

University of Southampton Research Repository ePrints Soton

Copyright © and Moral Rights for this thesis are retained by the author and/or other copyright owners. A copy can be downloaded for personal non-commercial research or study, without prior permission or charge. This thesis cannot be reproduced or quoted extensively from without first obtaining permission in writing from the copyright holder/s. The content must not be changed in any way or sold commercially in any format or medium without the formal permission of the copyright holders.

When referring to this work, full bibliographic details including the author, title, awarding institution and date of the thesis must be given e.g.

AUTHOR (year of submission) "Full thesis title", University of Southampton, name of the University School or Department, PhD Thesis, pagination

UNIVERSITY OF SOUTHAMPTON

FACULTY OF NATURAL AND ENVIRONMENTAL SCIENCES

CHEMISTRY

**A surface analytical chemistry approach to copper corrosion and its inhibition
with benzotriazole derivatives in oil-filled power transformers**

by

Marco Facciotti

Thesis for the degree of Doctor of Philosophy

October 2015

UNIVERSITY OF SOUTHAMPTON

ABSTRACT

FACULTY OF NATURAL AND ENVIRONMENTAL SCIENCES

Chemistry

Thesis for the degree of Doctor of Philosophy

A SURFACE ANALYTICAL CHEMISTRY APPROACH TO COPPER CORROSION AND ITS INHIBITION WITH BENZOTRIAZOLE DERIVATIVES IN OIL-FILLED POWER TRANSFORMERS

Marco Facciotti

In this thesis is discussed the possible application of surface analytical chemistry techniques to the study of copper corrosion and its inhibition in insulating oils. In particular, the techniques investigated were X-ray photoelectron spectroscopy (XPS) and secondary ion mass spectrometry (SSIMS). XPS was used, in combination with energy-dispersive spectroscopy (EDX), to study the formation and migration of the corrosion by-product copper sulfide on both copper conductors and paper insulation, as a consequence of their exposure to corrosive insulating oils. Its surface atomic sensitivity allowed the study of the influence of variables such as concentration of corrosive species, oxygen, time and copper-paper proximity on the corrosion process. This ultimately led to the formulation of a new bifurcated mechanism to explain how copper sulfide might contaminate the insulating system of power transformers filled with corrosive oils. Additionally, XPS could also be used to study the inhibitor layer formed by the benzotriazole derivative Irgamet®39 on copper immersed in oil. The corrosion inhibitor was detected as a local enrichment of nitrogen on copper substrates, solely induced by the presence of its surface-active tolyltriazole moiety. Remarkably, it was possible to identify a correlation between the amount of corrosion inhibitor present in the oil and that effectively protecting copper, while estimating the thickness of the protection layer and the optimal amount of corrosion inhibitor to be used in real-life applications.

SSIMS was used to increase the understanding of the copper inhibition process in oil by means of tolyltriazole. Thanks to its surface molecular sensitivity it was possible to obtain a new insight on the surface chemistry of the inhibitor, while investigating the effect of local temperature changes on the metal coverage and its stability under vacuum with the help of ion imaging. Moreover, it was also possible to estimate the energy of desorption of the tolyltriazole molecules from the copper surface. Finally, SSIMS ion imaging was shown to be a potentially valuable asset in forensic investigations, being able to track the distribution of corrosion inhibitor and by-products in decommissioned or failed power transformers.

Table of Contents

Table of Contents	i
DECLARATION OF AUTHORSHIP	v
Acknowledgements	vii
Abbreviations	ix
Thesis Outline.....	1
Introduction.....	2
1.1 Aim and outline of the chapter	2
1.2 Electricity transmission and distribution in Great Britain	2
1.3 Transformers.....	6
1.3.1 Magnetic core	8
1.3.2 Conductors.....	9
1.3.3 Insulating materials	10
1.3.3.1 Insulating fluids.....	11
1.3.3.2 Insulating paper and pressboards	13
1.3.4 Tank.....	14
1.4 The <i>corrosive sulfur</i> problem	15
1.4.1 Identification of corrosive compounds	16
1.4.2 Mechanism of formation of copper sulfide in transformers and its consequences	19
1.5 Detection of corrosive sulfur species and mitigation strategies	23
1.5.1 Detection of corrosive species in transformer oil.....	23
1.5.2 Oil reclamation and substitution.....	24
1.5.3 Addition of copper-targeted additives	25
1.5.3.1 Chelation agents	25
1.5.3.2 Surface inhibitor agents.....	25
1.5.4 Advantages and disadvantages of the proposed mitigation strategies	28
1.5.5 General consideration on benzotriazole derivatives as corrosion inhibitors	29

2.	Experimental methods	31
2.1	General notes	31
2.2	Oil sample and standard solutions	32
2.3	Corrosion tests	33
2.4	Large paper samples for copper sulfide deposition studies	33
2.5	Scanning electron microscopy (SEM)	34
2.5.1	Fundamental principles	34
2.5.2	Sample preparation	37
2.6	X-ray photoelectron spectroscopy (XPS)	38
2.6.1	Fundamental principles	38
2.6.2	Sample preparation	43
2.6.3	Experimental parameters	44
2.6.4	XPS signal assignments	47
2.7	Secondary ion mass spectrometry (SIMS)	48
2.7.1	Fundamental principles	48
2.7.2	Sample preparation	51
2.7.3	Experimental parameters	53
2.7.3.1	Constant temperature and imaging SSIMS	54
2.7.3.2	Ion imaging	54
2.7.3.3	Variable temperature SSIMS	54
2.7.3.4	Energy of desorption calculations	55
2.7.4	SSIMS ion mass assignments	55
3.	The effect of metal-insulation contact on copper sulfide deposition on Kraft paper	57
3.1	Aim and outline of the chapter	57
3.2	Overview on copper dissolution in oil and copper sulfide contamination of insulating paper by CIGRE WG A2.40	58
3.3	Optimisation of the ageing conditions: time and temperature	62
3.4	The effect of the concentration of DBDS in the oil	68
3.5	The role of ageing atmosphere	71
3.6	The importance of the contact between copper and paper	74
3.7	The proposed mechanism	75

3.8	Summary of the chapter and future work	77
4.	XPS studies on the tolyltriazole corrosion inhibitor layer.....	79
4.1	Aim and outline of the chapter	79
4.2	Previous applications of XPS to study copper inhibition by benzotriazole derivatives.....	80
4.3	Corrosion inhibition in base oil: feasibility, reproducibility and optimisation of the XPS analysis protocol.....	81
4.4	Corrosion inhibition in commercial oils: XPS results and their correlation with standard corrosion tests.....	89
4.5	Corrosion inhibition in oils: XPS estimation of the organic inhibition layer thickness	94
4.6	Practical recommendations consequence of this study.....	98
4.7	Summary of the chapter and future work	99
5.	SSIMS studies on the tolyltriazole corrosion inhibition layer.....	101
5.1	Aim and outline of the chapter	101
5.2	Previous applications of SSIMS to study copper inhibition by benzotriazole derivatives in different media	102
5.3	TPD-SSIMS on copper samples inhibited in oil.....	103
5.3.1	Quality of the copper surfaces and the oils.....	103
5.3.2	Secondary ion profiling	104
5.3.3	Secondary ion imaging	111
5.3.3.1	Visualising the surface coverage.....	111
5.3.3.2	The effect of electrical stresses on the inhibition layer.....	113
5.3.3.3	First application of secondary ion imaging as a transformer forensic tool: The case of a scrapped 400/275 kV substation autotransformer	115
5.3.4	Energy of desorption calculations	118
5.3.5	The influence of the metal surface on the interactions with the inhibitor: A study on Cu single crystals	120
5.4	Summary of the chapter and future work	123
6.	Conclusions	127
	Appendices.....	129

Appendix A.....	131
A.1 Copyright permission of reuse.....	131
A.2 ESEM micrographs of aged paper samples	132
A.3 Thermogravimetric Data.....	155
Appendix B.....	157
B.1 Copyright permissions to reuse	157
B.2 XPS sample holder	158
B.3 HD resolution CCD test results	158
Appendix C.....	161
C.1 Copyright permission to reuse	161
C.2 SSIMS data sets	162
Base Oil 20.....	162
Gemini X oil.....	166
HyVolt III oil	168
10 GBN oil.....	174
Cu(110) surface.....	180
Cu(111) surface.....	182
List of References.....	185

DECLARATION OF AUTHORSHIP

I, Marco Facciotti

declare that this thesis entitled

“A surface analytical chemistry approach to copper corrosion and its inhibition with benzotriazole derivatives in oil-filled power transformers”

and the work presented in it are my own and has been generated by me as the result of my own original research.

I confirm that:

1. This work was done wholly or mainly while in candidature for a research degree at this University;
2. Where any part of this thesis has previously been submitted for a degree or any other qualification at this University or any other institution, this has been clearly stated;
3. Where I have consulted the published work of others, this is always clearly attributed;
4. Where I have quoted from the work of others, the source is always given. With the exception of such quotations, this thesis is entirely my own work;
5. I have acknowledged all main sources of help;
6. Where the thesis is based on work done by myself jointly with others, I have made clear exactly what was done by others and what I have contributed myself;
7. Parts of this work have been published as peer reviewed journal papers (•) or conference contributions (–):
 - Facciotti, M.; Amaro, P. S.; Holt, A. F.; Brown, R. C. D.; Lewin, P. L.; Pilgrim, J. A.; Wilson, G.; Jarman, P. N. Contact-Based Corrosion Mechanism Leading to Copper Sulphide Deposition on Insulating Paper Used in Oil-Immersed Electrical Power Equipment. *Corros. Sci.* **2014**, *84*, 172–179.
 - Facciotti, M.; Amaro, P. S.; Holt, A. F.; Brown, R. C. D.; Lewin, P. L.; Pilgrim, J. A.; Wilson, G.; Jarman, P. N.; Fletcher, I.W. Static secondary ion mass spectrometry investigation of corrosion inhibitor Irgamet®39 on copper surfaces treated in power transformer insulating oil. *Corros. Sci.* **2015**, *98*, 450–456.
 - Facciotti, M.; Amaro, P. S.; Brown, R. C. D.; Lewin, P. L.; Pilgrim, J. A.; Wilson, G.; Jarman, P. N.; Barlow, A. X-ray photoelectron spectroscopy study of the correlation between surface saturation of copper and corrosion inhibition performance in insulating transformer oils. **2015**, *In Preparation*.

- Facciotti, M.; Amaro, P. S.; Brown, R. C. D.; Lewin, P. L.; Pilgrim, J. A.; Wilson, G.; Jarman, P. N. SSIMS Molecular Selective Imaging: A New Diagnostic Tool to Investigate Metal Passivators in Scrapped Transformers. In *2015 IEEE Electrical Insulation Conference (EIC)*; IEEE, 2015; pp. 388-391.
- Facciotti, M.; Holt, A. F.; Amaro, A. P. G. V.; Brown, R. C. D.; Lewin, P. L.; Wilson, G.; Jarman, P. N. XPS Study on Direct Detection of Passivator Irgamet 39TM on Copper Surfaces Aged in Insulating Mineral Oil. In *2013 Annual Report Conference on Electrical Insulation and Dielectric Phenomena*; IEEE, 2013; pp. 1097–1100.
- Facciotti, M.; Amaro, P. S.; Brown, R. C. D.; Lewin, P. L.; Pilgrim, J. A.; Wilson, G.; Jarman, P. N. Passivators, Corrosive Sulphur and Surface Chemistry. Tools for the Investigation of Effective Protection. In *MyTransfo 2014: Oil and Transformer*; 2014; pp. 27–35.
- Amaro, P. S.; Facciotti, M.; Holt, A. F.; Pilgrim, J. A.; Lewin, P. L.; Brown, R. C. D.; Wilson, G.; Jarman, P. Tracking Copper Sulfide Formation in Corrosive Transformer Oil. In *2013 IEEE Electrical Insulation Conference (EIC)*; IEEE, 2013; pp. 144–147.
- Holt, A. F.; Facciotti, M.; Amaro, P.; Brown, R. C. D.; Lewin, P. L.; Pilgrim, J. A.; Wilson, G.; Jarman, P. An Initial Study into Silver Corrosion in Transformers Following Oil Reclamation. In *2013 IEEE Electrical Insulation Conference (EIC)*; IEEE, 2013; pp. 469–472.

Signed:

Date:

Acknowledgements

I would like to thank:

Prof Richard C. D. Brown for his supervision during my Ph.D. studies and for allowing me to direct my research project.

The members of the Brown's group, past and present, for their help and for interrupting with enjoyable tea breaks my long hours at the desk.

Prof Paul L. Lewin for his support and availability throughout my stay at Southampton and for being the first to welcome me in the TDHVL family, where I could see the world, grow professionally, meet new friends and learn about the "balance".

Dr Pedro S. Amaro and Dr Alex F. Holt for sharing good and less good times in the lab.

Dr Gordon Wilson for his invaluable support, insight and feedback at all stages of the project.

I would also like to thank National Grid plc for the financial support together with all the collaborators from the University of Southampton, Intertek Wilton and University of Newcastle upon Tyne.

Abbreviations

Å	Ångstrom(s)	DBSO	Dibenzyl sulfoxide
AC	Alternating current	DC	Direct current
ASCII	American Standard Code for Information Interchange	DGA	Dissolved gas analysis
ASTM	American Society for Testing and Materials	DHDS	Diethyl disulfide
B.E.	Binding energy	DHS	Diethyl sulfide
BS EN	British Standard	DIN	Deutsches Institut für Normung
BSE	Backscattered electrons	DNO	Distribution network operator
BSI	British Standards Institution	DP	Degree of polymerisation
BTA	Benzotriazole	E	Energy
CCD	Covered conductor deposition	e	Electron
CCGT	Combined-cycle gas turbines	EAL	Effective attenuation length
CHP	Combined heat and power plants	E_{des}	Energy of desorption
CIGRE	Conseil International des Grands Réseaux Électriques	EDX	Energy-dispersive X-ray spectroscopy
cm	Centimetre(s)	EPSRC	Engineering and Physical Sciences Research Council
cP	Centipoise(s)	ESEM	Environmental scanning electron microscopy
CPR	Chemical preparation room	eV	Electronvolt
CPS	Counts per second(s)	FFT	Fast Fourier transformation
Cu_xS	Copper sulfides	g	Gram(s)
Da	Dalton(s)	GDD	Gaseous detection device
DBDS	Dibenzyl disulfide	GSE	Gaseous secondary electrons
DBPC	2,6-di- <i>ter</i> -butyl- <i>p</i> -cresol	h	Hour(s)
DBS	Dibenzyl sulfide	HD	High-definition
		HV	High voltage

IEC	International Electrotechnical Commission	MVA	Megavolt-ampere
IEEE	Institute of Electrical and Electronic Engineers	<i>n</i>	Principal quantum number
IFT	Interfacial tension	<i>n</i>⁺	n-tuple positive charge
IMFP	Inelastic mean free path	NEXUS	National EPSRC XPS Users' Service
IUPAC	International Union of Pure and Applied Chemistry	nm	Nanometre(s)
J	Joule(s)	NMR	Nuclear magnetic resonance
K	Kelvin degrees	°	Degrees Celsius
K.E.	Kinetic energy	Ø	Diameter
kg	Kilogram(s)	°C	Celsius degrees
kJ	Kilojoule(s)	Ofgem	Office for Gas and Electricity Market
<i>l</i>	Azimuthal quantum number	OFHC	Oxygen-free high conductivity
LMIG	Liquid metal ion gun	Pa	Pascal(s)
LV	Low voltage	PARXPS	Parallel Angle-Resolved XPS
m	Metre(s)	PET	Polyethylene terephthalate
M	Molecule	PLA	Pressure limited aperture
<i>m/z</i>	Mass-charge ratio	ppm	Part(s) per million
m/Δm	Mass resolution	PTFE	Polytetrafluoroethylene
mbar	Millibar	QP	Quadrupole
Me	Metal	RAW	Raw image file
mg	Milligram(s)	RGB	Red-green-blue
min	Minute(s)	RSF	Relative sensitivity factor
ml	Millilitre(s)	s	Second(s)
mm	Millimetre(s)	SDS	Sodium dodecyl sulfate
mN	Millinewton(s)	SE	Secondary electrons
mol	Mole(s)	SERS	Surface enhanced Raman spectroscopy

SO	System operator	XPS	X-ray photoelectron spectroscopy
SSIMS	Static secondary ion mass spectrometry	Z	Atomic number or generic atom
T	Temperature	Δ	Variation
tanδ	Dissipation factor	μm	Micrometre(s)
TB	Technical brochure	Ω	Ohm(s)
TGA	Thermogravimetric analysis	•	Radical
TO	Transmission operator	+	Positive charge
ToF	Time of flight	-	Negative charge
TPD	Temperature-programmed desorption	©	Copyright
		®	Registered
TPP2M	Tanuma-Powell-Penn-2M	±	Plus or minus
TTA	Tolyltriazole	<	Less than
UHV	Ultra-high vacuum	>	Greater than
V	Volt(s)	>>	Much greater than
W	Watt(s)	≥	Greater than or equal
Wb	Weber(s)	~	Circa
WD	Working distance	2D	Bi-dimensional
WG	Working group		

Thesis Outline

This thesis is organised into six chapters.

The first introductory chapter provides background on the literature knowledge on basic transformer design and materials, corrosion of copper in insulating oils, mechanism of formation of copper sulfide in the insulating system, possible mitigation strategies and, finally, a general overview of copper corrosion inhibition. Particular attention is paid to the chemistry of the processes involved in both corrosion and protection of copper conductors in oil, rather than on technical or physical aspects that are considered the domain of high-voltage engineering. Such multidisciplinary work however, cannot be completely exempt from overlapping expertise.

The second chapter details the physical-chemical processes on which the experimental techniques used lay their foundations, and then focuses on the definition of the experimental procedures and instrumental parameters used throughout the study.

The third chapter describes a series of experiments performed to increase the understanding of the variables that influence the process of copper sulfide formation in transformers, its migration and deposition on copper conductors and insulating paper, as a consequence of corrosion. It comprises a discussion on the development of a new sample preparation procedure, together with the outcomes of the characterisation of the materials obtained both empirically and by means of X-ray photoelectron spectroscopy (XPS) and energy-dispersive X-ray spectroscopy (EDX).

The fourth and fifth chapters include results of the investigation on corrosion inhibitor layer stability, characteristics and performance by means of surface specific analytical techniques: XPS and static secondary ion mass spectrometry (SSIMS), respectively. The fifth chapter is also partly dedicated to the possible exploitation of SSIMS ion imaging in real-life applications, together with the critical evaluation of its advantages and limitations, providing a successful example of how SSIMS imaging can help understanding the failure of a scrapped transformer.

Lastly, the conclusions of the work are concisely summarised.

Introduction

1.1 Aim and outline of the chapter

This chapter has been organised into subsections to facilitate the discussion of the literature on the subjects of corrosion phenomena in oil-filled power transformers and their countermeasures. Initially, an overview of high voltage transmission and power transformer design and construction is reported. This section does not aim to describe either technical or mathematical details to a large extent, outside the scopes of this work, but rather serve as background for readers not familiar with such topics. It provides a basic level of understanding necessary to appreciate the practical implication of the chemistry research work presented in the following chapters. This is followed by a discussion on sulfur-related corrosion in oil-filled transformers and finally, a summary detailing possible mitigation strategies. Special consideration was given to metal inhibition by means of benzotriazole derivatives, outlined while discussing the state-of-the-art chemistry involved.

1.2 Electricity transmission and distribution in Great Britain

Power is often produced far away from the place it is used. This is mainly due to the uneven distribution of energetic resources across the Planet, but also the environmental impact that power production sites undoubtedly have on their surroundings. Regardless of the cause of such occurrence, since the dawn of electrical power systems in the late 19th century, efficient and reliable transmission and distribution of electricity has been a primary concern. It led, especially after the Second World War, to the development of power networks in developed country, first for direct (DC) and then alternating current (AC).

Historically, Britain had a central role in both discovery and development of electricity and for this reason certain milestones cannot be left unmentioned, especially those involving the many accomplishments of Michael Faraday, who did so much for this area of engineering and technology. After the pioneering observations of the Dane Hans C. Ørsted that led to the discovery of electromagnetism, Faraday fathered revolutionary ideas such as electromagnetic rotation (1821) and induction,¹ the first electrical transformer and generator (1832) and the concept of electromagnetic field (1840-50's), later formalised by Lord Kelvin and James C. Maxwell in the form of the well-known equations.² After the

scientific breakthrough, dedicated technology was developed to take advantage of electromagnetic phenomena to improve people's lives, even if with some physiologic delay. In the following 40 years the first experimental electric lighthouses were installed, telegraph cables were laid across Europe and the Atlantic, the telephone and the light bulb were invented followed by public electric lighting (1881) and electric railways (1883).³ It is noteworthy to report that the first UK government actions towards the capillary connection of households to power were performed in the 1930's with the Assisted Wiring Scheme, allowing more than 12,000 wealthy people access to electricity by the end 1936.³ After the Great War, the energy sector expanded enormously thanks to the nationalisation of the electrical industry (previously divided in 625 electricity companies) and the diffused economic boost, in common with other European countries and the United States of America.³

The backbone of the electrical transmission and distribution network in the UK was completed by the 1960s and it is still mostly unchanged in 2015. Today, the British electricity network can be considered constituted of three main subsets, each of which is responsibility of one or more companies operating in the energy sector: generation, transmission and distribution. The simplest way to trace a boundary between these is looking at the rated voltage of the lines. The structure of the network and graphical explanation of this last concept are exemplified in **Figure 1**.

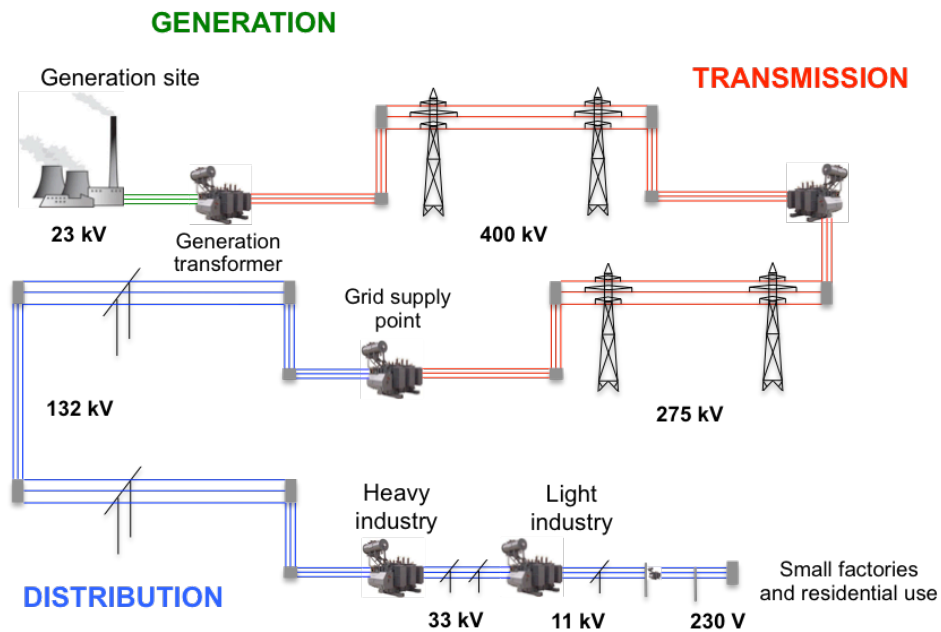


Figure 1 – Schematic representation of electricity generation, transmission and distribution network based on 400 kV/275 kV/132 kV connections in Britain.

Power generation across the whole United Kingdom, is today quite diversified between different power sources such as oil-/coal-/dual-fired stations, nuclear plants, combined-cycle gas turbines (CCGT), combined heat and power plants (CHP), gas turbines, diesel generators, hydroelectric stations and biomass conversion.⁴

Onshore power transmission is currently responsibility of three *transformer operators* (TOs): Scottish Power Transmission Ltd (southern Scotland), Scottish Hydro-Electric Transmission plc (Scotland and Scottish archipelago) and National Grid Electricity Transmission plc (England and Wales). As a consequence of the privatisation of the energy sector started in 1990,³ a controlling role is now being held by the latter company as *system operator* (SO) of the whole transmission grid of the island of Great Britain.

Power distribution instead is managed by fourteen licensed *distribution network operators* (DNOs), which are accountable for the capillary distribution of power, regionally. Due to the likelihood of the instauration of a monopole on the energy market, a regulatory body has been identified in the Office for Gas and Electricity Market (Ofgem). It monitors prices at the consumers' end, all major network investments and eventually penalises operators in case of repeated offences or persistent power outages.

The main challenges that this network faces today are three:

1. Integrate a variety of renewable sources in a system that was not meant to host them, coping with their intermittent nature, diverse tension and technological requirements (*e.g.* high voltage direct current applications, HVDC).
2. Establish links with foreign grids to redistribute power more efficiently across different countries and take full advantage of renewables, ideally, worldwide-scale.
3. Deal with an old but essentially working network that requires dedicated and continuous condition monitoring in order to plan interventions, minimising running costs and failure likelihood.

The last point is probably the core need of the industry, from the point of view of the SO (National Grid plc), that led to the formulation of the research questions subject of the work detailed in this thesis.

As a reference to the reader, the appearance of the national electric grid to date, based on 400 kV, 220 kV and 132 kV networks, is shown in **Figure 2**.



Figure 2 – Map of the generation, transmission and distribution grid in Great Britain.⁴

1.3 Transformers

As already anticipated, power is often produced far away from the final users' locations and needs to be transmitted efficiently, with minimum loss. High voltage (HV) distribution grids have been the technological answer to this fundamental need of modern society, providing a reliable connection between remote generation sites and the users. To transmit this power, at least onshore, modern society normally relies on copper-wired overhead high voltage lines.

Intuitively, such high voltages are incompatible with everyday applications and energy cannot be produced everywhere in the same condition. For these reasons transformers are needed to change voltage reversibly and tune power to needs, on both ends of the transmission line, as shown in **Figure 1**. These devices allow changing either voltage or current levels in the network, often automatically, while keeping an ideally constant power output. Together as a fleet, they serve to the SO as an invaluable capillary control system for the power flows in the network at any given time. Thanks to dedicated control rooms, continuously predicting demand and supply at the transmission and distribution level, while communicating energy requirements to generation power stations almost in real time, today it is possible to achieve an efficient distribution of energy minimising costs.

The complex nature of both transmission and distribution grids and the need of their integration in a cohesive power grid requires a considerable number of transformers, which need to cope with variable requirements, depending on their position with respect to the overall network. For this reason, many different designs and constructive solutions are available nowadays on the market with variations on core, conductors, insulating liquids and materials, tanks and bushings. These devices are generally very expensive (millions of pounds in the case of large HVDC transformers) and they represent a major asset investment for whoever commissions them. In normal rated operative conditions, their projected lifetime is expected to be between 30 and 50 years,⁵ although some transformers in service can be considerably older than that.^{6,7}

The simplest ideal transformer is a single-phase machine comprising two metal conductors, said solenoids, wound around a toroidal ferromagnetic core, as shown in **Figure 3**.

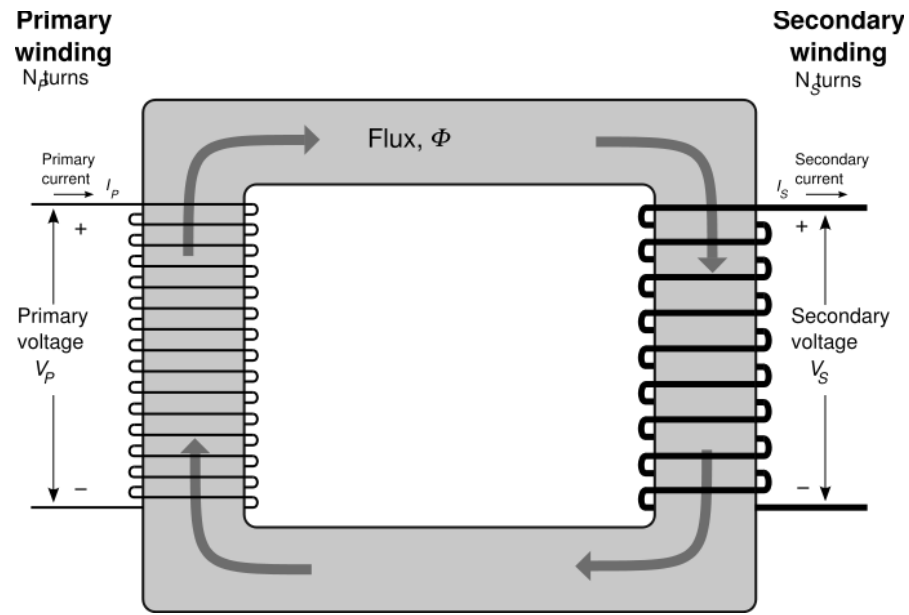


Figure 3 – Schematic representation of an ideal single-phase transformer.

Conventionally, the winding to which energy is provided is said primary while the one from which it is taken is said secondary. When an alternating sinusoidal voltage (AC) is applied on the primary winding a magnetic flux is generated due to magnetic induction in the iron core, which induces a sinusoidal voltage in the secondary, together with an electromotive force. The AC voltage produced in the secondary winding is then proportional to the ratio between the number of turns of the solenoids used, as known from the beginning of the 19th century,^{8,9} according to the equation:

$$\frac{V_P}{V_S} = \frac{N_P}{N_S} = k_0$$

Where V_P is the applied voltage to the primary winding, V_S the voltage induced on the secondary, N_P and N_S the number of turns of the above, respectively; k_0 is called transformation ratio. This phenomenon is an application of the electromagnetic induction, first described by M. Faraday¹ in the formulation of its Law of Induction (1832), reported below:

$$|\epsilon_{emf}| = \left| \frac{d\Phi_B}{dt} \right|$$

Where ϵ_{emf} is the electromotive force generated in the secondary winding in Volts (V) and Φ_B represents the magnetic flux through the circuit, measured in Webers (Wb).

One last complication needs to be addressed before continuing the discussion on the transformer's design and components, to avoid misleading oversimplifications: three-phase

power. Three-phase electric power is a method of AC generation, transmission and distribution that is based on power supplies with three conductors. Each of these carries AC with the same frequency and voltage as the other two, although normally separated by 120 electrical degrees, as shown in **Figure 4**.

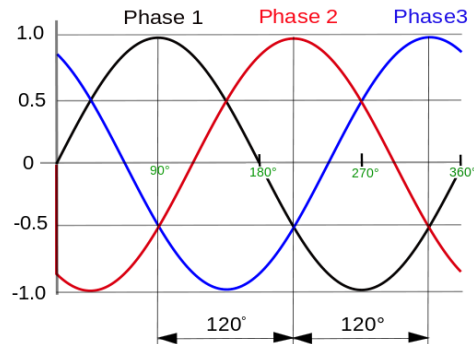


Figure 4 – Waveform of a three phase AC across one voltage cycle showing the instantaneous voltage variation over time.

The development of three-phase power helped to maximise the efficiency and the nominal load that a power grid can manage, which was fundamental in matching the growing demand of electricity supply during the last century.⁶ The reason for its convenience over single-phase power is that the phase delay between the conductors, ideally, allows constant power flow in balanced lines. Additionally, it uses less conductor material to transmit the same amount of power, making it also economically attractive. This obviously means that larger and more complex three-phase transformers are also required.

According to the extent of the scope of this work, despite of their rather obvious degree of engineering sophistication, transformers will be considered comprising mainly three main elements that are necessary to understand their basic operations: conductors, insulators and magnetic core. The following sections aim to briefly describe what these components are and the role they play in such complex pieces of equipment.

1.3.1 Magnetic core

The core, with a high magnetic permeability, has the function of facilitating the passage of the magnetic flux from the primary to the secondary winding through a low magnetic resistance (or reluctance) path, enabling electromagnetic induction to take place.

There are international regulations defining the materials to be used for such crucial components of transformers, such as IEC 60404.¹⁰ However, all suitable materials share

minimal magnetic hysteresis looping and high resistivity, to minimise eddy currents. The core itself can have a single-body or stacked sheets design and it can vary in layout to accommodate, for example, the three pairs of windings that are required in three-phase transformers. The most common layout in the UK, among the many possible, is the three-phase three-limb core, as shown in **Figure 5**.

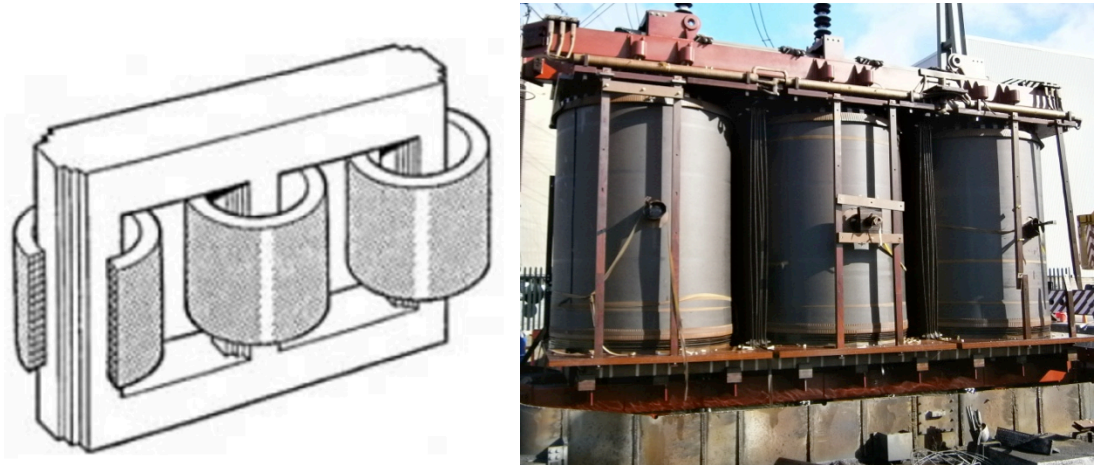


Figure 5 – Comparison between the schematic representation of a three-phase three-limb transformer core (left)⁶ and an example of its occurrence in a real application (right).

As a general rule, it is important to remember that all the theory and formalism described in Section 1.3 are strictly valid only in ideal systems. In real life, losses of some kind are always present due to deviation from ideal conditions. The core itself is source of some of said losses, experienced while the transformer is operational such as the generation of eddy currents, the insurgence of magnetic hysteresis phenomena, vibrations and noise due to the sudden change of polarity that is characteristic of AC.⁶

1.3.2 Conductors

Copper is second only to silver in terms of electrical conductivity but it is widely used for both cost and availability reasons.¹¹ Transformer windings consist essentially of electric grade copper alloys, normally with 0.1 to 0.3% Ag, in the form of rectangular-section wires or strips complying with BS EN 13601:2002.¹² Silver has no particular effects on conduction properties when in such low amount but helps in increasing the softening temperature of the alloy preventing changes in the shape of the windings, once operational, due to temperature fluctuations. Silver also provides additional hardness that increases the structural stability of the windings, especially needed in larger transformers where the ability of the conductor coils to bear their own weight becomes crucial.

The windings, serve the primary purpose of conducting electricity but they are also responsible for at least one undesired effect: temperature-related load losses. It is well known that a metal conductor, while having current flowing through it, experiences the phenomenon called Joule's heating. This is a major physical variable that has to be carefully taken into account when evaluating, for example, the cooling requirements of a transformer. As the heat generation is directly dependent on the cross-sectional area of the conductors and the applied load, its characteristics are typical for every single design/transformer. However, as the issue is much more complicated than described here, the eventual reduction of the cross-section of conductors wouldn't annihilate losses.⁶ Given all this, it should become clear why a great importance is given to the design of the conductors and cooling systems in power transformers.

Additionally it is necessary to mention that there are also significant differences between the conductors in the HV and low voltage (LV) windings. Due to the way in which transformers work, the high voltage winding is always subject to much smaller levels of flowing current therefore it can have smaller cross sectional area (although it requires to be significantly longer than the low voltage one to which it is paired). Mainly for size and efficiency reasons, the high voltage winding is normally wound to form discs, as shown in **Figure 6** (left). The pair of windings (LV and HV) is also wound around the same core (or core limb) with the low voltage end closer to it, as shown in **Figure 6** (right).^{6,7}

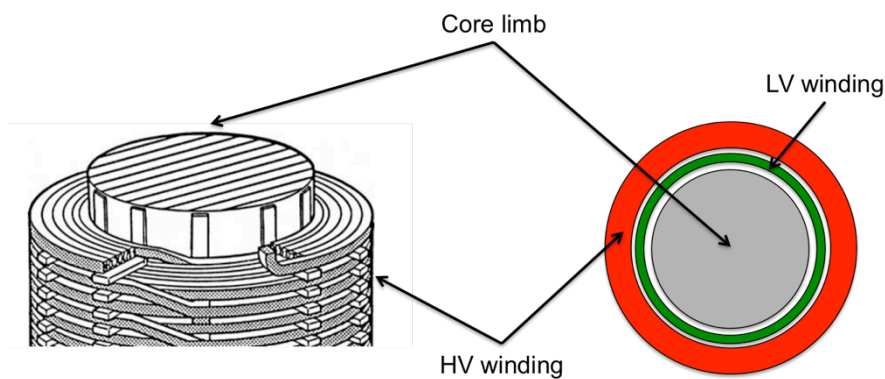


Figure 6 – Schematic representation of the discs arrangement of high voltage winding (left) and transverse section of core and windings (right).

1.3.3 Insulating materials

As discussed previously, transformers are electrical machines that work thanks to electromagnetic induction between two windings physically separated. For its correct operation, any electrical contact between the primary and the secondary winding must be

avoided, as well as between turns/discs of the same. If electrical insulation was not guaranteed at all times, it wouldn't be possible to observe the inductive phenomenon in the first instance and discharges or short circuits would be more likely to occur. Both solid and fluid insulators are used to ensure the correct operations of HV transformer and they are detailed in the next subsections.

1.3.3.1 Insulating fluids

As the focus of this project was to understand corrosion and corrosion inhibition of copper in oil-filled HV power transformers, the most relevant insulating fluid to be discussed is, for obvious reasons, mineral oil. Nonetheless, several different fluids can be used as insulators in transformers, depending on the final application and design characteristics of the piece of equipment for example:

- In some applications silicone liquids can be preferred due to their extremely high flash point ($> 350\text{ }^{\circ}\text{C}$), higher thermal stability and chemical resistance.
- Ester fluids (both natural and synthetic) might be desirable for their low toxicity and low environmental impact, thanks to their biodegradability, despite their relatively high cost.
- In specialist applications the use of a gas insulator, normally sulfur hexafluoride (SF_6), may be required although it is highly desirable for its use to be reduced in the future, as it is a well-known and highly persistent greenhouse gas.¹³

In addition to the insulating properties it expresses, the insulating fluid also allows the transformer (or parts of it) to operate at an average temperature between 60 and $80\text{ }^{\circ}\text{C}$, in the absence of other problems.¹⁴ Given all the above, insulating mineral oil represents the most widely available, low-cost and flexible solution and it is therefore used often in power transformers, in compliance with IEC 60296.¹⁵

As one of the heavy fractions of crude oil refinery, separated after atmospheric and reduced pressure distillation, mineral oils represent less than 2% of lubricants.¹⁶ Refinery processes are not only needed to separate different fractions from the crude, but also to produce uniform properties from such an intrinsically variable and complex fossil-derived raw material, reducing the concentration of contaminants (often peculiar to each extraction site) such as metals, oxygen, nitrogen, sulfur and tuning the aromatic/naphthenic/aliphatic ratio of the final product.

After distillation, the crude can undergo three main different treatments, in order of severity (intended as high temperature and pressure):¹⁶

- *Solvent refining*
- *Hydrotreating/hydropolishing*
- *Hydrocracking*

The first one is substantially an extraction with solvent to remove aromatic and heterocyclic impurities thanks to their partition coefficient and solubility in different solvents (*e.g.* liquid SO₂, furfural and methyl pyrrolidone). The second is a catalytic process at high temperature and pressure, promoting the hydrogenation of the impurities previously cited. The last treatment represents a more severe version of the previous and it substantially promotes the hydrogenation of the aromatic fractions as well, with saturation and ring opening reactions with increasing efficiency for highly condensed structures, leaving a paraffinic base oil as a result. As a general rule, it can be said that the higher the severity the higher the purity of the oil obtained.¹⁷ However, the objective of refining processes is not to remove all impurities but only those affecting the properties desired for the specific application for which the oil is intended. More often a combination of treatment is recommended so that certain desired oil fractions, such as aromatic compounds, may be retained in the final product ensuring better oxidation performance.⁵ To complete the treatments, the oil is normally filtered to remove particles and sludge while moisture content is reduced through vacuum stripping. It is due mentioning that mineral oils contain naphthenic, aromatic and paraffinic fractions, and each commercial product is characterized by carefully selected ratios of these common constituents, to achieve the desired properties.¹⁶

The development of specialist knowledge on these treatments and their management, acquired over decades, now allows the production of mineral oils in a remarkable variety. However, it is still unrealistic to pretend they should simultaneously meet all technological requirements and therefore a compromise at the users' end is often accepted.

In fact, there are many properties to be considered when choosing an insulating mineral oil (high dielectric constant, resistivity, interfacial tension, flash point, oxidation stability, good heat transfer coefficient, low dielectric loss, electrostatic charging, viscosity, pour point, *etc.*) but they will not be discussed in further detail unless functional to the discussion of results, since they are outside of the scope of this work. However, it is important to note that after all refinery processes some properties are found to be worse

and, therefore, various additives can be added to ensure that all (or most) technical requirements are met.^{18,19} Oils that are doped are now normally referred to as inhibited.¹⁵ Although in the past their use was common practice elsewhere especially to enhance the oxidation stability, in the UK additives were not permitted in electrical oils. As already discussed, this useful inhibition effect can be naturally expressed even by some oil constituents, such as some organosulfur compounds or aromatics, provided they are capable of terminating radical cycles. In commercial transformer oils, additives and impurities are regulated in compliance with international standards.^{15,18,19}

Thermal stresses and oxidation are the main reasons of the ageing of a mineral oil inside a transformer in service. In terms of specific property deterioration, ageing normally causes the reduction of breakdown voltage, interfacial tension and dielectric resistance with a parallel increase of the dissipation factor ($\tan\delta$), acidity of the oil and sludge precipitation. As the oil represents the main constituent of the insulation system that is fundamental for the correct operation of the transformers, it is often said that its lifetime (together with that of paper insulation) coincides with that of the transformer.⁶ For this reason, a great deal of work has been carried out in developing condition monitoring tools (both chemical and electrical) to assess the ageing status of the insulating system. Remedial strategies have also been developed to mitigate the effects of ageing or undesirable reactions, which will be discussed in detail in Section 1.5.

1.3.3.2 Insulating paper and pressboards

Kraft paper is one of the cheapest amongst the best electrical insulating materials known. It is, by definition, made entirely from unbleached softwood pulp (as residual bleaching agents might jeopardize its electrical properties) manufactured by the sulfate process. In its electrical applications it is generally characterized by high dielectric strength, dielectric constant similar to the one of the oil, low power factor (dielectric loss) and substantial freedom from conductive particles.⁶ Inside a transformer, paper is normally tightly wrapped around copper conductors and metal connections, often in multiple overlapping layers, to provide additional insulation to that ensured by the oil alone. For particular transformer applications, four kinds of paper-base products are widely available to match different technological requirements. These are:

1. *Crêped* paper – made with an irregular close crimp that increases its thickness and extensibility in the machine direction. However, it tends to loose elasticity over time.

2. *Highly extensible* paper – its elasticity is tuned in the roll-forming process in which the action of the rolls, in conjunction with heat and moisture, axially compresses the fibres in the machine direction enhancing stretch and cross-machine tear properties, whilst retaining the original tensile strength and dielectric properties.
3. *Thermally upgraded* paper – treated with the addition of stabilizers during manufacture to achieve better temperature stability and a reduced thermal degradation. It does not permit higher operating temperatures but it reduces the rate of decrease of the degree of polymerization (DP) of paper.
4. *Diamond-dotted presspaper* – pre-coated with two-stage adhesive resin in a diamond pattern. The resin dots create a large bonding surface whilst ensuring that the paper can be effectively dried and efficiently impregnated with oil. When the winding is heated for drying purposes, the adhesive dots melt and cure creating permanent bonding sites that give the structure its high mechanical strength, which remains unaffected by subsequent heating cycles.

Finally, pressboards are additional components of the solid insulation system. They consist of thick blocks of insulating material made by laying up multiple layers of paper at their wet stage in manufacture. Increased thickness can be achieved bonding together two or more pressboards using a suitable adhesive, otherwise absent. Their individual thickness in transformers usually ranges between 2 to 8 mm depending on their location within the tank and specific requirements of the transformer.⁶

1.3.4 Tank

The role of the tank is fairly simple: it has to physically contain and isolate from the environment all main parts of the transformer listed above whilst providing structural stability. It is made of steel and it usually fixed on a concrete basement. Its removal represents the first stage in the scrapping process of transformers as shown in **Figure 7**.



Figure 7 – Tank removal from a tri-phase 3-limb transformer in a coal-fired power station.

1.4 The *corrosive sulfur* problem

Corrosion is defined by IUPAC as an irreversible interfacial reaction of a material (metal, ceramic or polymer) with its environment, which results in consumption of the material or dissolution into the material of a component of the environment. Often, but not necessarily, corrosion results in effects detrimental to the usage of the material considered.²⁰ Metal corrosion, in particular, is a thermodynamically driven oxidative reaction that converts the refined metal to its more stable oxide (*i.e.* $\text{Me}^0 \rightarrow \text{Me}^{n+}$). Although in general sense this process is almost always linked to the aggressive presence of oxygen in contact with the metal surface, this is not always the case as some other chemical species are equally capable of inflicting damage. In fact, the subject of all studies related to copper corrosion in oil-filled transformers are chemical species in this latter category: sulfides.

Sulfide-mediated corrosion of copper and its alloys is a known issue in many applications of metallic materials, still subject of interest of the corrosion scientific community in both aqueous^{21–24} and non-aqueous environments such as lubricants, oils and fuels.^{25–29} Although its first appearances under the name of *corrosive sulfur* in oil-filled power apparatus go back to the beginning of the 21st century,³⁰ these were not investigated in great detail from the very beginning due to their isolated nature. The main observation made in such cases was the formation of copper sulfide (Cu_xS , complex mixture of CuS and Cu_2S)³¹ as a solid contaminant inside a failed transformer, the role of which in the failure mechanism will be detailed in Section 1.4.2. A few years later however, the increasing number of both affected and failed transformers worldwide was no longer

controllable nor geographically confined and remained substantially unexplainable by mere manufacturing problems.³² After some thought, the conclusion that was drawn was that the insulating oils, or better some new formulated additives, could be the cause of these corrosion-related failures.³² As a consequence, in the past decade or so, a lot of research has been carried out trying to:

- Identify potentially dangerous compounds.
- Understand their mechanism of action and the formation of Cu_xS .
- Develop efficient new ways to detect and monitor corrosive species in the oils.
- Prevent or mitigate the issue by means of *ad hoc* countermeasures.

1.4.1 Identification of corrosive compounds

Since shortly after its discovery, the denomination *corrosive sulfur* has been used as a nonspecific label to identify all chemical compounds capable of expressing corrosion towards copper in oil-insulated HV devices, regardless of their nature. Only after years of dedicated analytical chemistry studies aimed to detect such corrosive species, a more precise idea of the nature of the species involved was formed. In transformer oils, organosulfur compounds were identified to be the main culprits since the early stages of research, representing the most reasonable explanation to the observed formation of the main corrosion by-products of the reaction, copper sulfides (Cu_xS).^{33,34}

Although several different classes of sulfur-containing organic compounds have been postulated to contribute to the formation of copper sulfide inside transformers, the most typical molecular sources of sulfur in transformer oil are (listed in order of increasing reactivity towards copper):^{35,36}

- Monosulfides and thiophenes
- Mercaptans and oxidised sulfur compounds
- Disulfides
- Elemental sulfur

These were experimentally ranked in different base, paraffinic and naphthenic oils fortified with various organosulfur compounds at different temperatures, in accordance to IEC 62535.³⁷ Results clearly showed that benzyl mercaptans are the most prone to react with copper in oil at temperature as low as 80 °C.³⁶

It is indeed important to remember that these chemical compounds are not corrosive to copper *per se* but they are observed to become corrosive under certain environmental conditions, such as a local increase in temperature.

As already discussed, it is widely accepted that corrosive sulfur compounds are not created as a result of natural processes occurring inside a perfectly functional transformer in operation therefore, when present, it has been considered legitimate to assume they were added later (even if only in the form of precursors and/or unwillingly).³⁸ There are only two reasonable ways in which these undesirable substances could start manifesting themselves in insulating oils:

- Low grade of sophistication in the oil manufacturing and refining process.
- The addition of additives used to enhance the performance of the oil, which may be precursors of potentially corrosive species.³⁰

However, refinery processes are generally considered to substantially decrease the sulfur content.³⁹ Additionally, the simple and interesting observation³⁸ detailed below strongly led the scientific community to think of a predominance of the second scenario. **Figure 8** shows how, over the last two decades, sulfur content after the refining processes has indeed dropped mostly due to technological advances of the refinery industry.

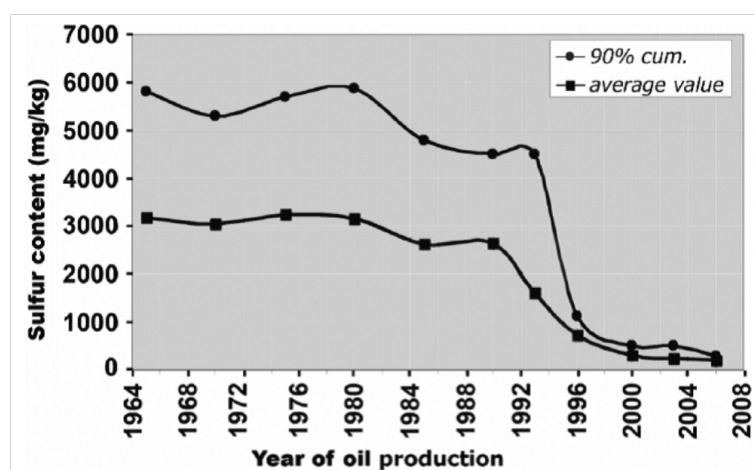


Figure 8 – Average sulfur content of mineral insulating oil manufactured in the last 50 years.³⁸ © 2009 IEEE

On the other hand **Figure 9** shows an opposite trend when looking at the occurrence of corrosive sulfur in transformer oils, across same period of time. Based on these data, refinery processes alone cannot be held responsible for the corrosive sulfur issue.

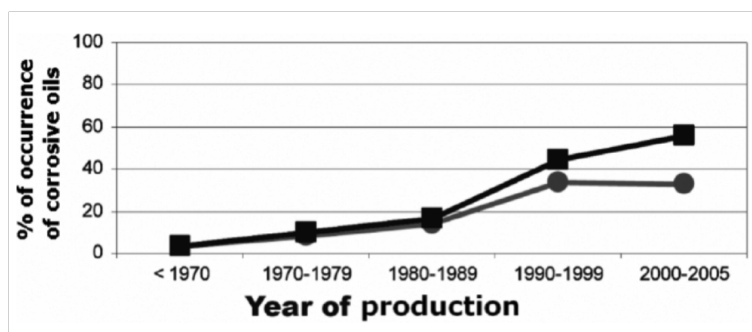


Figure 9 – Percentage occurrence of corrosive oils as for D1275A^a normal (circles) and extended to 48 h (squares).³⁸ © 2009 IEEE

One compound in particular was identified to play a crucial and representative role, although not alone, in corrosive sulfur-related failures of transformers: dibenzyl disulfide (DBDS). DBDS was originally employed as an antioxidant for transformer oils since, in its stable form at low temperature (below 150°C), it acts as a good oxidation inhibitor *via* oxidation of S–S bond and reduction of hydroperoxides. Nonetheless, according to the opinion of very few, this process occurs through cleavage of the S–S bond.⁴⁰ Outside the electrical industry, it also finds application as flavouring agent in food products and extreme-pressure additive in gear lubricants.⁴¹

Interestingly enough DBDS can indeed be present in crude oil but, due to its relative low thermal stability, it should be easily removed by the normal refining techniques, leading even less doubts on its origin when first found in transformer oils. Nonetheless, DBDS has been appointed as one of the major causes of corrosive sulfur related faults³⁵ when it was discovered to be present in relevant concentration (notably higher than all the other organosulfur compounds) and very efficient in promoting Cu_xS deposition. In fact, extremely low concentrations of DBDS (1 mg kg⁻¹) have been shown to be able to cause detectable corrosion with copper sulfide deposition, under controlled laboratory conditions.^{42,43} Its efficiency in promoting this undesirable process inside oil-filled HV devices is far greater than other similar compounds shown in **Figure 10** like dihexyl sulfide (DHS), dihexyl disulfide (DHDS), dibenzyl sulfide (DBS) and dibenzyl sulfoxide (DBSO).⁴⁴ This is the reason why DBDS has been so intimately intertwined with all research work carried out on corrosive sulfur and remedial strategies.

Reinforcing what was already discussed, a worldwide investigation carried out in 2005/2006 demonstrated that DBDS was practically absent in all oils based on furfural

^a Further details will be provided in Section 1.5.1.

refining (not used anymore), in opposition to more recent hydro-refined products containing 100-200 mg kg⁻¹ of DBDS. This led the oil manufacturing industry to extensive reformulation of transformer oils over the following years to be DBDS-free,³⁶ in order to comply with standard specifications for the supply of unused mineral insulating oils (*i.e.* IEC 60296).¹⁵

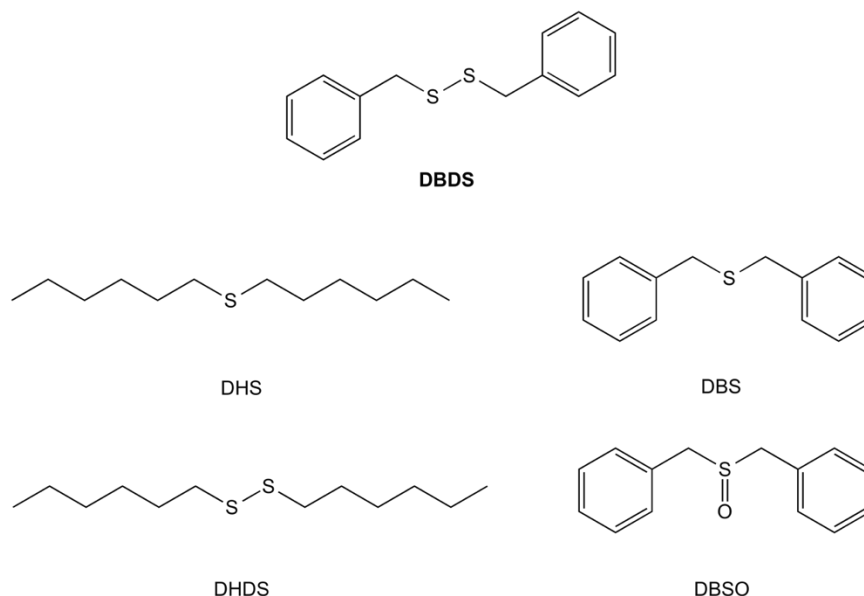


Figure 10 – Chemical structures of DBDS and some other corrosive compounds towards copper in transformer oil environment.

1.4.2 Mechanism of formation of copper sulfide in transformers and its consequences

The formation, migration and deposition of Cu_xS in a transformer in service is a delicate issue as this conductive compound is able to participate in the disruption of the insulating performance of solid and liquid dielectrics, creating the conditions for electrical and/or thermal faults to occur.

Regardless of the failure mechanism (discussed at the end of this section) in which copper sulfide undoubtedly takes part, a clear mechanistic explanation on the way in which it is generated is still debated by the scientific community. For this reason, a comprehensive state-of-the-art investigation into the understanding of the mechanism of the chemical processes involved in the formation of copper sulfide in transformer oil was recently carried out by CIGRE (Working Group A2.40: Copper sulphide long-term mitigation and risk assessment),³⁶ and will be discussed in more detail in Section 3.2.

Its main conclusion was that the most likely mechanistic explanation of this process involved copper dissolution in oil, followed by complexation, diffusion and adsorption of copper species on the insulating paper, where the actual generation of copper sulfide occurs. However, as a consequence of results detailed in this thesis (Chapter 3), a contact-based contribution to this mechanism was also included, taking into account the peculiar phenomena observed in the presence of both oxygen and close proximity of copper and paper insulation.⁴⁵ A comprehensive scheme of the postulated mechanism is shown in **Figure 11**,³⁶ reflecting the underlying complexity of the process investigated by many researchers.^{33,45–47}

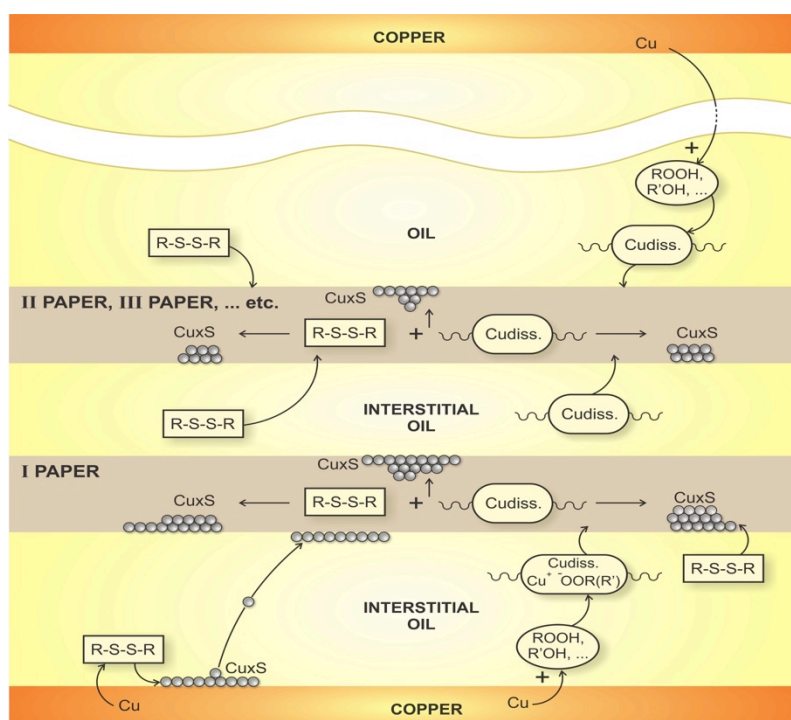


Figure 11 – Proposed mechanism for the formation, migration and deposition of Cu_xS on paper.³⁶ © 2015 CIGRE

It was also observed how the formation of Cu_xS does not always occur simultaneously on both metal and insulating paper, leaving the mechanism still to be expanded and adapted to fit each case (*i.e.* temperature, oil composition and refining grade, oxygen content, inhibitors, additives, *etc.*).³⁶ However, this rather complex mechanism has the advantage of taking into account both:

- The formation of copper sulfide at the copper surface together with its following detachment/migration, which would largely account for the observed contamination of paper layer in close proximity to the copper.

- The formation of complexes (possibly based on hydroperoxides)^{33,48} that enhance solubility of dissolved copper in oil, allowing its migration through the hydrocarbon medium to all transformer parts even though particles should be blocked as a consequence of the filtering action of multiple paper layers.

The presence of two cooperative but different parallel mechanisms was therefore a necessity, trying to explain the vast variety of real cases observed. In failed transformers in fact, it is quite frequent to find that the paper layers closer to the copper conductors show higher Cu_xS contamination. Nonetheless, it has also been reported (in very limited cases), the sole contamination of paper layers far away from the metal surface. Of course, a simpler explanation to this second observation is that copper sulfide found on paper layers far from the metal surface of the windings could be originated from corrosion of some of the many other bare copper components in the transformer tank. However, the magnitude of the phenomenon observed in such cases did not seem to agree with the hypothesized cause.

Generally, the Cu_xS deposition rate at constant temperature has been observed to be significantly dependent on the nature of the oil,⁴⁹ inversely proportional to the test duration and directly proportional to the concentration of DBDS in the oil.⁴² The effect of temperature was also extensively studied, especially while trying to define standard test conditions of accelerated ageing (see Section 1.5.1), and it was found to be directly related to the corrosion rate.^{38,42} Atmosphere, as will be discussed in Chapter 3,⁴⁵ also plays a crucial role in the deposition process as the absence of oxygen has been linked to incomplete development of the Cu_xS deposition and migration process in oil.^{50,51} Finally, the presence of other oil additives has been found to be critical in boosting the undesired deposition process, such as the antioxidant 2,6-di-*tert*-butyl-*p*-cresol (DBPC) that was observed to express a synergistic effect with DBDS in favouring Cu_xS deposition.^{52,53}

Although still controversial, the cause of faults was recently postulated to be triggered, ultimately, by the degradation of the thermal stability of the insulation system as a consequence of copper sulfide deposition.⁵⁴ In addition to thermal degradation of the insulation system, Cu_xS migration in the oil and its deposition in form of conductive particles on the insulating paper can lead to significant deterioration of the insulating performance of both materials. For example suspended copper species, or worse dissolved/complexed copper species generated by corrosion processes, were shown to significantly affect the insulating properties of insulating oils,^{55,56} as soon as their contribution to the total copper content could be isolated.⁵⁷ However, Cu_xS deposits in

particular were shown able to affect paper insulation performance quite substantially,^{38,42,58} as exemplified in **Table 1**.

Table 1 – Example of the effects on dissipation factor ($\tan\delta$) and resistivity of increasing Cu_xS contamination on insulating paper.³¹

Sample	$\tan(\delta)$	Resistivity ($\Omega \text{ m}^{-1}$)
Clean insulating paper	0.003	5×10^{12}
Insulating paper with low Cu_xS contamination	0.005	5×10^{10}
Insulating paper with high Cu_xS contamination	> 1	5×10^4

As the dissipation factor increases so does the temperature of the deposits under normal operating conditions, which can lead to the formation of hotspots on paper that in turn promote thermal degradation of the insulator. Many studies largely ignore this thermal contribution of copper sulfide deposits, blaming the failures only on the reduced breakdown strength of the contaminated solid/liquid insulation could lead to turn-to-turn breakdown (characterised by high short-circuit currents).³⁸ This could be described as a *pure electrical failure event*.

However, it has been objected that the presence of multiple layer of insulating paper should greatly reduce the likeability of a full electrical breakdown of the solid insulation in the presence of a relatively low turn-to-turn field stress.⁵⁴ Conversely, others are in favour of what could be described as a *thermo-electrical failure event*. In this case, a point is reached where the heat generated by these Cu_xS deposits on paper cannot efficiently dispersed by the material causing a thermal runaway and breakdown, as a consequence of thermal degradation of the solid insulation.⁵⁴ This is supported by extrapolations of the power generated in copper sulfide contaminated areas of insulating paper, estimated approximately 500 times greater than in uncontaminated ones.³⁸

Due to the many real failure cases investigated and their variety, it was not possible to unify all phenomena under only one mechanism. The sole common ground shared by all hypothesis is the observation that corrosive sulfur-related faults are commonly located at the top of the transformer winding, where the temperature is usually high enough to activate the corrosion reaction cascade^{59,60} or damage the corrosion inhibition layer.^{61–63}

1.5 Detection of corrosive sulfur species and mitigation strategies

Summarising what has been discussed, when a power transformer is in service it is possible to observe the formation of copper sulfide due to the reactions of some sulfur-containing organic corrosive compounds with the metal, which most likely acts as a heterogeneous catalyst. Copper sulfide can be formed at the copper surface in the oil due to interaction with dissolved copper species or on insulating paper and, when the contamination reaches a critical value, parts of the insulating system can experience a sudden collapse with catastrophic outcomes. In order to prevent this scenario, over the years engineering and chemistry have developed some detection and mitigation strategies that are detailed in the following subsections.

1.5.1 Detection of corrosive species in transformer oil

Being able to detect the presence of corrosive sulfur species by means of some sort of chemical analysis is understandably of crucial importance in real life applications. Even though manufacturers regularly test oils in order to provide insulating fluids that comply with the relevant standards, the system operator performs most of the monitoring on the quality of the oil in service. Standard corrosion tests normally involve a metal (Cu or Ag) strip that has to be immersed in the oil to be tested under a set of specified conditions (*e.g.* time, temperature, atmosphere, *etc.*). As for every standard, multiple procedures from different Standardising Bodies or versions/implementations of the same have existed over the years. Some examples are reported in **Table 2**.

Table 2 – Comparative list of experimental conditions in different standard corrosion tests.

Method	Metal	Oil/Metal/Paper	Temperature (°C)	Time (h)	O ₂
DIN51353	Ag	100 ml/1600 mm ² / -	100	18	Limited
ASTM D1275A	Cu	250 ml/300 mm ² / -	140	19	-
ASTM D1275B	Cu	250 ml/300 mm ² / -	150	48	-
IEC 62535*	Cu	15 ml/540 mm ² /540 mm ²	150	72	Limited

* Used in the experimental work detailed in this thesis.

As both DIN and ASTM standards were considered too subjective in their interpretation and not very reliable, since based on the visual comparison of the metal strip tested with a

standard reference colour chart, CIGRE developed the IEC 62535.³⁷ In this test a 30 mm copper strip is immersed in 15 ml of oil to be tested in a sealed vial then aged 72 hours at 150 °C (more details available in Section 2.3). This procedure, also known under the name of covered conductor deposition (CCD) test, allows both the evaluation of the intrinsic corrosivity and the tendency of the oil to deposit Cu_xS on paper insulation. None of the tests detailed in **Table 2** is specific for any chemical species and therefore they are aimed to assess corrosivity or copper sulfide deposition tendency in qualitative terms. More specific and quantitative analytical methodologies were developed to detect and monitor corrosive species of special interest in oil like DBDS,^{35,43,64–69} antioxidants (*e.g.* DBPC)^{65,66} and inhibitors (*e.g.* Irgamet[®]30 and Irgamet[®]39)⁶⁶ and they are summarised in the final report of CIGRE WG A2.40.³⁶

1.5.2 Oil reclamation and substitution

Whenever routine prevention strategies fail (*e.g.* load control or temperature management) more severe, expensive and time-consuming procedures might be needed to mitigate the effects of corrosion. Online oil reclamation, by means of heat treatment on activated clays, is one of the possibilities chosen more often in the UK. As it is unnecessary to turn the transformer off during the reclamation of the oil, money losses due to power outages that might derive from that are thus kept to a minimum. However, recent cases where reclaimed oil have developed silver corrosivity as a consequence of the regeneration process have been reported and much attention has been focussed on understanding the reasons of such occurrences.^{70–72}

On the other hand, oil substitution is to be considered a most extreme solution and it is generally used in very few circumstances, although considered by CIGRE the most robust procedure based on the long term stability of the properties of the insulating oil.³⁶ The cost of the volume of oil needed to fill the main tank and all additional components of the transformer (*i.e.* tens of thousands of litres) is often prohibitive.⁵⁸ Moreover, additional costs for mineral oil disposal under environmental waste management regulations and the necessity of putting the transformer offline make this approach the most expensive of all. As if economical reasons would not be enough, it has been reported of cases in which residual corrosiveness manifested (most likely due to incomplete rinsing of the active parts) even after the oil was changed. Effects of residual corrosiveness were usually weak, but varied with the amount of residual oil and concentration of corrosive sulfur compounds originally present.³⁶

1.5.3 Addition of copper-targeted additives

They are meant to decrease the catalytic effect and the total amount of dissolved copper in the insulating media in order to reduce oil oxidation and corrosion phenomena while keeping other oil properties (*e.g.* $\tan\delta$, acidity) as stable as possible.⁷³ These tasks can be accomplished by using molecular systems that could be classified in two main families according to their mechanism of action:⁷⁴ chelation agents and surface inhibitor agents.

1.5.3.1 Chelation agents

Perhaps better known in the field as *metal deactivators*, chelation agents inhibit the catalytic effect of Cu^{n+} ions in enhancing generation of free radicals and side-products from otherwise harmless molecular species. They work by strongly occupying the coordination sphere of free metal ions, hindering their reactivity. An example is reported in **Figure 12**.

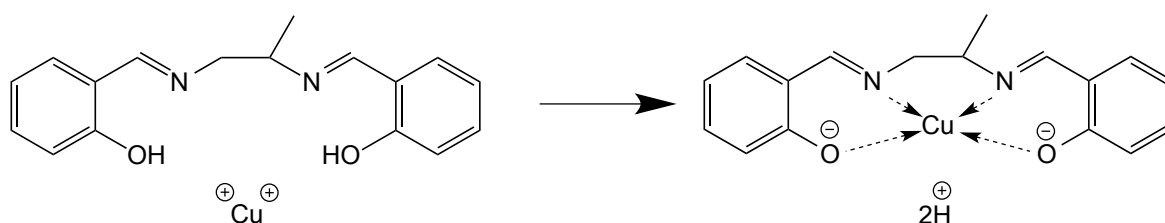


Figure 12 – *N,N*-Disalicylidene-1,2-propane diamine, chelation agent commonly used in fuels.⁷⁴

In transformer applications, the most commonly referred example of this class of additives is Irgamet[®] 30 (BASF), shown in **Figure 13**. This triazole derivative is believed to act through the loss of its aliphatic amine moiety and liberation of the heterocyclic ring, being then capable of forming complexes with copper ions dissolved in the oil.

1.5.3.2 Surface inhibitor agents

The addition of organic corrosion inhibitors, commonly referred to as *passivators*, often ensures the best cost-performance ratio and represents, to date, the most common chemical countermeasure against corrosion.³⁶ Already well known in lubricants and fuel industries since the late 1940s (first registered patent in 1947),⁷⁵ organic corrosion inhibitors have been applied in transformers since the 1970s. They are molecules expressing high affinity for metal ions or atoms, by definition bound to a surface, capable of retarding or delay attack of corrosive compounds.⁷³ In contrast with their inorganic counterparts that act through stable oxide film formation on the metal surface (normally triggered by the metal

itself, *e.g.* Fe or Al), organic inhibitors normally function through their absorption and self-organization to form a protective layer on the surface of the metal. This layer is believed to be both a physical barrier to reactive species and to act as copper dissolution retardant.⁷⁶

They work by inhibiting the reactivity of copper atoms on the metal surface exposed to the environment. In non-aqueous media, they are commonly heterocyclic compounds (O, N, S) with free electron pairs, often polycyclic and containing at least one aromatic ring and an alkyl groups to optimise their solubility. In this family, due to their high temperature stability and ability to form films on metal surfaces, benzotriazole (BTA) and its derivatives are widely used^{75,77} and a more detailed overview of their applications will be provided in Section 1.5.5. Substituents also play a role in the development of high inhibition efficiency. For example, 5-substituted electron-acceptor groups were shown to promote better interactions between BTA derivatives and copper.⁷⁷ BTA derivatives and triazoles, if opportunely engineered, have been shown to provide protection against corrosion even in the most harsh chemical environments such as strongly acidic media or elevated concentrations of aggressive ionic species such as sulfides.^{77,78}

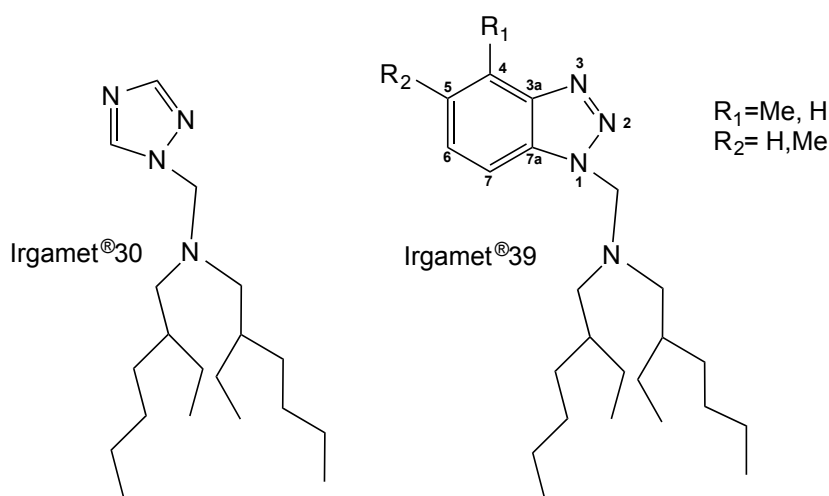


Figure 13 – Comparison between the chemical structures of the metal deactivator Irgamet®30 and the corrosion inhibitor Irgamet®39.

Nowadays the addition of Irgamet®39 (liquid, BASF, shown in **Figure 13**), is probably the most common strategy adopted to fight copper corrosion in oil-filled power equipment.³⁶ Irgamet®39 is normally mixed together with some base oil or a portion of oil from the transformer (if not bought already pre-diluted) and then added into the main tank up to the desired concentration. It is then the natural thermally-driven convection of the dielectric liquid that ensure it is brought right where it is needed, in the proximity of copper parts. This operation, like any other intervention on a transformer, needs planning and timing is

essential. In principle, if corrosion has already occurred to the copper inside the transformer there should be little benefit (if any) in the late addition of a metal inhibitor. Nonetheless, this practice was born and developed as a corrosive sulfur mitigation/containment countermeasure and therefore, by its own definition, added when corrosion is already manifested. Nonetheless an early addition is recommended by CIGRE A2.40.³⁶

Academic and industrial research on this particular application of metal inhibitors gained followers in the last 15 years when the first contributions describing the catalytic deactivation of copper by Irgamet[®]39 in insulating mineral oil were published.⁷³ As Irgamet[®]30, Irgamet[®]39 is believed to undergo a cleavage of the aliphatic amine to liberate tolyltriazole which, being surface-active, is capable of establishing chemical interactions with the surface of the copper conductors. It is believed that once added to the oil it can migrate towards copper components within the transformers and undergo a chemical reaction that allows it to become surface active and therefore express its corrosion inhibition properties. The hypothesised mechanism involves a retro-Mannich reaction,^{48,79} as shown in **Figure 14**. However, some details such as the destiny of the amine moiety after the reaction has taken place are still unknown.⁴⁸ Final experimental evidence of the cleavage of the molecule was nonetheless collected *via* mass spectrometry.⁶⁸

Application-wise, some limitations of this mitigation strategy deserve mention. BTA and its derivatives suffer the presence of hydroperoxide species, which are deemed capable of jeopardizing the integrity of the inhibition layer due to the generation of highly reactive radical species.^{48,80,81} The formation of such reactive species is held accountable for the observed depleted concentration of corrosion inhibitor in oil inside transformers in service, accelerated in the presence of oxygen, elevated temperatures, high operating loads and advanced oil oxidation.^{44,82,83}

In fact, it has been shown that if its concentration in the oil drops below the recommended 100 to about 30 mg kg⁻¹, the corrosiveness is basically restored⁸² even though more recent results detailed in Chapter 4 indicate much higher values. The addition of Irgamet[®]39 has also been linked to the undesired phenomenon known as passivator-induced stray gassing,⁸⁴ which is the evolution of H₂, CO and CO₂ from the oil in the first days/weeks after its addition to the insulating fluid. This normally does not cause abnormal changes of chemical or physical properties of oil like acidity, interfacial tension or dissipation factor (tanδ), but can interfere with routine condition monitoring tools such as dissolved gas analysis (DGA) results.³⁶ Finally, some researchers also attributed to the insulating paper

layers around copper a role as reservoirs of corrosion inhibitor,⁴⁸ which appeared able to interfere to some extent in the copper sulfide deposition process.³³ Evidence of this phenomenon was not observed in experiments detailed in the next chapter by means of X-ray photoelectron spectroscopy.⁸⁵

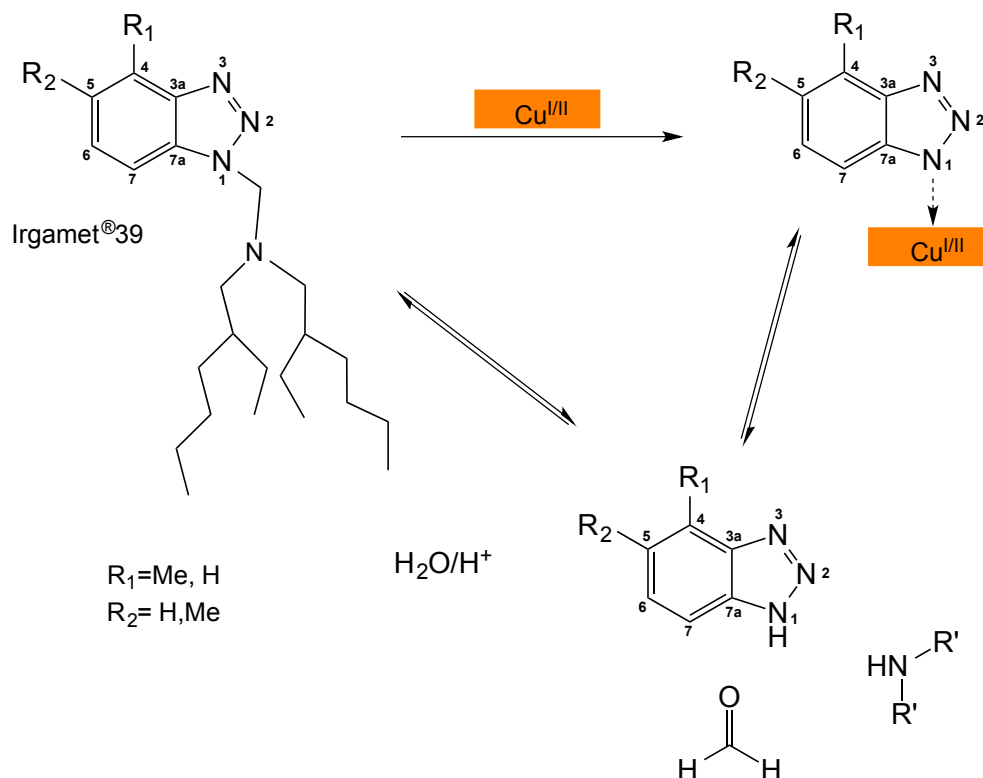


Figure 14 – Retro-Mannich reaction of Irgamet® 39 in oil to bind the copper surface.

1.5.4 Advantages and disadvantages of the proposed mitigation strategies

To conclude this section detailing the possible mitigation strategies when dealing with corrosive oils in power transformers, a short summary of their main advantages and disadvantages is reported in **Table 3**.

It can be observed that all approaches carry both advantages and disadvantages, which make the decision of the one to be undertaken a very complex task for the SO. Additionally, although a general strategy or preference could be present, most of the time an evaluation for each of the units needing care is necessary.

Table 3 – Main advantages (+) and disadvantages (–) of corrosive sulfur mitigation techniques according to CIGRE WG A2.40.³⁶

Mitigation strategy	+	–
Replacement of the oil	Restoration of properties, long-term performance	Cost, offline process, environmental impact
Oil regeneration	Restoration of properties, long-term performance, online process	Complexity, duration
Addition of metal inhibitor	Simple, fast, low cost, online process	No restoration of properties, poor stability over time

1.5.5 General consideration on benzotriazole derivatives as corrosion inhibitors

As for most metal corrosion inhibitors it was empirical observation, rather than chemistry knowledge of the mechanisms involved, which led to the use of certain corrosion inhibitors on various substrates and in a different media. Benzotriazole (BTA) and its derivatives have been known as effective copper corrosion inhibitors for almost 70 years now, but the protective layer they form on copper surfaces was not studied in depth for many years mostly due to instrumental limitations.

For the relevance of their applications in industry, most of the studies on corrosion inhibitors for copper and its alloys were historically carried out in aqueous media.^{77,86,87} However, with the development of the oils and lubricants industry more and more attention was dedicated to corrosion inhibition in hydrocarbon media.^{26,28,74,87–91} Starting from the late 40's, several attempts were carried out trying to chemically characterize the inhibition layer at least in aqueous solution but, until very powerful *in situ* surface sensitive techniques were developed, no molecular information was available.⁹²

In 1963 a pioneering work by Cotton *et al.* on the inhibiting effect of BTA on copper corrosion in water studied the effects of this corrosion inhibitor extensively, but did not investigate the mechanisms involved in depth. In 1967 an article by Melchiorre and Mills (Sun Oil Company) reported the formation of a layer of a BTA derivative on a copper surface used as a catalyst in an accelerated oxidation experiment: both catalytic effects and amount of copper in the insulators were observed to decrease.⁷³

In the early 1990s some further studies on the interaction of BTA derivatives with the metal surface have been carried out while studying aircraft fuel systems, already subject of study since the early 1950's for military purposes in jet aircraft.⁹³ BTA has been object of several studies during the following decade when Cao *et al.* carried out a comparative study of its inhibition effects on different metals using surface enhanced Raman spectroscopy (SERS) in which metal-organic complexes such as $[\text{Cu}^{\text{I}}(\text{BTA})_2]_n$ were observed for the first time, as shown in **Figure 15**.^{94,95}

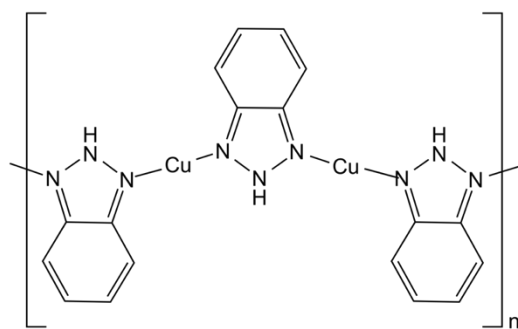


Figure 15 – Molecular structure of the surface $[\text{Cu}^{\text{I}}(\text{BTA})_2]_n$ complex.⁹⁴

More recently, thanks to the development of computer atomistic simulations, increasing theoretical knowledge has been built on the geometry and energy of BTA-copper interactions on clean single crystals^{96–103} and oxidised surfaces.^{104–106} However, experimental confirmation is still lacking and, as the structure of the surface assemblies should significantly vary depending on the medium in which corrosion inhibition takes place, this subject is still very controversial.⁸⁷

As already mentioned, surface sensitive analytical techniques play a crucial role in the experimental confirmation of predicted properties for these molecular systems and they have been used quite extensively in the past. In particular, X-ray photoelectron spectroscopy indeed contributed in the study of corrosion inhibitors, delivering a great deal of information on the transformation that the metal undergoes in terms of oxidation state variation.^{26,78,87,92,93,107–111} Conversely, SSIMS and its variations helped in the understanding of the process at the molecular level.^{93,112–114} These represent the main reason why a surface analytical chemistry approach was chosen for the work detailed the next chapters of this thesis, describing sulfide corrosion and inhibition of copper in a very specific non-aqueous medium: insulating mineral oils for HV applications.

2. Experimental methods

This chapter details the experimental methods, procedures and equipment used during the course of the project. After some general notes describing the fundamental pieces of equipment used, details on the preparation of mineral oil solutions and standards are provided. Subsequently, procedures to perform corrosion tests and prepare large paper samples contaminated with copper sulfide are described. Scanning electron microscopy (SEM), X-ray photoelectron spectroscopy (XPS) and static secondary ion mass spectrometry (SSIMS) are briefly discussed for the benefit of the wider readership, together with the relevant sample preparation and experimental parameters. Unless otherwise specified and justified in the following chapters, in the specific context of custom-designed experiments, no modifications of these procedures have been made.

2.1 General notes

All chemicals used were used as supplied and without any further purification or treatment. Solvents were used directly from the bottle and used without additional drying or purification. Commercial insulating transformer mineral oils were obtained through National Grid UK plc, with the only exception of Nynas Nytro Gemini X that was supplied directly by Nynas Naphthenics Ltd. A research sample batch of Irgamet[®]39 (1000 g) was kindly provided by BASF, free of charge. Oxygen-free high conductivity (OFHC) and engineering grade copper samples were obtained through National Grid UK plc or supplied by Siemens. Conventional SEM was carried out using a JEOL560, while environmental SEM was conducted using a Philips XL-30 instrument. All SEM was performed without preventive conductive coating of the samples. XPS was carried out using a Thermo Scientific Theta Probe at the National EPSRC XPS Users' Service (NEXUS) at Newcastle University, while SSIMS was performed with a ION-TOF ToFSIMS 4 instrument at Intertek Wilton laboratories. Sample preparation was carried out in the chemical preparation room (CPR) of the Tony Davies High Voltage Laboratory at the University of Southampton, together with thermal ageing under vacuum, air or inert atmosphere using digital fan and vacuum ovens. Due to the focus of the project on surface properties of the samples, handling was always performed with clean stainless steel tweezers and wearing clean nitrile gloves, minimising the exposure of bare metal surfaces to both unnecessary contact and atmosphere. Copper single crystals (100), (110) and (111) were obtained from

PI-KEM Ltd and stored, double-bagged and under vacuum, until used. They were polished and had a geometric surface area of 10 x 10 x 0.5 mm.

2.2 Oil sample and standard solutions

Oils used were Base Oil 20 (SPEXCertiPrep, Inc.), Nytro Gemini X, Nytro 10GBN (Nynas Naphthenics Ltd.) and HyVolt III (Ergon, Inc.). Gemini X and HyVolt III are classified, as per the relevant international standards,^{115,116} as inhibited oils while 10GBN as uninhibited and inherently corrosive.^b All oils were free from detectable dibenzyl disulfide (DBDS) and corrosion inhibitor Irgamet[®]39. All solutions were always prepared using dilutions by weight. Stock solutions of Irgamet[®]39 were prepared dissolving the solute in warm oil (temperature between 40 °C and 50 °C, controlled through a fitted thermocouple) with efficient mechanical stirring using a stirrer-hotplate to ensure thorough mixing of the oil, to obtain a clear solution. If the simulation of a corrosive environment was requested, DBDS (Sigma Aldrich, 98%) was added as solid to obtain the required concentration. To ensure thorough dissolution, the headspace vials underwent additional 60 minutes of mechanical shaking (oil initial temperature 60 ± 2 °C, then allowed to naturally cool down).

Whenever solid insulation was not required in the experiment to be carried out, any residual layer of insulating paper was removed immediately before the beginning of the experiment. Copper samples were then degreased three times with fresh cyclohexane (Fisher Scientific, $\geq 99\%$) before being placed in the oil.

Copper samples for copper inhibition studies were degreased with fresh cyclohexane (Fisher Scientific, $\geq 99\%$) three times and then placed in 20 ml headspace glass vials with 15 g of desired oil solution. After being sealed with butyl/PTFE septa, vials were placed in fan oven at 70 ± 2 °C for 24 hours to allow metal inhibition to occur. When removed from the oil, the samples were degreased by rinsing three times with fresh cyclohexane before being wrapped in clean aluminium foil to be shipped to either NEXUS or Intertek facilities.

^b In the new IEC 60296 (ed.4), the definition of “uninhibited” and “inhibited” transformer oils is linked to IEC 60666. If any of the antioxidant described in IEC 60666 are added, the oil should be declared as either “trace inhibited” or “inhibited”. In the previous edition of IEC 60296, inhibitors improving the oxidation stability of the transformer oil were strictly limited to those described in the IEC 60666 but now it is not anymore. As a consequence, oil manufacturers can now add any antioxidant additive not described in the IEC 60666 and declare the oil as “un-inhibited”, even though the transformer oil contains a synthetic antioxidant.

2.3 Corrosion tests

Corrosion tests performed were compliant to the standard procedure detailed in IEC 62535.³⁷ Non-overlapping-paper-insulated copper samples, suitable for transformer conductor windings, were cut to length of 30 mm ($\sim 100 \text{ mm}^2$) then unwrapped to leave only one layer of insulating paper, placed together with the appropriate mineral oil samples in 20 ml headspace glass vials fitted with PTFE-faced silicone septa and aged for 72 hours in fan oven at $150 \pm 2 \text{ }^\circ\text{C}$. In this test, the result is positive if the copper strip has one of the following colours: graphite grey, dark brown or black based on the ASTM copper strip corrosion standard D130.¹¹⁷ Variations of these standard conditions, both for corrosion tests or ageing purposes, will be detailed discussing specific experiments.

2.4 Large paper samples for copper sulfide deposition studies

A procedure to prepare large paper samples (9 cm by 9 cm) uniformly contaminated by copper sulfide was developed using DBDS in oil at high temperature, in collaboration with Dr Pedro S. Amaro.^{45,54} On such large contaminated paper samples multiple experimental techniques were applicable such as spectroscopic studies⁴⁵ and electrical breakdown measurements. The copper square sheets were highly ductile C106 engineering grade, phosphorous deoxidised, non-arsenical copper 99.85% pure. They had a nominal thickness of 0.5 mm and approximate geometric area of 1800 mm^2 . The metal surface was prepared by means of a polishing wheel and residuals were rinsed with fresh cyclohexane. The insulating paper used was standard electrical grade Kraft paper with a nominal thickness of 0.07 mm. The square copper plates had to be curved to a roughly constant radius, giving rise to concave and convex surfaces. Prior to the experiment, a new Kraft paper sheet was cut to a dimension of 90 mm by 180 mm, wrapped around the polished metal and secured using plastic zip ties to increase surface contact. The convex surface of the curved copper plate was therefore in closer contact with the inner side of insulating paper, as shown in **Figure 16**. The covered copper plates were then placed in Gemini X oil (453 g, 512 ml). Ageing experiments were performed in a crystallising dish (140 mm outer diameter by 73 mm high). DBDS (Sigma Aldrich, 98%, 906 mg) was used to simulate a corrosive environment and therefore allow copper sulfide deposition to take place across the surface of the paper sample in close contact with the copper. The final nominal concentration of DBDS was 2000 mg kg^{-1} . Depending on the type of atmosphere, nitrogen or air, a vacuum or fan oven was used respectively during the ageing period. For experiments conducted in nitrogen-enriched atmosphere, the vacuum oven was purged three times with fresh N_2 at

the beginning of the experiment. The optimised ageing condition was found to be 7 days at 140 °C.

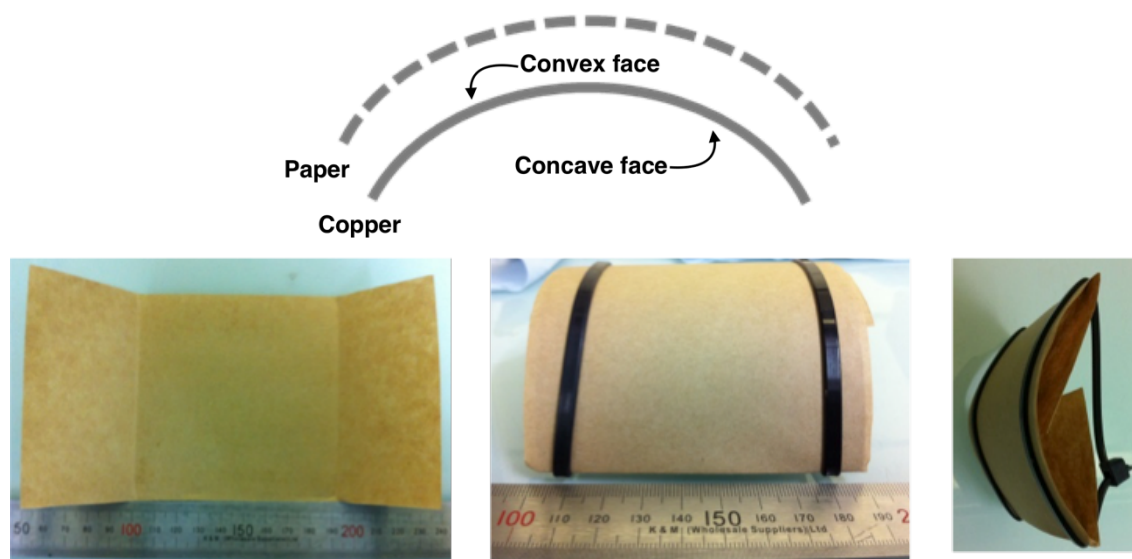


Figure 16 – Schematic representation (top) of a curved copper sample covered in insulating Kraft paper, and example of a wrapped copper plate (bottom)⁵⁴.

2.5 Scanning electron microscopy (SEM)

Scanning electron microscopy images were obtained using the facilities available in the department of Chemistry within the University of Southampton, as detailed in Section 2.1. Data collection and processing were performed entirely by the author.

2.5.1 Fundamental principles

A scanning electron microscope (SEM) is a reflector-type electron microscope that is able to generate images collecting signals arising from the surface of a sample as a consequence of its interactions with accelerated electrons. In a typical experiment a focussed electron beam is used to scan, in a raster pattern, the surface of a sample while a set of detector is fitted to collect all reflected signals generated. In fact, when electrons impact a solid sample (and to a certain extent penetrate it), several phenomena can be observed, as shown in **Figure 17**. Once scattered within a rather small and superficial region of the bulk sample, also called interaction volume, electrons interact with the atoms in the sample and with each other generating three main kinds of detectable responses:¹¹⁸

1. Secondary electrons (SE) → With energy < 50 eV and coming from the outermost regions of the interaction volume, they can deliver the best topographic information as they interact with fewer atoms before they escape the sample bulk.
2. Backscattered electrons (BSE) → With energy ≥ 50 eV, they are by all means energetically comparable with the primary scanning electron beam and coming from regions relatively far from the surface of the samples. They can deliver the best density contrast, since they are more influenced by neighbour atoms encountered in their escape path from the sample bulk, from which they manage to emerge thanks to their higher energy content, with respect to SE.
3. X-rays → Emerging from deep below the surface of the sample, X-rays are generated by the sample in the attempt of dissipating the excess of energy, provided by the incident primary electron beam, without the emission of any more particles. They are characterised by components (or lines) that are typical for each different atom and therefore can deliver the best elemental composition information.¹¹⁹

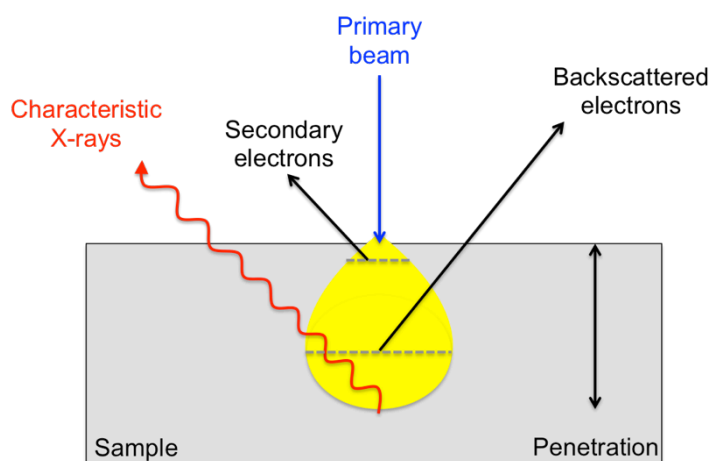


Figure 17 – Schematic representation of the interaction volume (in yellow) between the primary scanning electron beam and sample analysed *via* SEM, showing the main detectable signals and their origin within the solid bulk (in grey).

As shown in **Figure 17** and already mentioned, the SEM-detectable signals are generated in different regions of the *pear-shaped* interaction volume and all provide complimentary information to each other. This volume is directly proportional to the accelerating voltage of the electron beam and inversely proportional to the density of the sample (or atomic number of the atoms). These parameters also strongly affect the sampling depth of the technique.

Usually, characteristic X-rays emitted are widely used in energy-dispersive spectroscopy (EDX) detectors to obtain the elemental composition of a small area of the sample

analysed. Although in theory this kind of analysis can be fully quantitative when supported by specific reference materials, where available, it is often used without external standardisation and therefore referred to as a semi-quantitative analysis. This latter definition is the most appropriate for the work that is described in this thesis.

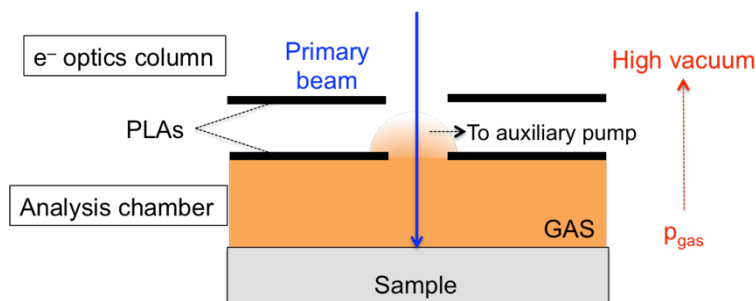


Figure 18 – Representation of differential pumping allowed by the presence of two pressure limiting apertures (PLAs).

A few words need to be said on the so-called *Environmental SEM* (ESEM). ESEM came into existence in the late 1980s^{120,121} and was originally devised to allow the observation of liquid water and live samples in electron microscopy, operating with a specimen chamber in which a positive gas pressure (usually H₂O) can be maintained, instead of the high vacuum of the traditional SEM. High vacuum though, still needs to be present in the electron optics column and this is achieved by means of differential pumping, exemplified in **Figure 18**.

Pressure limiting apertures (PLAs), small orifices that allow the entrance of primary electrons and back-diffusion of small quantities of gas (quickly removed by dedicated pumps), separate the specimen chamber from the optics thus keeping the pressure gradient between these roughly constant.¹²² The absence of vacuum is problematic, in traditional SEM, since gaseous species can dissipate the charges emitted by the sample, as a consequence of electron collisions with gas molecules while being accelerated towards the detector. In fact, after a relatively short distance, emitted electrons lose their energy ionising or exciting the gas molecules present. Assuming this process occurs as many times as the secondary electrons are emitted, the original signal from the sample can then be imagined to produce an avalanche of gaseous electron-ion pairs, shown schematically in **Figure 19**, which can be monitored through a special gaseous detection device (GDD).

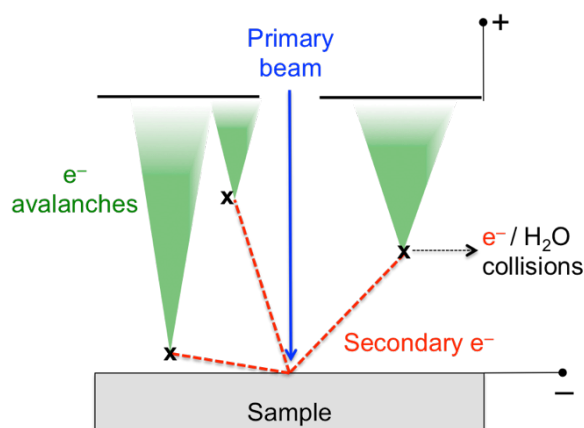


Figure 19 – Principle of gaseous detection showing how secondary electrons, interacting with the gas in the analysis chamber, are multiplied to an avalanche that is detected.

GDDs normally exploit scintillating materials, emitting photons of light when hit by charged particles or ionising radiations, coupled with photomultipliers that amplify the original avalanche signal generated in the environmental analysis chamber.¹²²

2.5.2 Sample preparation

Copper samples were analysed using the following settings: working distance (WD) = 10.000 mm, spot size parameter = 38-42, accelerating voltage = 10 kV, magnification = 500 x, 1000 x, 1500 x. Secondary electrons (SE) were collected in imaging mode when vacuum was established. EDX quantification was carried out using INCA microanalysis software suite (Oxford Instruments plc).

Paper samples were analysed in environmental mode ($p_{\text{H}_2\text{O}} = 93\text{-}133 \text{ Pa}$) using the following settings: working distance (WD) = 10.000 mm, spot size parameter = 38-42, accelerating voltage = 10 kV, magnification = 100 x, 500 x, 1000 x. Gaseous Secondary Electrons (GSE) were collected in the imaging mode and pressure limited aperture (PLA) was not necessary. Vacuum in the chamber was considered established after six flushes of water vapour, to replace all air in the analysis chamber. In case of samples showing lower contamination of conductive particles (*i.e.* copper sulfide), the spot size and the partial pressure of water were decreased to minimise charging. EDX quantification was carried out using the NSS Spectral Analysis software suite (Thermo Scientific).

Whenever necessary, images at different magnification were taken on a discontinued basis. Conductive carbon tape was used to secure the samples on the stage, as shown in **Figure 20**. No significant stigmatism was ever observed; contrast and brightness were adjusted manually where needed. EDX measurements were always performed at 500 x

magnification and each image was analysed on three rectangular selections covering all relevant features. Although all elements present were identified, only C (*K* line), S (*K* line) and Cu (*L* line) were quantified as a percentage. Carbon, being ubiquitous, was kept as a reference.



Figure 20 – Paper samples secured onto the ESEM sample holder.

2.6 X-ray photoelectron spectroscopy (XPS)

X-ray photoelectron spectra were obtained at the National EPSRC XPS Users' Service (NEXUS) at Newcastle University, an EPSRC Mid-Range Facility. Data collection was performed as part of several different projects submitted to the facility. Dr Anders Barlow and Dr Naoko Sano were responsible for data collection on copper and paper samples respectively.

2.6.1 Fundamental principles

X-ray photoelectron spectroscopy (XPS) is a surface sensitive ultra-high vacuum technique ($<10^{-7}$ Pa) suitable for investigation of the top 10 nm of the surface of a material. XPS can provide information such as empirical formula and, under appropriate conditions, even the chemical state of its atoms. It provides virtually unambiguous analysis and can be applied with equal facility throughout the periodic table, for $Z > 2$.¹²³ Kai Siegbahn, Nobel Prize for Physics in 1981, developed the technique of XPS in its modern form.¹²⁴ This technique is applied preferentially on solid samples, unless cooling precautions or other sophistications¹²⁵ are used, due to the extreme vacuum conditions within the analysis chamber that cause sudden evaporation even of low boiling point solids (*e.g.* Zn).

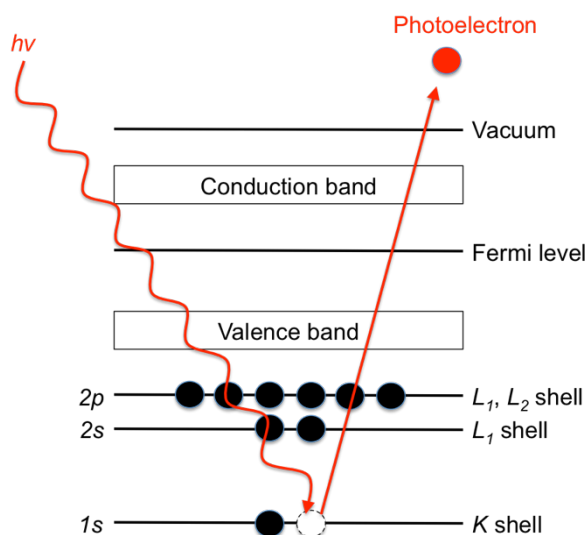


Figure 21 – Graphic representation of the photoelectric effect, first observed by Albert Einstein in 1905, schematically showing the extraction of a core electron in the *K* shell of a nucleus (and the generation of the paired inner core vacancy) by means of an electromagnetic radiation.

Figure 21 schematically represents what happens during a typical XPS experiment, when a highly mono-energetic collimated X-ray beam irradiates the surface of a sample. The sample, due to the photoelectric effect, emits photoelectrons with a characteristic kinetic energy.¹²⁶ In practice however the binding energy (B.E.), which is the force that keeps the electrons close to their nuclei, is often preferred over the kinetic energy (K.E.) when plotting, discussing and comparing results. The reason for this choice is that the position of any photoelectric peak is independent from the X-ray energy, once plotted using binding energy in abscissa, making the comparison easier between samples collected in different conditions. These two expressions of energy are related by the equation shown below:¹²⁷

$$E_{K.E.} = h\nu - E_{B.E.} - \Phi$$

Where $h\nu$ is the photon energy (that varies with the X-ray anode material used), $E_{K.E.}$ and $E_{B.E.}$ are the kinetic and binding energy of the ejected electron respectively, and Φ the work function of the material. Regardless of the abscissa convention used, quantifying the number of the electrons of all given energy values produces a spectrum, which intrinsically retains the information on the nature of the atom from which the electrons have been extracted. In fact, binding energies, in principle, are well defined for all the electronic states of the atoms.¹²⁷ Furthermore, the chemical environments of the atoms can influence the spectra promoting well-defined energy shifts of the photoelectric lines with respect to the B.E., similarly to the concept of chemical shifts in NMR spectroscopy.

It is also important to point out that not all lines visible in a spectrum are due to photoelectrons¹²⁷ and the most common causes of the arising of these other signals are three:

1. Auger electrons → Generated when an inner core vacancy left by the ejected photoelectron is filled by a more energetic electron from within the atom. The excess energy (*i.e.* difference between the states involved in the transition) can be dissipated by emitting an electron, characterised by the same energy content. As Auger electrons are produced by auto-ionization, changing the primary X-ray characteristic energy does not alter their position, unlike photoelectric lines.
2. X-ray satellite peaks → Usually caused by the imperfect achromacy of the radiation source, they are characterised by an offset from the primary spectral lines that is related to the resonance effects of the polychromatic radiation.
3. Plasmon peaks → Caused by resonant scattering of electrons by the surface of the material.

Despite its undoubted standards in qualitative analysis, XPS cannot be considered a fully quantitative technique. Indeed, the total number of electrons collected at a given energy is proportional to the number of those present on the surface of the sample however, single measurements reporting atomic concentrations are typically quoted with a 10% error. In other words, although XPS is a very precise analytical technique its accuracy cannot be assumed *a priori*.¹²⁷

For this reason, the direct comparison of peak area is not a recommended way to compare XPS spectra, for at least two different reasons: firstly, the efficiency of the photoelectric signal generation depends on the kinetic energy of the emitted electrons (which is related to the operating conditions of the instrument and its radiation source). Secondly, not all the electrons emitted by the samples are collected and quantified by the detector. The use of percentage atomic concentration is therefore very common, allowing the expression of intensity as a ratio between a certain signal and the total intensity of electrons during any single measurement. This approach was used in all XPS data processing reported in this thesis.

In theory, further complications of the ideal experiment described could arise when considering, for example, that there are multiple core electrons that can be emitted from a single atom as a consequence of the same X-ray irradiation. In reality these homonuclear

transitions do happen and they are designated quoting the principal (n) and azimuthal (l) quantum numbers after the element symbol transitions (e.g. C1s and C2p).

These transitions are also not equally likely to occur therefore, in practice, peaks with different area are observed, although generated by the same number of identical atoms. Data must therefore be scaled to ensure the same amount of each element is quantified, regardless of the transition chosen. To ensure precision when quantifying XPS spectra, Relative Sensitivity Factor (RSF) libraries are used to scale the measured peak areas so that all variations are representative of the amount of material in the sample surface. It has to be noted that tabulated RSF values are considered strictly valid for homogeneous materials only.¹²⁷

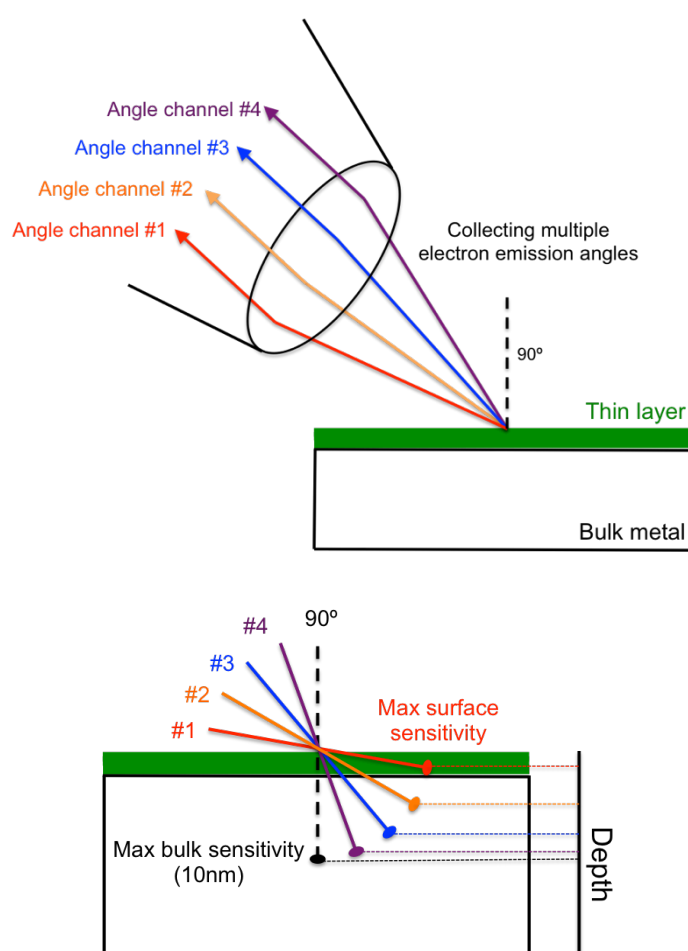


Figure 22 – Principles of simultaneous PARXPS collection (top) and representation of the angle-information relationship (bottom), picturing intuitively why angle channel #4 is less surface sensitive than angle channel #1.

In simplistic terms, the setup features a radiation source, a sample holder, an electron spectrometer and a detector.^{123,124} Some modifications are needed to the latter should depth profiling of the sample be required, when working in the so named parallel angle-resolved

(PARXPS) mode. This mode of operation, which allows the collection of photoelectrons emitted at different angles from the surface, is particularly useful when trying to investigate or model the composition of a sample as a function of its depth without damaging the sample, as shown in **Figure 22**.

Another peculiarity of PARXPS is the possibility of collecting different angular channels without the need, otherwise present in the past, of actually tilting the sample on the sample holder (hence the designation parallel). The arrangement of all the components enabled the instrument used in this study to collect data over a range of 60° with an angular resolution of approximately 1° . This is achieved specifically thanks to a 2D detector capable of dispersing electrons according to their kinetic energy in one direction while according to the angle at which they were emitted from the surface of the sample in the other, as exemplified in **Figure 23**.

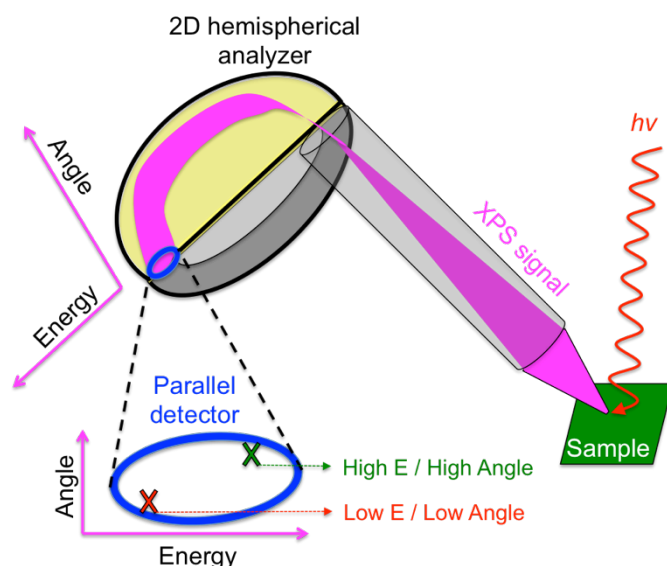


Figure 23 – Representation of a 2D analyser, capable of detecting multiple angle channels (*i.e.* X and X) thanks to its ability of dispersing the XPS signal as it was made of the two separate components, energy and emission angle.

The great advantage of the parallel mode of operation over more conventional approaches is that it can, to a certain extent, perform depth profiling measurements in a non-destructive fashion, meaning without surface etching/analysis reiteration, as shown schematically in **Figure 24**. Further theoretical detail is provided in Section 2.6.3. Generally, there are three main ways in which XPS data collected can be processed: generation of spectra, depth profiling or compositional imaging. To conclude, it is very important to reiterate that XPS is characterised by atomic selectivity only.

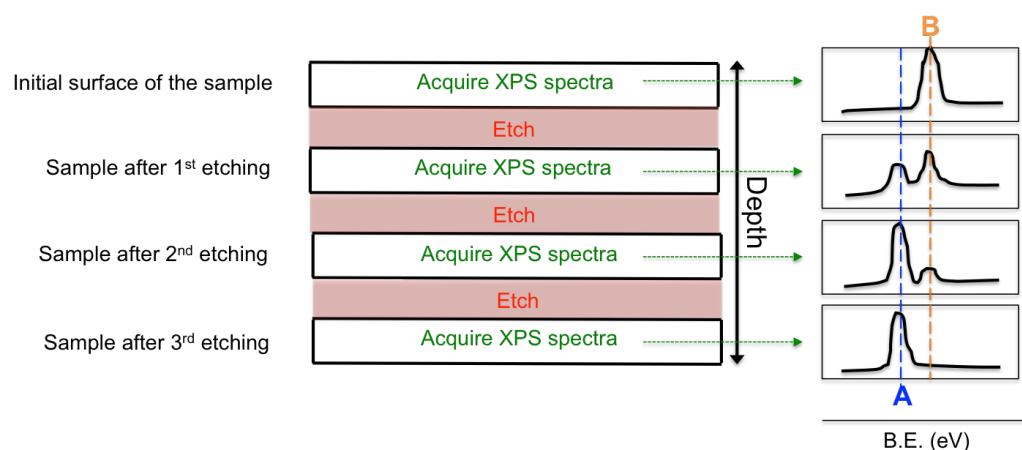


Figure 24 – Sketch of XPS destructive depth profiling through collection of discontinuous spectral series from each newly etched surface of a samples (*i.e.* enriched in **B** on the surface).

2.6.2 Sample preparation

Samples were prepared following the procedure described in Section 2.2 then mounted on the XPS sample holder and analysed, as shown in **Figure 25** and more in detail in Appendix B2.

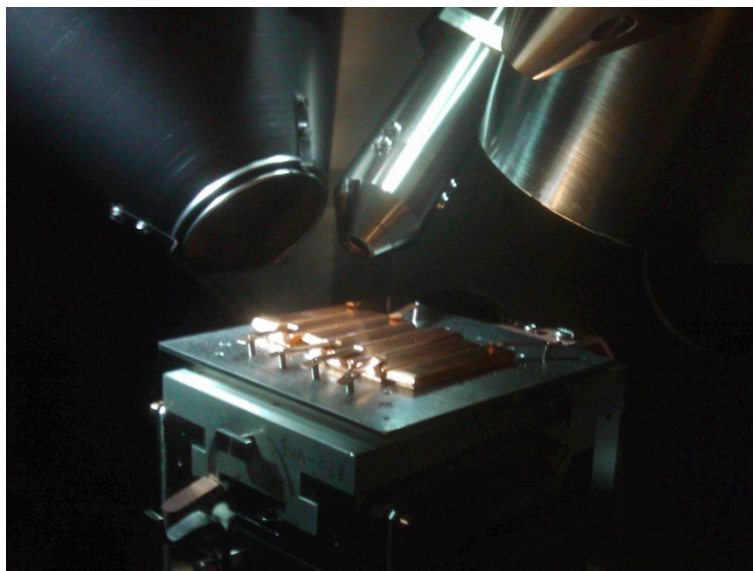


Figure 25 –Side view of some samples loaded on the Theta Probe XPS sample holder under the guns and detectors in the analysis chamber.

2.6.3 Experimental parameters

XPS spectra were collected using the XPS Theta Probe shown in **Figure 26** (Thermo Scientific, East Grinstead, UK) equipped with a monochromatic Al K α X-ray source of 1486.6 eV operated at 100 W.

The system maintains a base pressure of $< 10^{-9}$ mbar, and typical analysis pressures for the copper samples were in the 10^{-9} mbar range. Due to the high conductivity of the copper substrates no charge compensation was found to be necessary for this analysis. Paper samples, on the other hand, required the use of a charge compensation device, here a flood gun. This accessory compensates for the depletion of electrons of the sample, which occurs due to the photoelectric emission, providing a steady flow of low energy electrons towards the sample. In the absence of such a technological solution, already investigated in the late 1980s,¹²⁸ the electron depletion of the sample generates a retarding electric field (as a consequence of the induced positive polarity of the sample) that is able to modify the kinetic energy of the emitted electrons, jeopardising any measurements. In the case of conductive samples, electrically connected with the metal sample holder, charge compensation is not necessary because charge balance is easily restored; in fact, the excess bulk metal electrons naturally counterbalances electron emission from the sample.

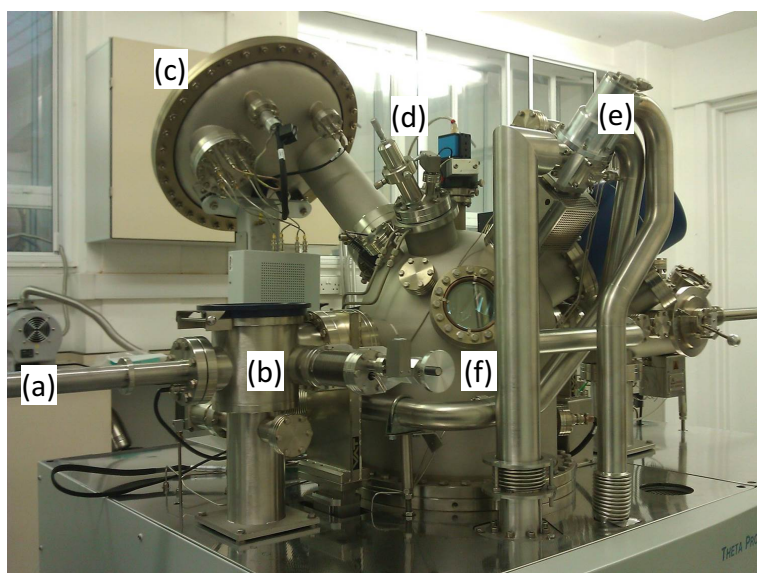


Figure 26 – Overview of the XPS equipment used at NEXUS showing the loading rod (a), pre-treatment chamber (b), hemispheric analyser (c), charge compensation flood gun (d), X-ray source (e) and analysis chamber (f).

Survey spectra of copper samples, (3 sweeps) from 1350 to -15 eV (Binding Energy, B.E.) were collected with pass energy of 200 eV and step size of 1 eV. High-resolution scans

were made (10 sweeps) for quantification on C1s, O1s, N1s and Cu2p peaks with pass energy of 40 eV and step size of 0.1 eV. Survey spectra of paper samples, (3 sweeps) from 1350 to -10 eV (B.E.) were collected with pass energy of 200 eV and step size of 1 eV.

High-resolution scans were made (10 sweeps) for quantification on C1s, S2p and Cu2p peaks with pass energy of 40 eV and step size of 0.1 eV. Integration was always performed using CasaXPS and a Shirley background was used. Finally, as already mentioned, a well-established normalization technique has been used to make data sets comparable when integration results were expressed in CPS eV (Counts Per Second eV). Quantifying nitrogen for example, the area of the N1s peak was divided by the sum of the area of all other major signals (here C1s, O1s, S2p and Cu2p) in the same spectrum. The ordinates in the graphs reporting XPS results in the following chapters reflect this normalization expressing an area ratio, dimensionless.⁶²

The depth penetration of this technique is estimated to be in the range of 10–20 nm.¹²⁷ To extract the film thickness information, in corrosion inhibition studies, all high-resolution spectra were collected in Parallel Angle-Resolved XPS (PARXPS) mode, using 16 angular channels. Electrons were detected from angles between 20° and 80° from the surface normal, in steps of 3.75 degrees. Overlayer thickness was calculated using the Single Overlayer Thickness Calculator in the Avantage Software (Thermo Scientific).

This process uses PARXPS data and the Lambert-Beer law to estimate the thickness of the overlayer based on the variation in the attenuation of the substrate signal with respect to the electron emission angle. The substrate signal was chosen to be the Cu2p peak area, while the overlayer signal was taken as either the C1s or N1s peak area, for reasons that will be clarified in the discussion of the results. The overlayer density was taken to be that of tolyltriazole (1.24 g cm^{-3}) while the substrate was taken as the density of copper metal (8.96 g cm^{-3}). Asymmetry factors for the C1s, N1s and Cu2p shells were calculated using the known kinetic energy of the electron shells and the resulting attenuation lengths were calculated using the Tanuma-Powell-Penn-2M (TPP2M) formula described in detail below, both performed within the software.^c

^c Asymmetry parameters take into account the anisotropy of the photoemission process, resulting from the different shapes of the different orbitals (or more precisely their wavefunctions) and how achromatic X-rays interact with them at different angles. The Avantage Single Overlayer Thickness Calculator software performs this operation automatically.

For the benefit of the reader, a brief discussion on the physical nature of the terms and the broad scopes of the TPP2M equation is reported, although purposely not fully addressing its underlying complexity that is beyond the purpose of this work.

TPP2M is a predictive equation that helps quantify the inelastic mean free path (IMFP) of a photoelectron travelling through an organic material. The IMFP is defined as the distance that an electron can travel through a solid before undergoing an inelastic scattering event.¹²⁹ In molecular collision theory, an inelastic scattering event is defined by IUPAC as a process characterised by a transfer of energy among degrees of freedom without a chemical reaction occurring, where the kinetic energy of the incident particle is not conserved.²⁰ TPP2M can be expressed in the form:

$$\lambda = \frac{E}{E_p^2 [\beta \ln(\gamma E) - (C/E) - (D/E^2)]}$$

$$\beta = -0.10 - 0.944(E_p^2 + E_g^2)^{-1/2} + 0.069\rho^{0.1}$$

$$\gamma = 0.191\rho^{-1/2}$$

$$C = 1.97 - 0.91U$$

$$D = 53.4 - 20.8U$$

$$U = \frac{N_v\rho}{M} = \frac{E_p^2}{829.4}$$

Where λ is the IMFP (Å), E is the electron energy (eV) and γ, β, C, D are a complex series of material-related parameters that take into account the atomic weight, density, valence electrons and the band gap energy. E_p represents the free electron plasmon/delocalised electron at the interface energy (eV), N_v the number of valence electron per atom, ρ the density (g cm⁻³) and M the atomic/molecular weight (g mol⁻¹).¹³⁰

The IMFP can indeed be determined experimentally for metals and inorganic materials but, due to the intrinsic difficulties in analysing organic materials that are usually electrical insulators, such predictive equations provide a valuable alternative for its estimation. Simplifications of this equation exist and, ignoring elastic interactions, provide the related value of the effective attenuation length (EAL), by definition smaller than the IMFP.¹²⁹

2.6.4 XPS signal assignments

XPS spectra collected from copper samples shared the same photoelectric signals, varying only in intensity in accordance with the experimental conditions to which the samples were subjected. The major signals of this survey, common to all samples discussed in this work, identified as Cu2p, O1s, N1s, C1s, S2p and Si2p are also shown in **Figure 27**, together with their high resolution scans with relative peak fitting using Gaussian components.

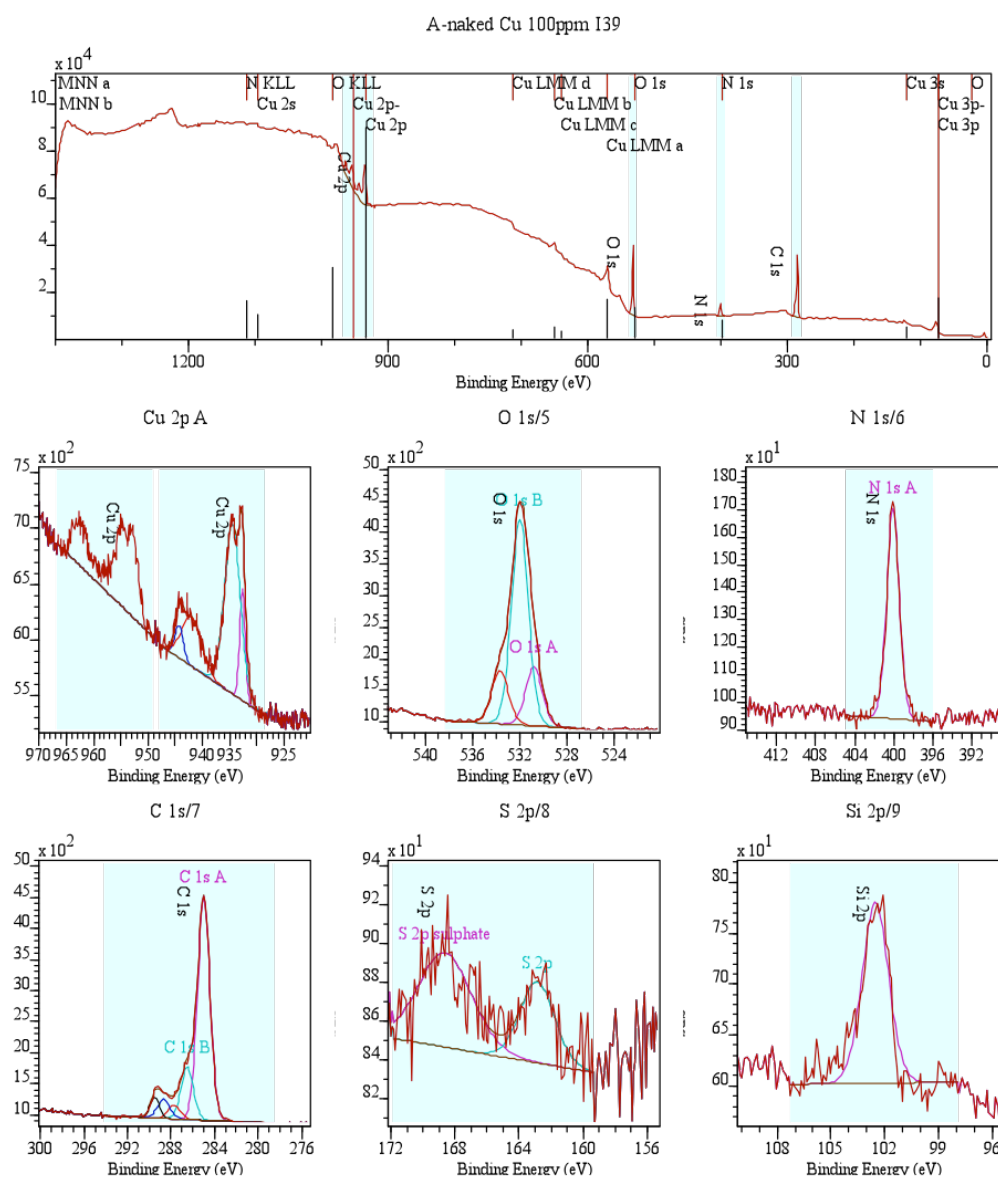


Figure 27 – Example of a survey spectra (top) and high-resolution photoelectric peaks for Cu2p, O1s, N1s, C1s, S2p and Si2p on a copper sample treated with 100 mg kg⁻¹ of Irgamet[®] 39 in mineral oil, as they appear in the data processing software CasaXPS.

Table 4 – Tabulated values of binding energy for elements relevant to this study in specific chemical environments.

Element	Chemical environment	Electronic transition	Binding energy (eV)
C	Graphite, sp ³	1s	284.8
N	Pyridine	1s	400.0
O	SiO ₂	1s	532.9
S	Cu ₂ S	2p	161.7
Cu	Metallic Cu	2p 1/2	952.5
	CuO	2p 1/2	953.2

Data retrieved from NIST X-ray Photoelectron Spectroscopy Database, Version 4.1 (National Institute of Standards and Technology, Gaithersburg, 2012); <http://srdata.nist.gov/xps/>

It has to be clarified that silicon was only sometimes tentatively detectable as an impurity. Traces of sulfur, however, were common on samples treated in Nytro 10GBN, which is inherently corrosive. For the benefit of the reader, tabulated values of elements of interest in selected environments are provided in **Table 4**.

2.7 Secondary ion mass spectrometry (SIMS)

Secondary ion mass spectra were obtained at Intertek Wilton. Data collection was performed as part of different projects submitted to the facility. Dr Ian W. Fletcher was responsible for spectra collection and initial data processing.

2.7.1 Fundamental principles

SIMS is a particular kind of mass spectrometry that allows the study of a material both on the atomic and the molecular level. In a typical SIMS experiment a focused ion beam, rather than an electromagnetic one (*e.g.* XPS), is directed on the sample causing sputtering and desorption of secondary ions from its surface, as a consequence of elastic and inelastic scattering interactions. Secondary ions that are generated, only around 5% of the total sputter yield,¹³¹ are then extracted into a mass analyser, which finally yields a mass spectrum. SIMS is characterised by molecular selectivity and the depth penetration of this technique is estimated, in organic materials such as polymers to be around 1 nm in static mode.¹³¹ A schematic representation of the physical process is shown in **Figure 28**.

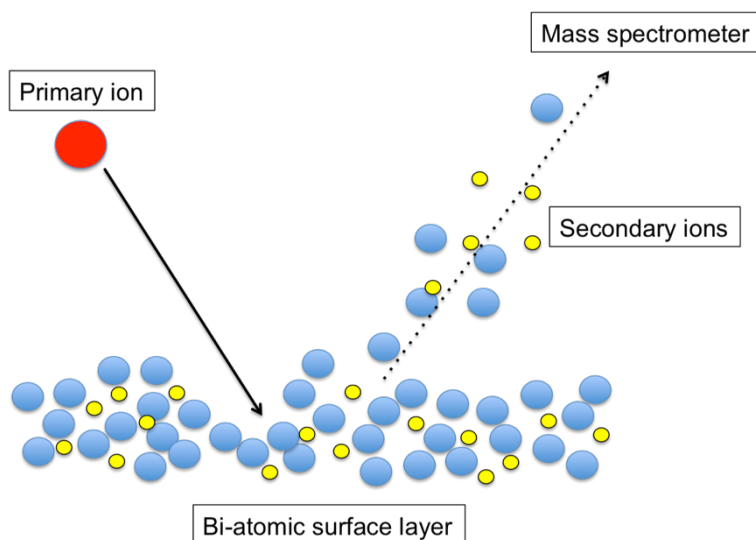


Figure 28 – Graphic representation of the secondary ion signal generation from a bi-component surface hit by a primary ion beam during a SIMS experiment.

Additionally, focusing and rastering the ion beam on the sample it is possible to generate mass spectrometric images, monitoring the secondary ion intensity for given m/z species as a function of the position on the sample.¹³² However, in the work detailed in this thesis, a variation from more traditionally SIMS ion beams has been used, which exploits clusters, conglomerates of atoms that do not yet exhibit physical properties of condensed matter.¹³³ In fact, while in conventional experiments atomic projectiles are generally used (Ga^+ , Cs^+ , Ar^+), it is also possible to employ ion clusters such as, but not limited to:^{133,134}

- Fullerene-type ions (C_{60}^+)
- Heavy metal trimers and pentamers (Au_3^+ , Bi_3^+ , Bi_5^+ , SF_5^+)
- Massive Ar_n^+ gas clusters ($n > 500$)

The reason for this can be explained by the equation below¹³² where E_c is the final energy of one of the constituent atoms of the cluster after impacting the surface, E_0 that of the cluster before the impact, M_c the mass of the constituent and M_t the total mass of the cluster:

$$E_c = E_0 \left(\frac{M_c}{M_t} \right)$$

When a cluster impacts the surface of the sample and breaks apart, each of the constituent atoms retains only a fraction of the original energy (*i.e.* E_c), proportional to its mass ratio with the cluster. Since the penetration depth of an ion is proportional to its impact energy, when cluster ions are used less penetration and damage of the surface can be achieved.

It is important to understand that the important parameter to be considered is not the total energy or mass of the cluster but rather energy and momentum of the constituent atom. Sputtering and desorption of secondary ions from the surface of the sample depend on how efficiently energy is transferred from the beam to the material after the impact, and according to elementary physics that is strongly affected by the masses of colliding particles. Without indulging into excessive detail, the more similar the masses the more efficient the energy transfer is going to be, therefore a highly energetic cluster is theoretically preferred over an equally energetic atomic projectile.^{133,135}

In this study Bi_3^{2+} cluster ions were used. They were generated by means of a liquid metal ion gun (LMIG), which is a type of source that is considered ideal for imaging applications thanks to its high spatial resolution,¹³⁶ exemplified in **Figure 29**. It consists of a needle or capillary covered or filled with bismuth heated above its melting point (271.4 °C) to which an electric potential is applied. The combination of this applied electric field and the liquid metal surface tension leads to the formation of a protrusion called the Taylor cone, due to space charge, from which ions are emitted and accelerated (from the very same field that has generated them). The equilibrium and mass/charge balance is guaranteed by the presence of the reservoir of liquid metal.¹³⁷

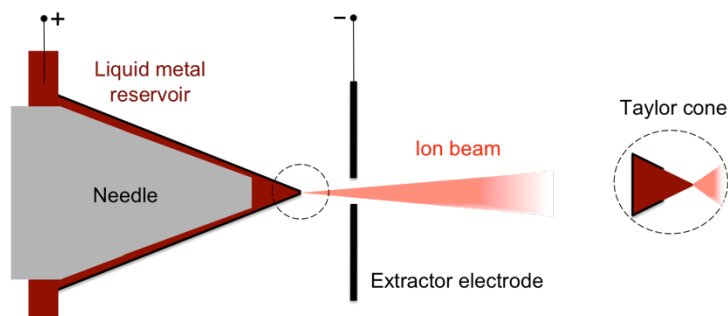


Figure 29 – Sketch of the cross-section of a liquid metal ion gun (left) and detail of the space-charge-induced protrusion known as the Taylor cone (right).

The analyser used in this work was a Time of Flight (ToF). ToF analysers are capable of simultaneously detecting all secondary ions of a selected polarity with excellent mass resolution^d in tandem with very low current pulsed (or *bunched*) ion beam, which minimizes chemical damage of soft materials.¹³²

^d This would be the principal drawback of another common analyser, the quadrupole (QP), attributed to its inability to resolve more than one peak per nominal mass (low unit mass resolution). QPs use oscillatory electromagnetic fields to promote a stable exit trajectory to the detector only for species with selected m/z values.

While XPS needs to be equipped with some etching devices, SIMS can be a destructive depth profiling technique on its own, when operated in *dynamic* mode.^e However, the operational mode used in the applications described in the following sections is named *static* (SSIMS). It uses a low energy primary ion beam, allowing a more delicate sputtering of the surface of the sample that can be considered substantially unperturbed for the duration of the experiment,¹³¹ since the accumulated ion dose during spectral acquisition is kept sufficiently low (never more than 10^{13} ions cm^{-2}).¹³⁸ In fact, it can be safely assumed that during the time scale of the experiment, very much less than 1% of the top surface layer of atoms or molecules receive an ion impact.¹³⁸ This is ideal when trying to collect information on organic materials on the surface, such as an organic inhibition layer on copper, which is normally insulating, energy-labile and therefore subject to either surface charging or decomposition. Moreover, the low ion dose to which the sample is subject minimizes charging effects and fragmentation of organic molecules, which usually can be more easily observed. However, in SSIMS analysis of organic overlayers on metal substrates, clusters do not necessarily provide a benefit in preserving organic deprotonated molecules with respect to more traditional monoatomic beams, as reported experimentally and through simulations.¹³³ Some drawbacks and limitation of clusters were observed in some cases such as increased cross-linking damage processes with the increase of atomicity, but generally it is now an established practice to use these sources in the SSIMS analysis of soft samples.^{134,135} However, even though traditional ionic projectile sources were not investigated for the specific system that will be discussed in the following chapters, none of these limitations of cluster beam technology were ever observed.

2.7.2 Sample preparation

Samples were prepared following the procedure described in Section 2.2. For measurements at constant temperature and imaging, the copper samples were attached to a suitable sample holder using clean metal clips, as shown in **Figure 30** (left). The samples for analysis were handled using clean stainless steel tweezers at all times.

^e Typically uses analysers that can cope well with high operating currents and continuous primary beams such as QPs or Magnetic Sectors. This latter uses a magnetic field to physically separate, thanks to their momentum, the trajectories of species with different m/z in conjunction with an electrostatic field that removes chromatic aberrations.

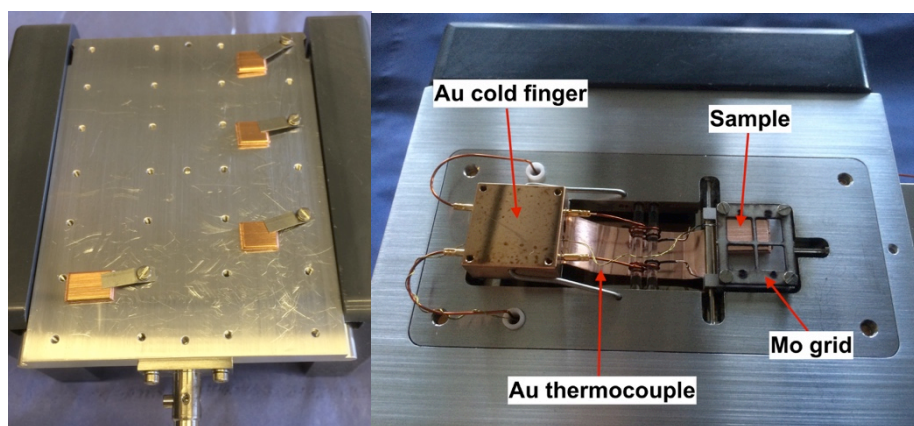


Figure 30 – Copper samples, kept in place by metal clips, on the SSIMS room temperature sample holder (left) and details of the variable temperature sample holder.

For measurements at variable temperature, the copper samples were mounted individually on to a main chamber heating/cooling sample holder under a clean Mo grid, as shown in **Figure 30** (right), featuring a Au cold finger target for temperature control. The fitted Au thermocouple used to measure the sample temperature was trapped between the sample surface and the underside of the molybdenum grid.

The preparation of the microwire sample described in Section 5.3.3.2 was more complex. A portion of polyurethane-insulated copper microwire (99.99%, Ø 25 µm, 5 µm insulation thickness, Goodfellow Cambridge Ltd.) was sealed into a glass pipette by means of a glowing resistor wire. This produced a bubble-free glass embedded copper wire that was then polished, using abrasive paper and paste, down to 1 µm and sonicated in deionized water for 5 minutes to obtain a flat mirror-finished copper surface. Two of these samples were prepared: one sample was kept as reference while the other underwent multiple surface breakdowns. The pipettes were then cut down to a total length of 15 mm and were treated in Gemini X in the presence of 100 mg kg⁻¹ of Irgamet[®]39 following the procedure detailed in Section 2.2.

The copper wire was earthed and kept standing by means of some Sn-alloy soldering wire. Although the setup appeared to be a needle-to-plane arrangement, due to the size of the cross-section of the copper wire in reality the field arrangement had to be considered more like a needle-to-needle setup. Once the needle was positioned over the sample, a drop of Gemini X oil was deposited between the two allowing surface tension only to keep it in place, in order to perform the breakdown in the presence of the oil while simultaneously ensuring a perfect alignment (otherwise impossible due to optical aberrations). The measured voltage breakdown was approximately 19 kV ± 2kV, with a voltage ramp of 50

V/s and electrodes at 1 mm distance. The breakdown was repeated a few times to increase the chances of identifying the breakdown site in the copper wire cross-section surface using SSIMS. A graphical summary of the experiment is shown in **Figure 31**.

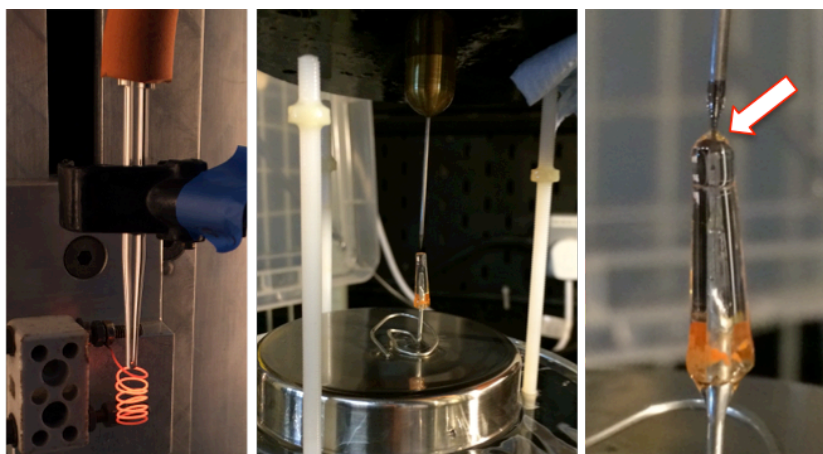


Figure 31 – Graphical summary of the steps to obtain a copper sample subject to surface breakdown: glass pipette containing copper wire, under suction, melting using a glowing resistor wire (left); overview of the setup used (middle); detail of the alignment between sample and needle, connected by a drop of Gemini X oil (arrow on the right).

2.7.3 Experimental parameters

SSIMS spectra were collected with the ION-TOF ToFSIMS 4 instrument shown in **Figure 32**.

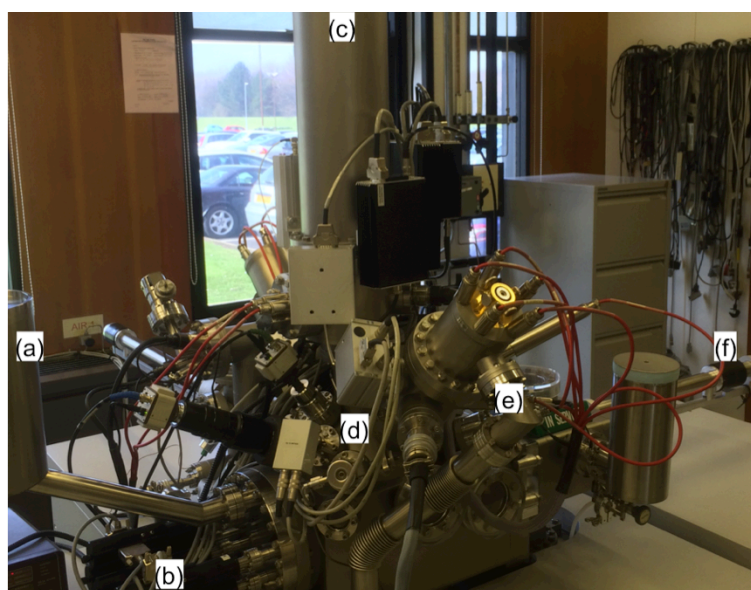


Figure 32 – Overview of the SIMS equipment used at Intertek Wilton showing details of liquid N₂ reservoir for sample holder cooling (a), sample holder heating supply (b), ToF analyser (c), main analysis chamber (d), Bi₂³⁺ ion source (e) and loading rod (f).

2.7.3.1 Constant temperature and imaging SSIMS

Positive and negative ion spectra were recorded with 200 μm x 200 μm analysis areas. The total ion dose for each acquisition was $\approx 5 \times 10^{11}$ ions cm^{-2} . This was within the accepted ion dose limit for static SIMS of 5×10^{12} ions cm^{-2} . The Bi_3^{2+} ion source was used in all cases reported. Data were recorded from the samples using a primary cluster beam operating in bunched mode (nanosecond length pulses) to allow high mass resolution to be realised without reducing primary currents even further. The spatial resolution achieved in the images was $\approx 4 \mu\text{m}$ and the mass resolution, $m/\Delta m$, was around 5000. Reference spectra for the liquid samples were collected by analysing the pure liquid spread as a thin layer on clean PET film.

2.7.3.2 Ion imaging

Ion images reflect, in each pixel, the secondary ion intensity of a selected species. Each of the composed images is generated by superposition of the three ion channels collected in red-green-blue mode (RGB) representing $^{63}\text{Cu}^-$, $[\text{C}_7\text{H}_6\text{N}_3]^-$ and S^- species respectively. Each one of the separate feeds shows the intensity, scaled from 0 to 225 for display purposes, of the relative species. When a specific pixel is shared between multiple feeds the resulting colour is the addition of the three components, scaled by their respective intensities. When mixed overlaid contributions are present on one pixel because 2 or 3 of the species are detected simultaneously, the resulting colour represents the addition of the 3 components once scaled by their respective intensities. The intensity parameter is scaled linearly from 0 to 255 for display purposes. For example, if all 3 species chosen showed maximum signal they would all have intensity of 255 and would combine to give a white pixel. Hence, whichever species shows the most intensity tends to dominate the final colour.

2.7.3.3 Variable temperature SSIMS

For the thermal desorption work, the sample was stabilised at the starting temperature of 27 $^\circ\text{C}$ (300 K) for approximately 10 minutes. The temperature-programmed desorption (TPD) SSIMS profile acquisition was started and the temperature ramp (5 K min^{-1}) began after 20 s acquisition time. The data collection was stopped manually at 400 $^\circ\text{C}$ (673K). The main chamber pressure during analysis was less than $\approx 5 \times 10^{-7}$ mbar from a base pressure of $\approx 5 \times 10^{-9}$ mbar. Negative ion thermal desorption profiles, images and spectra were recorded from fresh areas of the samples using a 500 μm x 500 μm analysis area in

each case. The total ion dose for each profile was $\approx 2 \times 10^{12}$ ions cm^{-2} , which was within the accepted ion dose limit for static SIMS of 5×10^{12} ions cm^{-2} . Data were recorded from the samples using a primary cluster beam operating in bunched mode. The spatial resolution achieved in the images was $\approx 4 \mu\text{m}$ and the mass resolution, $m/\Delta m$, was around 5000. The profiles and images were recorded using the 'raw' data stream mode (RAW). Data sets for intensity in the profiles were smoothed using a 5 points FFT (Fast Fourier Transformation) in Origin 8.6, to minimise noise at low intensity and their scale was plotted as linear.

2.7.3.4 Energy of desorption calculations

Data were reprocessed in order to plot intensity vs. time for the representative ion at m/z 132, in the form of a TPD-SSIMS profile. Data were exported from the instrument 'IonSpec' software in ASCII format and then processed using Excel2000 and Origin 9.1. 5 points FFT and adjacent averaging smoothing (100 points) was used to reduce the data noise at low temperature and the first derivative plots were obtained. The temperature at maximum desorption rate (T_p), the minimum of the second first derivative plot, was then used to calculate the energy of desorption into vacuum (E_{des}) assuming a first order process and absence of intramolecular interactions and re-adsorption. The equation used is shown below.¹³⁹

$$E_{des} = T_p R \left\{ \ln \left[\frac{\nu_i T_p}{B} \right] - 3.64 \right\}$$

Where R is the molar gas constant ($8.314 \text{ J K}^{-1} \text{ mol}^{-1}$), B is the heating rate ($5 \text{ K min}^{-1} = 0.08333 \text{ K s}^{-1}$) and ν_i is the estimated rate constant (10^{13} s^{-1}).

2.7.4 SSIMS ion mass assignments

During all the experiments performed, many ions were observed and monitored although some of them were, understandably, more relevant to the study of inhibition of copper samples treated in insulating oil with Irgamet[®]39. Those pivotal to the discussion carried out in the following chapters are reported in **Table 5** and **Table 6**.

Table 5 – Negative ion secondary ion assignments for signals detected on oil samples.

<i>m/z</i>	Ionic formula
68	C ₂ H ₂ N ₃ [−]
132	C ₇ H ₆ N ₃ [−]

Table 6 – Negative ion secondary ion assignments for signals detected on copper samples.

<i>m/z</i>	Ionic formula	Measured exact mass (Da)	Δ from theoretical exact mass (ppm)
68	C ₂ H ₂ N ₃ [−] (triazole)	68.0262	19
132	C ₇ H ₆ N ₃ [−] (tolyltriazole)	132.0534	21

The measured masses could be improved in their accuracy by employing a calibration reference of higher mass. Calibration references for the measurements were instead easily identifiable relatively low mass fragments (H₂[−], CH₂[−] and CH₄[−]). This was not an issue, as the determination of the exact mass of such ions was beyond the scopes of the investigations. Additionally, some specific ionic species detected and their possible different sources are hypothesised below for completeness, although none of these speculations are about species directly relevant to this study:

- tris(2,4-di-*tert*-butylphenyl)phosphite (Irgafos[®]168)

$m/z = 663$ {O=P–[OC₆H₃(C₄H₉)₂]₃H}⁺ from oxidation.

$m/z = 473$ from fragmentation and/or oxidation loss of [M–OC₆H₃(C₄H₉)₂] to leave the oxidized fragment {O=P–[OC₆H₃(C₄H₉)₂]₂O}[−].^f

- Sodium dodecyl sulfate (SDS)

$m/z = 263$ (C₁₂H₂₃OSO₃)[−], 265 (C₁₂H₂₅OSO₃)[−] from 2H loss in the ionisation process or presence of common impurities with unsaturation in the alkyl chain.

$m/z = 293$ (C₁₄H₂₉OSO₃)[−], probably for the homologous impurity with two additional methylene units in the alkyl chain (*i.e.* sodium tetradecyl sulfate).

^f M = P–[OC₆H₃(C₄H₉)₂]₃

3. The effect of metal-insulation contact on copper sulfide deposition on Kraft paper

Part of the results in this chapter have been previously published as:

Facciotti, M.; Amaro, P. S.; Holt, A. F.; Brown, R. C. D.; Lewin, P. L.; Pilgrim, J. A.; Wilson, G.; Jarman, P. N. Contact-Based Corrosion Mechanism Leading to Copper Sulphide Deposition on Insulating Paper Used in Oil-Immersed Electrical Power Equipment. *Corros. Sci.* **2014**, *84*, 172–179.

Copyright permission can be found in Appendix A1.

3.1 Aim and outline of the chapter

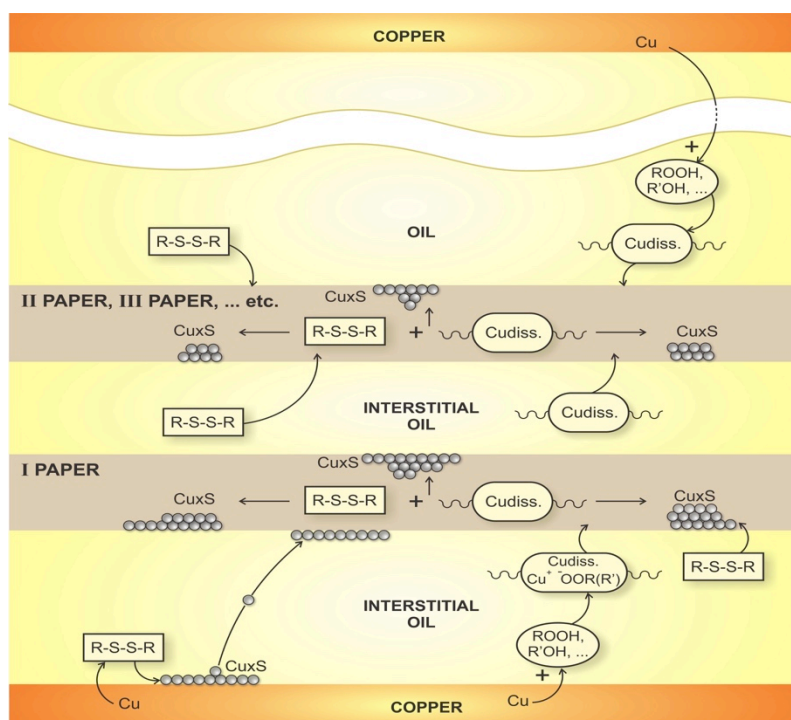
In this chapter is discussed a series of experiments meant to expand and complement the knowledge on the process of copper sulfide formation, mobilisation and deposition in oil-filled power transformers. Initially, a summary of the current state of understanding of this process in terms of its mechanism is provided. Given the literature detailed, this work aims to focus on a peculiar observation that seemed to receive less attention in previous research, trying to understand the mechanism behind copper sulfide contamination of solid insulation: copper-paper proximity. In fact, Cu_xS found on contaminated paper insulation is believed to be generated mainly locally, by reaction between soluble complexes containing copper and organosulfur compounds, as will be discussed in Section 3.2. On the contrary, our work highlighted that the formation, migration and decomposition of organic copper complexes could not be the only mechanism taking place in insulating oil and the only explanation to the observed phenomena. Contextually, evidence was provided to support a contributing role of a mechanism that strongly depends on the vicinity of copper conductor and paper insulation.

The influence of some crucial experimental variables in the production of contaminated paper samples such as time, temperature, concentration of DBDS (*i.e.* a representative

corrosive compound) and atmosphere were taken into account, while discussed with the support of experimental observations made with XPS and ESEM/EDX. These two techniques, thanks to their elemental selectivity together with their diverse and complimentary depth resolutions, allowed a semi-quantitative evaluation of the Cu and S contamination of paper, both its bulk and surface, providing an invaluable new insight. Finally, a discussion of the mechanistic significance of the results is carried out leading to the formulation of the proposed bifurcated mechanisms, a part of which strongly affected by copper-paper proximity, which aims to further detail the process of copper sulfide contamination of insulating paper inside transformers.

3.2 Overview on copper dissolution in oil and copper sulfide contamination of insulating paper by CIGRE WG A2.40

As already briefly discussed in Section 1.4.2, a rather comprehensive work has been carried out by CIGRE WG A2.40 in collecting and rationalising all proposed mechanisms for the formation of copper sulfide in oil-filled transformers, derived both from laboratory investigations and field observations. Although few pivotal works have been cited in this section, the reader is referred to the relevant soon-to-be-published CIGRE Technical Brochure (TB) for additional references.³⁶



A graphical representation of its conclusion has been shown in **Figure 11**, which is reported again above. As already discussed most of the mechanisms proposed for the

formation of Cu_xS , are based on the initial dissolution of copper in oil to form soluble intermediates. This process comprises four different steps:

- Occurrence of free and highly reactive copper species at the metal surface, characterised by very limited solubility in oil, possibly due to local thermal excitation or electrical stresses.
- Formation of dissolved copper intermediates, facilitated in the presence of oxygen and some antioxidants, due to the complexation activity of organic components of the oils (*e.g.* hydroperoxides).
- Displacement/diffusion of the intermediates into the oil and paper insulation.
- Reaction of dissolved copper intermediates with reactive sulfur species to form Cu_xS as corrosion by-product on paper.

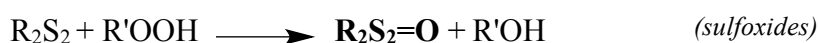
The source of Cu_xS contamination of paper held accountable for the vast majority of the deposits found in the insulation system is considered, to date, that described above. The second minor source is represented by copper sulfide originally formed at the surface of the corroded copper conductor and then migrated. This Cu_xS might be referred to as metal-generated contamination, as opposed to that generated by reaction of precursors in the paper.

Generally, dissolution of copper is clearly the rate-determining step of this chain of events. Previous studies have shown how oxygen is able to promote this phenomenon, particularly in uninhibited oils, together with elevated temperatures (*i.e.* $> 140\text{ }^\circ\text{C}$). However, very high temperatures and O_2 in the oil were also linked to reduced copper dissolution efficiency in oil when compared with milder experimental conditions ($100\text{ }^\circ\text{C} < T < 140\text{ }^\circ\text{C}$, lower O_2).¹⁴⁰ This reduction in dissolved copper, otherwise available to undergo complexation, can be explained by the observed formation and precipitation of copper-rich sludge in the oil when these harsh conditions are used.⁶⁴ Regarding the following step, involving Cu_xS contamination of paper insulation, similar observations were made. The presence of oxygen was shown to promote deposition of copper sulfide on the insulating paper,^{29,33,45,48,58,64,140} increasing from inner to outer layers in accordance to a non-steady-state Fick's diffusion pattern,⁴⁷ thus supporting a mechanism that involved soluble copper species in oil (the only ones able to diffuse across multiple layers of oil impregnated paper). Surprisingly, even high concentrations of phenolic inhibitors such as DBPC, which protect the oil from oxidation, were observed to favour copper deposition on paper over dissolution in oil.¹⁴⁰

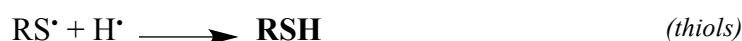
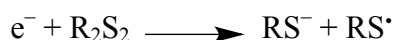
Nonetheless, once copper is dissolved and it has migrated in the insulation systems, Cu_xS has somehow to be formed. This process, however, is not fully understood mainly due to the enormous variety of chemical species present in the oil that could potentially take part in it. Nonetheless, several postulations have been made trying to elucidate the formation of reactive species and copper sulfide contamination of both copper surfaces and paper, to best explain phenomena observed in real life applications.

At first one can think of solid-state reactions at the copper surface, which acts as an heterogeneous catalyst, where reactive corrosive sulfur compounds such as disulfides can decompose. The proposed route to the formation of metal-generated copper sulfide in the presence of oxygen is through decomposition of said disulfides and formation of mercaptans and oxidised sulfur species, which can in turn attack the metal.⁶⁴ The formation of these reactive species, consequences of the secondary antioxidant properties of some disulfides, is believed to follow two main pathways. These take into account the reactivity of the compounds involved while in the presence of the most relevant and viable environmental conditions in transformers³⁶:

- *Oxidation of S atoms by hydroperoxides in the presence of dissolved O_2*



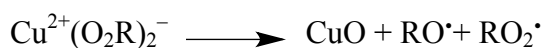
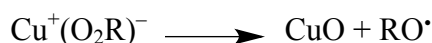
- *Temperature and/or accelerated electron-mediated C–S bond cleavage*



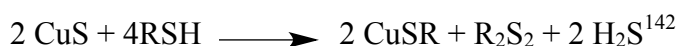
In the representative case of DBDS, the reaction products would be DBS and toluene; DBS could then undergo further decomposition to produce benzyl mercaptans and, upon reaction with the oxidised surface of the conductor, copper sulfide. Additionally, the local formation of elemental sulfur, highly reactive towards copper, is also contemplated although it has been observed to be a viable reaction pathway for DBDS only above 200 °C.¹⁴¹

To explain how dissolved copper could be transformed in copper sulfide contamination of paper insulation, the formation of complexes by reaction between hydroperoxides in the oil and copper oxides at the surface of the metal has to be taken into account. In fact, at least partial oxidation of the surface of any copper conductor has to be formally expected even though, for simplicity, all reactivity and mechanisms are often discussed with respect to metallic copper. These soluble species could then migrate into the insulating paper layers where they react with organosulfur compounds yielding Cu_xS deposits. This in turn could be the origin of the observed increased levels of elemental sulfur, mercaptans and toluene. It is known that both radicals and peroxides formed as a consequence of the partial oxidation of the oil are capable to attack oxidised copper surfaces to promote dissolution of copper.²⁹ This free copper is then capable of being complexed, diffuse through the insulating system and undergo further reactions with reactive sulfur species. A proposed set of reactions for these process is detailed below³³:

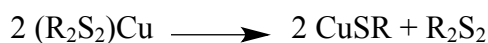
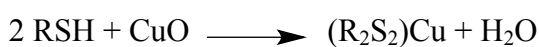
1. *Hydroperoxide-mediated formation of **dissolved copper complexes***



2. *Generation of **copper sulfide** deposits due to mercaptans*



and/or



This last proposal is based on the well-known mercaptans/disulfide exchange equilibrium, promoted by copper cations,¹⁴³ which could be the cause of reactive species regeneration (allowing corrosion to continue in a self-sustained fashion). This mechanism also requires the intermediate species CuO to be locally formed, and later converted in Cu_xS. Interestingly, mercaptans in hydrocarbon media were also reported to react with sulfides to regenerate disulfide species, providing a pathway for a corrosive sulfur species regeneration equilibrium.¹⁴²

Given these hypotheses based and experimental results of Lukic *et al.*,³³ a rather close relationship exists between the oxidation processes occurring in the oil and the formation of copper sulfide, although this was not so commonly observed in laboratory tests. Provided enough oxidation has occurred to the oil and in the presence of reactive sulfur species (*e.g.* thiols, sulfur oxyacids) the formation of copper sulfide was shown to be possible. Supporting this, some precursors of Cu_xS appear more reactive towards copper as a consequence of their oxidation. The most notable examples are disulfide secondary antioxidants, additives meant to decompose peroxides species formed in oil due to the oxidative degradation of the oil that is not completely prevented by primary antioxidants (*e.g.* DBPC).^{58,144} Disulfides, under such conditions, can be converted to oxidised species like sulfoxides and sulfur oxyacids (as shown above), which are reactive towards the metal and could ultimately form more copper sulfide.

Summarising, different processes seem to co-exist regarding the generation of Cu_xS. However the number of compounds involved, the complexity of the possible reaction pathways and virtually endless short-lived highly reactive intermediates simply make this problem too complex to be systematically described.

3.3 Optimisation of the ageing conditions: time and temperature

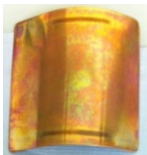









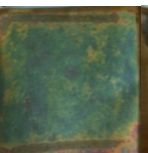
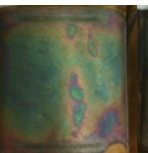

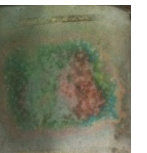

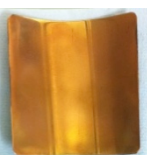

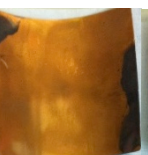
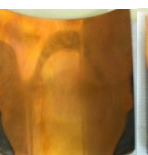

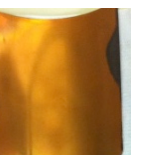
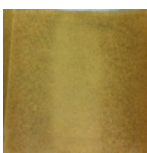
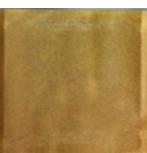
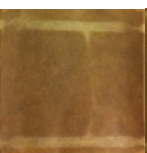
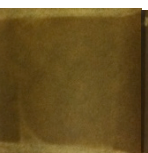

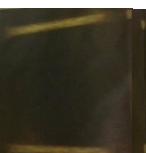
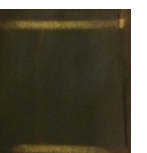
As a first step, a visual qualitatively investigation was carried out to identify the optimal experimental conditions promoting the most uniform contamination of a paper sample by copper sulfide. The aim of this optimization was to define a reproducible method to produce large insulating paper samples (9 x 9 cm²) with homogeneous Cu_xS contamination to be used in all tests to follow, detailed in Section 2.4. Subsequently, a spectroscopic analysis of the paper samples was also carried out by means of XPS and EDX in order to assess the degree of contamination of the paper at the surface and bulk respectively. Both

XPS and EDX are, in fact, fully able to deliver data in terms of atomic % concentration of C, Cu and S, which are the main constituents of the samples. However, the reason behind the application of both techniques rests in their complimentary depth resolution: while XPS selectively returns elemental information only from the top 10-20 nm of the sample, EDX is capable of analysing deeper within a sample, thanks to its vertical resolution of 0.5-5 μm (see Sections 2.6.1 and 2.7.1 for more details). As a consequence, a comparison of all the data collected by means of the two techniques allowed the construction of a comprehensive quantitative representation of the Cu_xS contamination of the surface and the bulk of the paper samples when exposed to a variety of experimental conditions. The full set of the SEM and ESEM images, of copper and paper samples respectively, can be found in Appendix A2.

Any accelerated ageing experiments, aimed to simulate several years of natural ageing of the insulation system over a few hours, need to be designed carefully to avoid misleading conclusions. Temperature, for example, is increased in order to accelerate the kinetics of the (ideally only) chemical reactions involved. However, a delicate balance is needed, as very high temperatures might also change the thermodynamics of other reactions that might not be relevant in real life ageing. In other terms, one might end up studying the effects of processes that are thermodynamically disfavoured at service temperature inside an operating transformer, which may lead to the misinterpretation of the experimental results. Additionally, excessive heating might even degrade the materials irrecoverably (*i.e.* oil flash point and oxidation, paper thermal degradation/carbonisation). For this reason, designing the experiments detailed in this chapter, both ageing time and temperature were carefully and systematically evaluated to better study the chemical processes that lead to the contamination of paper insulation by Cu_xS . It is known that both parameters are directly proportional to the amount of copper sulfide deposits found on paper. Luckily, this problem has already been largely dealt with by international working groups and standardising bodies (*i.e.* CIGRE, IEC and BSI) while determining the standard test conditions to be used in monitoring corrosion phenomena in insulating oil. Unfortunately, some of these parameters might serve their purpose only under the stringent conditions detailed in the relevant standard procedures, as IEC 62535.³⁷ Its standard conditions were, in fact, evaluated at the beginning of this study in order to be used due to their relevance to the context. However, a temperature of 150 °C was found unsuitable for the purpose of the production of Cu_xS -contaminated large paper samples. Due to the significantly higher amount of oil used when compared to a standard corrosion test in headspace vials, the amount of oil vapours over multiple days ageing was just unmanageable. As a

consequence, the ageing temperature employed throughout the study was selected to be 140 °C. This has been shown to be a good compromise between the unavoidable partial thermo-chemical degradation of the paper samples and the desired acceleration of the reaction kinetics.¹⁴⁵ The effect of time on samples aged in oil containing 2000 mg kg⁻¹ of DBDS under air atmosphere over an 8 day period is shown in **Table 7**.

Table 7 – Visual appearance of both copper plates and paper samples after ageing over 8 days in oil at 140 °C in the presence of air and 2000 mg kg⁻¹ of DBDS. TGA data are available in Appendix A3.

	Ageing days						
	1	2	3	5	6	7	8
Convex surface (copper)							
Inner side (paper)							
Concave surface (copper)							
Outer side (paper)							

At this point a few observation could be made, before any instrumental analysis was performed on both copper and paper. Firstly, the most uniform and homogeneous deposition of copper sulfide on paper was observed on the inner side of the sample aged for 7 days under these conditions. Secondly, areas in which copper and paper were not aged in close contact were observed to be significantly less corroded and less contaminated by Cu_xS, as can be observed in images of copper concave surfaces and paper outer sides in **Table 7**. The procedure was found to be very reproducible once optimised, as can be seen in **Figure 33** (bottom). Good consistency was also found in EDX results to assess the total sulfur contamination of the samples, as shown in **Figure 33** (top). Longer ageing times, even if potentially yielding thicker contamination layers were not deemed worth pursuing, largely to avoid unnecessary thermo-chemical degradation of the paper insulation. ESEM micrographs available in Appendix A2, on which EDX semi-quantitative analysis was

performed, did not show noteworthy features. The samples appeared uniformly conductive, although not showing the presence of particulate and deposits, suggesting a diffuse contamination of the bulk of cellulose (otherwise insulating).

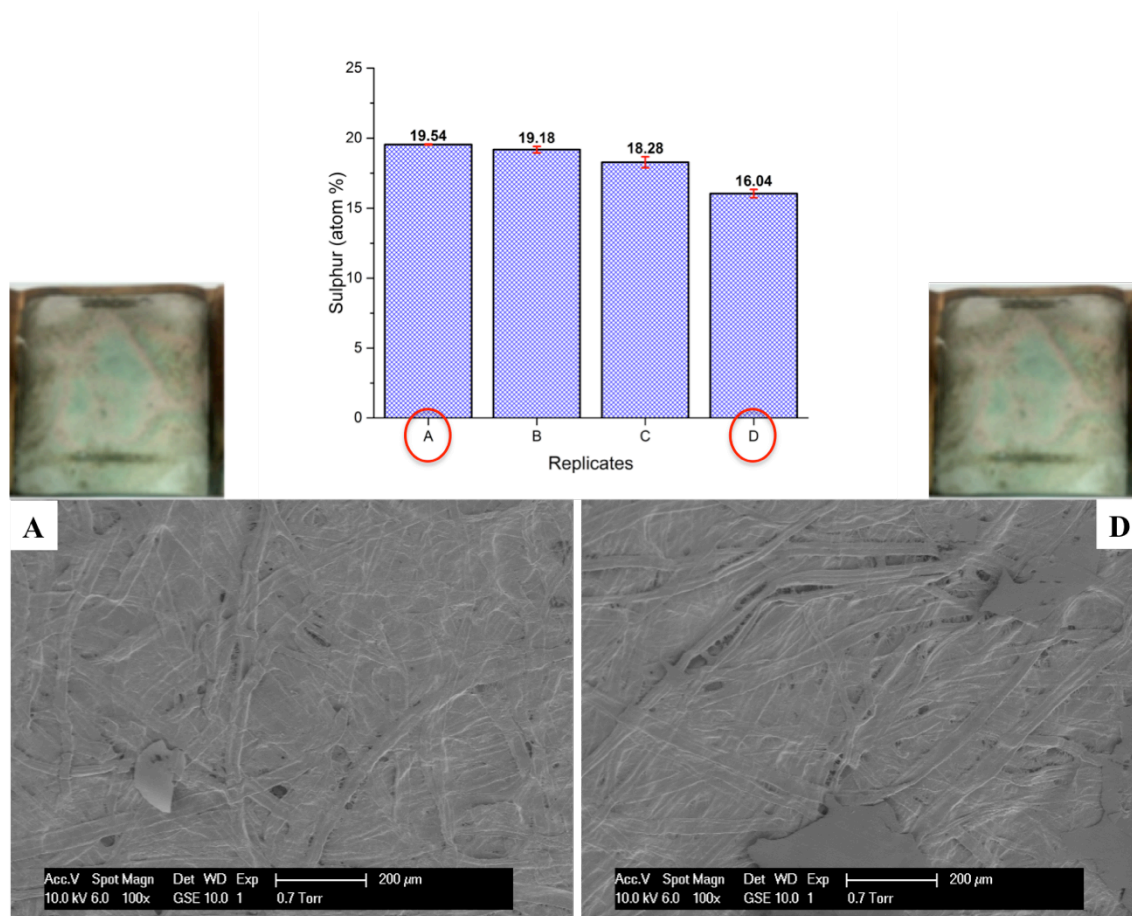


Figure 33 – Visual inspection, corresponding ESEM micrographs and total sulfur determined by EDX of replicates **A** and **D** produced using the optimised procedure.

For completeness, EDX analysis was performed on copper samples confirming the presence of copper sulfide on the surface of corroded copper sheets but, from there on, focus was on the analysis of paper samples. EDX analysis of paper revealed how the ageing time influenced the contamination of paper in the bulk of the sample. The more contaminated inner side of paper samples, that in close proximity with copper during the ageing experiments, was analysed. Apart from the expected ubiquitous carbon signal arising from the cellulosic background, copper and sulfur signals were clearly visible and their trend is shown in **Figure 34**. From the data collected it could be observed that the amount of copper and sulfur contamination, which are solely products of corrosion processes, progressively increased during the ageing period reaching a plateau after 6 days. This was consistent with the outcomes of the visual inspection of paper samples, as shown

in **Table 7**. An approximate apparent ratio $\text{Cu:S} = 2$ was found in the bulk of paper, suggesting the predominant presence of Cu_2S .

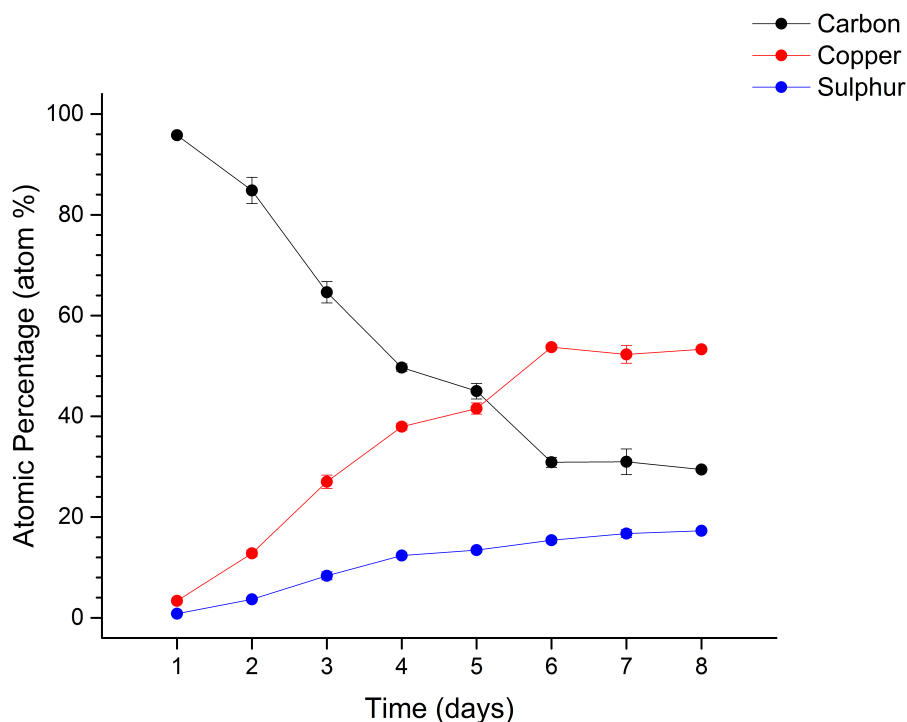


Figure 34 –EDX results for C, S and Cu from the inner surface of paper samples aged over an 8 day period.

All paper samples analysed shared very similar XPS spectra, significantly varying only for the intensity of the characteristic $\text{Cu}2p$ and $\text{S}2p$ signals. An example of the appearance of the collected XPS survey spectra on paper samples, highlighting the signal assignment, is shown in **Figure 35**. Carbon, oxygen, copper and sulfur were the major elements detected on most of the samples (with the exception of some traces of nitrogen). In addition to core electron photoelectric peaks, also Auger's transitions for all elements were also observed (for further details see Section 2.6.1), although not quantified. These latter signals are conventionally named after the element (Z) from which they originate from and a set of three letters, *e.g.* Z_{XYZ} . This notation describes the decay process of an energetic electron towards the core vacancy generated by the emitted photoelectron (responsible for the main photoelectric peak), coupled with the emission of another electron of an energy characteristic of the differences between the states involved in the process.¹²⁷ For example, the signal O_{KLL} refers to the emission of an L-shell electron as a consequence of the decay of another L-shell electron to fill a K-shell vacancy within the same atom of oxygen.

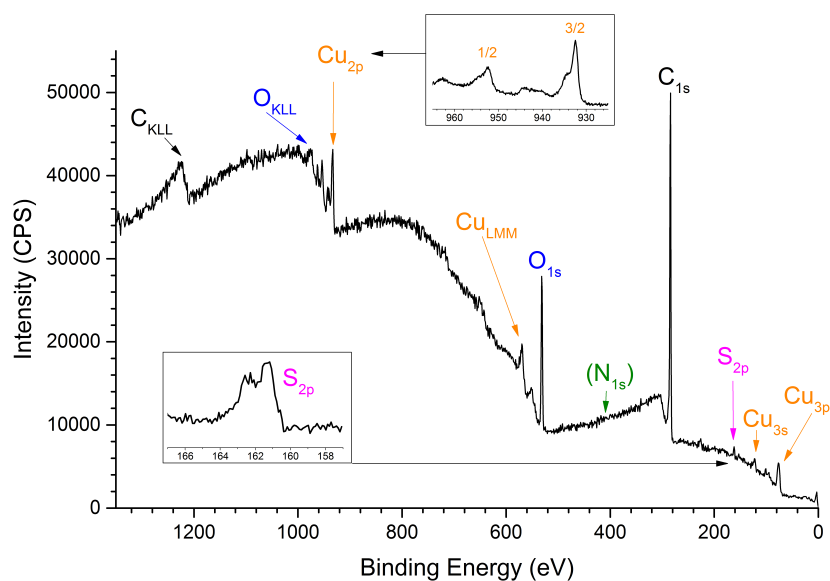


Figure 35 – Appearance of a typical XPS spectrum (and relative signal assignment) of a paper sample aged for 8 days in oil at 140 °C in the presence of air and 2000 mg kg⁻¹ of DBDS.

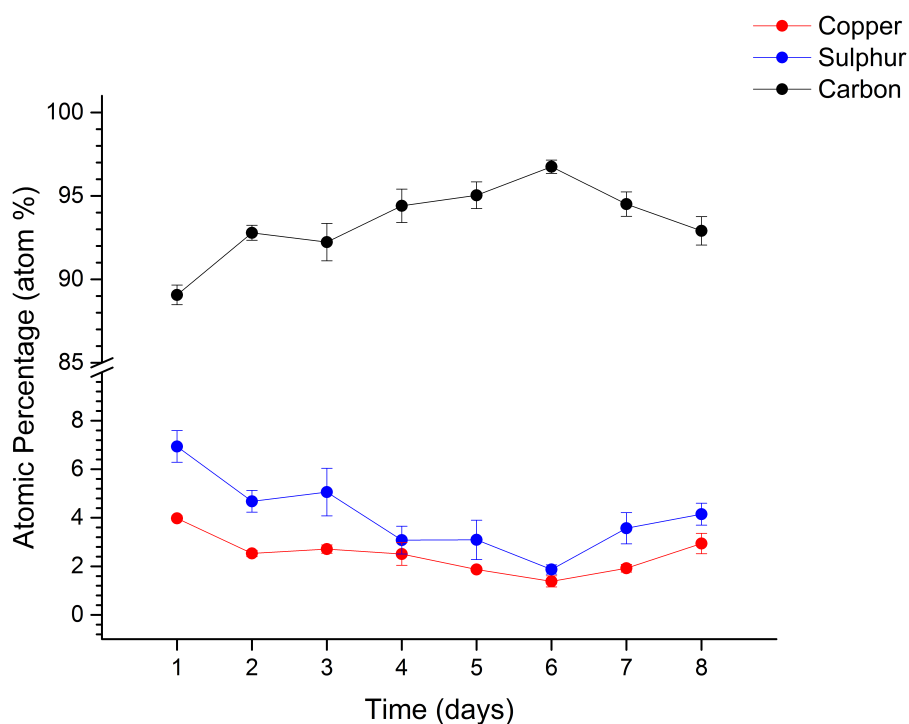


Figure 36 –XPS results for C, S and Cu from the inner surface of paper samples aged over an 8 day period.

Interestingly, XPS results obtained for the compositional analysis of the surface of the samples (top 10-20 nm) were significantly different and they are shown in **Figure 36**.

Substantially no variation in Cu and S content was observed, with the exception of a rather small decrease after the first 2 days of ageing. The combined concentration of paper contaminants from corrosion processes was found never to exceed 5-10 atomic%. These values were significantly smaller than those observed in the bulk of the samples *via* EDX, closer to a combined 80 atomic% of the total signal detected. Additionally an almost reverse Cu:S ratio was found, suggesting perhaps a more complex stoichiometry of the observed deposits.

Looking at the sole distribution of the paper contaminants, an interesting observation could be made: in correspondence to the apparent decreased amount of Cu and S on the surface of the paper sample, the bulk experiences the fastest build-up of said species. This suggested that a diffusion process of the contaminant elements (in speciation yet to be determined) was happening at that point in time. This also explained the absence of an increasing trend for these species on the surface. Once the diffusion reached a steady state, in fact, Cu and S on the surface appeared constant over time as they were dynamically diffusing through the cellulose network, accumulating as shown by EDX results.

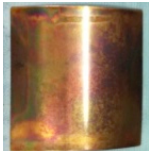









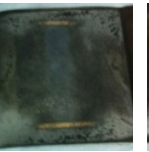


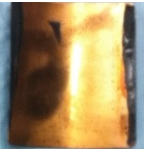
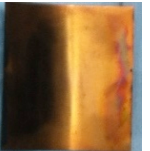
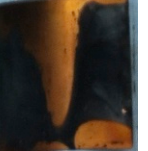
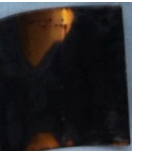

In other words, an initial migration of copper and sulfur occurs towards the paper insulation surface that leads to its contamination. After the surface has been saturated in contaminants, these start to diffuse into the cellulose matrix (probably in form of soluble complexes) where it is easier to find heterogenic nucleation and growth sites for Cu_xS crystals thanks to the intrinsic roughness generated by cellulose fibres. These observations on the relevance of diffusive processes in explaining how the insulation system can get contaminated even far away from the copper conductors, is in substantial agreement with what has been previously reported in the XPS work by Castle *et al.*⁴⁷

3.4 The effect of the concentration of DBDS in the oil

As the oil used in the experiments detailed in this chapter (*i.e.* Gemini X) was not corrosive, the addition of the representative corrosive compound DBDS was necessary to promote corrosion and thus allow the deposition of Cu_xS on paper. In the experiment detailed in Section 3.3, copper samples were exposed to as much as 2000 mg kg⁻¹ of DBDS during the ageing period. The reason such an elevated (and unrealistic) concentration of the compound was necessary is rather simple: as the aim of the procedure was to produce as much copper sulfide as possible the ageing had to be conducted in great excess of its precursor, here DBDS. Nonetheless this parameter was not treated lightly, as

its relevance to the problem demanded, therefore an investigation of the effects of the concentration of DBDS ($0 - 10000 \text{ mg kg}^{-1}$) on the paper contamination was carried out and the results are shown in **Table 8**.

Table 8 – Visual appearance of both copper plates and paper samples after ageing over the optimal 7 days period in oil at 140°C in the presence of air and increasing DBDS. TGA data are available in Appendix A3.

	DBDS (mg kg^{-1})					
	100	500	1000	2000	5000	10000
Convex surface (copper)						
Inner side (paper)						
Concave surface (copper)						

For copper, it was again observed that the face of the copper plate more affected by corrosion was that in closer proximity to paper during ageing. However, for extremely high concentrations of DBDS in oil ($> 2000 \text{ mg kg}^{-1}$) copper corrosion became evident on both sides of the metal plate. Additionally, the copper convex surfaces appeared to be going through some sort of formation-detachment cycle of Cu_xS deposits. It could be seen that, at very high DBDS concentration, bare copper became visible again. This could be probably explained by the formation of a thicker copper sulfide layer, more prone to cracking and detachment, together with the effect of the ageing atmosphere that will be detailed in Section 3.5. As before, paper was only found contaminated by Cu_xS in its inner side, as shown in **Table 8**. Interestingly, it was noted that at lower concentrations of corrosive compounds the both copper corrosion and deposition of its by-products on the surface of paper insulation appeared like smooth and uniform layers. On the contrary, at higher concentration of DBDS, copper sulfide appeared patchy and loose. This difference was considered the underlying reason of the apparent cyclic behaviour mentioned above.

EDX and XPS analysis of the contaminated paper samples was performed and results are discussed below. For paper samples produced under these ageing conditions a similar trend was visible in data collected with both instrumental techniques used. Seemingly, the top

nanometres investigated with XPS were less contaminated by Cu_xS than the bulk, as observed and discussed already in Section 3.3. Data shown in **Figure 37** and **Figure 38** appeared, at first inspection, fairly similar to each other in trend.

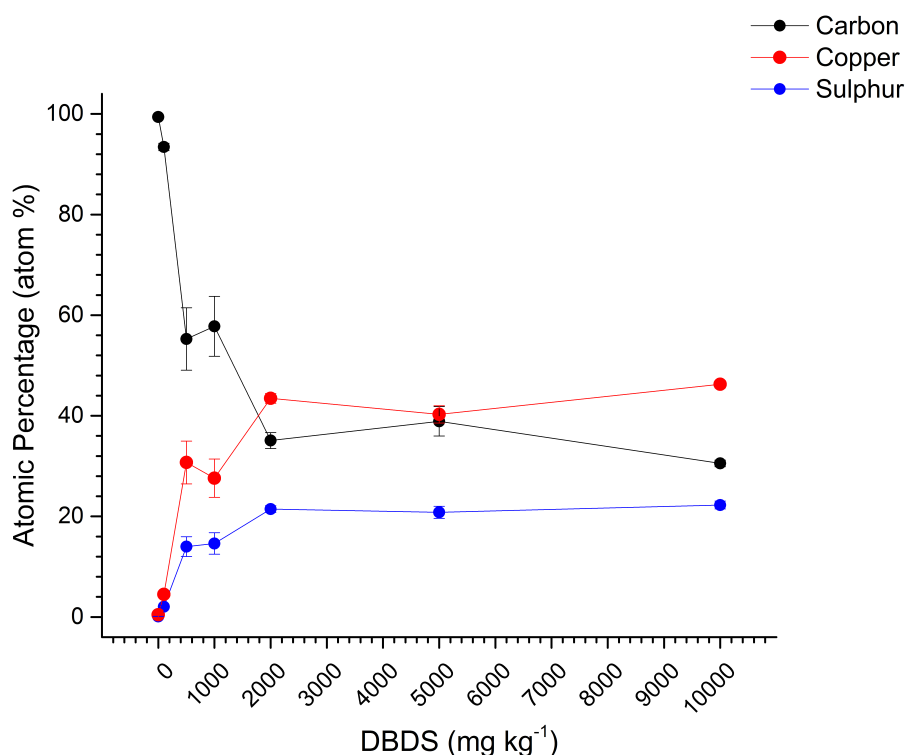


Figure 37 – EDX results for C, S and Cu from the inner surface of paper samples aged over the optimal 7 day period in oil at 140 °C in the presence of air and increasing DBDS.

However, the relative percentage of corrosion by-product deposits is different in EDX and XPS: the combined concentration of paper contaminants from corrosion processes was found close to 60 atomic% using EDX while only around 25 atomic% using XPS. This can be explained once again by the different and complimentary depth resolutions of the two spectroscopic techniques used. As a more general consideration it is noteworthy that XPS showed consistently less Cu and S contamination of the paper analysed. ESEM micrographs, reported in Appendix A1, started to show evidence of deposit formation at DBDS concentration as low as 100 mg kg⁻¹. This process reached its apex for the sample aged in the presence of air and 10000 mg kg⁻¹ of DBDS in oil, where large flakes of copper sulfide were clearly visible. Such large deposits, retained by the paper layer as a filter, were most likely formed at the surface of the copper plate and then detached as a consequence of unknown reactions. Interestingly, due to the high surface sensitivity of XPS, after the surface of the paper was saturated in contaminants, a relatively stable surface composition could be reached quite quickly. Subsequently, XPS was not able to follow compositional variation occurring within the paper bulk.

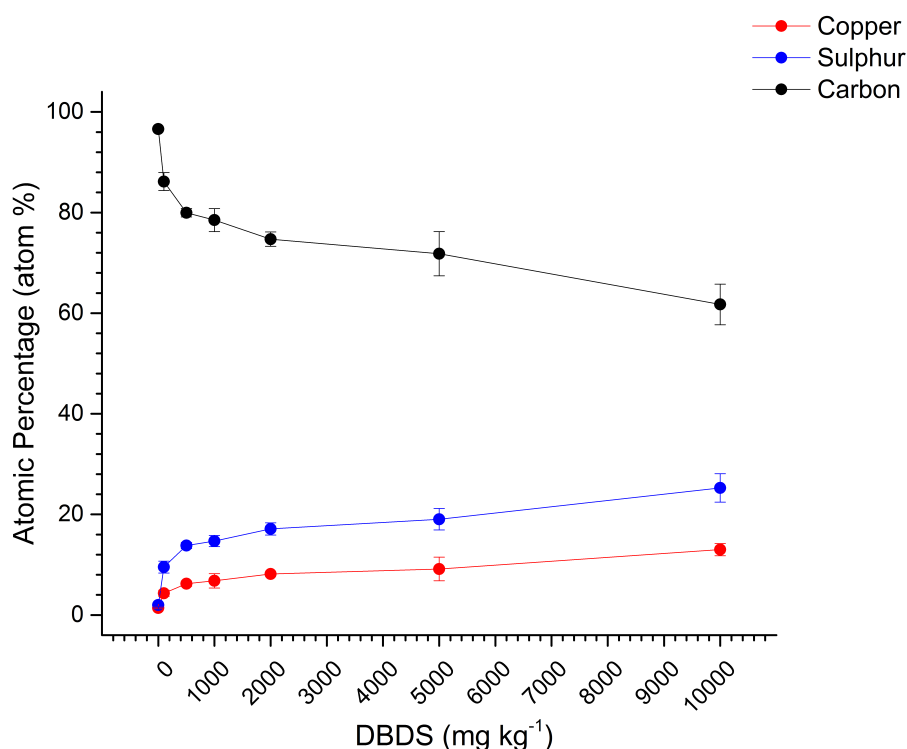


Figure 38 – XPS results for C, S and Cu from the inner surface of paper samples aged over the optimal 7 day period in oil at 140 °C in the presence of air and increasing DBDS.













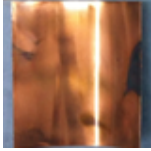
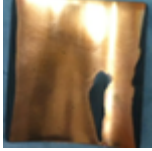
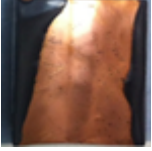
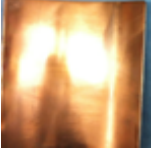


3.5 The role of ageing atmosphere

The effect of the ageing atmosphere on the Cu_xS deposition on paper was also investigated. Even though it is well known, as discussed before, that the presence of oxygen in insulating mineral oils has the effect of enhancing Cu_xS deposition phenomena on paper insulation, a set of experiments under inert N_2 atmosphere was performed. An overview of the visual inspection carried out on both copper and paper samples after ageing in the presence of DBDS is shown in **Table 9**. The appearance of the samples after ageing in inert atmosphere was very different from that observed in previous experiments reported in Sections 3.3 and 3.4.

Although the appearance of both concave and convex copper surfaces in the presence of low concentrations of DBDS recalled the one observed in **Table 8**, for samples aged in the presence of air significant differences were observed at higher concentrations. In fact, Cu_xS deposition was not at all observed on paper, while extensive copper corrosion was clearly visible, mostly in areas close to the paper layers. In contrast to the samples aged in air (**Table 8**), the surface of the corroded metal appeared to have diffuse copper sulfide contamination, in form of smooth, shiny and varnish-like layer rather than being patchy and loosely attached. This observations suggested that, even if copper sulfide was

generated on the surface of the metal rather than only as a consequence of *in situ* transformation of soluble complexes, Cu_xS could only migrate (after detachment) towards the insulation system in the presence of oxygen.³³

Table 9 – Visual appearance of both copper plates and paper samples after ageing over the optimal 7 day period in oil at 140 °C under inert N_2 atmosphere and increasing DBDS.

	DBDS (mg kg^{-1})					
	100	500	1000	2000	5000	10000
Convex surface (copper)						
Inner side (paper)						
Concave surface (copper)						

In practice, this would mean that the amount of Cu_xS deposits on paper, originally formed at the metal surface, could be greatly reduced by simply controlling the atmosphere composition (*i.e.* monitoring oxygen intake of the transformer). N_2 was therefore observed to reduce the contribution of copper-generated Cu_xS to the overall contamination of the insulating paper and simultaneously the failure risk associated with the presence of large amount of corrosive compounds (*i.e.* DBDS). Notably, the possible contribution of copper-generated Cu_xS to an overall bifurcated mechanism of contamination of the insulation materials was therefore considered for the first time, and will be expanded in Section 3.7.

ESEM micrographs of paper, reported in Appendix A1, showed hardly any Cu_xS contamination. As a consequence, paper samples were poorly conductive and this led to surface charging, charring and poorer imaging quality. EDX and XPS data collected from paper samples shown in **Table 9** substantially reinforced the visual inspection outcomes, as it can be seen in **Figure 39** and **Figure 40**. Both techniques showed no significant contamination of paper in terms of Cu and S, as neither of those element were present in quantifiable atomic concentrations on the samples aged under N_2 atmosphere, while the major signal detected was the C from the cellulosic matrix. Experimental evidence collected highlighted the primary role of oxygen availability in this complex chemical process occurring in oil.

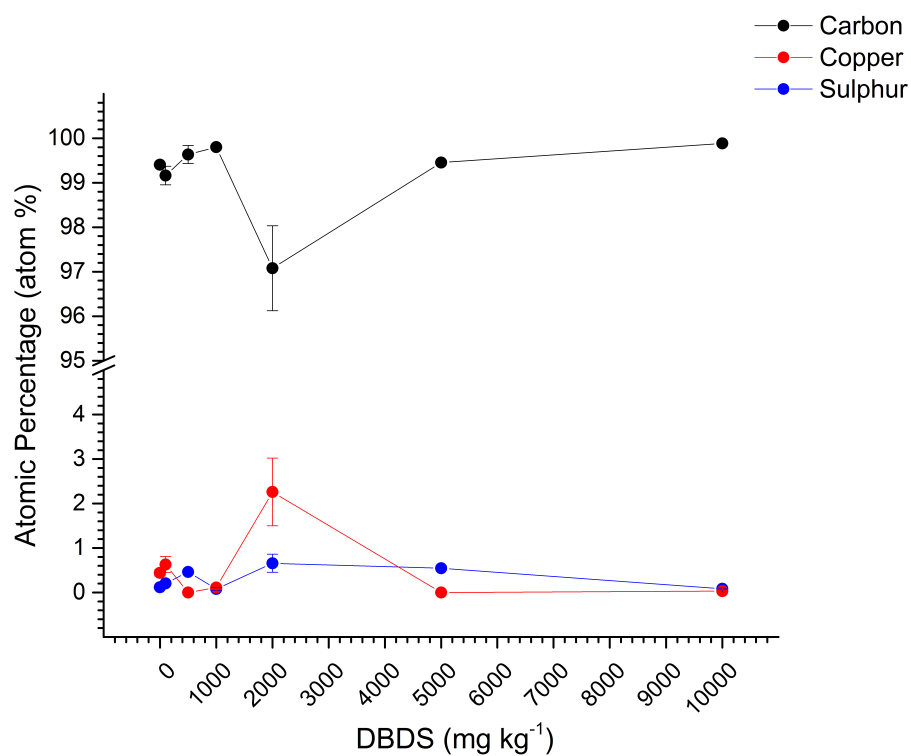


Figure 39 – EDX results for C, S and Cu from the inner surface of paper samples aged over the optimal 7 day period in oil at 140 °C under inert atmosphere (N₂) and increasing DBDS concentrations

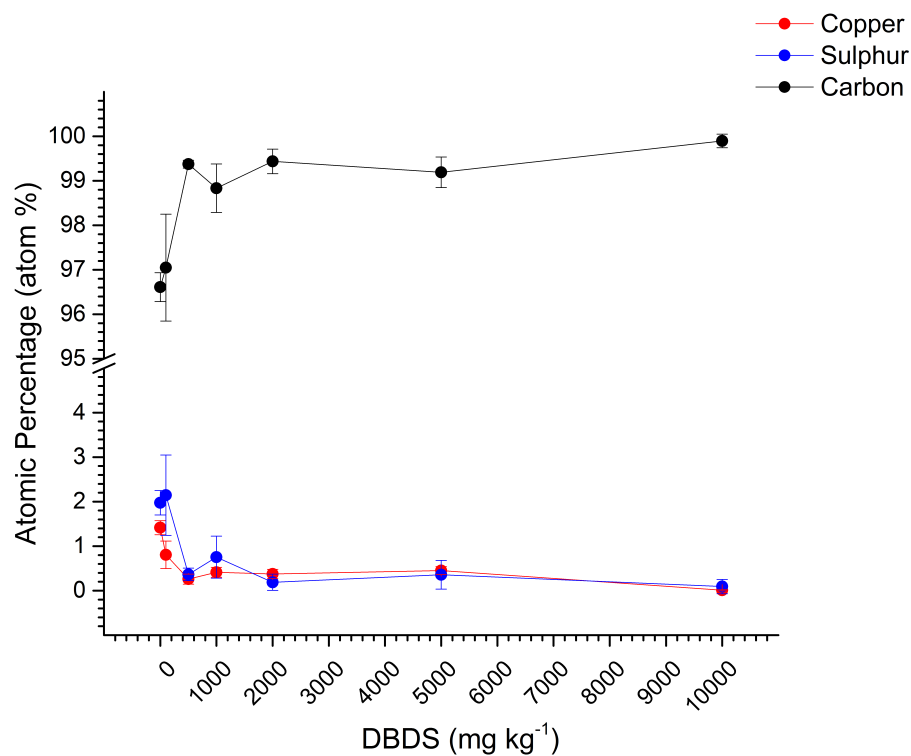


Figure 40 – XPS results for C, S and Cu from the inner surface of paper samples aged over the optimal 7 day period in oil at 140 °C under inert atmosphere (N₂) and increasing DBDS concentrations.

Even if the role of oxygen was not a completely new finding, the clear observation of its influence on copper-generated Cu_xS was noteworthy, although the mechanism that causes copper sulfide detachment is still not clear. In these ageing experiments, oxygen clearly interfered with the surface interaction between the metal and Cu_xS , causing its displacement. This “flaking” from the surfaces not only represented the first stage of the contamination of the surrounding insulation system as a whole (oil and paper) but also did cause the exposure of reactive bare copper free sites. These exposed metal sites were substantially made available for further corrosion. In essence oxygen, provided enough corrosive compounds are available, was found to facilitate corrosion to occur by constantly exposing fresh copper surface.

3.6 The importance of the contact between copper and paper

Perhaps the most interesting of the observations, made possible by the use of such large copper and paper samples, was that of the role of the proximity between copper and paper in influencing both corrosion of copper and contamination of paper by copper sulfide deposits. In all experiments detailed in the previous sections of this chapter, a clear relationship between the most corroded metal surface and its proximity with the surface of paper was found. In particular, the presence of paper in close contact with the metal (*i.e.* the convex surface of the copper plates used) seemed to promote corrosion phenomena. Copper convex surfaces were systematically found to be more attacked by corrosive compounds regardless of the ageing conditions used. Trying to emphasize and further characterise this unexpected phenomenon while confirming that corrosion of the metal was highly dependant on the surface contact between the two materials investigated, a dedicated experiment was designed. On one of the same type of large samples used in previous experiments, a portion of paper was removed from that covering the convex face of the metal plate to expose bare copper to the corrosive oil environment. The sample was then aged in Gemini X oil with 2000 mg kg^{-1} of DBDS for 7 days at 140°C and results are shown in **Figure 41**.

After this experiment there was no doubt that the sole presence of paper in close contact with the metal surface largely influenced the observed rate of corrosion. This effect was attributed to the ability of paper to slow down the mixing of the thin layer of interstitial oil between itself and the copper surface. Paper was then hypothesized to build up a concentration polarisation layer of reactive chemical species (*e.g.* corrosive compounds, peroxides) and corrosion by-products nearby the copper surface. This increase could then

cause an increased rate of corrosion, especially if locally aggravated by limited oil mixing/replacement rates at the interface.



Figure 41 – Appearance of the sample before (left) and after (middle) ageing for 7 days in oil at 140 °C in the presence of air and 2000 mg kg⁻¹ of DBDS. An overview of the status of both copper and paper is shown (right).

3.7 The proposed mechanism

As a consequence of the experimental evidence collected in this study, a simple but rather comprehensive mechanism was proposed to account for copper sulfide contamination of insulating paper in power transformers. This was a bifurcated mechanism, comprising both Cu_xS generated at the surface of the copper conductor and that produced by decomposition and reaction of soluble complexes in the paper. This was meant to compliment the existing mechanistic knowledge, detailed previously in this chapter, while trying to find an explanation for the observed differences between the contamination of surface and bulk of the paper insulation by copper sulfide. A graphical summary of the proposed pathways is shown in **Figure 42**.

The first mechanism is believed to be the one primarily responsible for the initial contamination of the surface of the paper insulation layer closer to the metal surface. In the presence of oxygen, it was observed to be the fastest-yielding process to form copper sulfide deposits. This phenomenon was based on the formation of Cu_xS on the surface of the corroded metal, which can then detach and migrate towards the neighbouring paper layer in form of particles and flakes. There, the size of larger particles prevents further diffusion through the oil-impregnated cellulose fibres, which act as a filter and causing a local increase in both Cu and S. This process is believed to yield the saturation of the paper's top surface (10-20 nm) fairly quickly, as was observed in XPS data discussed previously. In summary, corrosive sulfur species such as DBDS attack the copper to create a film of Cu_xS (approx. 2:1 stoichiometry). The Cu_xS layer, otherwise strongly attached to

the surface of copper, is displaced more readily in the presence of oxygen, after the interaction with the bulk surface is broken. Paper retains most of the Cu_xS particles due to their size, explaining why deposits are rarely found confined in the outer layers of paper insulation. Supporting this, the concentration of contaminants on the surface of the paper measured with XPS was higher than that in the bulk measured using EDX (at least in the first stages of the process) This, as already discussed, suggested a process with fast kinetics.

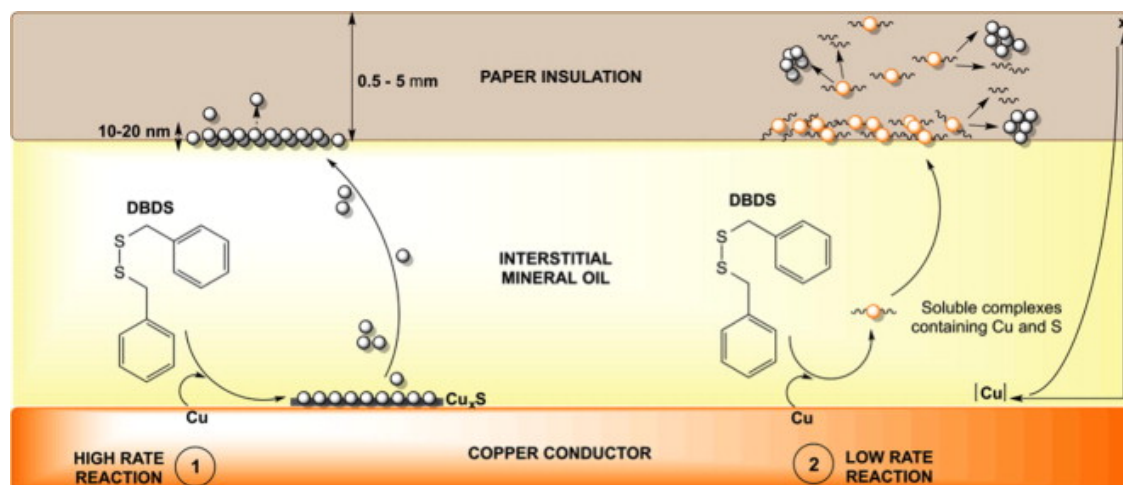


Figure 42 – Schematic representation of the bifurcated mechanisms proposed for: surface contamination (1) and bulk contamination of insulating paper (2).

The second half of the hypothesised mechanism has slower kinetics but is held accountable for the bulk contamination of the paper insulation (0.5-5 mm), experimentally assessed by EDX spectroscopy. Here, corrosive compounds (*i.e.* DBDS) attack copper to form metal soluble complexes that diffuse away from the copper surface into the oil. These species are able to freely diffuse through the oil-impregnated layer until suitable conditions are found for their reaction and decomposition to form copper sulfide deposits, anywhere in the paper insulation bulk. Paper is thought to provide sites for the Cu_xS formation in its bulk as a consequence of the decomposition of complexes.

Despite their intrinsic ability to diffuse, an increased probability of finding suitable nucleation sites for the contaminant crystals is still expected in regions of the insulating paper closer to the copper, as the concentration profile of such complexes is expected to follow an exponential decay with the distance from their source. The observation of deposits, however rare, on outer insulating layers while no traces are found in the inner ones can indeed be explained by this mechanism. In fact, although the likelihood of forming Cu_xS deposits will decrease exponentially with distance from the copper surface

due to dilution phenomena, it will never annihilate thus providing a way to explain the (occasionally found) deposition occurring far from the conductors while closer ones remain unaffected.

3.8 Summary of the chapter and future work

XPS and ESEM/EDX proved to be useful tools to study the process of copper sulfide deposition on insulating Kraft paper, allowing a clear separation between bulk and surface contamination thanks to their complimentary depth resolution. After the development of an optimised procedure to produce large insulating paper sample uniformly contaminated in copper sulfide, the effect of time, temperature, ageing atmosphere and DBDS on the magnitude of the deposition process on paper insulation was investigated. It was found that increase of either temperature ($\leq 140\text{ }^{\circ}\text{C}$) or [DBDS] ($\leq 10000\text{ mg kg}^{-1}$) had a similar effect in increasing the rate of Cu_xS formation, which could be valuable when designing ageing experiments in the presence of unavoidable constraints to the conditions (*e.g.* oils with low flash point). The presence of oxygen in ageing experiments was found implicated in the promotion of detachment and mobilisation of Cu_xS deposits from the copper surface to the inner layer of paper, apparently following a stochastic process. Spectroscopic evidence collected demonstrated the ability of paper to enhance corrosion of copper conductors and copper sulfide deposition on paper insulation, only when in close contact with the metal. As a consequence of this study and the formulation of a new simple bifurcated mechanism, a better comprehension of the nature of the mechanism involved in copper sulfide deposition in insulating mineral oils was achieved.

To conclude, in future experimental work it would be important to start transcending the use of DBDS in order to focus also on other potentially problematic species, developing a more comprehensive, general and flexible theory. Even though DBDS has been so far a useful means of unification of the research effort across the scientific community, it is not likely to be a primary problem for the power industry forever. Industries and technologies evolved very much in the past 20 years and research must also be able to look beyond its immediate needs, trying to the best of its ability to equip for the next challenge.

4. XPS studies on the tolyltriazole corrosion inhibitor layer

Part of the results in this chapter are being considered for publication or has already been published as:

- Facciotti, M.; Amaro, P. S.; Brown, R. C. D.; Lewin, P. L.; Pilgrim, J. A.; Wilson, G.; Jarman, P. N.; Barlow, A. X-ray photoelectron spectroscopy study of the correlation between surface saturation of copper and corrosion inhibition performance in insulating transformer oils. **2015**, *In Preparation*.
- Facciotti, M.; Amaro, P. S.; Brown, R. C. D.; Lewin, P. L.; Pilgrim, J. A.; Wilson, G.; Jarman, P. N. Passivators, Corrosive Sulphur and Surface Chemistry. Tools for the Investigation of Effective Protection. In *MyTransfo 2014: Oil and Transformer*; **2014**; pp. 27–35.
- Facciotti, M.; Holt, A. F.; Amaro, A. P. G. V; Brown, R. C. D.; Lewin, P. L.; Wilson, G.; Jarman, P. N. XPS Study on Direct Detection of Passivator Irgamet 39TM on Copper Surfaces Aged in Insulating Mineral Oil. In *2013 Annual Report Conference on Electrical Insulation and Dielectric Phenomena*; IEEE, **2013**; pp. 1097–1100.

Copyright permission can be found in Appendix B1.

4.1 Aim and outline of the chapter

In this chapter the possible use of X-ray photoelectron spectroscopy in the study of corrosion inhibition of copper conductors in transformer insulating mineral oils is investigated. This work is part of a greater effort trying to identify new analytical tools, previously not considered or perhaps not fully exploited, for the study of corrosion and its inhibition in high voltage oil-filled power transformers. The reasons this technique, XPS, was approached is dual: firstly, it is able to perform non-destructive analysis on solid samples and secondly, it is characterised by a remarkable atomic selectivity and sensitivity (Section 2.6.1). The corrosion inhibitor under study, Irgamet[®]39, could be considered the

only source of possible enrichment in nitrogen atoms on the surface of the copper samples. Therefore, it was thought that N1s signal could be selected as a representative for the presence of the organic corrosion inhibition layer. Once this hypothesis was proved, XPS was used mostly in concentration-dependant studies. These were aimed to assess the optimal amount of Irgamet[®]39 to be used in different oils and some of the physical characteristic of the organic inhibition layers produced under different experimental conditions (*i.e.* estimated thickness, patchiness) in order to ultimately propose an educated recommendation for the most effective application of this corrosion inhibitor in real life. The effects of different non-aqueous inhibition environments (one base oil and three commercial mineral oils), pre-existent corrosive sulfur compounds and added DBDS were also considered, and their significance verified by means of standard corrosion tests.

4.2 Previous applications of XPS to study copper inhibition by benzotriazole derivatives

As already anticipated, the molecular structure of benzotriazole (BTA) derivatives can be easily imagined to be detectable by XPS, despite its limitation to atomic selectivity. As shown schematically in **Figure 43**, the nitrogen content of the active moiety of Irgamet[®]39, an isomeric tolyltriazole, provides a suitable mean of detection with XPS.

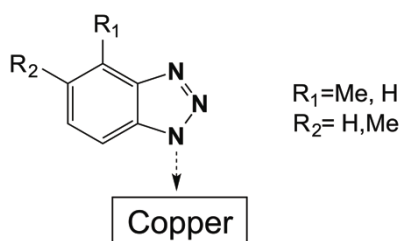


Figure 43 – Graphical highlight of the basis of Cu-adsorbed tolyltriazole detectability with XPS.

There are many literature examples of applications of XPS to the study of copper corrosion inhibition and there are two main reasons for that: Firstly, samples to be analysed usually require relatively minor preparation (if any), often related to the removal of the medium where protection occurred, thus preserving the surface to be analysed. Secondly, corrosion protection itself is a phenomenon that is confined to the surface of a metal, hence particularly suitable to be investigated with a surface-selective technique. There are many examples of the use of XPS to study BTA derivatives on copper and copper oxides in aqueous,^{78,107,109,111,146} hydrocarbon^{26,93,147,148} and vacuum¹⁴⁹ environments. In more recent

years some of this pre-existing knowledge, especially on hydrocarbons and fuel systems, was also rather fragmentally exploited in the topic of corrosion in oil-filled transformers and its inhibition.^{28,47,150,151} However, XPS (as many other surface chemistry analytical techniques) is still far from being considered other than an unconventional technique, if not even exotic, in this field of applied research. This is mostly due to its poor availability in non-specialised/academic laboratories together with its elevated installation and running costs, even without considering the necessity of developing a dedicated expertise for data collection and interpretation.⁶¹ The work detailed in the following sections aimed to assess what was foreseen to be a broader potential range of X-ray photoelectron spectroscopy in this field. This was accomplished by taking advantage of its peculiar ability to pinpoint the presence of the corrosion inhibitor Irgamet[®]39 on the surface of metal samples. Thus, allowing a direct assessment of its status under different experimental conditions, in opposition to the conventional indirect evaluation of oil-mediated analytical information, more easily accessible for a transformer in service, through analysis of the oil.

4.3 Corrosion inhibition in base oil: feasibility, reproducibility and optimisation of the XPS analysis protocol

The first experiments were carried out on inhibited copper samples treated in Base Oil 20. The reason for this choice was the need to optimise the analysis protocol on a reasonably simple and clean system, before moving onto more complex oils. Additionally, reference base oils, like the one used in this study, guarantee a greater consistency in both chemical and physical properties due to their high degree of refining. These preliminary consideration made Base Oil 20 the most appropriate medium for these first tests, aimed to assess the feasibility and reproducibility of the sample production/handling procedure and of the XPS analysis itself.

All experiments in this chapter were designed in order to investigate the characteristic saturation curves of the corrosion inhibitor Irgamet[®]39 (*i.e.* tolyltriazole moiety) on the surface of copper samples treated in different oil environments. To achieve this, a series of metal samples were inhibited in the presence of increasing concentration of Irgamet[®]39. In addition, further modifications of this experiment that will be discussed later on, required the addition of variable amounts of DBDS to simulate corrosivity in otherwise non-corrosive oils. Nominal concentrations used are detailed in **Table 10** and samples were prepared following the procedure described in Section 2.2.

Table 10 – Nominal concentration of the solutions used for the sample preparation for XPS saturation studies.

Solute	Concentration (mg kg ⁻¹)
Irgamet [®] 39	0, 5, 10, 25, 50, 100, 200, 300, 400, 500, 600, 700, 800, 900, 1000
DBDS	0, 25, 50, 100, 200, 300, 400, 500, 600, 700, 800, 900, 1000, 1500, 2000

All copper samples analysed shared very similar XPS spectra, most of the times significantly varying only for the intensity of the characteristic N1s signal. An example of the appearance of the collected XPS survey spectra, highlighting the signal assignment, is shown in **Figure 44**. Copper, carbon, nitrogen and oxygen were the major elements detected on most of the samples. In addition to core electron photoelectric peaks, Auger's transitions for all elements were also observed (for further details see 2.6.1), although not quantified.

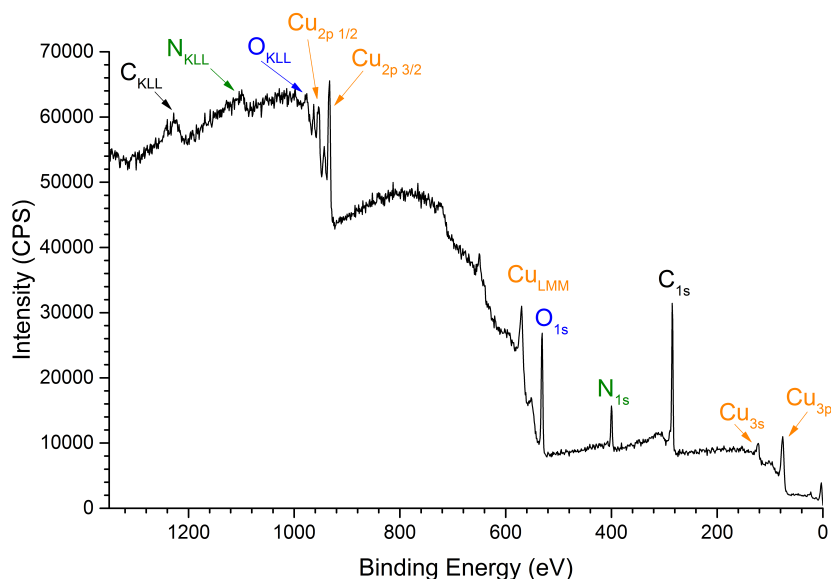


Figure 44 – Appearance of a typical XPS spectrum (and relative signal assignment) of a copper sample treated in the presence of 100 mg kg⁻¹ of Irgamet[®]39 in Gemini X oil.

In the experiments detailed in this chapter the detection of the tolyltriazole inhibitor was carried out taking advantage of the relatively high abundance of N atoms within its structure. The increased nitrogen abundance was expected to cause an increase in the N1s photoelectric peak as a consequence of the corrosion inhibition process of copper samples carried out in oil, as previously reported by Feng *et al.*⁸¹ An example of the impact of the

corrosion inhibitor presence on the surface a copper sample treated in the presence of 100 mg kg⁻¹ of Irgamet[®]39 in Base Oil 20 on an XPS survey spectrum is shown in **Figure 45**.

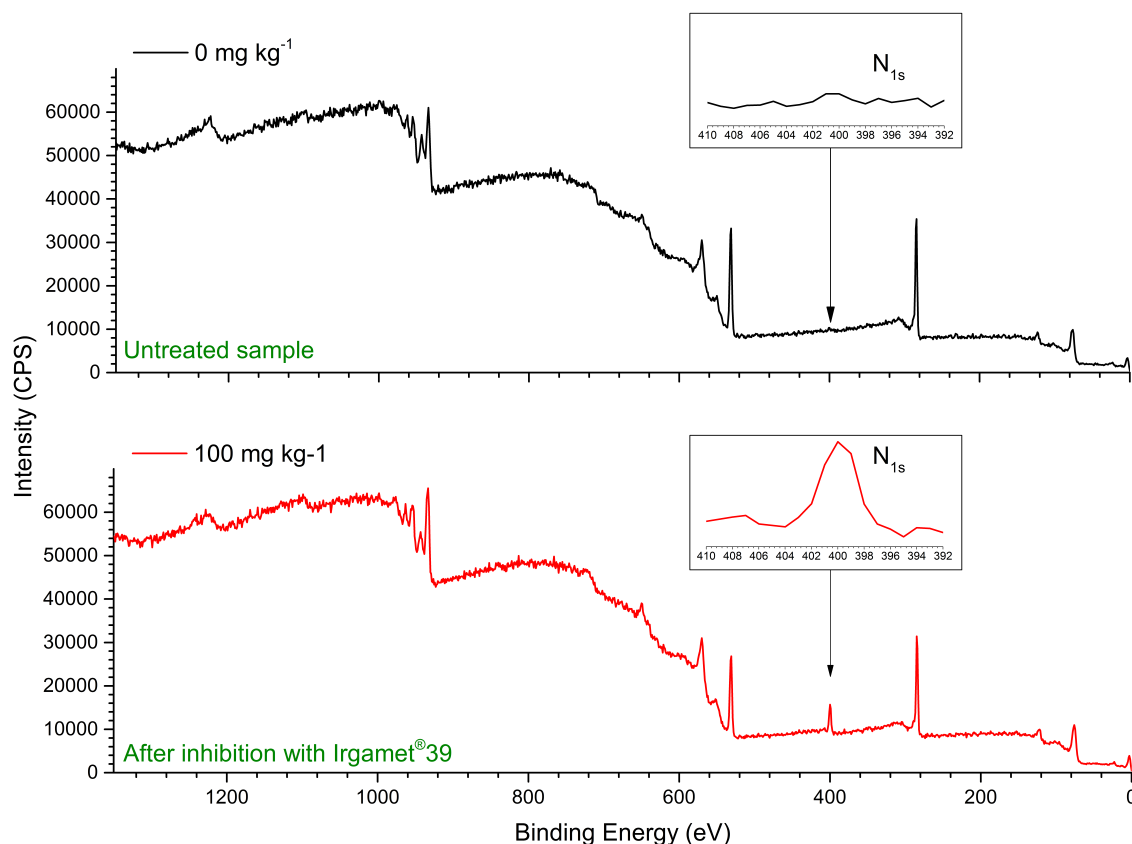


Figure 45 – Example of the typical XPS spectra of a blank copper sample and one treated in the presence of 100 mg kg⁻¹ of Irgamet[®]39 in Base Oil 20. The inset graphs show details of the high-resolution N_{1s} peak.

The addition of Irgamet[®]39 yielded a clear photoelectric contribution of N_{1s}, confirming once again the feasibility of this detection approach. In all cases observed, copper samples showed an excellent nitrogen signal with single photoelectric peak energy, suggesting the presence of nitrogen atoms in a similar chemical environment, as shown in **Figure 46** (left). This was not necessarily expected given the molecular structure of tolyltriazole and the predicted distribution of the delocalised electrons on the heterocyclic moiety, which could have led to expect the presence of at least two nitrogen environments. Confirming this, no *shake-up* features were observed on N_{1s} high resolution peaks, normally generated as a consequence of the interactions between some of the emitted photoelectrons with the delocalised aromatic π electrons. These should in fact appear as small satellite signals at higher B.E. values (*ca.* 7-10 eV above the main photoelectric peak).

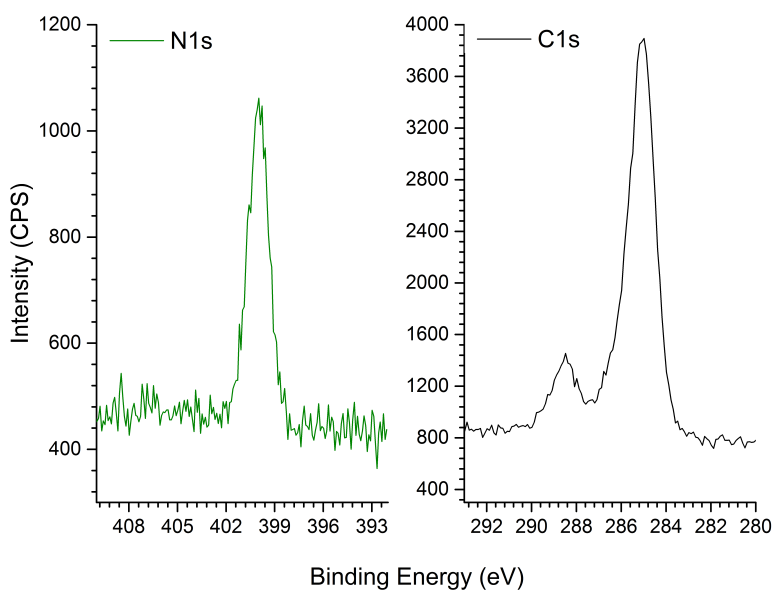


Figure 46 – Example of the typical high resolution XPS spectra of the N1s (left) and C1s (right) peaks on a copper sample treated in the presence of 100 mg kg⁻¹ of Irgamet[®]39 in Base Oil 20.

The absence of these *shake-up* features meant that the atomic selectivity of XPS could not confirm the presence of aromatic nitrogen atoms, otherwise observable using molecular selective techniques such as SIMS.^{79,150–152} The C1s peak however, showed multiple peaks, as shown in **Figure 46** (right), derived from the different chemical environments for the carbon atoms both in the monitored species and the ubiquitous contaminations. These contaminations are always present, as a consequence to exposure to environmental contamination, unless the sample is etched under vacuum to destructively clean its surface prior to the analysis. The characteristic peak position of nitrogen at 400.1 eV was found compatible with tabulated values for related molecules (pyridines ~ 400.0 eV, charged imides ~ 402 eV) and therefore it could be concluded that the energy of the observed signal was reasonable for the N atoms within the tolyltriazole active moiety of Irgamet[®]39.

Interestingly, the viscosity of the oil used during copper inhibition was observed to be of fundamental importance, if not for the inhibition process itself, for the ability to produce easily analysable samples. It has to be specified that Base Oil 20 is named after its viscosity expressed in Poise, namely 20 cP. Its more viscous analogue Base Oil 75 (similarly, 75 cP), was also originally tested as a candidate, but an additional problem led to it being excluded from further studies. As shown in the XPS spectrum of an untreated copper surface exposed to different base oils in **Figure 47**, the simple degreasing procedure used (3 rinses with fresh cyclohexane) was not able to remove all residual Base

Oil 75 from the metal. As a consequence a thin layer of oil, thicker than the maximum depth penetration of XPS, was left on the surface of the metal that became totally undetectable. For this reason Base Oil 75 was abandoned and Base Oil 20 was used for all further experiments, as it was much more easily removed from the metal samples prior to analysis.

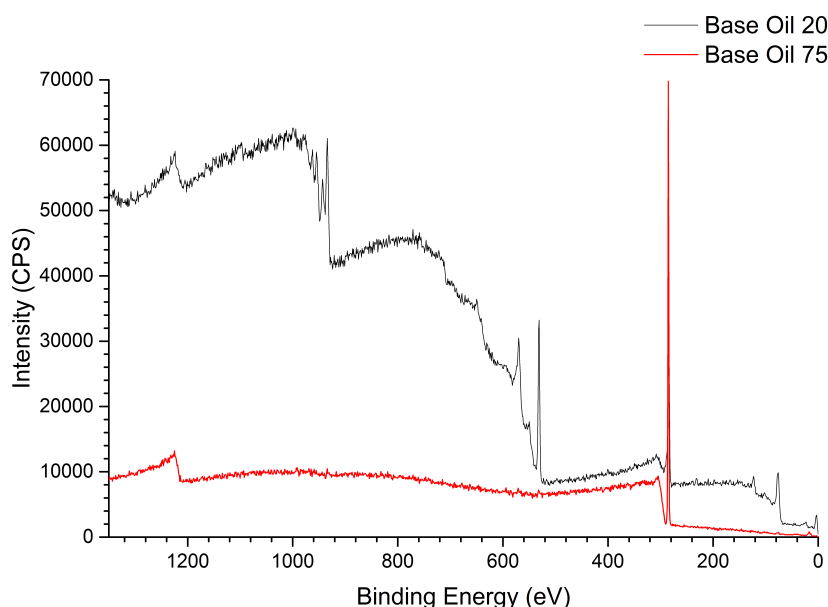


Figure 47 – XPS spectra of a blank copper sample immersed in Base Oil 20 compared to that of a similar sample immersed in its more viscous analogue, Base Oil 75.

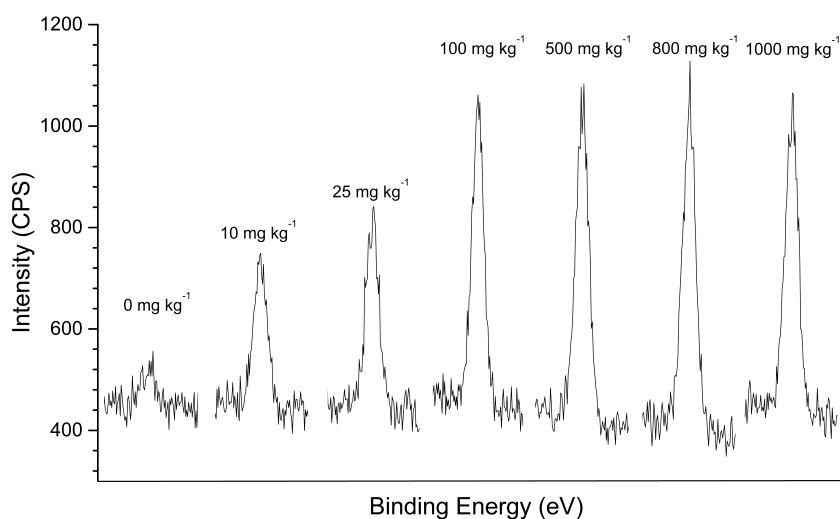


Figure 48 – Example of the typical high resolution XPS spectra of the N1s peak between 395 and 405 eV showing its evolution in the presence of increasing concentrations of Irgamet[®] 39 used for sample inhibition treatment.

Conversely, residual traces of commercial oils were always easily removed by simple solvent rinse of the metal samples. As a consequence, the organic inhibition layer was normally detected together with characteristic copper signals arising from below the layer itself or from exposed areas present during the early stages of the surface inhibition, when the protective layer was still patchy. The effect of the increase in concentration of Irgamet[®] 39 in oil during the inhibition treatment of the copper surface on the high resolution N1s peak is exemplified in **Figure 48**. As originally hypothesised, the intensity of the signal was observed to increase with the concentration of inhibitor used in the treatment of the metal. Once the surface exposed reactive sites have been completely covered in adsorbed tolyltriazole molecules the N1s signal intensity reaches a plateau.

In order to assess this process more quantitatively, raw data as shown in **Figure 48** had to be processed as detailed in Section 2.6.3. As a consequence of data processing all results will, from now on, be reported as normalised areas, dimensionless. The results of XPS experiments for copper samples inhibited in Base Oil 20 environment, investigating repeatability and reproducibility of the procedure, are shown in **Figure 49**.

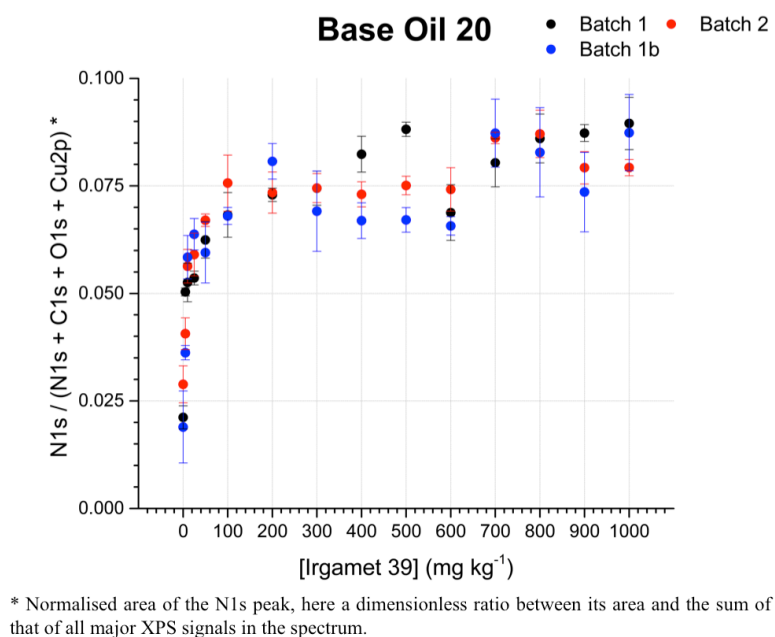


Figure 49 – Comparison between the normalised areas of N1s peak, over 3 repetitions, on copper surfaces treated in Base Oil 20 in the presence of increasing concentrations of corrosion inhibitor Irgamet[®] 39.

In this graph are shown the results of three experiments conducted in Base Oil 20 under the same experimental conditions. *Batch 1* and *Batch 1b* dataset are relative to the very same series of 15 inhibited copper samples treated in base oil environment, albeit analysed one

month apart from one another. Conversely, *Batch 2* dataset was obtained from a duplicated series of inhibited copper samples. The agreement between the three series is remarkable, especially considering the expected grade of cleanness of the surface of the samples. All samples were analysed three times on different regions of their surface and the error bar on each data point shows the calculated standard deviation between the readings. Deviations appeared to be reasonably small, both within and between series, although some discontinuities in the saturation trend were sometimes observed. An example of this occurrence can be found in correspondence with abscissa value of 600 mg kg^{-1} .

The trend observed in all cases reflected, as expected, a progressive saturation of the surface of the metal when treated in oils with increasing amounts of corrosion inhibitor. The values of normalised area of the N1s peak in spectra collected from these samples showed a characteristic trend, which could be separated into two main phases. The first one was characterised by a rapid build up in N1s counts, before the saturation of the metal reactive surface sites was obtained; the second could be assimilated to a plateau. The intersection of these two limiting regimes in the saturation process appeared to be laid between 100 and 200 mg kg^{-1} of corrosion inhibitor Irgamet[®]39 originally present in the oil used to treat the copper samples prior to the XPS analyses. Notably, the scatter of data points seemed to be smaller for *Batches 1* and *2* than that of *Batch 1b*. This increased scattering was originally ascribed to possible oxidative degradation of the organic inhibition layer, exposed to the atmosphere for a month before being analysed. However, before oxidative ageing could be held accountable for this observed deterioration of the samples, further tests were needed to exclude another possible cause of damage of the organic inhibition layer on the copper sample: exposure to radiation. The capability of highly energetic electromagnetic radiation to affect the integrity of organic matter on the molecular scale is a well-known phenomenon, and this case was potentially no exception. As already discussed, *Batch 1b* was analysed previously (*i.e. Batch 1*) and therefore already dosed with a significant amount of X-ray radiation. Results of the experiments aimed to assess the radiation damage potentially inflicted onto the organic inhibition layer formed in oil by Irgamet[®]39 are shown in **Figure 50** and **Figure 51**. In these experiments a high dose of X-ray radiation was used to irradiate the same area of a copper sample treated in the presence of 100 mg kg^{-1} of corrosion inhibitor Irgamet[®]39 in Base Oil 20. Two different radiation density values were tested, modifying the dwell time between the X-ray impulses used, for a total of 20 scans each. In other words, in the presence of a reduced dwell between X-ray impulses, samples have less time to dissipate the incoming energy and therefore they are subject to higher radiation density. The reduced data scattering

observed from 100 ms to 500 ms of dwell time is a direct consequence of this phenomenon.

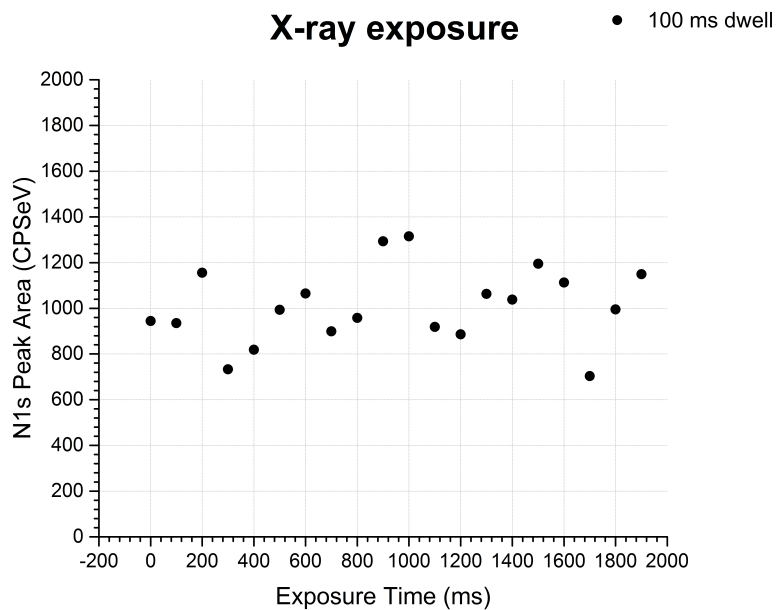


Figure 50 – Measured areas of N1s peak, over 20 repetitions separated by 100 ms of dwell time, on the same region of a copper surface treated in Base Oil 20 in the presence of 100 mg kg⁻¹ Irgamet[®] 39.

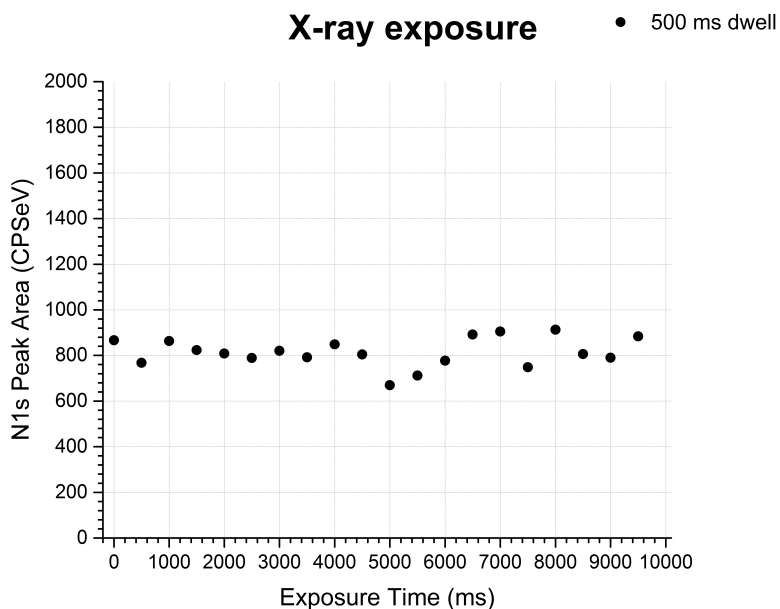


Figure 51 – Measured areas of N1s peak, over 20 repetitions separated by 500 ms of dwell time, on the same region of a copper surface treated in Base Oil 20 in the presence of 100 mg kg⁻¹ Irgamet[®] 39.

As the datasets shown in **Figure 50** and **Figure 51** were originated in the same analysis session and on the very same sample region no normalization of the N1s areas was necessary. In this case, as it can be seen, no significant changes in the detected N1s signal was observed over the course of the experiment. Notably, the radiation dose any of the sample detailed in this thesis was exposed to during XPS analysis was significantly lower than that tested in this experiment. Therefore, it was concluded that mainly oxidative ageing took part in the observed lost of homogeneity of the organic inhibition layer on the copper samples of *Batch 1b* when compared to *Batch 1*. As a consequence, it recommended avoiding any unnecessary prolonged exposure of inhibited copper surfaces to the atmosphere before the XPS analysis could be performed.

It could be concluded that the experiments detailed in this section confirmed the feasibility of producing a semi-quantitative saturation profile of the corrosion inhibitor Irgamet[®]39 on the surface of copper samples treated in oil environments with XPS. Additionally, the reproducibility of repeated measurements was found satisfactory when prolonged exposure to the atmosphere was avoided, while no influence of the radiation dose on the N1s signal arising from the organic inhibition layer was observed.

4.4 Corrosion inhibition in commercial oils: XPS results and their correlation with standard corrosion tests

The study was successfully extended also to commercial insulating oil systems, which were far more relevant due to their application in oil-filled power transformers. As already discussed, saturation curves generated from XPS data were relative to copper samples treated in the presence of increasing amount of corrosion inhibitor Irgamet[®]39 in oil. However, in order to identify a correlation between the measured surface saturation in inhibitor and the effective protection corrosion tests had to be performed to experimentally assess the efficacy of the corrosion protection. To achieve this, 2000 mg kg⁻¹ of DBDS were spiked in all the oil solutions before the inhibition treatment started, so that they would be available as corrosive species during the corrosion tests that followed. XPS results for Gemini X are reported in **Figure 52** (top).

It was immediately noticed how the overall trend resembled the very same saturation behaviour shown in **Figure 49** where, after an initial steep increase in detected N1s signal, a steady saturation was reached between 100 and 200 mg kg⁻¹ of corrosion inhibitor in oil. XPS saturation data collected were then compared to the results of the corresponding

modified standard CCD tests, reported in **Figure 52** (bottom). As anticipated, it was observed that the saturation of at least the most exposed and reactive copper sites was achieved, hence protecting the metal from any further corrosive attacks of DBDS. As it can be visually appreciated, this was in substantial agreement with results from XPS, reinforcing the predicted ability of this technique to assess (by means of the characteristic N1s signal abundance) the presence of tolyltriazole on the surface of copper treated in insulating mineral oils containing Irgamet[®] 39.

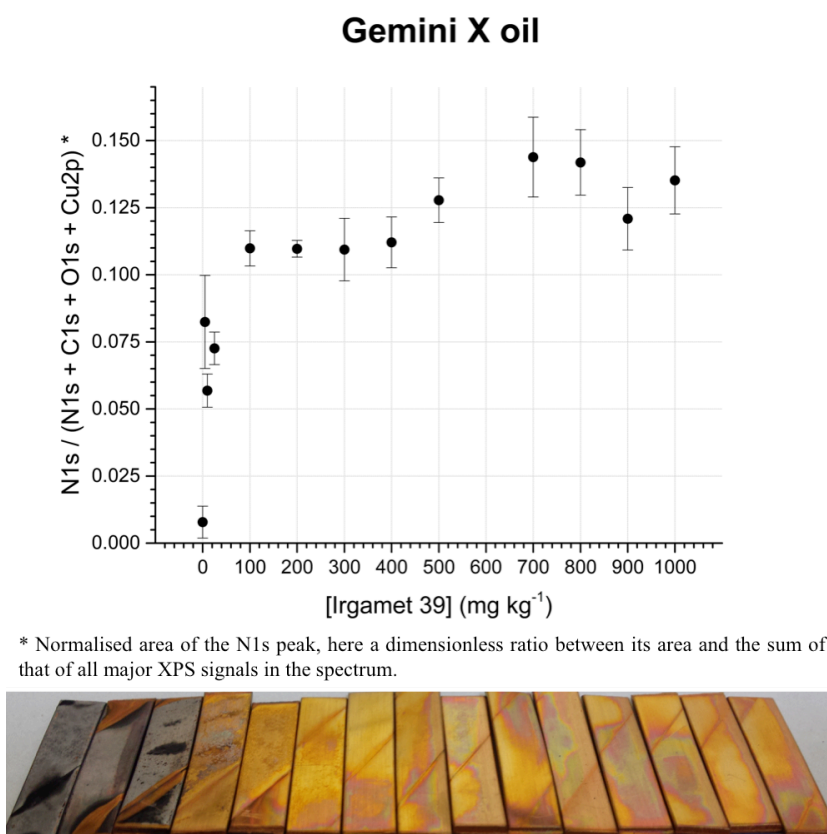


Figure 52 – XPS saturation profile of N1s signal recorded on copper surfaces treated with increasing concentrations of Irgamet[®]39 in Gemini X oil (top) and results of the corresponding modified CCD test (bottom). See Appendix B3 for HD quality pictures.

Similarly, the results for samples inhibited in HyVolt III oil were obtained and they are shown in **Figure 53**. It is worth remembering that Gemini X and HyVolt III oils are fairly similar in their nature, as they both are naphthenic oxidation inhibited oils. For this reason, there was little surprise in finding similar trends in the XPS data of copper samples produced in either one of those oils. However, even though the overall trend looked similar, the standard deviation of repeated measurements appeared to be larger, perhaps suggesting the occurrence of oxidative ageing phenomena of the samples prior to the analysis (as discussed in Section 4.3).

Regarding the correlation between the saturation curve and the results of the modified CCD test, results were consistent with what reported above for samples corrosion inhibited in Gemini X oil. The remarkable peculiarity of the samples treated in HyVolt III oil was an apparently more clear and sudden transition between situations of severe corrosion to extremely satisfactory corrosion inhibition of the copper samples produced by the modified CCD tests. In both cases discussed so far, the most interesting and reassuring observation was (from the point of view of the final users) that the organic inhibition layer proved to be effective even in the presence of very high concentrations of corrosive species (*i.e.* DBDS, 2000 mg kg⁻¹).

Such concentrations are, in fact, substantially impossible to be found in an operating transformer. Normally values as low as 20 mg kg⁻¹ are deemed a warning sign for the health status of the transformer.³⁶ The performance of Irgamet[®] 39 in these conditions were therefore observed to be truly fit for purpose, provided it was present at concentrations of at least 100 mg kg⁻¹ in the oil used to perform the metal inhibition.

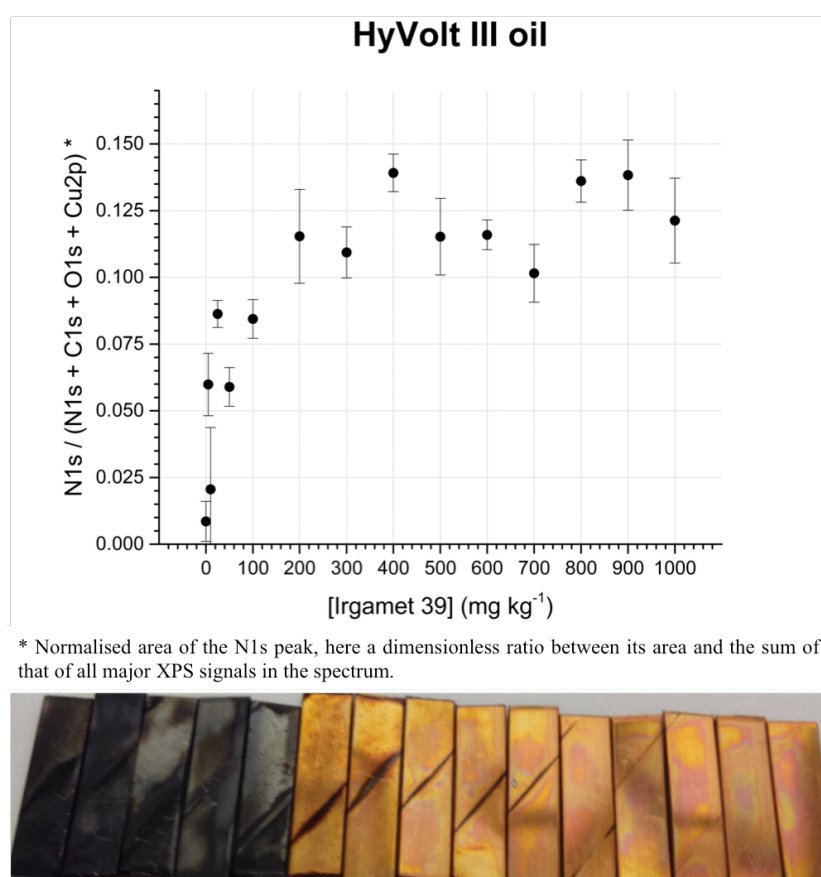


Figure 53 – XPS saturation profile of N1s signal recorded on copper surfaces treated with increasing concentrations of Irgamet[®]39 in HyVolt III oil (top) and results of the corresponding modified CCD test (bottom). See Appendix B3 for HD quality pictures.

Lastly, samples treated with increasing concentration of Irgamet®39 in the uninhibited and corrosive 10 GBN oil were tested in the same conditions. Results of both the XPS experiment and the corresponding modified CCD test are shown in **Figure 54**.

The saturation profile observed did not show huge differences from the ones discussed before other than a less smooth trend and lower intensity counts. However, although the first could be due to some underlying differences in the oils used during the copper inhibition, the latter is most likely to be attributed to momentarily fluctuations in the equipment conditions (*e.g.* vacuum level, X-ray energy) or sample-related issues (*e.g.* bending). In contrast to earlier corrosion tests shown in **Figure 52** and **Figure 53**, the results of the CCD experiment in the presence of additional 2000 mg kg⁻¹ of DBDS show all samples in the series failing the test.

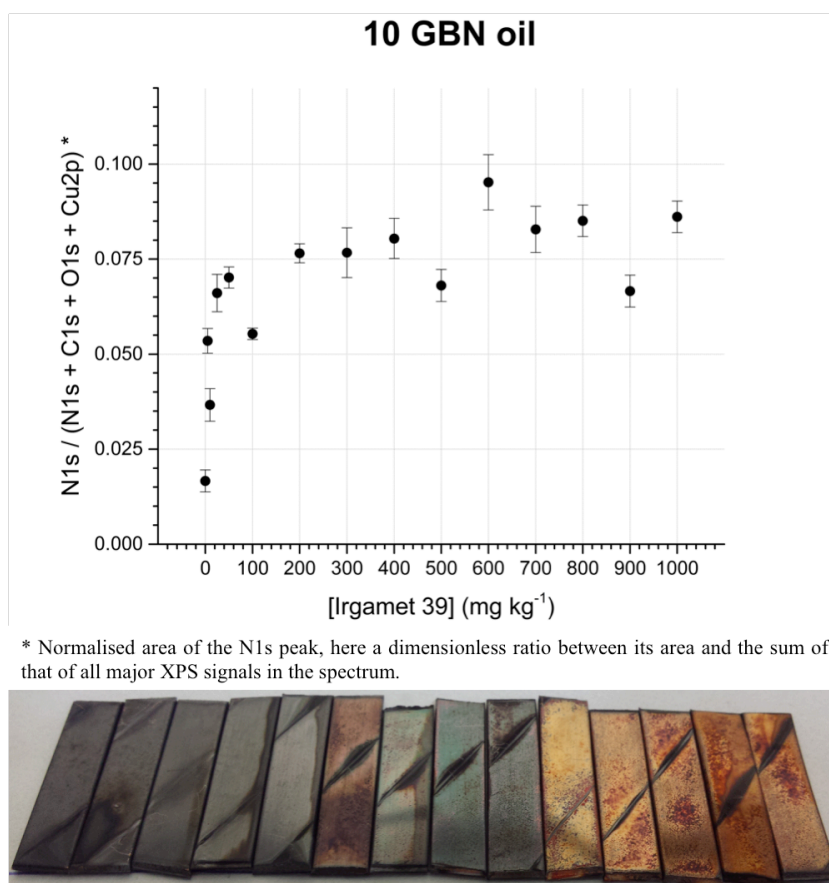


Figure 54 – XPS saturation profile of N1s signal recorded on copper surfaces treated with increasing concentrations of Irgamet®39 in 10 GBN oil (top) and results of the corresponding modified CCD test (bottom). See Appendix B3 for HD quality pictures.

This was a very interesting observation because, even if already agreed that such high concentrations of DBDS are virtually impossible to be found in a transformer in service, copper samples inhibited in the other commercial oils investigated could nonetheless cope

with it remarkably well. The occurrence of another peculiar event is shown in **Figure 55**, where it can be seen how 10 GBN lost transparency, as a consequence of its use in the CCD tests, suggesting that oil oxidative degradation phenomena were occurring.

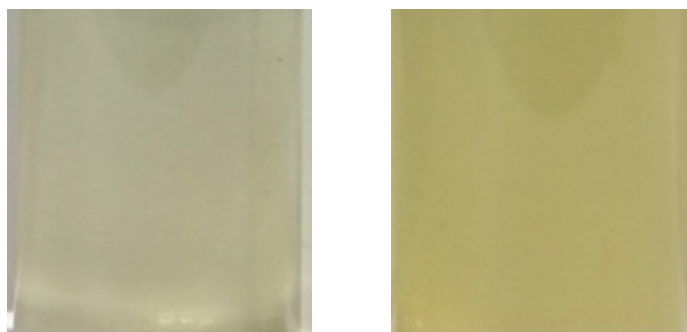


Figure 55 – Change in appearance, colour and transparency, of 10 GBN oil before (left) and after (right) the modified CCD corrosion test as a possible consequence of oxidative degradation.

Thinking of the corrosive nature of the oil itself, a postulation was made trying to explain the observed results. It was thought that, perhaps, a synergistic effect could exist between the added DBDS and the mixture of corrosive compounds already present in the oil matrix in enhancing corrosion of copper even in the presence of above reasonable quantities of Irgamet[®]39. It has to be said that some differences in corrosivity were indeed expected, especially remembering that both Gemini X and HyVolt III were non-corrosive inhibited oils, before being spiked with DBDS. In order to study this hypothesised synergy between corrosive compounds and added DBDS, two more experiments were devised trying to isolate the single contributions to the final observed phenomenon.

Firstly, it was investigated how copper corrosion was affected by the presence of increasing amounts of dissolved DBDS in 10 GBN oil, inhibited at the recommended concentration of 100 mg kg⁻¹. Results of this experiment are shown in **Figure 56** (top). It was observed that, under these experimental conditions, the increase in DBDS in oil did not lead to severely corroded samples as those shown previously in **Figure 54**, until very high concentrations of the corrosive compounds were present. This suggested that, if a synergistic effect did exist, it would be expressed only in the presence of extremely high concentrations of DBDS, although through a mechanism yet to be understood.

Secondly, the inherent corrosivity of the 10 GBN oil was assessed in the presence of increasing concentration of corrosion inhibitor Irgamet[®]39 and results are shown in **Figure 56** (bottom). The observed behaviour throughout the series of copper samples that underwent the corrosion test independently confirmed that Irgamet[®]39, in the absence of

added DBDS, was indeed fully capable of suppressing corrosion phenomena occurring at the metal surface as a consequence of the intrinsic corrosivity of 10 GBN oil.

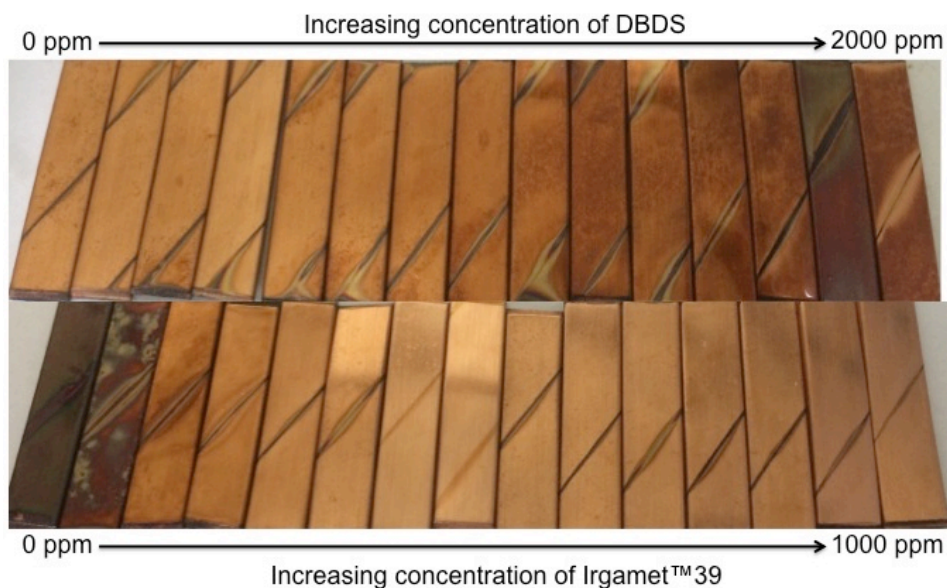


Figure 56 – Results of the modified CCD tests for copper samples treated with increasing concentrations of DBDS in the presence 100 mg kg^{-1} of Irgamet[®] 39 (top) and variable concentration of Irgamet[®] 39 in the absence of DBDS (bottom) in 10 GBN oil.

4.5 Corrosion inhibition in oils: XPS estimation of the organic inhibition layer thickness

As discussed in detail in Section 2.6.3, PARXPS is theoretically able to deliver an estimation of the thickness of the organic overlayer formed by the corrosion inhibitor on copper. Here, this was carried out through the estimation of the IMFP of emitted photoelectrons by means of the TPP2M model. This approach made it possible to evaluate how the thickness of the inhibition layer on the metal was varying with respect to its concentration in both base and commercial oils. This kind of experiment assimilates the development of the inhibition layer on the surface of the metal to two XPS-detectable complimentary phenomena:

1. The attenuation of the background signal of Cu2p photoelectrons as the inhibition layer was being formed.
2. The evolution of characteristic signals arising from the layer itself, in this case C1s and N1s.

Originally, it was planned to use only the nitrogen signal as it is unique and characteristic for the absorbed tolyltriazole molecules investigated, as discussed previously. However, a reduced signal to noise ratio was observed in the high-resolution spectra around 400 eV and therefore also C1s was included for completeness, as it was found to be less affected by this issue. In theory, C1s taken alone could be expected to grossly overestimate the thickness of the layer, due to its ubiquitous presence as an environmental contaminant of all samples exposed to atmosphere. In this case, however, a minimal carbon contamination was detected on the reference uninhibited copper samples before the treatment with the corrosion inhibitor Irgamet[®]39. Results for samples inhibited in base and commercial oils are shown in **Figure 57**, **Figure 58**, **Figure 59**, and **Figure 60**. The overall trend observed when plotting the calculated thickness of the inhibition layer with respect to the concentration of Irgamet[®]39 in both commercial and base oils appeared very similar to that observed in Section 4.3 and 4.4, recalling a saturation profile.

As already anticipated, as a result of the calculations a slightly thicker organic overlayer was expected when estimated by means of the C1s signal. Nonetheless, almost superimposable trends were found for both C1s- and N1s-derived thicknesses while lower scatter over three replicates was found to affect C1s data, as reflected by the error bars. The data scatter was found to be particularly elevated in cases where corrosion inhibitor concentrations were below 100 mg kg⁻¹.

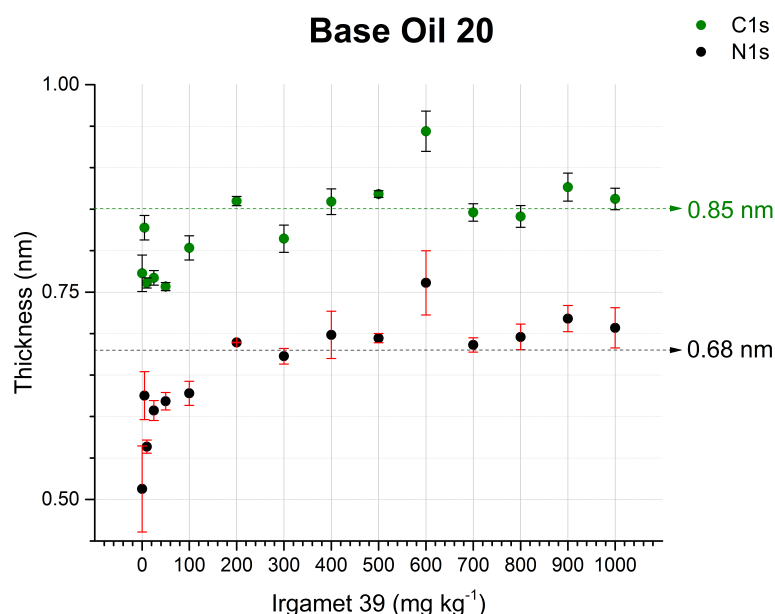


Figure 57 – Calculated thickness profile, based on PARXPS measurements of both C1s and N1s peaks, of the organic inhibition layer formed by Irgamet[®]39 on copper samples inhibited in Base Oil 20.

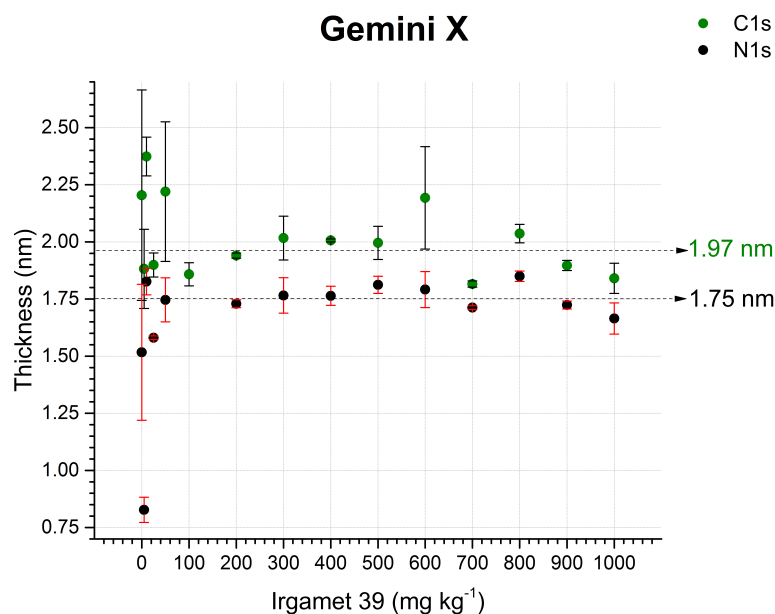


Figure 58 – Calculated thickness profile, based on PARXPS measurements of both C1s and N1s peaks, of the organic inhibition layer formed by Irgamet[®]39 on copper samples inhibited in Gemini X oil.

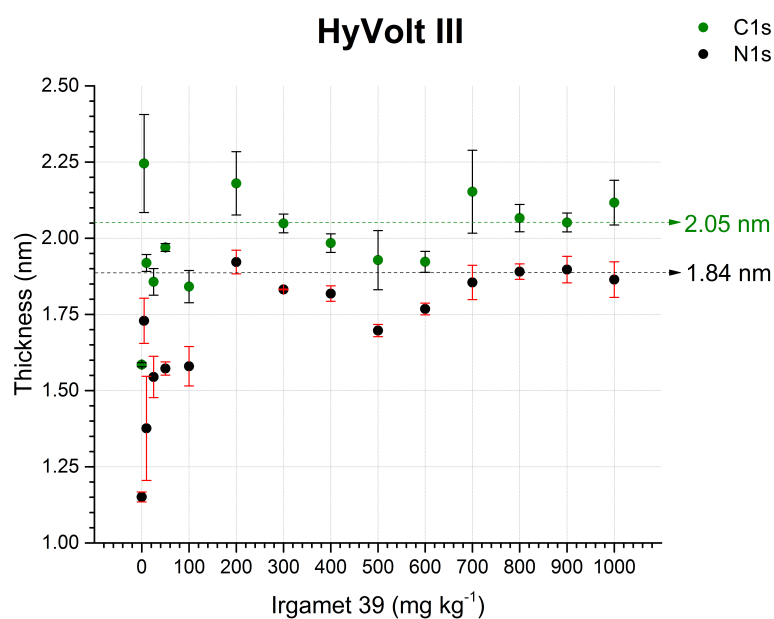


Figure 59 – Calculated thickness profile, based on PARXPS measurements of both C1s and N1s peaks, of the organic inhibition layer formed by Irgamet[®]39 on copper samples inhibited in HyVolt III oil.

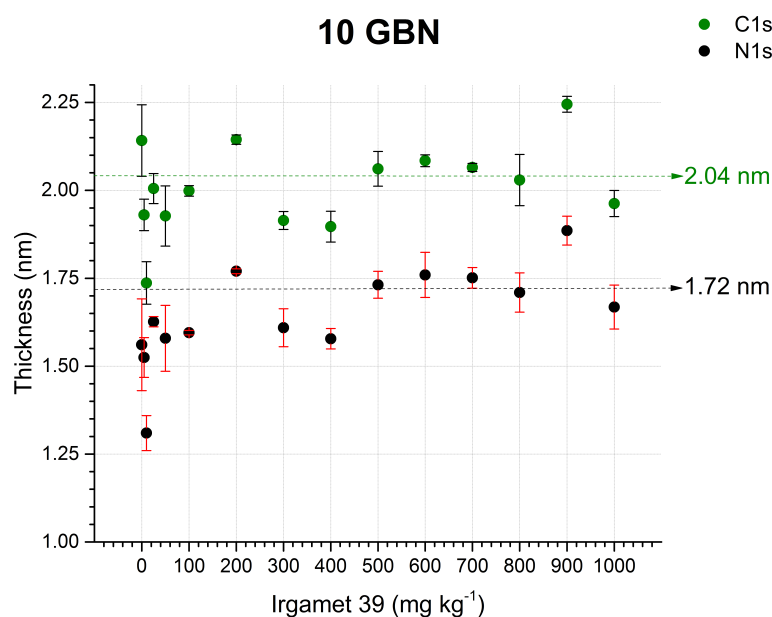


Figure 60 – Calculated thickness profile, based on PARXPS measurements of both C1s and N1s peaks, of the organic inhibition layer formed by Irgamet[®]39 on copper samples inhibited in 10 GBN oil.

The observed data scatter also suggested a lack of uniformity and completeness of the organic inhibition layer in the early stages of development. The patchiness of the inhibitor layer at low concentration of Irgamet[®]39, led to difficulties in the estimation of thickness values. The determination of the thickness, once saturation was reached, was performed by obtaining the intercept value of the linear regression of the saturated region of the data set, namely 200 – 1000 mg kg⁻¹. Results of the calculations are shown in **Table 11**, which contains estimated thickness values at saturation obtained considering either a C1s or a N1s overlayer.

The agreement between the results relative to commercial oils was found to be very good, while a thinner layer was estimated to have formed on the surface of copper samples inhibited in Base Oil 20. Interestingly, despite the results reported in Section 4.4, no significant variations were observed between inhibited (Gemini X, HyVolt III) and uninhibited and corrosive oils (10 GBN), at least in terms of thickness of the protection layers. For commercial oils, the estimated thickness resulted higher than that previously reported in the literature, by around 0.7 nm. However, these values were estimated by means of ellipsometry data, which might have been affected in their processing by the educated, but arbitrary choice of some required parameters such as the refractive index of the organic layer.^{28,79} Moreover, it has to be considered that variations in composition of the oils used might have played a role in changing the observed response.²⁸

Table 11 – Estimated thicknesses of the organic inhibition layer, by means of either the main carbon or nitrogen photoelectric peak, after saturation of a copper surface treated in different oils with Irgamet[®]39.

Insulating oil	Estimated thickness (nm)	
	C1s signal	N1s signal
Base Oil 20	0.8	0.7
Gemini X	2.0	1.8
HyVolt III	2.0	1.8
10 GBN	2.0	1.7

4.6 Practical recommendations consequence of this study

After the XPS experiments had been concluded, in an effort to make an impact on the electrical distribution industry (*i.e.* National Grid) and the broader electrical engineering community with the interesting observations made, a recommendation was formulated on the basis of the results collected. It was suggested that the optimal recommended concentration of 100 mg kg⁻¹ of Irgamet[®]39 in oil might not be sufficient to maintain a satisfactory degree of protection of the copper conductors immersed in corrosive insulating oils. This critical value was indeed observed to represent the lowest possible concentration of inhibitor in oil capable of saturating the metal surface, thus protecting it from corrosion. Although this might therefore seem the most cost-effective solution on the large scale, it was recommended that an increase of the minimum level to 200 mg kg⁻¹ could be a better solution, albeit arguably too conservative. However this would prevent that, should any depletion of corrosion inhibitor content occur in the oil during the operational life of the transformer, its concentration could fall to values below 100 mg kg⁻¹. Such low concentration values could, at least in principle, cause the reduced protection of the metal surface due to the perturbation of the dynamic equilibrium conditions. In other words, a buffering effect could be achieved working in slight excess of inhibitor in the oil, which in turn could greatly reduce the impact of small variations in inhibitor concentration while maintaining the desired protection. Interestingly enough, the impact of such change in operating procedure at the central electricity distribution level was not judged

economically undesirable, as one might perhaps expect while proposing a 100% increase in the amount of an additive to be used. This was due to the fact that, in terms of costs-per-intervention, increasing the amount of inhibitor to be used has a minor impact on the total expenditure that the SO has to account for every time the oil within a transformer requires the addition of corrosion inhibitor

4.7 Summary of the chapter and future work

In this chapter it was demonstrated how X-ray photoelectron spectroscopy (XPS) could be used to detect and quantify the presence of the organic inhibition layer formed in transformer insulating oils by the common tolyltriazole derivative Irgamet[®]39. Thanks to its ability to pinpoint its N-rich molecular structure on the surface of copper, XPS could produce profiles describing the saturation process that the metal underwent once exposed to increasing concentration of the corrosion inhibitor in oil. Although the reproducibility of the results was found satisfactory and consistent with the expected cleanness of the system as a whole, it was found significantly affected by oxidative ageing processes of the samples. The saturation process was shown completed, upon deactivation of the more reactive copper surface sites, when the metal was inhibited in oils with a concentration comprised between 100 and 200 mg kg⁻¹ of Irgamet[®]39. No significant influence on the inhibition process was found correlated to the nature of the oil used to produce the samples however, an interesting synergistic effect was shown to exist between inherently occurring corrosive compounds in uninhibited oils and large amounts (> 1000 mg kg⁻¹) of DBDS. Additionally, an estimation of the thickness of the tolyltriazole-based inhibition layer on copper was performed by means of dedicated XPS data collection and processing, which returned values in good agreement with those previously reported in literature. In particular, it was observed that thicker inhibitor layers were formed on copper surfaces treated in commercial oils when compared to those in base oil. Finally, as a direct consequence of the discussion of the data collected, a practical recommendation for an increase of the concentration of corrosion inhibitor Irgamet[®]39 to be used in transformer oils was formulated.

To conclude, in future work it would be interesting to exploit the imaging capabilities of XPS, although its atomic sensitivity remains its main disadvantage compared to other techniques such as SSIMS imaging. However, the most recent developments in the field of *in operando* XPS analysis,¹²⁵ which allow the study the solution/metal interfaces at

ambient pressure, could pave the way to a complete new way of observing the development of the corrosion inhibition layer as it forms in oil.

5. SSIMS studies on the tolyltriazole corrosion inhibition layer

Part of the results in this chapter have been previously published as:

- Facciotti, M.; Amaro, P. S.; Brown, R. C. D.; Lewin, P. L.; Pilgrim, J. A.; Wilson, G.; Jarman, P. N.; Fletcher, I. W. Static secondary ion mass spectrometry investigation of corrosion inhibitor Irgamet[®]39 on copper surfaces treated in power transformer insulating oil. *Corros. Sci.* **2015**, 98, 450–456.
- Facciotti, M.; Amaro, P. S.; Brown, R. C. D.; Lewin, P. L.; Pilgrim, J. A.; Wilson, G.; Jarman, P. N. SSIMS Molecular Selective Imaging: A New Diagnostic Tool to Investigate Metal Passivators in Scrapped Transformers. In *2015 IEEE Electrical Insulation Conference (EIC)* **2015**, pp. 388–391.

Copyright permission can be found in Appendix B1 and C1.

5.1 Aim and outline of the chapter

This chapter describes the application of static secondary ion mass spectrometry in the study of corrosion inhibition of copper conductors in transformer insulating mineral oils. Particular attention was paid to the description of the surface chemistry of the samples, with the identification of several species (related both to the corrosion inhibitor or the oil environment) that were monitored across a wide range of temperatures under vacuum. The imaging capabilities of this technique were also exploited in order to provide new detailed insight on the thermal desorption processes of topical species. Moreover, desorption experiments on inhibited copper single crystals surfaces were carried out trying to understand how the nature of the metal structure could influence the stability of the organic inhibition layer, as suggested by theoretical calculations found in the literature. Finally, after the imaging technique was tested on laboratory-prepared samples, it was applied for the first time on copper specimens from the windings of a scrapped substation

autotransformer. This helped to understand if such an exotic approach could be applicable and useful in assessing the performance of the corrosion inhibitor Irgamet[®]39 in real life applications.

5.2 Previous applications of SSIMS to study copper inhibition by benzotriazole derivatives in different media

The application of secondary ion mass spectrometry to the study of corrosion inhibitors on metal surface is not new. In fact, this analytical technique was already being exploited in the early 1990's for the study of corrosion inhibitors for stainless steel and other alloys to be used in contact with liquid jet fuels.^{93,114} The interest for benzotriazole and its derivatives came shortly after and spanned a vast variety of technologically relevant metals such as Ag, Ni, Au and, obviously, Cu and its alloys.^{112,113} However, most of the early work (with the important exception of those carried out within the fuel industry), studied the inhibition layers formed in extremely clean and controlled fluid media such as water, simple organic solvents (*e.g.* methanol) or even ultra-high vacuum (UHV). Nonetheless they represented an essential first step for the development of the main technique used in this study, TPD-SSIMS.^{112,153} Some observations of this early stream of research were, in fact, pivotal for the development of the approach detailed in this thesis. Firstly, the work of Brusic *et al.*,¹⁵⁴ which was the first to provide direct experimental evidence of the formation of the Cu^IBTA surface polymer complex on inhibited metals and secondly, that of Oertel *et al.* who was able to study the desorption from copper surfaces of tolyltriazole (TTA) deposited under UHV conditions, reporting a desorption temperature of around 580 K.¹¹² The application of SSIMS to the field of benzotriazole-based corrosion inhibitors to be used in insulating oils has indeed been reported in recent years. Unfortunately, this approach was incapable of attracting much interest from the scientific community, perhaps due to its rather exotic nature, and its exploitation somehow lost drive as the years passed. The first SSIMS experiment on these systems reported in the literature was by Levin *et al.*,⁷⁹ confirming the ability of amino-functionalised tolyltriazole inhibitors (*i.e.* Irgamet[®]39) to adsorb on the copper surface as intact TTA molecules in insulating oils. Similar observations were later confirmed by Wan *et al.* and,¹⁵¹ most recently by our group.^{62,63} However, the literature was found to lack examples of specific applications of TPD-SSIMS and secondary ion imaging that became, therefore, the focus of the research work detailed in the rest of this chapter. In summary, this work was meant to deliver a

more thorough evaluation of what this technique could offer to both chemists and engineers dealing with corrosion inhibition in insulating oils.

5.3 TPD-SSIMS on copper samples inhibited in oil

5.3.1 Quality of the copper surfaces and the oils

The spectra from the reference clean and untreated copper sample showed no evidence of any significant contamination or surface treatment from the manufacturing process and were always consistent with a clean, albeit naturally oxidised copper surface. The spectra from blank samples, exposed to the oil environment in the absence of corrosion inhibitor were always found similar to those from the reference, showing mainly the presence of metallic and oxidised copper species. However, in the case of a copper sample exposed to Base Oil 20 a significant signal intensity due to CN^- and oxidised phosphorus species (PO_2^- , PO_3^-) was also observed along with $\text{Cu}(\text{CN})_2^-$. This peculiar observation of phosphorus species was probably related to the evidence of the presence of the antioxidant Irgafos[®] 168, shown in **Figure 61**, in the oils.

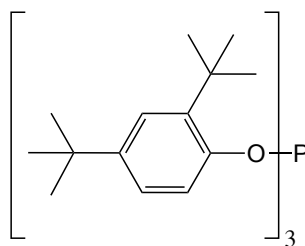


Figure 61 – Molecular structure of tris(2,4-di-*tert*-butylphenyl)phosphite, antioxidant also commercially known as Irgafos[®] 168.

However, the apparent concentration of tris(2,4-di-*tert*-butylphenyl)phosphite in Base Oil 20 was not found significantly larger than in other oils, even though this seemed to have a much more significant impact only on mass spectra of samples treated in this particular medium, as will be discussed later. More details on the observed species and mass assignments can be found in Section 2.7.4. Both positive and negative polarity secondary mass spectra were registered from the oil systems used to perform the copper surface inhibition, by means of Irgamet[®] 39. They were all found consistent with that of highly refined oil products and can be found in Appendix C.2.1-4. Both base and commercial oils showed spectra expected of long chained hydrocarbon liquids, characterised by “un-zipping fragmentation signals” relative to methylene units. For commercial fluids, the peak

corresponding to the average relative intensity distribution for hydrocarbon-like species appeared to be bimodal only for Gemini X oil (370 Da and 480 Da), while it was found to be a single peak for both HyVolt III and 10 GBN oils (390 Da and 410 Da, respectively). Interestingly the spectra of 10 GBN oil were dominated by the presence of Si-based ions, which have a well-known tendency to segregate in the outermost surface of the sample (*ca.* 1 nm) under SSIMS analysis conditions. From the negative spectra assignment, these were shown to be compatible with poly(dimethyl siloxane)-like species and were also observed, although in far lesser amount, in HyVolt III oil spectra.

5.3.2 Secondary ion profiling

Ion profiling was the first possible way of processing and visually deliver the results of variable temperature SSIMS experiments in the most effective and easily interpretable fashion. All the graphs reported in this section show the intensity of secondary ions of interest, as detailed in Section 2.7.4, with respect to the temperature of the sample being analysed. In other words, it was possible to monitor both the nature and the amount of ions desorbed from the copper surface as a function of its increasing temperature under vacuum. Given what was discussed in Section 2.7.3.3 and being the energy of the primary ion cluster beam kept constant, the relative abundance of a secondary ion at a particular temperature could be considered dependent on the strength of the interaction of its parent species with the surface of the metal. Specifically, here I measured the ease in causing its desorption as a consequence of a constant ionisation driving force (*i.e.* primary ion bombardment).

Copper surfaces, inhibited with the recommended concentration of 100 mg kg⁻¹ of Irgamet[®]39 in the same four oil systems detailed in Chapter 4, were analysed using TPD-SSIMS. For each of the samples, a set of profiles of the major secondary ions of interest was obtained between 27 °C and 400 °C and their complete mass assignment is available in Section 2.7.4. Following a methodology similar to that discussed for XPS analysis, samples inhibited in the model Base Oil 20 environment were tested. Once the experimental conditions were optimised, samples inhibited in Gemini X, HyVolt III and 10 GBN oils were tested.

However, in the body of the chapter, it has been chosen to include a selection of plotted results mostly referring to samples exposed to either Base Oil 20 or Gemini X oil. In doing so, the reader is allowed to focus on both the reasoning and the significance of each of the

steps of data processing and discussion, without having to deal with replicate measurements (having perhaps very similar outcomes). Whenever significant differences were observed between the systems investigated, a clear reference was made to the relevant dataset reported in Appendix C. Consequently, when not explicitly indicated otherwise, the discussion was considered applicable to all other samples. Once the sample preparation procedure was established, secondary ions were identified and all the instrument parameters were optimised analysing copper samples based in Base Oil 20, the study could move to the more relevant commercial insulating oil inhibition environments. Results for copper treated in the presence of 100 mg kg^{-1} of Irgamet[®] 39 in Gemini X are discussed below.

To facilitate the discussion of the ion profiles obtained all species were divided in two groups. At first, attention was given to background species or those not directly related to the corrosion inhibitor itself, as shown in **Figure 62** for an inhibited copper sample treated in Gemini X oil. The most intense signal detected was that of CN^- ions, supposedly from fragmentation of the triazole ring of the corrosion inhibitor. As perhaps expected, a steady flow of $^{63}\text{Cu}^-$ ions from the metal substrate was detected throughout the temperature range investigated. On the contrary, the presence of Cl^- ions at temperature below 100°C , most likely from environmental contamination as no other possible source of these species could be suggested, remained a surprising finding.

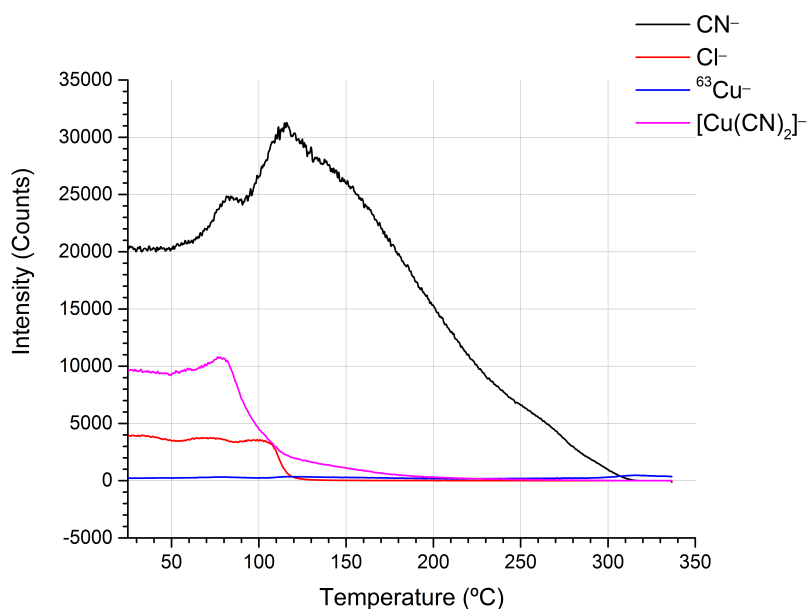


Figure 62 – TPD-SSIMS profiles for Cu^- , Cl^- and $\text{Cu}(\text{CN})_2^-$ on copper treated with 100 mg kg^{-1} of Irgamet[®] 39 in Gemini X at 70°C for 24 hours.

A similar trend was also found for $\text{Cu}(\text{CN})_2^-$, a cyano-complex formed by combination of ionised or excited copper species and organic fragments during the desorption process. This observation was in agreement with the increased desorption rate shown by CN^- ions, above 100 °C, as a consequence of the breakdown of $\text{Cu}(\text{CN})_2^-$ species. CN^- was then found to decrease at temperature above 130 °C, probably due to the depletion in tolyltriazole ions (the hypothesized source of such cyanides) that will be discussed in **Figure 64**.

As already anticipated in Section 5.3.1, significant signal intensity due to oxidised phosphorus species (PO_2^- , PO_3^-) was observed on the surface of copper samples treated in Base Oil 20. An example of the effect that such prominent signals had on the appearance of the same dataset described in **Figure 62** is shown in **Figure 63**. As a consequence of the relative abundance of oxidised phosphorus species and their related complexes, which can be visually appreciated in comparing the ordinate scales, the intensities of the monitored ion signals resulted halved, potentially making the discussion of trends more speculative. Fortunately, such contaminations did not have any effect on the analysed copper samples treated in any of the commercial oils and the intensity of the secondary ions of interest was found high enough to be well-above the background noise.

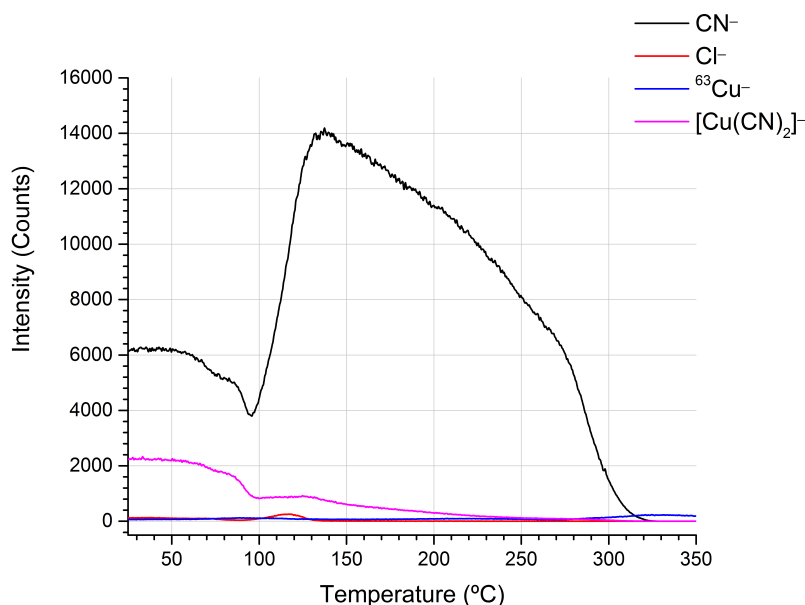


Figure 63 – TPD-SSIMS profiles for Cu^- , Cl^- and $\text{Cu}(\text{CN})_2^-$ on copper treated with 100 mg kg^{-1} of Irgamet[®]39 in Base Oil 20 at 70 °C for 24 hours.

More interesting for the scopes of the experiment were the ions directly related to the tolyltriazole corrosion inhibitor, collected in the dataset shown in **Figure 64**. The

representative ions, in negative polarity mode, for the surface-active moiety of the corrosion inhibitor molecules were: a deprotonated tolyltriazole molecule ($[\text{C}_7\text{H}_6\text{N}_3]^-$, m/z 132), which was also the most abundant species observed in the set for samples treated in commercial oils, and a deprotonated triazole as its main fragmentation product ($[\text{C}_2\text{H}_2\text{N}_3]^-$, m/z 68).

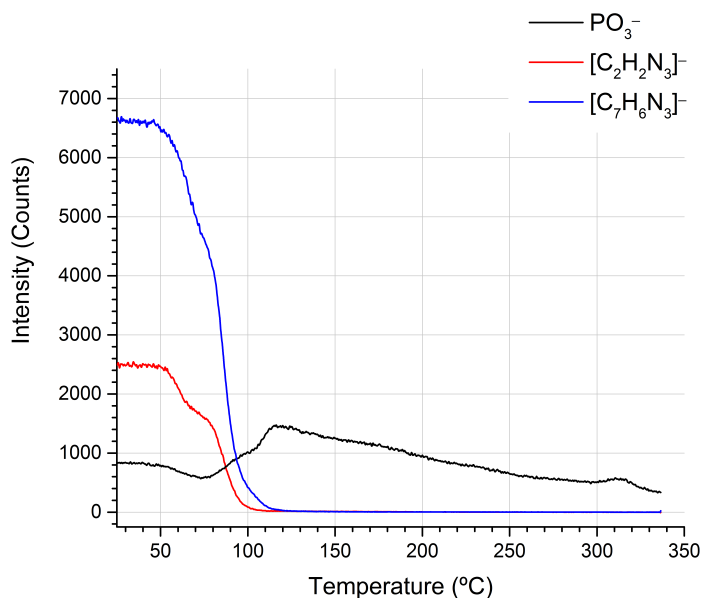


Figure 64 – TPD-SSIMS profiles for representative ions for the corrosion inhibitor and PO_3^- on copper treated with 100 mg kg^{-1} of Irgamet[®]39 in Gemini X oil at 70°C for 24 hours.

As already discussed, metaphosphate ion (PO_3^-), was the predominant ion for samples treated in Base Oil 20, as it can be seen in **Figure 65**, despite being observed also in all mass spectra of commercial oils. This species was indicative of the presence of oxidized phosphorus on the metal surface. The source of these oxidized phosphorus species was hypothesised to be blending of phosphorus-based secondary antioxidants, such as triarylphosphite-based hydroperoxide deactivators commonly used in lubricant and polymer applications.⁸⁸

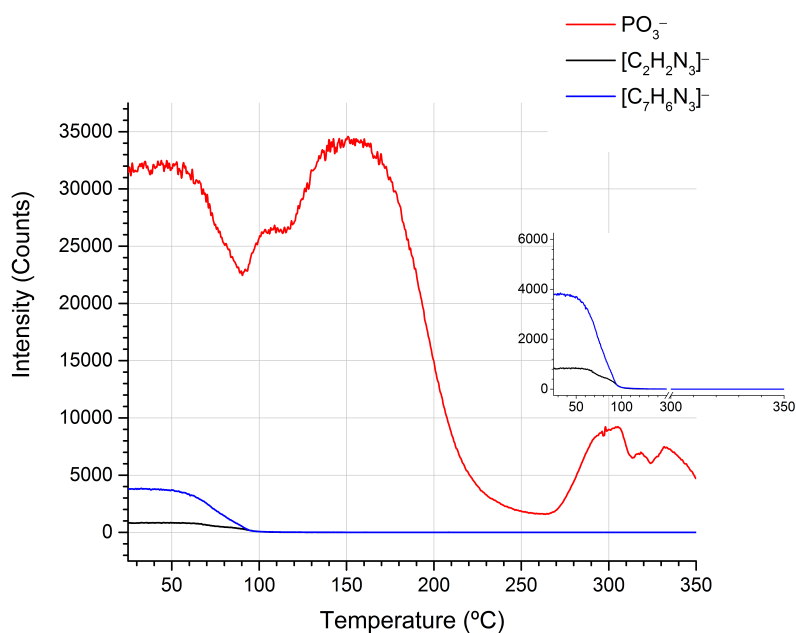


Figure 65 – TPD-SSIMS profiles for representative ions for the corrosion inhibitor and PO_3^- on copper treated with 100 mg kg^{-1} of Irgamet[®] 39 in Base Oil 20 at 70°C for 24 hours (inset showing trends excluding phosphorus contamination).

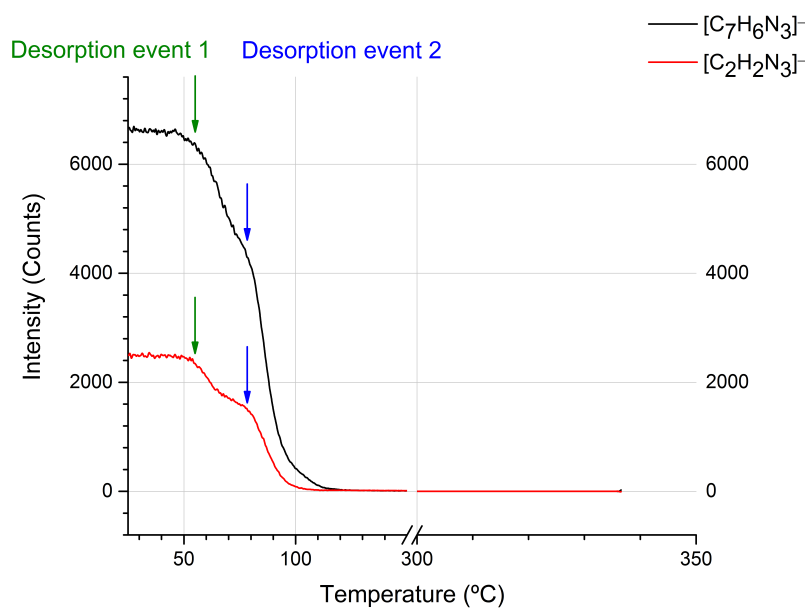


Figure 66 – TPD-SSIMS profiles for TTA deprotonated molecule (m/z 132) and TA ion (m/z 68) on copper treated with 100 mg kg^{-1} of Irgamet[®] 39 in Gemini X oil at 70°C for 24 hours.

This assumption was also supported by evidence of characteristic ions for tris(2,4-di-tert-butylphenyl)phosphite and it was also consistent with the fact that base oil products are subject to more severe hydrotreatment during manufacturing, which destroys any natural inhibition thus making them far more likely to contain larger amounts of antioxidant

additives.¹⁵⁵ Regardless of the source of these oxidized phosphorus species, they were always present on the surface of copper samples following exposure to any of the oils used in this study.

Focussing on the corrosion inhibitor, the deprotonated tolyltriazole species (TTA, $[\text{C}_7\text{H}_6\text{N}_3]^-$), it could be observed how its desorption profile was characterised by a complex nature. For most of the samples, at least two minor events were observable both for this species and the deprotonated triazole fragment (TA, $[\text{C}_2\text{H}_2\text{N}_3]^-$), as shown in **Figure 66**. This fact was interesting as it could indicate the theoretically expected non-equivalence of different copper sites (belonging to different crystallographic facets or having an incomplete coordination sphere), as suggested by computational calculations on single crystal substrates.⁹⁶ It also has to be pointed out that the reproducibility of these measurements, tested on samples treated in the presence of Base Oil 20 was evaluated and found satisfactory, regardless of the presence of the oxidised phosphorus impurities on the metal surfaces. A comparison between two replicate samples is shown in **Figure 67**.

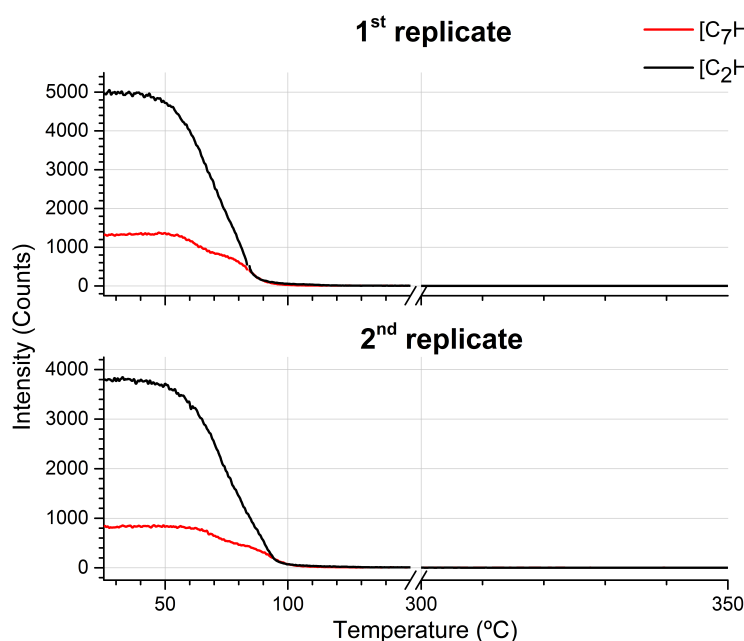


Figure 67 –Stacked comparison between TPD-SSIMS profiles for TTA deprotonated molecule (m/z 132) and TA ion (m/z 68) on copper treated with 100 mg kg^{-1} of Irgamet[®] 39 in Base oil 20 in 1st and 2nd replicates.

As anticipated, a similar behaviour to that discussed above was observed on copper samples treated in the other oils but some more fine distinctions could be made looking closely at the TTA deprotonated molecule profile. A comparison between the corresponding datasets for samples treated in different oil environments is shown in **Figure 68**. Under ultra-high vacuum conditions, the thermal desorption was found completed by

ca. 105 °C for all samples. An apparently reduced stability of tolyltriazole was observed for the layer formed in Base Oil 20, where surface oxidized phosphorus species may have disrupted the normal action of the corrosion inhibitor. Additionally, it is worth specifying that the variability of absolute intensity of secondary ion yield observed between samples in **Figure 68**, resulted from minor variations of instrument operating parameters and the nature of the sample (corrosion inhibitor coverage, topography, composition or oxidation state of the surface) and represented an intrinsic reproducibility limitation of the technique. The relative position of the curves, however, was already shown to be reproducible and therefore a good means of comparison. A more thorough exploitation of these data, after more processing, was nonetheless carried out and will be detailed in Section 5.3.4, as instrumental for the description of estimation of the energy of desorption of the corrosion inhibitor from the metal surface.

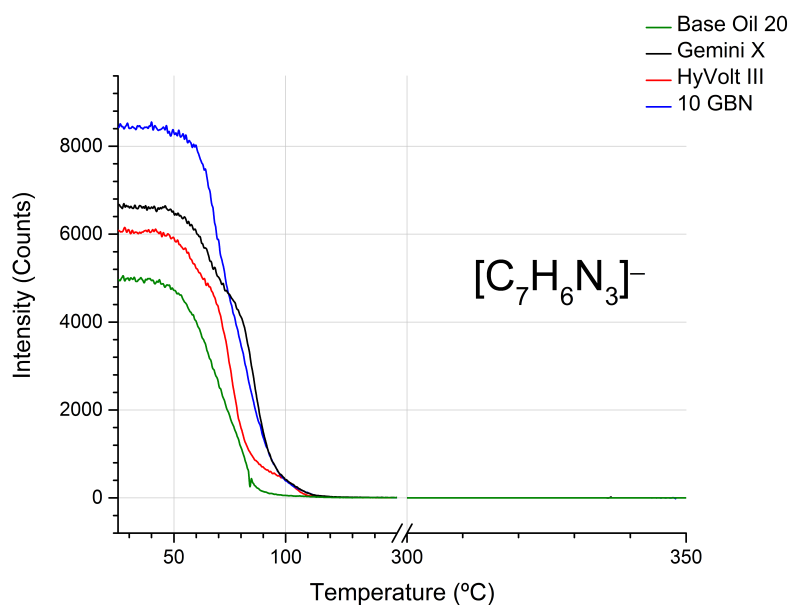


Figure 68 – Comparison of TPD-SSIMS profiles of tolyltriazole negative ion ($[C_7H_6N_3]^-$) for copper samples treated with 100 mg kg^{-1} of Irgamet[®]39 in different oils at 70 °C for 24 hours.

To conclude, it is necessary to reiterate that, obviously, these conditions differed significantly from those within an operational transformer, where equilibrium exists between corrosion inhibitor absorbed on the surface and in the oil. Therefore, the desorption temperatures observed in the TPD-SSIMS must not be directly extrapolated to real transformers but only serve as an indication of the relative thermal stability of TTA on copper surfaces treated in different oils.

5.3.3 Secondary ion imaging

The ability of processing the huge datasets produced by every single SSIMS experiment at variable temperature into colour-coded images was perhaps the most convenient and exciting way of reporting the experimental results collected. Ion imaging made possible the almost unique experience of being able to see the process of the thermal desorption of the inhibitor from the metal surface in ultra-high vacuum conditions. As it is clear that those images do not carry more information than their corresponding datasets, their convenience for the purpose of the discussion of the results was undeniable. In fact, ion imaging provided a visual description of the effect of increasing the temperature of copper upon the corrosion inhibitor layer with an unprecedented degree of detail for these systems. Due to processing software limitations, only a maximum of three secondary ion species could be imaged simultaneously. The reason is that the separate contribution from each species needed to be processed as one of the three available channels (RGB) in order to obtain the final composed image, as described in more detail in Section 2.7.3.2.

5.3.3.1 Visualising the surface coverage

The matrix of imaging results shown in **Figure 69**, represents an example of the conversion of 10 discrete points of a TPD-SSIMS ion profile for $^{63}\text{Cu}^-$ and $[\text{C}_7\text{H}_6\text{N}_3]^-$, taken from the datasets plotted in **Figure 63** and **Figure 65**.

It could be clearly seen that, as soon as the temperature of the metal substrate increased, a progressive destabilisation of the inhibition layer occurred, to leave copper exposed starting from around 100 °C. An identical matrix was generated for each of the samples analysed and can be found in Appendix C.2. 1-4 however, no significant differences could be visually appreciated in these cases. Conversely, ion imaging will be shown later (Sections 5.3.3.2 and 5.3.3.3) to be able to provide invaluable information virtually not extractable from unprocessed datasets. Notably, to avoid any possible misinterpretation of the results, the reader should note that black pixels could appear in the images as a consequence of one or more of these four factors:

- Holes or pits in the sample surface.
- Shadows due to surface topography.
- Relatively low signals and poor counting statistics.
- None of the selected species were actually present.

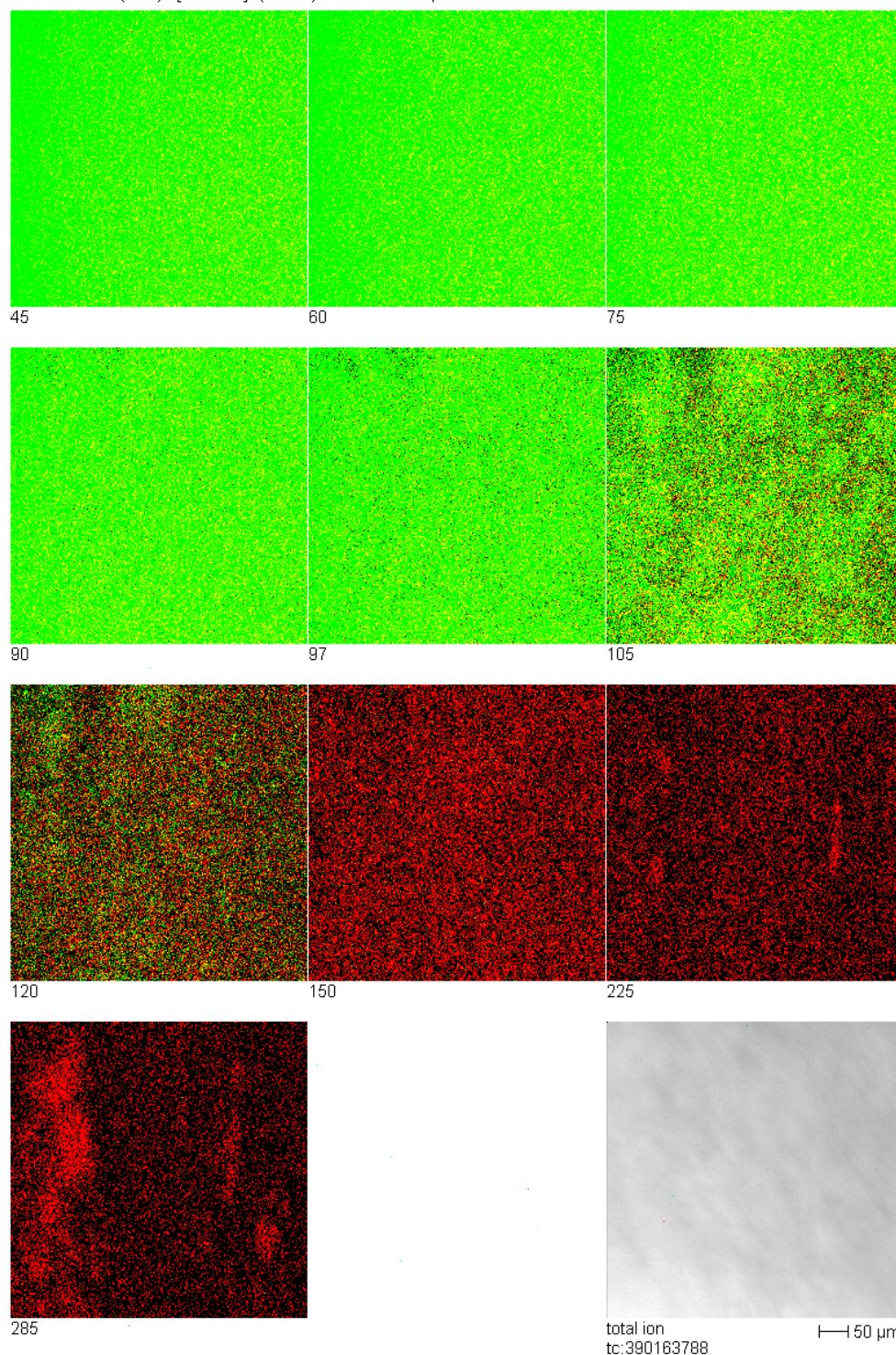
6651G3A Cu- (Red) / [MBTA-H]- (Green) 500.0 × 500.0 μm²

Figure 69 – Negative ion image from 45 °C to 285 °C of Cu (red) treated with 100 mg kg⁻¹ of Irgamet[®]39 (*i.e.* m/z 132, green) in Base Oil 20 at 70 °C for 24 hours.

In an effort to obtain a more quantitative assessment of the desorption process the tolyltriazole deprotonated molecule (m/z 132), its signal intensity between 40 °C and 100 °C was compared to that of the other samples, showing how the coverage in corrosion inhibitor was influenced as the temperature of copper changed, as reported in **Figure 70**. TTA was shown to be most readily desorbed from the sample inhibited with Irgamet[®]39 in

Base Oil 20, where the intensity of the tolyltriazole deprotonated molecule was observed to decrease more rapidly across the temperature range investigated. As already discussed in Section 5.3.2, this observation could be related to the presence of oxidised phosphorus species on the metal surface capable of affecting the corrosion inhibitor layer stability.

The three commercial insulating mineral oils (Gemini X, HyVolt III and the corrosive 10GBN) exhibited similar coverage, although the first appears to have higher corrosion inhibitor coverage in the range 80–90 °C, followed by samples treated in 10 GBN and HyVolt III oils respectively.

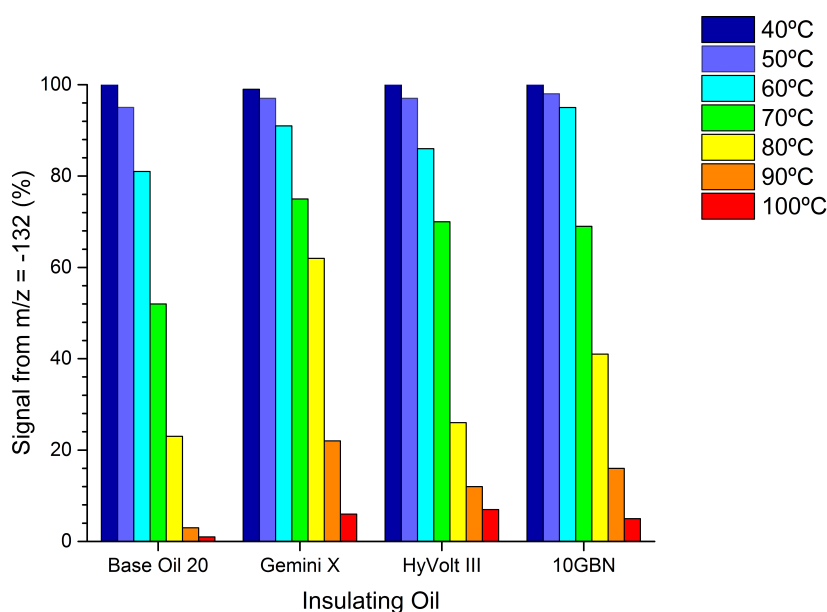


Figure 70 – Tolyltriazole deprotonated molecule (m/z 132) surface signal or corrosion inhibitor coverage variation between 40 °C and 100 °C in ultra high vacuum conditions for samples treated with 100 mg kg⁻¹ of Irgamet® 39, in different oils, at 70 °C for 24 hours.

5.3.3.2 The effect of electrical stresses on the inhibition layer

SSIMS imaging was also applied to investigate whether the development of surface breakdown events on a transformer winding in service was able to cause any damage to the corrosion inhibitor organic layer, hence increasing the probability of the insurgence of corrosive phenomena. It was hypothesised that, since a surface breakdown could deliver phenomenal amounts of energy onto the metal surface, this could be reasonably expected to greatly damage the organic inhibitor layer on the copper surface, striking it with such intensity. Results collected on samples prepared as detailed in Section 2.7.2 are shown below and they substantially confirmed this hypothesis. Firstly, the reference nanowire samples that did not undergo surface breakdown, was analysed and the corresponding ion

imaging results are shown in **Figure 71**. Looking at the intensity of each of the single image feeds separately in **Figure 71 (a, b, c)**, it was possible to observe how the latter, representing the tolyltriazole deprotonated molecule, appeared to be predominant. The appearance of the sample was therefore that of a metal surface uniformly covered by tolyltriazole molecules, which was consistent with a well-inhibited copper surface, at room temperature, not subjected to particular stresses. This could be still visually appreciated in the composed picture in **Figure 71 (d)**, where the contribution from the active moiety of Irgamet[®] 39 was even more striking, since it was able to outshine the signals arising from other two species.

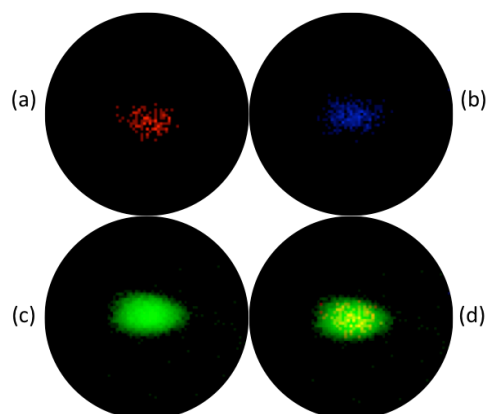


Figure 71 – SSIMS imaging of the section of an inhibited copper microwire (\varnothing 25 μm) embedded in glass showing the separate counts for copper (a), sulfur (b) and tolyltriazole (c) respectively and the resulting composed image (d).

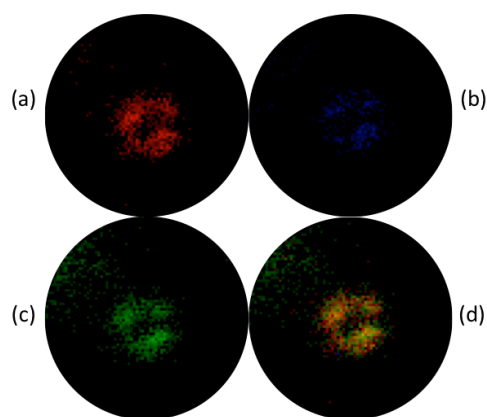


Figure 72 – SSIMS imaging of the section of an inhibited copper microwire (\varnothing 25 μm) embedded in glass and subject to a surface breakdown in oil showing the separate counts for copper (a), sulfur (b) and tolyltriazole (c) respectively and the resulting composed image (d).

However, as a consequence of the repeated surface breakdowns in oil, performed with the setup shown in **Figure 31**, differences in the integrity of the corrosion inhibitor layer on copper could clearly be seen, as shown in **Figure 72**. As expected, as a consequence of the amount of energy released on the surface of copper during the surface breakdown events, the intensity of the ion contribution of TTA detected in **Figure 72 (c)** decreased substantially. On the contrary, more copper ions in **Figure 72 (a)** were detected from the substrate, while sulfur remained substantially unchanged in **Figure 72 (b)**. The composed ion image, shown in **Figure 72 (d)**, once again completed the dataset. Results of this proof of concept experiment clearly showed how the organic inhibition layer could be negatively influenced by electric phenomena occurring on a copper conductor inside an energised transformer. In fact, the localized destruction of the tolyltriazole inhibition layer could pave the way to the development of pit corrosion that could then expand, especially towards the hottest parts of the windings, as will be discussed in the next paragraph.

5.3.3.3 First application of secondary ion imaging as a transformer forensic tool:

The case of a scrapped 400/275 kV substation autotransformer

The aim of this experiment was to show how the unique capabilities of the static secondary ion mass spectrometry imaging could be exploited in the forensic investigation of corrosion phenomena and their inhibition in oil-filled power transformers. The goal was to test the applicability of ion imaging in real life, as a tool to investigate the distribution of both corrosion inhibitor and corrosion by-products inside a transformer in order to link this with either design of the unit or its operating conditions.

As a topical example, the case of a proactively scrapped 400/275/13 kV 1000 MVA autotransformer was reported here. The unit was installed in 1995 and the first addition of corrosion inhibitor (Irgamet[®]39) occurred in 2008, only for the transformer to be finally scrapped in 2012, after 17 years of service. The unit was known to have suffered prolonged overheating of the top discs of the windings, most likely due to design issues and manipulation of thermostat regulations of its cooling fans, as a consequence of noise complaints risen from the neighbourhoods of the substation. Additionally, as a consequence of its inspection after decommission, manufacturing issues such as the misalignment of some insulation blocks were reported.

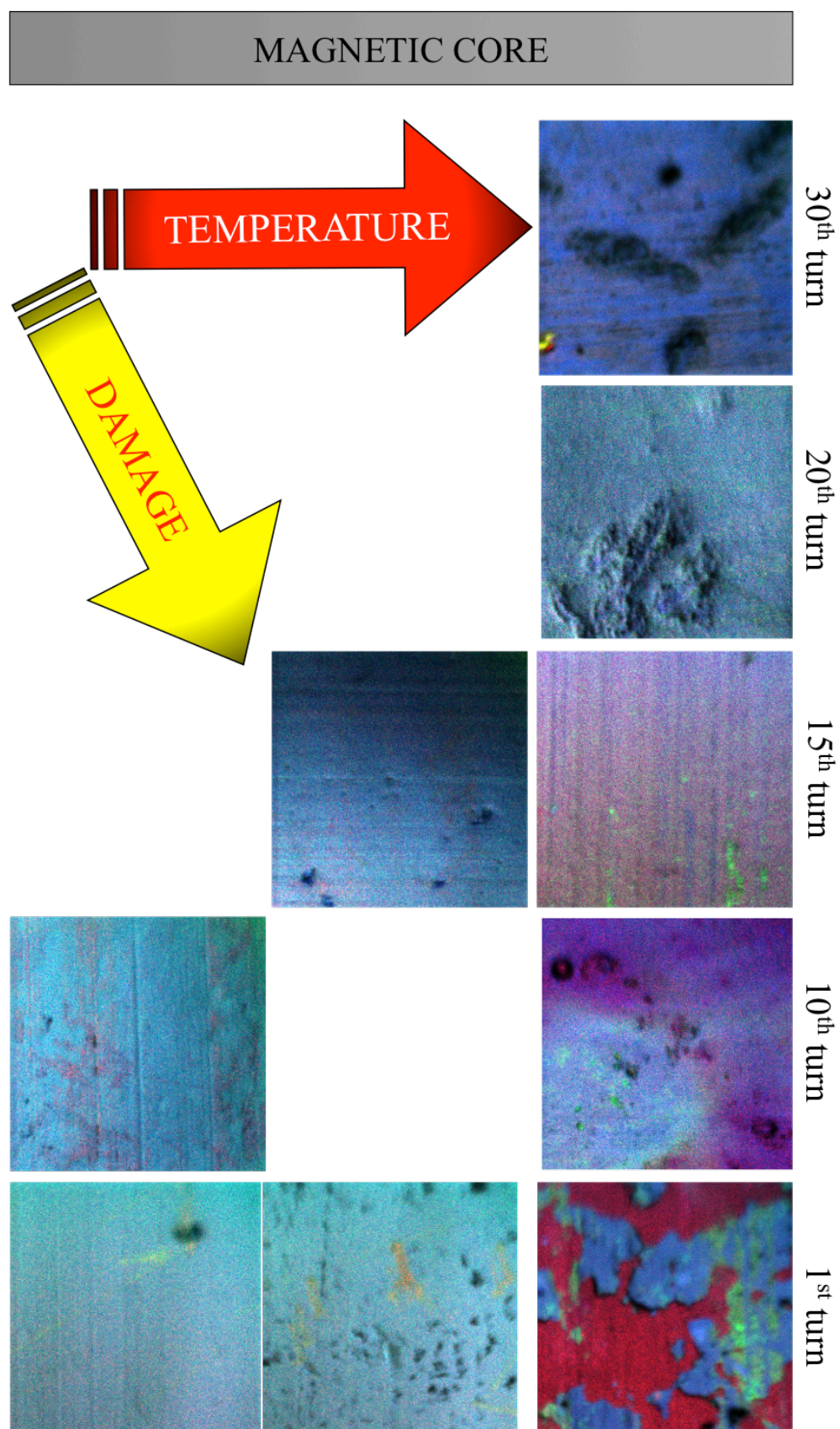


Figure 73 – Sketch showing the distribution of the ion imaging results (Cu, red; S, blue; TTA, green), as a function of the position of the analysed copper samples in the winding, highlighting the correlation between the temperature of the conductor in operation and the integrity of the inhibitor layer.

The consequences of these problems, which led to overall “poor conditions” result according to IEC 60422, are listed below:

- Diffuse corrosion of the top discs of the windings and failed IEC 62535 test.
- Acidity $> 0.1 \text{ mg KOH g}^{-1}$.
- Interfacial tension (IFT) drop from 21 to 17 mN m^{-1} between 2004 and 2006.
- Corrosion inhibitor content after one year (2009) dropped to 16 mg kg^{-1} (– 84%).

Additionally, abnormal paper thermal ageing and increased detected levels of H_2 and CO were observed. A total of nine bare copper samples, collected during the scrapping procedure from different locations within the B phase winding of the unit by Dr H. Ding (Doble Engineering Company) were analyzed to obtain the ion images shown in **Figure 73**.

The main difference between all samples collected was the temperatures to which they were subjected during the operational life of the transformer, which in turn was a consequence of their location in the winding. In fact, it is reasonable to assume that the bottom of an energised winding is generally colder than its top.

The appearance of the metal surfaces from the colder bottom and middle discs were quite similar, as delivered by their rather uniform false turquoise appearance, as a consequence of an optical aberration. This was originated from the mixed contribution of highly dispersed neighbouring green and blue pixels in the final composed image, representing tolyltriazole and sulfur-containing ions respectively. Interestingly, moving towards the magnetic core, more and more sulfur-containing ions were detected.

The samples from the top discs of the windings were, conversely, very different from the others and between each other, suggesting a more complex influence of temperature. No substantial presence of corrosion inhibitor was detected, if not in small areas, suggesting its destruction due to prolonged thermal stresses. The inner regions of the top disc appeared heavily corroded as mostly signal from sulfur-containing ions generated from corrosion by-products was collected. Additionally, no evidence of the copper substrate underneath was detected in this region of the winding, suggesting a well-attached corroded layer. Moving away from the core and towards the edges of the winding progressively more exposed copper was detected, together with minor residual traces of corrosion inhibitor. Finally, the outer region of the top disc seemed to be the most affected by advanced corrosion signs such as exposed copper (potentially vulnerable to further corrosion) and

poorly attached and flaky sulfur-rich formations constituted of corrosion by-products (e.g. copper sulfide).

There could be no doubt in considering this region of the winding as the most probable source of the copper sulfide contamination of the whole insulating system of the unit, as a consequence of the thermal stresses at which the corrosion inhibitor layer was subjected to during the operational life of the transformer, which caused its failure. Moreover, this also confirmed the hypothesised vulnerability of corrosion inhibition in case of prolonged exposure to abnormal high temperatures in units known to have the largest winding temperature gradients.

5.3.4 Energy of desorption calculations

With the term “energy of desorption” (E_{des}) was herein intended the amount energy to be provided to break the interaction between the adsorbed tolyltriazole molecule and the copper surface, which here was considered chemisorption rather than simple physisorption.¹⁵⁶ The results of the energy calculations, details of which are provided in Section 2.7.3.4, for the main desorption events were estimated for copper samples inhibited in different oil environments. This was performed thanks to some further processing of the TPD-SSIMS ion profiles for the TTA deprotonated molecule. As the model used required, it was necessary to extract from the experimental data a value of T_p , which was simply defined as the temperature at maximum desorption rate. A graphical summary of the data processing necessary to extrapolate its value is shown in **Figure 74**.

As a consequence of the sigmoidal nature of the desorption profile, by definition, the maximum rate of change was found as the absolute maximum of the 1st differential of the dataset (*i.e.* minimum, due to the negative sign of the function). However, due to experimental scatter, no peak could be observed as a consequence of differentiation of the raw data, as shown in **Figure 74** (top). Therefore, an optimised curve smoothing protocol was used, as detailed in Section 2.7.3.4, to reduce the data noise at low temperature and expose the sought first derivative plots with the necessary degree of detail, as shown in **Figure 74** (middle). At this point, the characteristic temperature value of T_p was extracted, as it can be seen in **Figure 74** (bottom). The complete collection of graphs showing the same process described here for all samples can be found in Appendix C.2. 1-4. For all samples analysed, E_{des} was calculated by means of the equation below using, the obtained temperature at maximum desorption rate (T_p) and assuming a first order process with absence of intramolecular interactions (*i.e.* low coverage) and re-adsorption.

$$E_{des} = T_p R \left\{ \ln \left[\frac{v_i T_p}{B} \right] - 3.64 \right\}$$

Where R is the molar gas constant ($8.314 \text{ J K}^{-1} \text{ mol}^{-1}$), B is the heating rate ($5 \text{ K min}^{-1} = 0.08333 \text{ K s}^{-1}$) and v_i is the estimated rate constant (10^{13} s^{-1}).

Energy values are shown in **Table 12** and were found to be between 99 kJ mol^{-1} and 103 kJ mol^{-1} , which were in the range of density functional theory (DFT) predicted values for similar systems under vacuum.^{96,157}

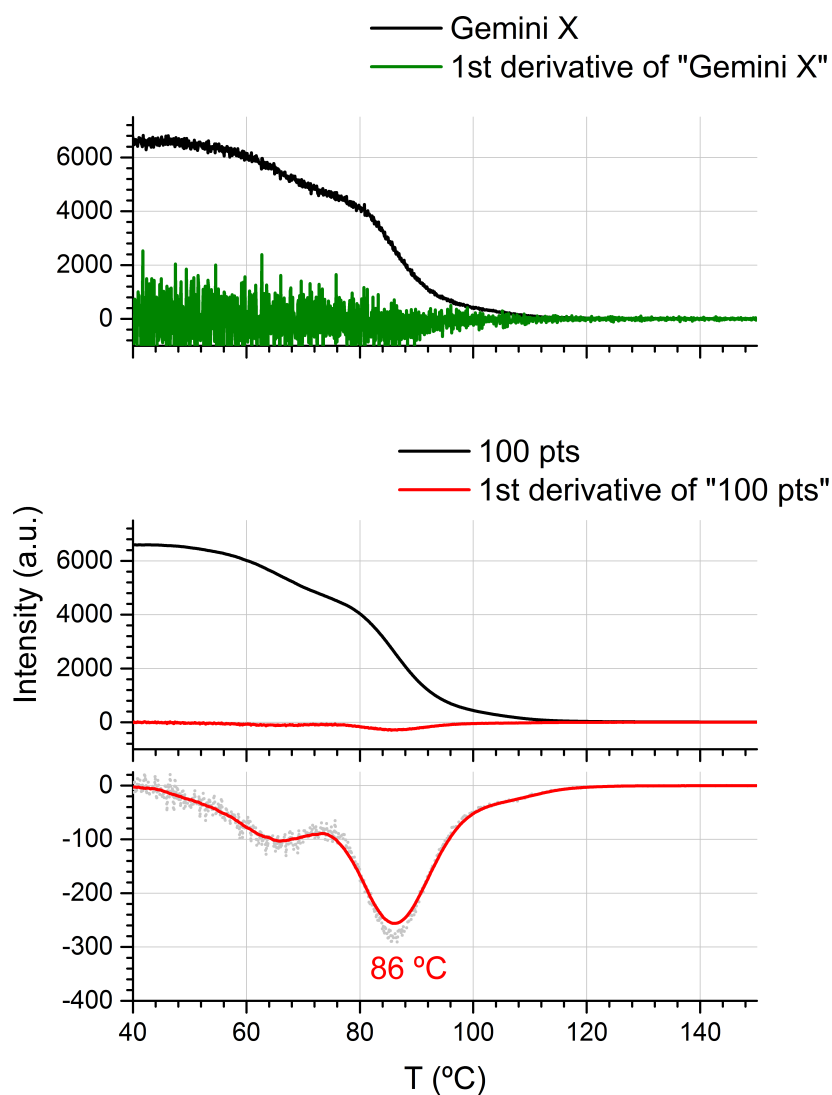


Figure 74 – Summary of the determination of T_p through TPD-SSIMS profiles processing: 1st differential (top) for m/z 132 on copper treated with 100 mg kg^{-1} of Irgamet[®]39 in Gemini X oil at 70°C for 24 hours; adjacent averaging smoothing at 100 points (middle); identification of the absolute minimum in the 1st differential plot (bottom).

Table 12 – Energy of desorption of tolyltriazole on copper inhibited in different oils.

Oil environment	T_p (°C)	E_{des} (kJ mol ⁻¹)
Base Oil 20	72	99
Gemini X	86	103
HyVolt III	76	100
10 GBN	75*	100

* Two comparable minima in the first differential were found therefore an average value was used.

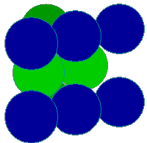
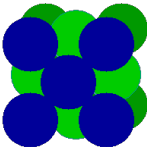
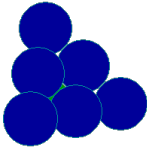
Notably, these energy values were also substantially lower than typical tabulated covalent bond energies such as C–C (347 kJ mol⁻¹), C–N (305 kJ mol⁻¹), C=C (614 kJ mol⁻¹) and N=N (418 kJ mol⁻¹).¹⁵⁸ This was consistent with the occurrence of a non-destructive desorption event rather than molecular decomposition of the adsorbed molecules, which was supported by the observation of tolyltriazole deprotonated molecule (m/z 132) in all experiments that were ever performed. The maximum value was found for the sample treated in Gemini X, while the minimum for that treated in Base Oil 20 however, at least using this simplistic approach to the calculation, the nature of the oil in which the corrosion inhibitor was used had relatively little effect on the calculated E_{des} values. A larger effect would be expected in the case of substantial surface modification and for this reason, in order to estimate the impact of the nature of the copper surface in the inhibition process, experiments on single crystal surfaces were performed and will be detailed below.

5.3.5 The influence of the metal surface on the interactions with the inhibitor: A study on Cu single crystals

Recently Kokalj *et al.*^{96,106} reported that the strength of the inhibitor-metal interaction should be expected to increase with decreasing coordination of surface atoms (due to either defects of crystallographic orientation), thus following the order Cu(111) < Cu(100) < Cu(110).⁹⁶ In this study, BTA molecules were hypothesised to coordinate copper sites with their molecular plane almost perpendicular to the surface and therefore that high coverage could influence the likelihood of unfavourable intermolecular interactions between adsorbed species. Unfortunately, results collected on inhibited copper single crystal surfaces did not show a clear influence of the degree of order of the metal surface on the desorption characteristics of the tolyltriazole molecules. In fact, after the experimental data sets were processed, all the three extrapolated values of T_p were found to be not

significantly different from both one another and that of the previously reported polycrystalline surfaces, as shown in **Table 13**.

Table 13 – Energy of desorption of tolyltriazole on copper single crystals inhibited in Gemini X oil.

Cu surface	Graphical representation	T_p (°C)	E_{des} (kJ mol ⁻¹)
110		76	99
100		72	100
111		74	100

As it can be appreciated below, for an inhibited Cu(100) surface, the same conclusions drawn in Section 5.3.4 for polycrystalline copper surfaces still hold. The possible explanation for this lack of differentiation was therefore postulated: In the absence of particular precautions to prevent the natural atmospheric oxidation of copper samples being handled, it is believed that any fine structural differences could have been masked by the presence of diffuse surface oxidation, which also proceeds with different kinetics on different crystallographic facets (due to their inherent reactivity). The corresponding set of graphs for Cu(110) and Cu(111) can be found in Appendix C.2.5-6.

Notably, when single crystals were used, a more uniform copper signal was collected from the substrate at $T \gg T_p$ and the desorption transition was observed to be less gradual, probably due to the homogeneity in the reactivity of the surface sites, as shown for example in **Figure 75**. Interestingly, the evolution of circular spots with the increasing temperature was observed, which then disappeared as the corrosion inhibitor had desorbed completely. This highly localised phenomenon was tentatively ascribed to contaminated areas that reduced the adsorption of the inhibitor, thus leading to a thinner organic overlayer on the metal. However, it has to be reiterated that no such feature was ever observed on the samples discussed within Section 5.3.3.

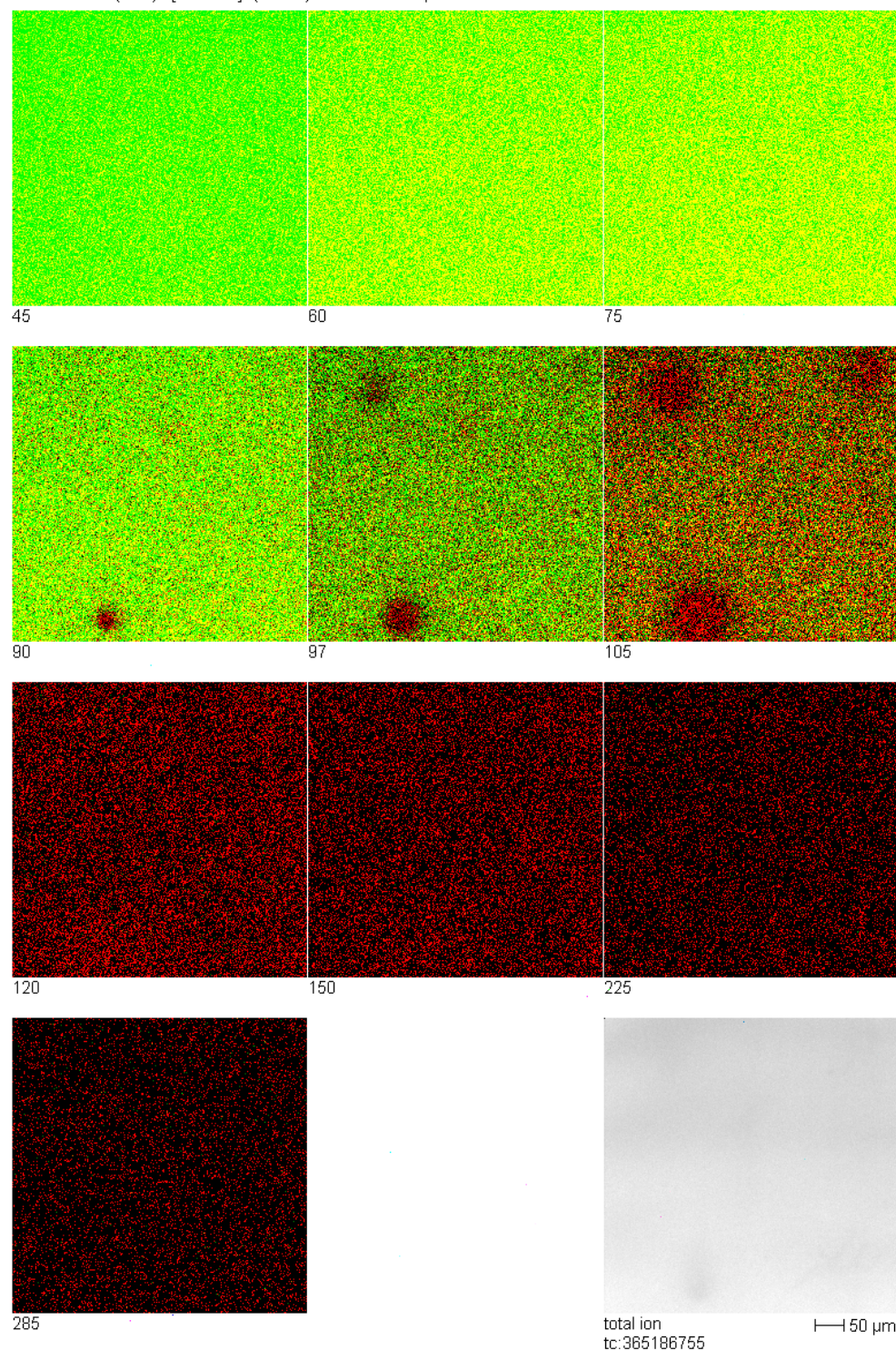
8465E1A Cu- (Red) / [MBTA-H]- (Green) 500.0 x 500.0 μm^2 

Figure 75 – Negative ion image from 45 °C to 285 °C of Cu(100) (red) treated with 100 mg kg⁻¹ of Irgamet[®] 39 (*i.e.* m/z 132, green) in Gemini X oil at 70 °C for 24 hours.

As anticipated, also the shape of the desorption profile for the tolyltriazole deprotonated molecule and the position of the minimum of its 1st derivative representing T_p were found to be remarkably similar to those observed on polycrystalline samples subject to the same analysis, as exemplified in **Figure 76**.

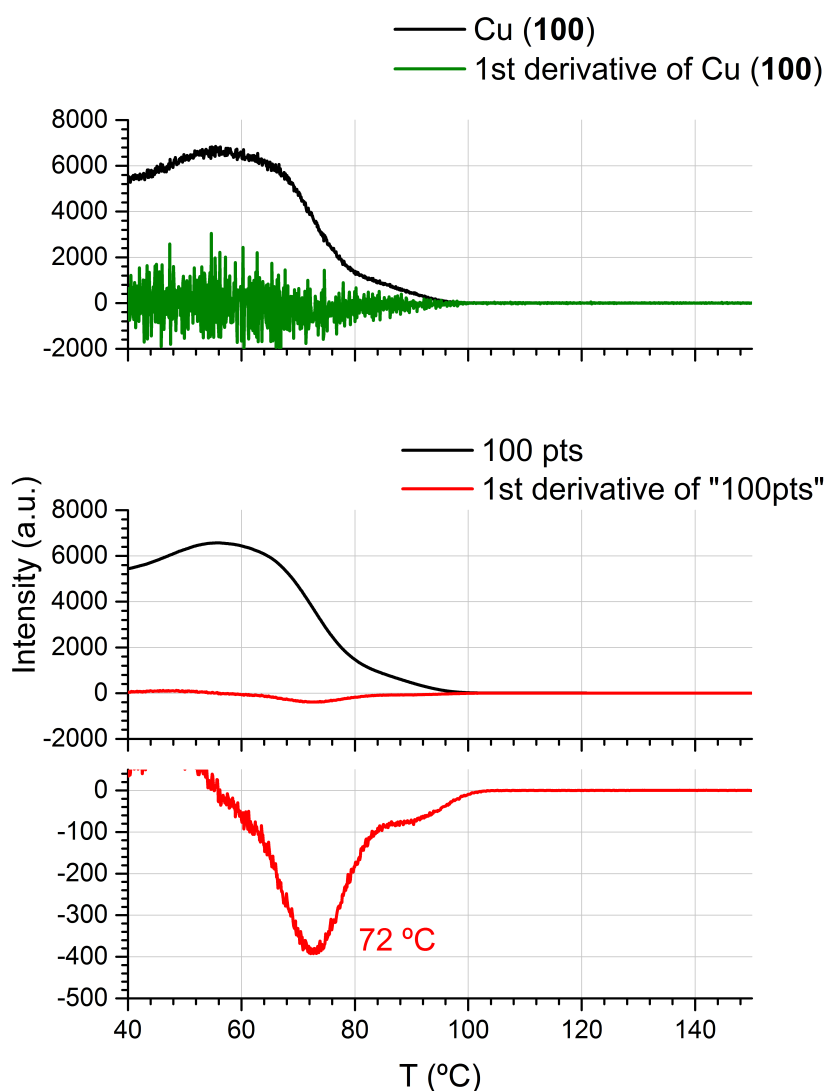


Figure 76 – Summary of the determination of T_p through TPD-SSIMS profiles processing: 1st differential (top) for m/z 132 on Cu(100) treated with 100 mg kg⁻¹ of Irgamet[®]39 in Gemini X oil at 70 °C for 24 hours; adjacent averaging smoothing at 100 points (middle); identification of the absolute minimum in the 1st differential plot (bottom).

5.4 Summary of the chapter and future work

In this chapter it was described how SSIMS was applied to identify molecular species adsorbed at the surface of copper samples that underwent corrosion inhibition with Irgamet[®]39 in insulating transformer oils. The application of this advanced surface analytical technique allowed a more precise description of the chemistry at the surface of copper in the presence of tolyltriazole-based inhibitors in these particular non-aqueous environments. Additionally, it was possible to obtain information on the absolute stability of several adsorbed species, under ultra-high vacuum conditions, across a wide range of temperatures. Interestingly, the observation of the detrimental effect that oxidised

phosphorus (*i.e.* represented by the metaphosphate ion PO_3^-) impurities had on the quality of the metal surface and thus the stability of the interactions with tolyltriazole molecules was also described. Additionally, in depth data processing was reserved for the most relevant species detected, here the deprotonated molecule for TTA (m/z 132) representative of the active tolyltriazole corrosion inhibitor and its major fragment ion TA (m/z 68).

It was observed how the vast majority of species related to the corrosion inhibitor molecule were completely desorbed at a temperature above *ca.* 100 °C, under SSIMS operating conditions. No significant differences in the ion profiles could be seen between commercial oils, however, Base Oil 20 was shown to be affected by the high levels of phosphorus-containing impurities accumulated at the metal surface (apparently able to partially undermine the efficiency of the inhibitor). Ion imaging was also exploited in order to deliver desorption data in a more immediate fashion, allowing a visual qualitative description of the desorption processes together with a more quantitative evaluation of the surface coverage at different temperatures for samples inhibited in different oils. Contextually, it was shown for the first time that SSIMS imaging could indeed provide useful forensic information on decommissioned or failed transformers affected by corrosive sulfur issues. Being able to track the distribution of the corrosion inhibitor and also sulfur-containing corrosion by-products on copper conductors and deliver data as colour-coded images, SSIMS was demonstrated an indubitable aid in understanding the effect of operating conditions on the corrosion inhibition efficacy and integrity.

Finally, thanks to some dedicated data processing it was possible to estimate the energy of desorption, under ultra-high vacuum conditions, for tolyltriazole molecules on copper surfaces treated in different insulating oils that, in all cases, was found around 100 kJ mol⁻¹. Moreover, a more rigorous study on the influence of the nature of the metal surface on the inhibition efficacy was carried out using copper single crystals surfaces. However, at least under the described experimental conditions, it was not possible to observe any significant dependence between the crystallographic facets and the desorption process, although theoretically predicted.

To conclude, possible future work need probably to be towards more applications of SSIMS imaging in forensic investigations of failed transformers in order to provide a more complete and rigorous insight of the chemical processes involving corrosion by-products and the inhibitor, which might in turn drive changes in both use and design of units. It would be interesting to replicate the experiment on single crystals inhibited in oil under

more controlled conditions, in order to possibly link theoretical predictions on the role of the surface reactivity for an efficient inhibition and TPD-SSIMS experimental results.

6. Conclusions

The original aim of this thesis was to increase the understanding of copper corrosion in insulating mineral oils and its inhibition by means of benzotriazole-based corrosion inhibitors, such as Irgamet[®]39. The chosen experimental approach, based on surface analytical chemistry techniques, was selected in order to obtain high quality information on the chemistry of the inhibitor at the metal surface, which was not reported previously in the literature. The main instrumental techniques used were XPS and SSIMS.

As a consequence of the use of XPS coupled with SEM/EDX, it was possible to study the phenomenon of copper sulfide deposition on insulating paper aged in mineral oils with an unprecedented detail. Thanks to a range of experiments performed under variable conditions (*i.e.* ageing time, temperature, oxygen availability and paper-copper proximity), it was possible to conclude that: (1) Oxygen in oil appears profoundly implicated in the promotion of detachment and mobilisation of copper sulfide deposits from the metal surface to the inner layer of paper; (2) Within the ranges investigated, the increase of either temperature or [DBDS] has a similar effect in increasing the rate of formation of copper sulfide; (3) A closer proximity between insulating paper and copper seems to enhance corrosion phenomena, probably due to its ability to concentrate corrosion by-products nearby the copper surface, hindering the efficient mixing of interstitial oil. These results were also formalised as an ancillary contact-based contribution to the overall copper sulfide deposition mechanism proposed by CIGRE WG A2.40. XPS was also exploited in the direct detection and monitoring of the corrosion inhibitor on the copper surface, by means of the exceptional atomic selectivity of the technique towards nitrogen. This approach, together with parallel angle resolved data collection and processing, also afforded an elegant way to estimate the thickness of the inhibition layer on copper, formed in the presence of different commercial mineral oils. Consequently, it was possible to suggest of a new optimal dosage for Irgamet[®]39 in transformers (*ca.* 200 mg kg⁻¹), which was considered to greatly reduce the impact of small variations in inhibitor concentration in corrosive oils, often encountered in real life applications.



SSIMS, thanks to its molecular selectivity, allowed: (1) The identification of molecular species closely related to the corrosion inhibitor on the surface of copper samples treated in different commercial mineral oils; (2) The confirmation of their nature, which also supports the proposed mechanism of action of this class of inhibitors and, subsequently, (3)

their thermal stability under ultra-high vacuum conditions, by means of desorption studies. Remarkably, dedicated data processing afforded easily interpretable secondary ion imaging, which helped visualising the desorption process of the corrosion inhibitor, occurring at *ca.* 100 °C under these conditions. The same imaging protocol was also successfully exploited in the study of the detrimental effects of electrical breakdown stresses on the inhibition layer and as a forensic tool, to help the assessment of its integrity in different regions of the copper windings a failed, decommissioned transformer. Interestingly, it was indeed possible to link the health status of the corrosion inhibitor layer with thermal stresses at which the copper conductors had been subjected during their years of service, thus demonstrating the incredible practical potential of a rather unconventional analytical tool.

Appendices

Appendix A

A.1 Copyright permission of reuse





Home

Account Info

Help

Live Chat



Title: Contact-based corrosion mechanism leading to copper sulphide deposition on insulating paper used in oil-immersed electrical power equipment

Author: Marco Facciotti, Pedro S. Amaro, Alex F. Holt, Richard C.D. Brown, Paul L. Lewin, James A. Pilgrim, Gordon Wilson, Paul N. Jarman

Publication: Corrosion Science

Publisher: Elsevier

Date: July 2014

Copyright © 2014 Elsevier Ltd. All rights reserved.

Logged in as:
Marco Facciotti

Account #:
3000897539

LOGOUT

Order Completed

Thank you very much for your order.

This is a License Agreement between Marco Facciotti ("You") and Elsevier ("Elsevier"). The license consists of your order details, the terms and conditions provided by Elsevier, and the [payment terms and conditions](#).

[Get the printable license.](#)

License Number	3663010901996
License date	Jul 06, 2015
Licensed content publisher	Elsevier
Licensed content publication	Corrosion Science
Licensed content title	Contact-based corrosion mechanism leading to copper sulphide deposition on insulating paper used in oil-immersed electrical power equipment
Licensed content author	Marco Facciotti, Pedro S. Amaro, Alex F. Holt, Richard C.D. Brown, Paul L. Lewin, James A. Pilgrim, Gordon Wilson, Paul N. Jarman
Licensed content date	July 2014
Licensed content volume number	84
Licensed content issue number	n/a
Number of pages	8
Type of Use	reuse in a thesis/dissertation
Portion	full article
Format	both print and electronic
Are you the author of this Elsevier article?	Yes
Will you be translating?	No
Title of your thesis/dissertation	A surface analytical chemistry approach to copper corrosion and its inhibition with benzotriazole derivatives in oil-filled power transformers
Expected completion date	Nov 2015
Estimated size (number of pages)	180
Elsevier VAT number	GB 494 6272 12
Permissions price	0.00 USD
VAT/Local Sales Tax	0.00 USD / 0.00 GBP
Total	0.00 USD

[ORDER MORE...](#)
[CLOSE WINDOW](#)

Copyright © 2015 [Copyright Clearance Center, Inc.](#) All Rights Reserved. [Privacy statement](#). [Terms and Conditions](#).
Comments? We would like to hear from you. E-mail us at customer@copyright.com

A.2 ESEM micrographs of aged paper samples

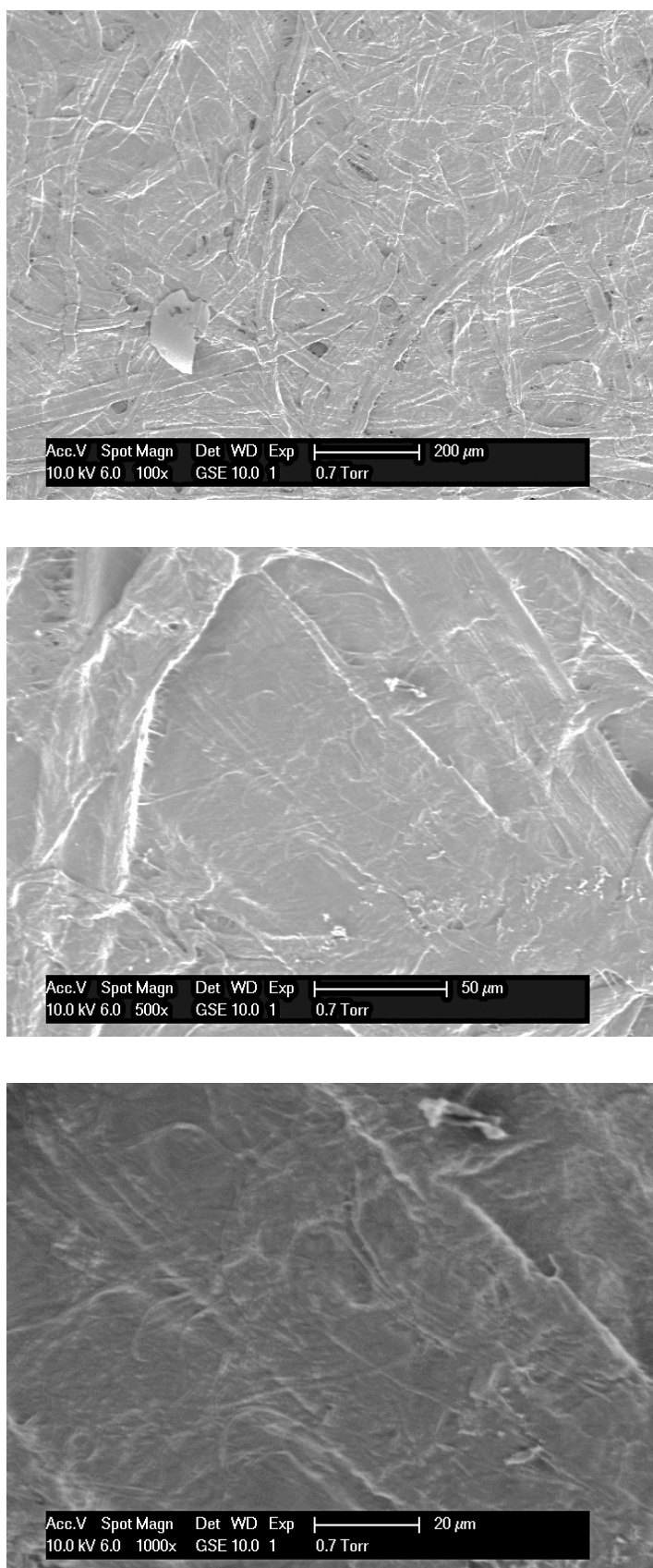


Figure A77 – Micrographs of paper sample at 100 x, 500 x and 1000 x magnification (7 days, 140 °C, 2000 mg kg⁻¹ DBDS, Air atmosphere, 1st replicate).

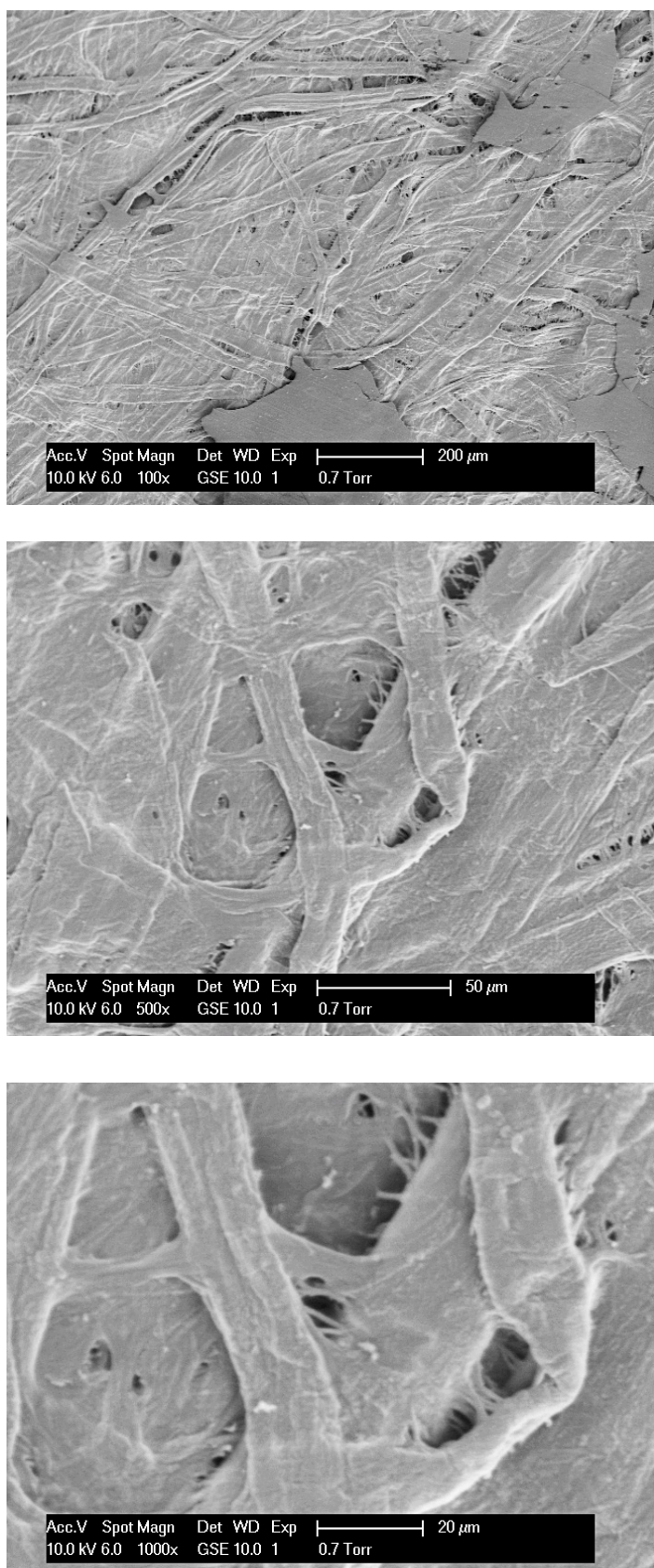


Figure A78 – Micrographs of paper sample at 100 x, 500 x and 1000 x magnification (7 days, 140 °C, 2000 mg kg⁻¹ DBDS, Air atmosphere, 2nd replicate).

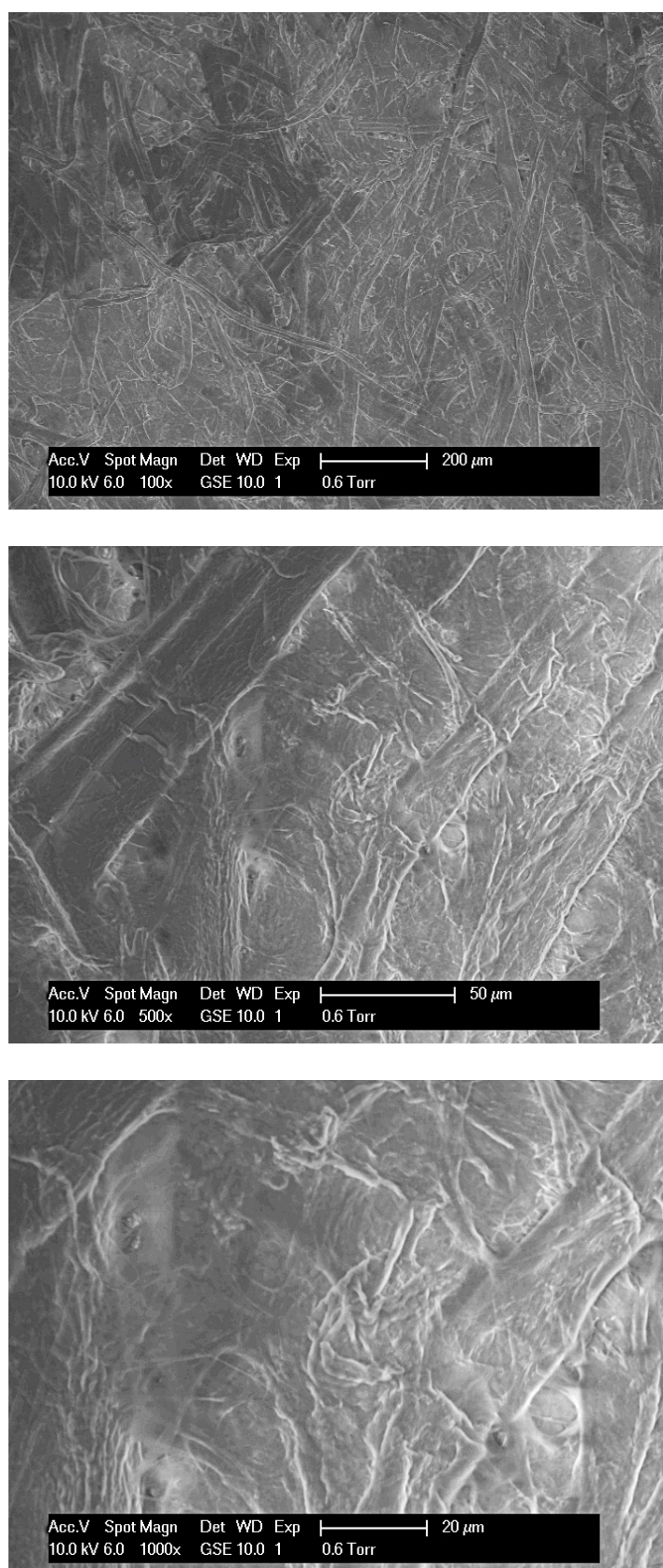


Figure A79 – Micrographs of paper sample at 100 x, 500 x and 1000 x magnification (1 day, 140 °C, 2000 mg kg⁻¹ DBDS, Air atmosphere).

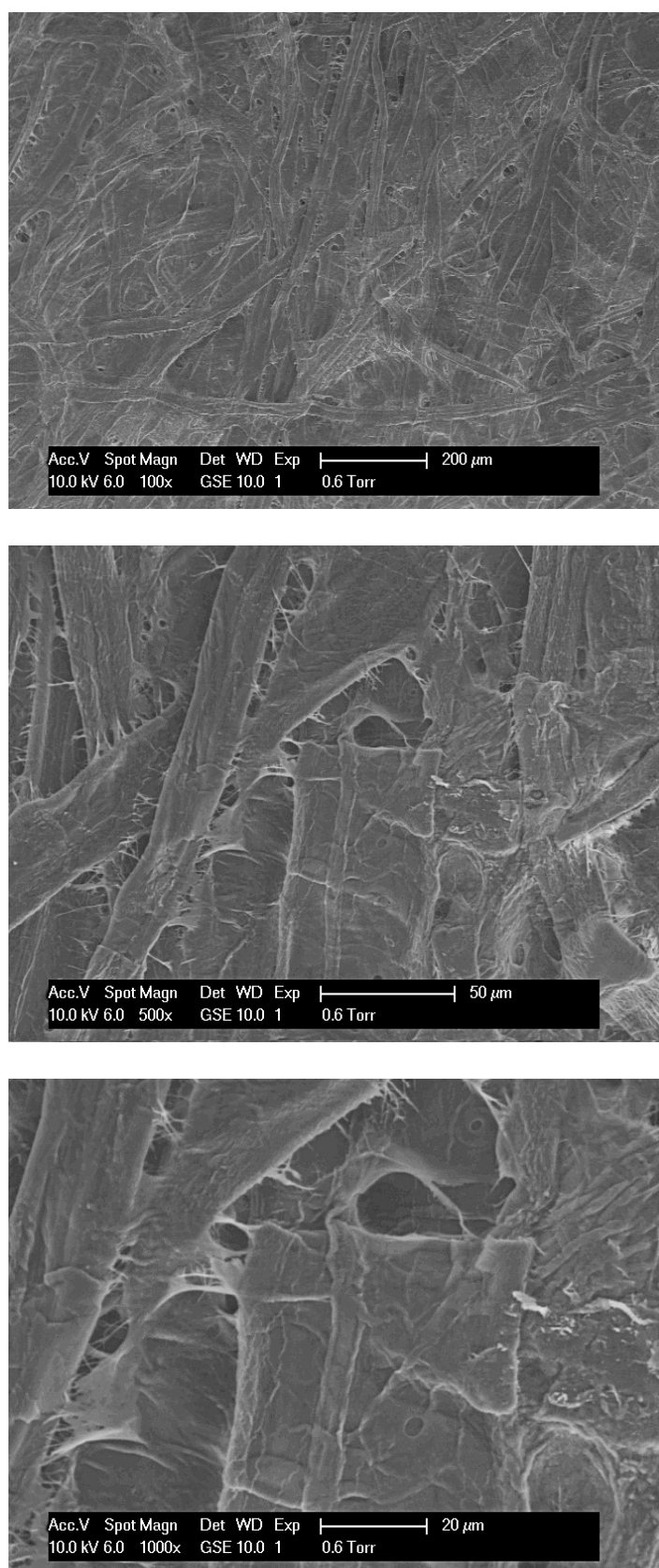


Figure A80 – Micrographs of paper sample at 100 x, 500 x and 1000 x magnification (2 days, 140 °C, 2000 mg kg⁻¹ DBDS, Air atmosphere).

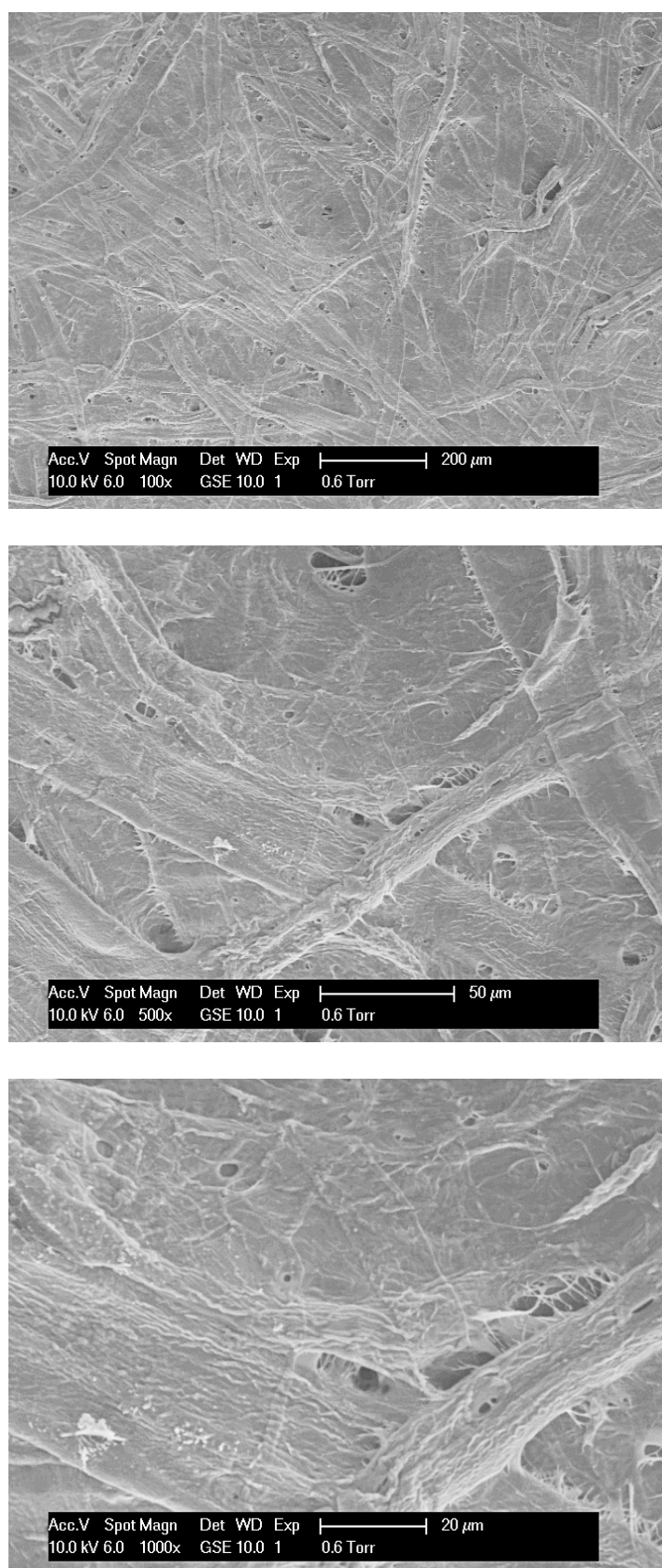


Figure A81 – Micrographs of paper sample at 100 x, 500 x and 1000 x magnification (3 days, 140 °C, 2000 mg kg⁻¹ DBDS, Air atmosphere).

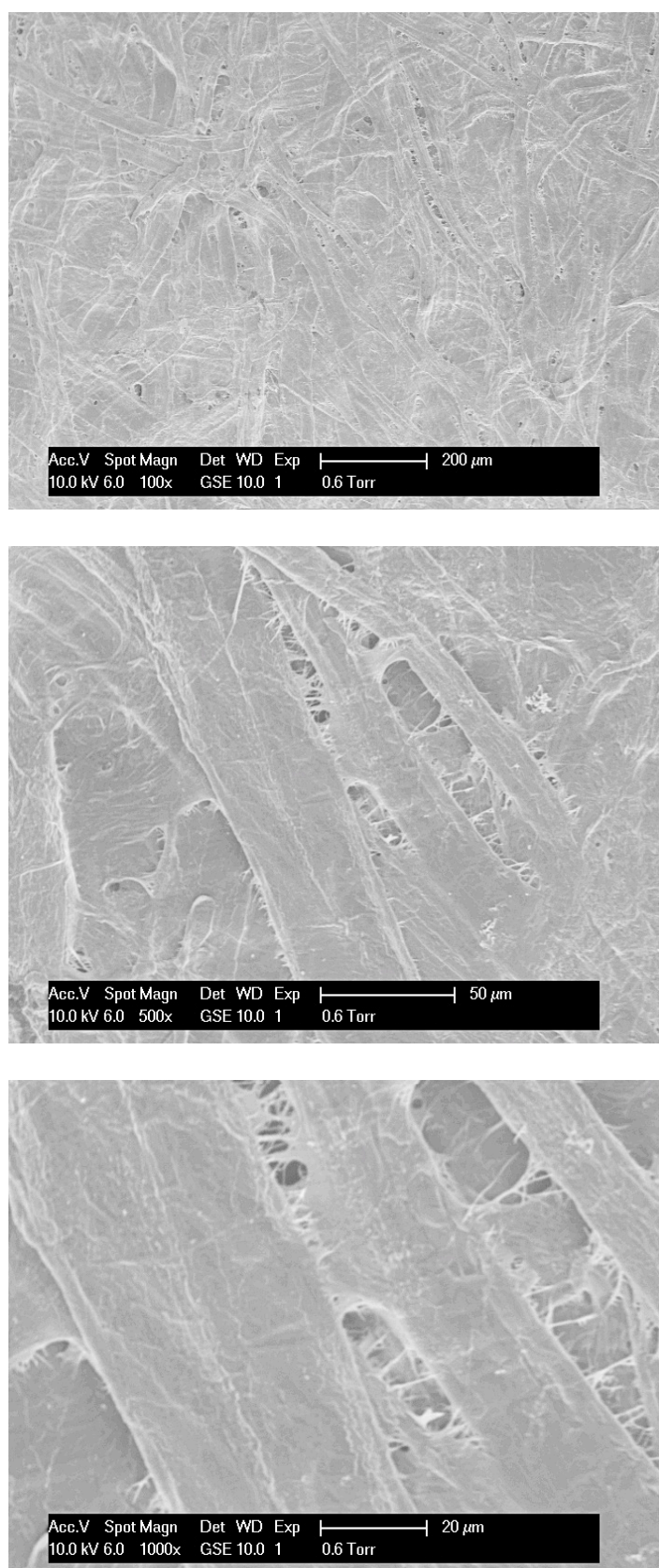


Figure A82 – Micrographs of paper sample at 100 x, 500 x and 1000 x magnification (4 days, 140 °C, 2000 mg kg⁻¹ DBDS, Air atmosphere).

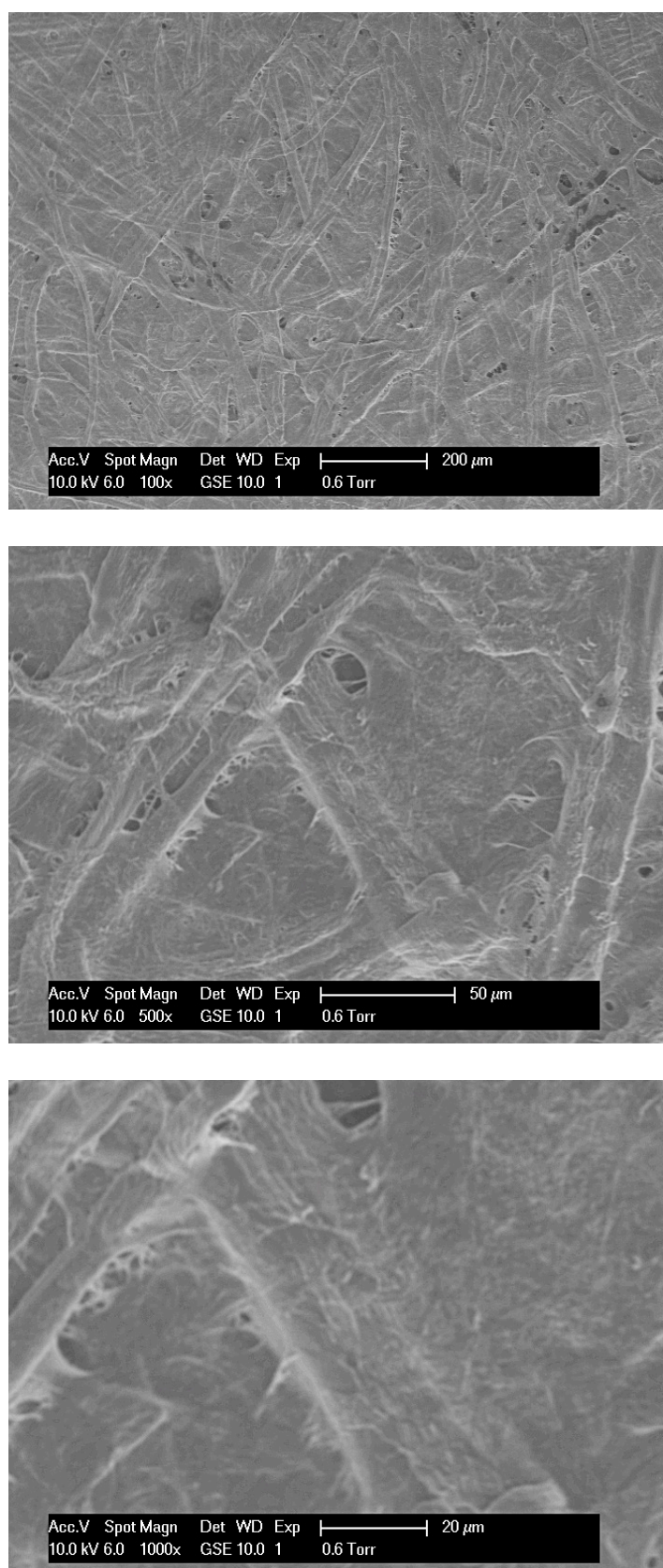


Figure A83 – Micrographs of paper sample at 100 x, 500 x and 1000 x magnification (5 days, 140 °C, 2000 mg kg⁻¹ DBDS, Air atmosphere).

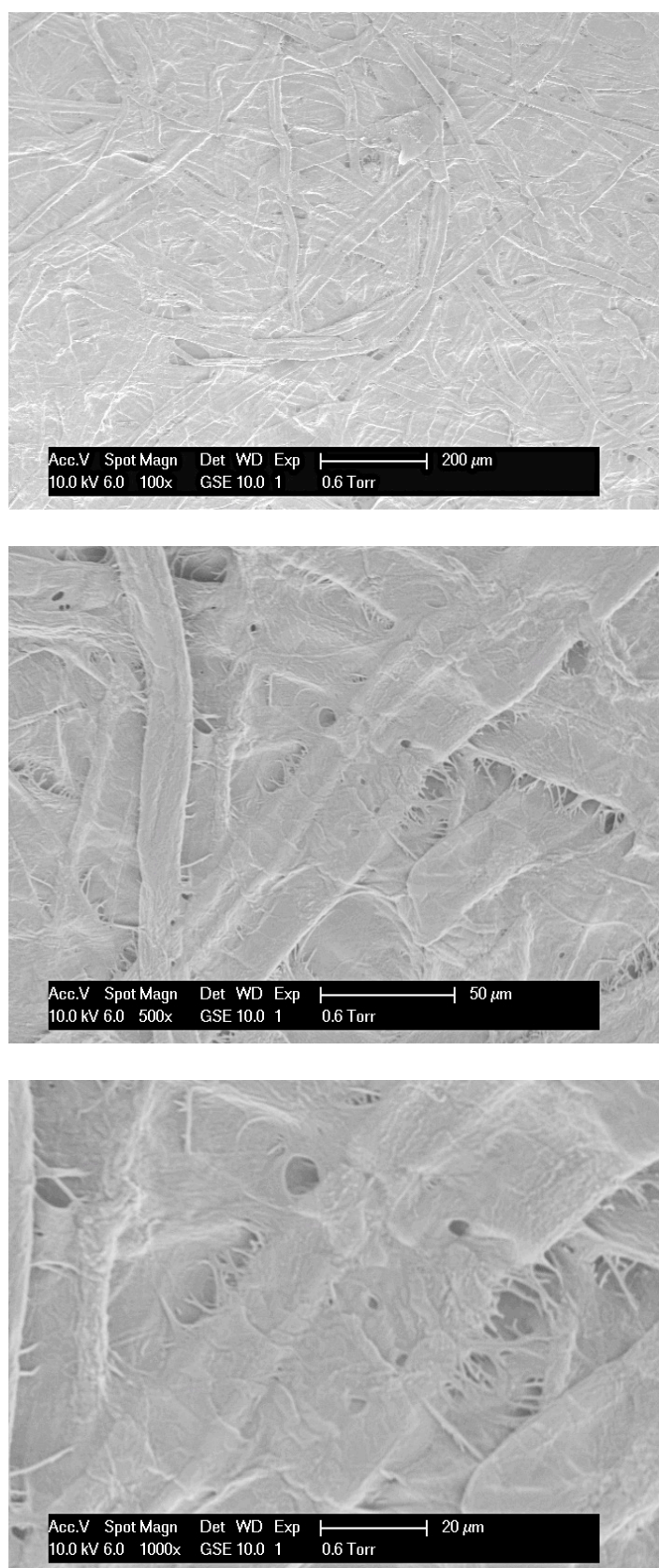


Figure A84 – Micrographs of paper sample at 100 x, 500 x and 1000 x magnification (6 days, 140 °C, 2000 mg kg⁻¹ DBDS, Air atmosphere).

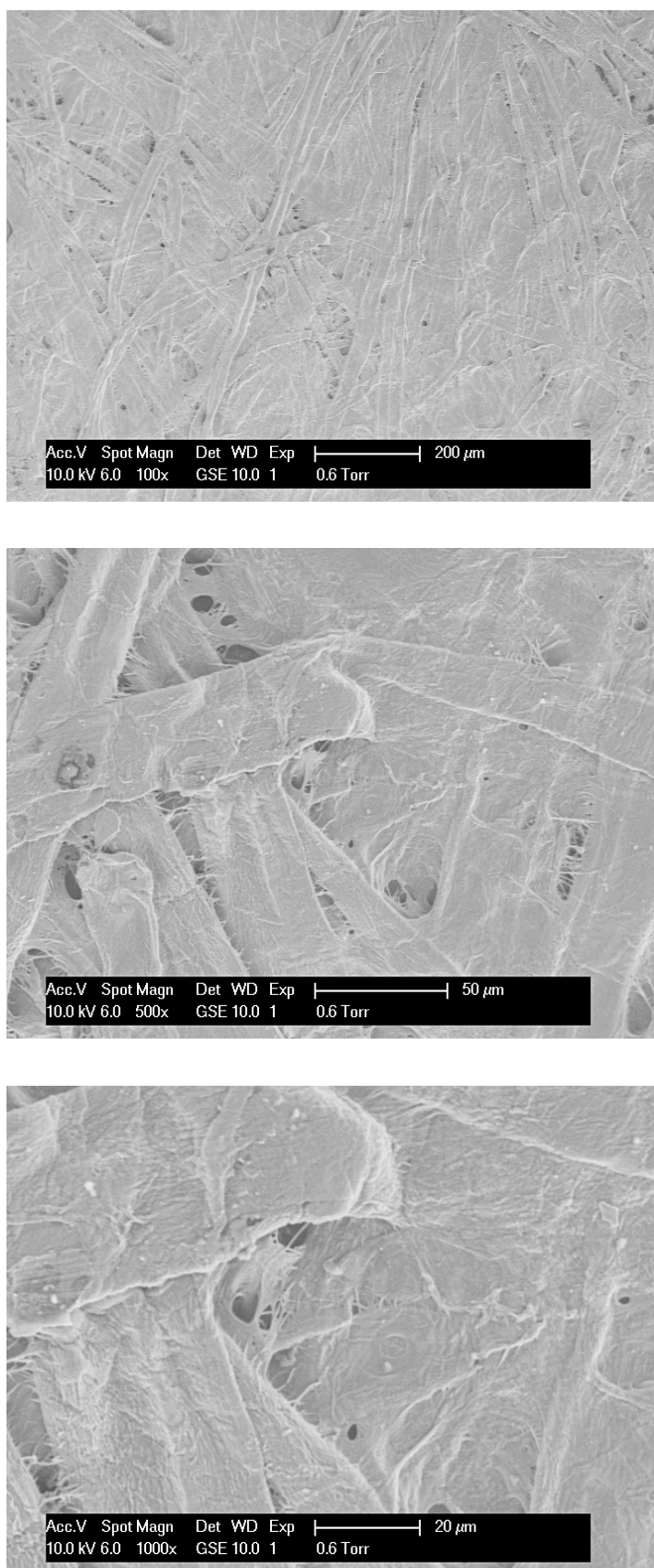


Figure A85 – Micrographs of paper sample at 100 x, 500 x and 1000 x magnification (7 days, 140 °C, 2000 mg kg⁻¹ DBDS, Air atmosphere).

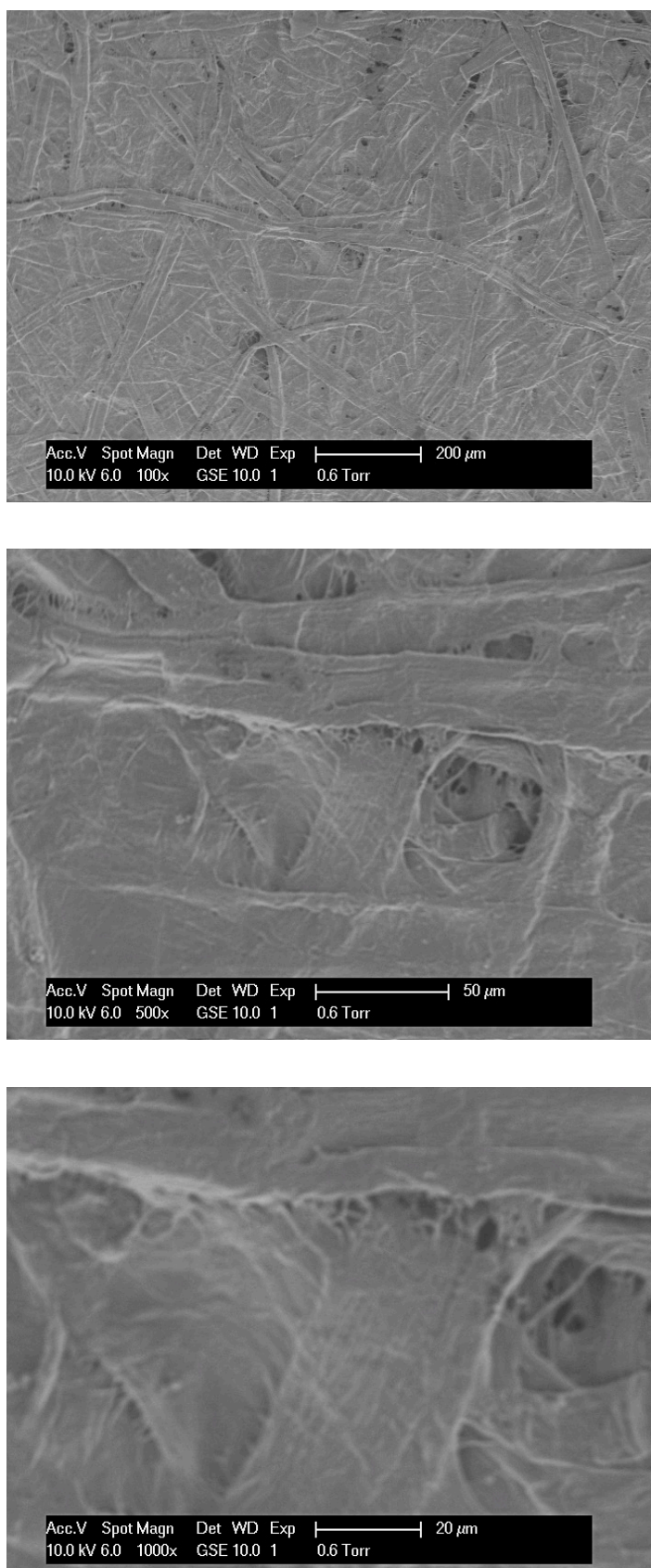


Figure A86 – Micrographs of paper sample at 100 x, 500 x and 1000 x magnification (8 days, 140 °C, 2000 mg kg⁻¹ DBDS, Air atmosphere).

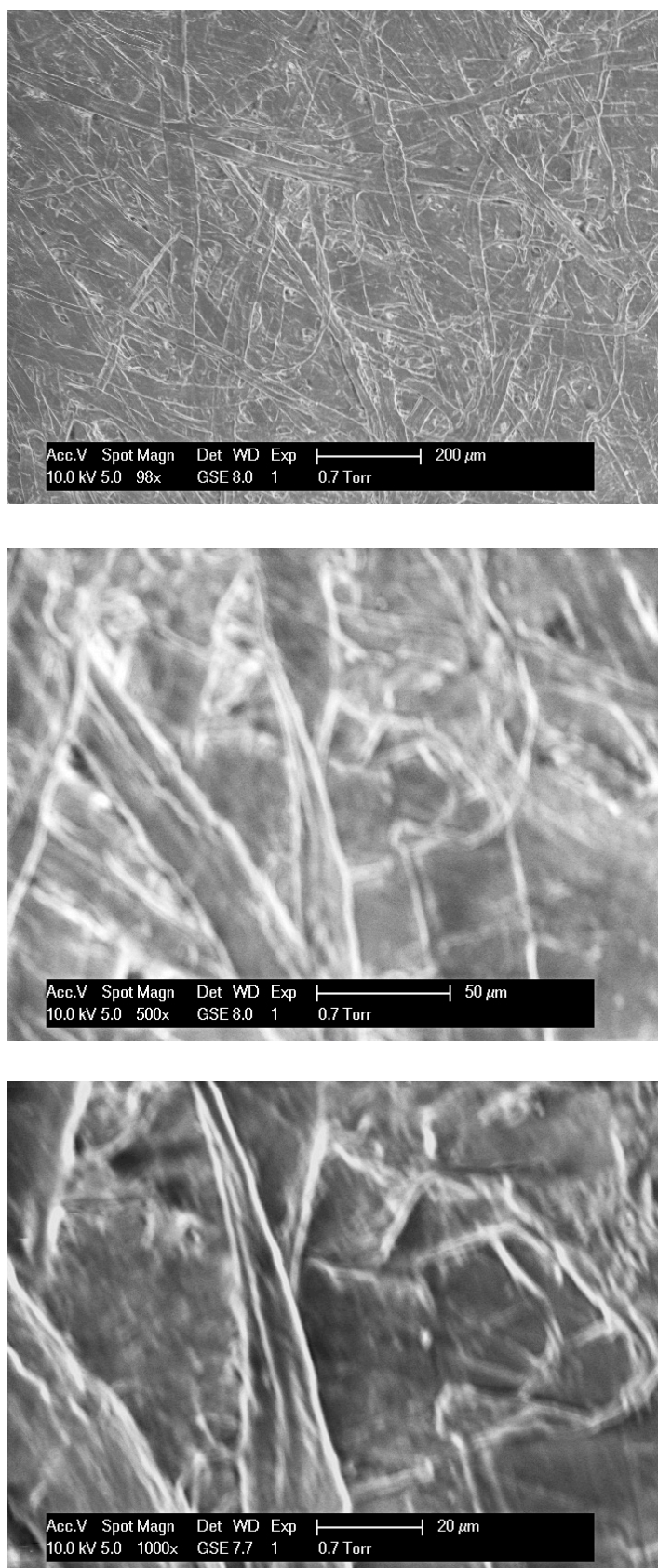


Figure A87 – Micrographs of paper sample at 100 x, 500 x and 1000 x magnification (7 days, 140 °C, 0 mg kg⁻¹ DBDS, Air atmosphere).

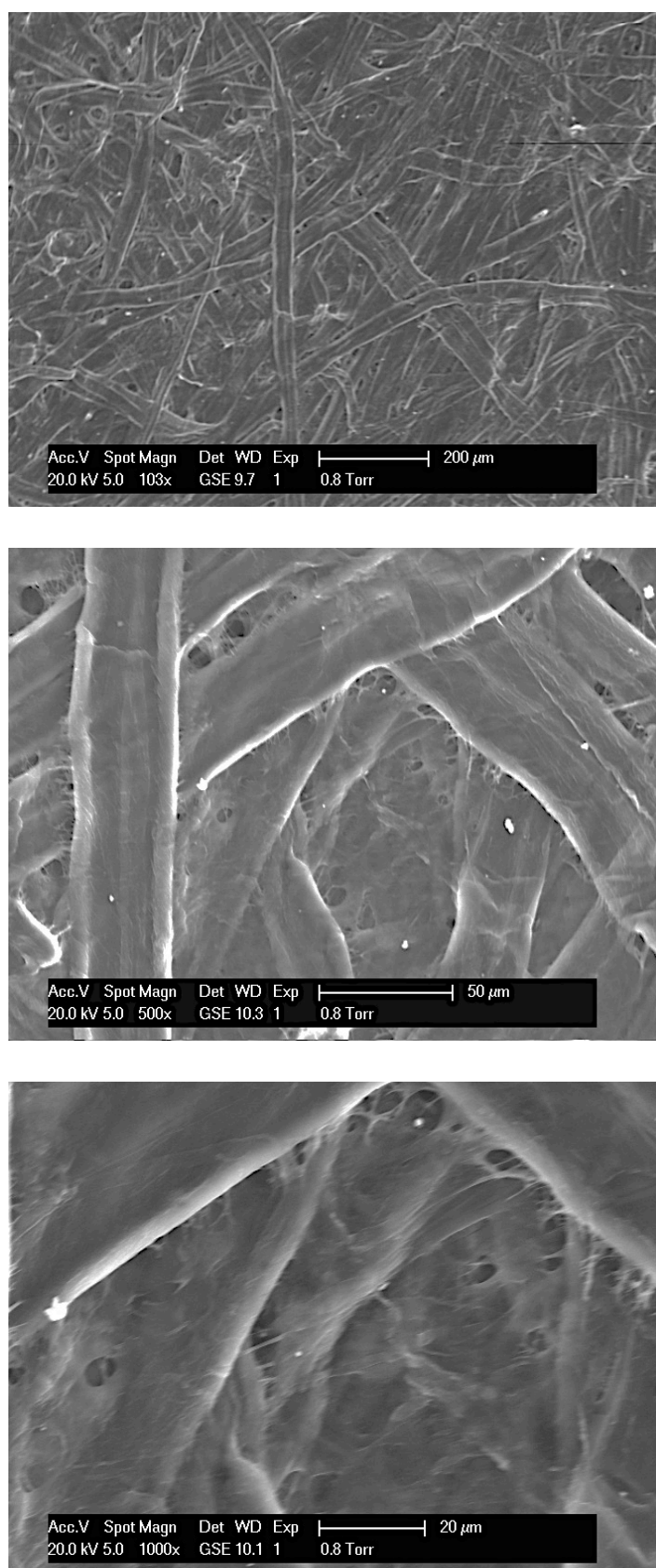


Figure A88 – Micrographs of paper sample at 100 x, 500 x and 1000 x magnification (7 days, 140 °C, 100 mg kg⁻¹ DBDS, Air atmosphere).

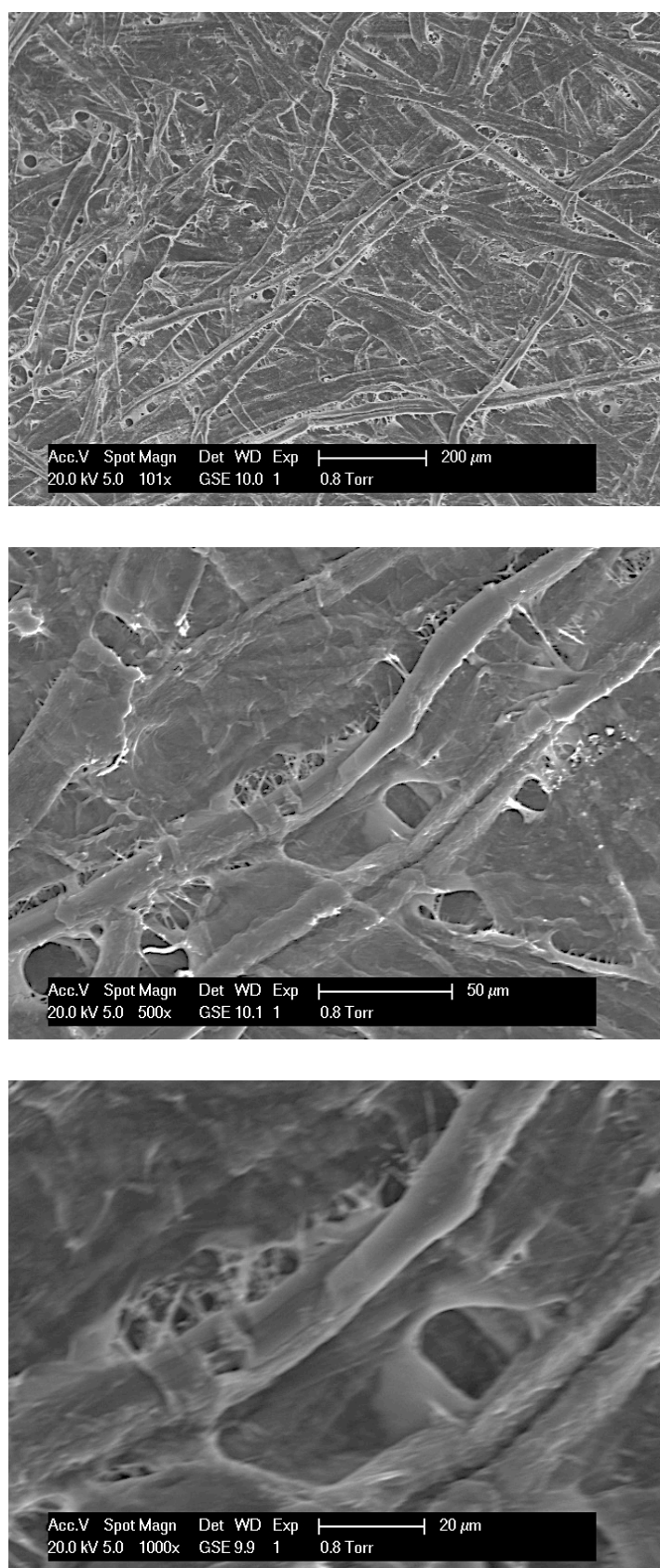


Figure A89 – Micrographs of paper sample at 100 x, 500 x and 1000 x magnification (7 days, 140 °C, 500 mg kg⁻¹ DBDS, Air atmosphere).

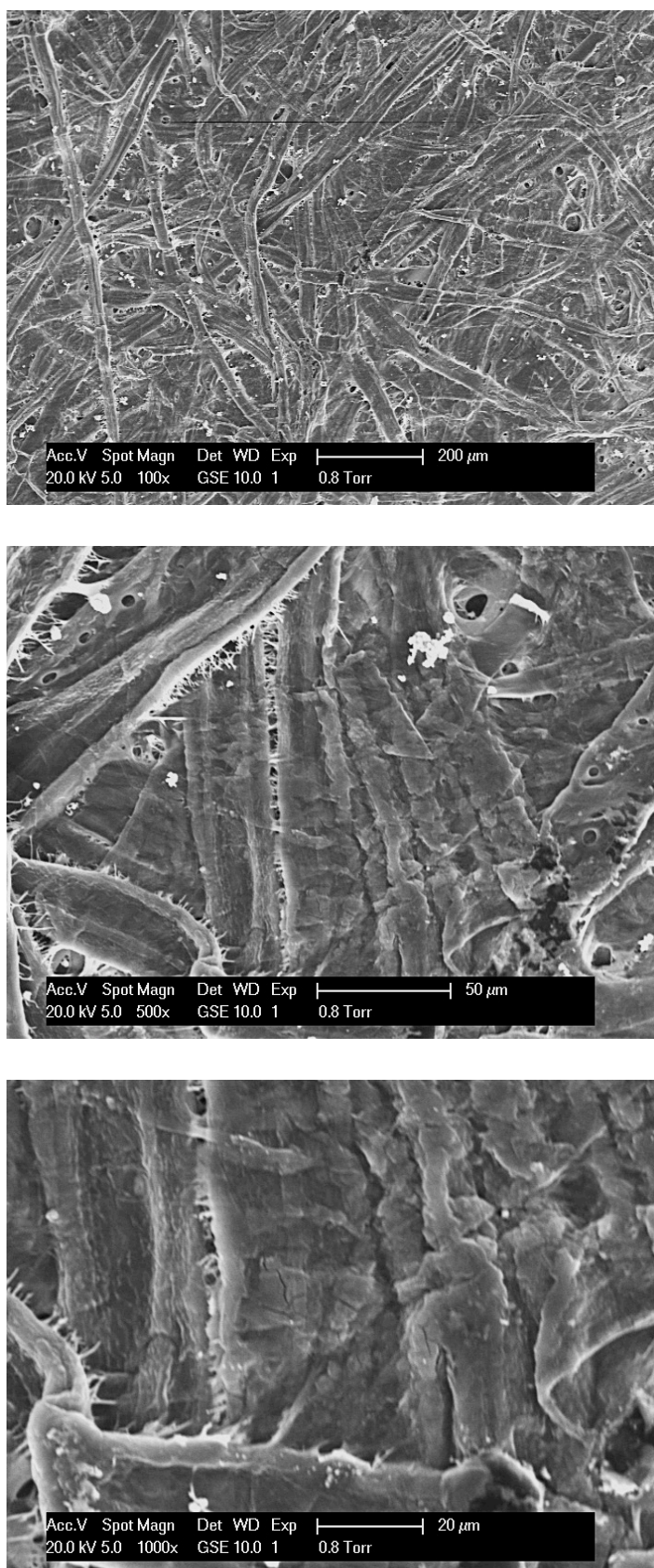


Figure A90 – Micrographs of paper sample at 100 x, 500 x and 1000 x magnification (7 days, 140 °C, 1000 mg kg⁻¹ DBDS, Air atmosphere).

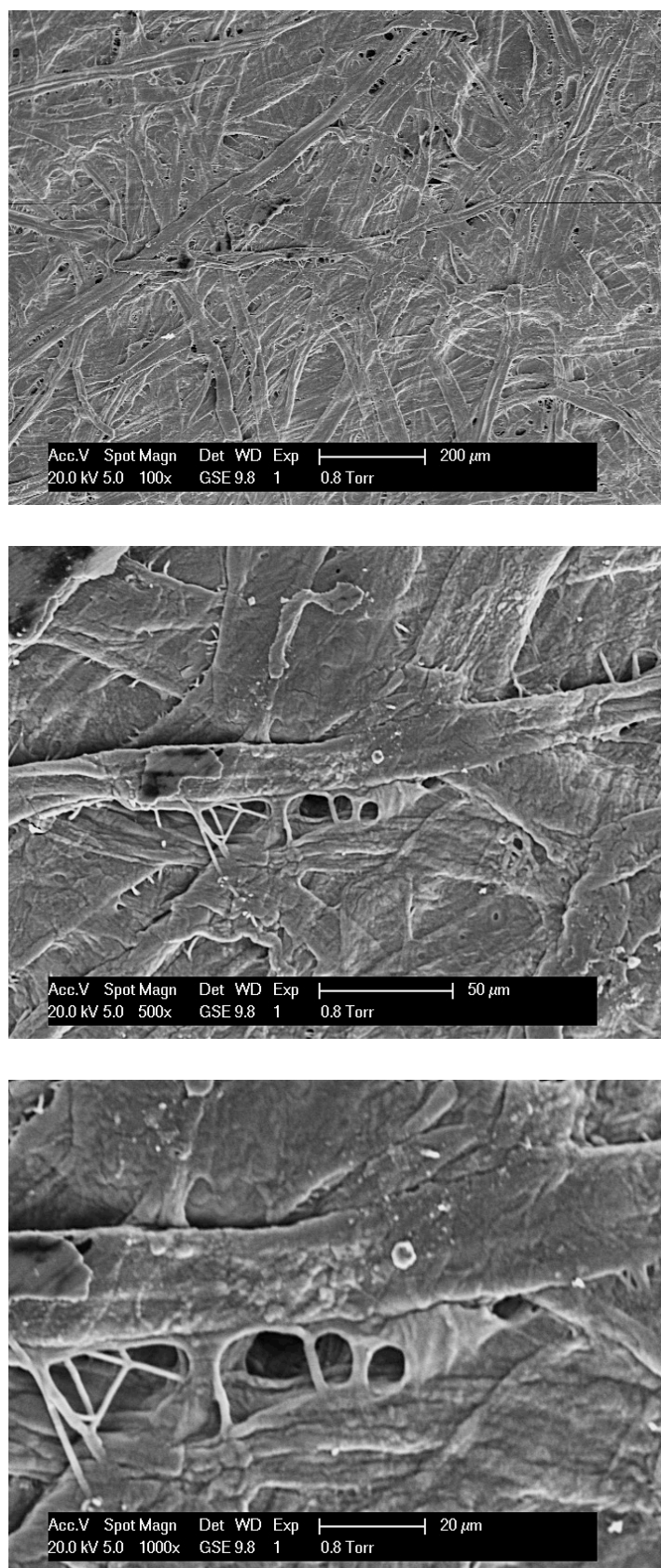


Figure A91 – Micrographs of paper sample at 100 x, 500 x and 1000 x magnification (7 days, 140 °C, 2000 mg kg⁻¹ DBDS, Air atmosphere).

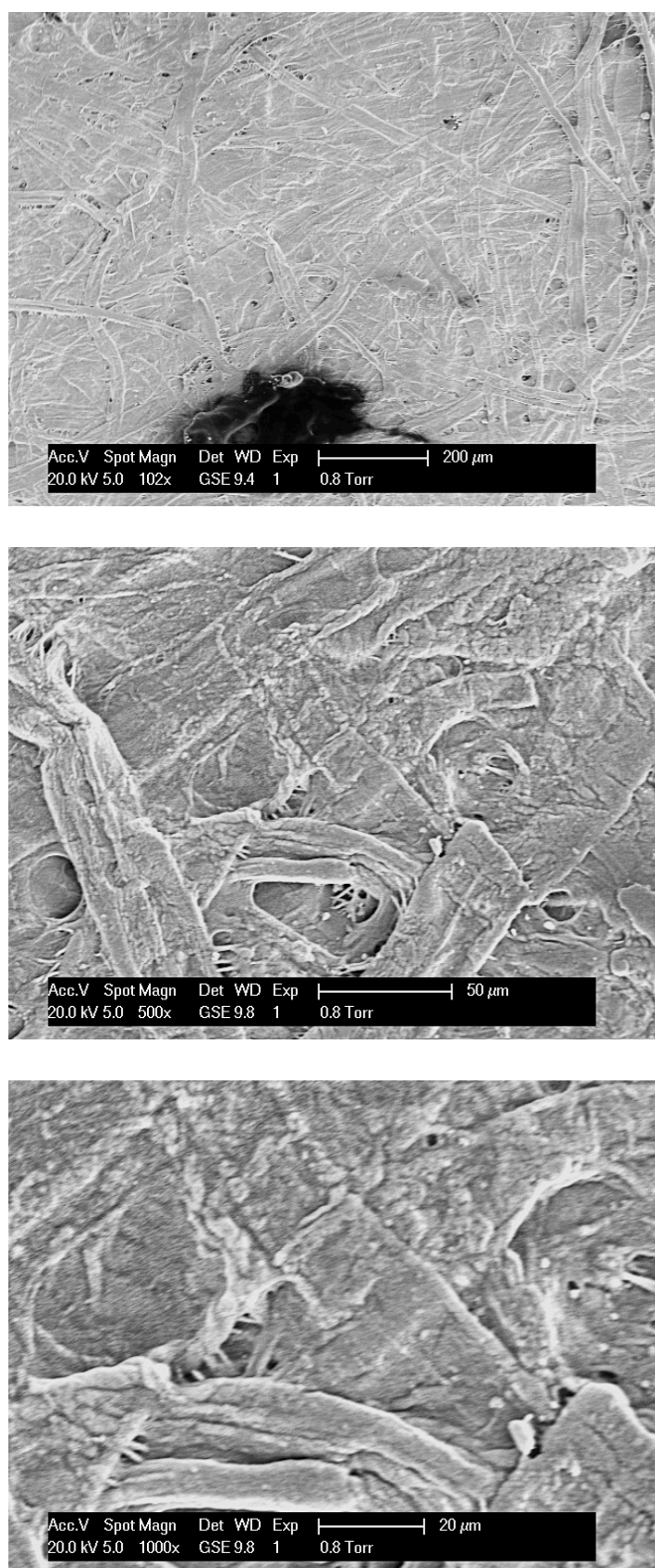


Figure A92 – Micrographs of paper sample at 100 x, 500 x and 1000 x magnification (7 days, 140 °C, 5000 mg kg⁻¹ DBDS, Air atmosphere).

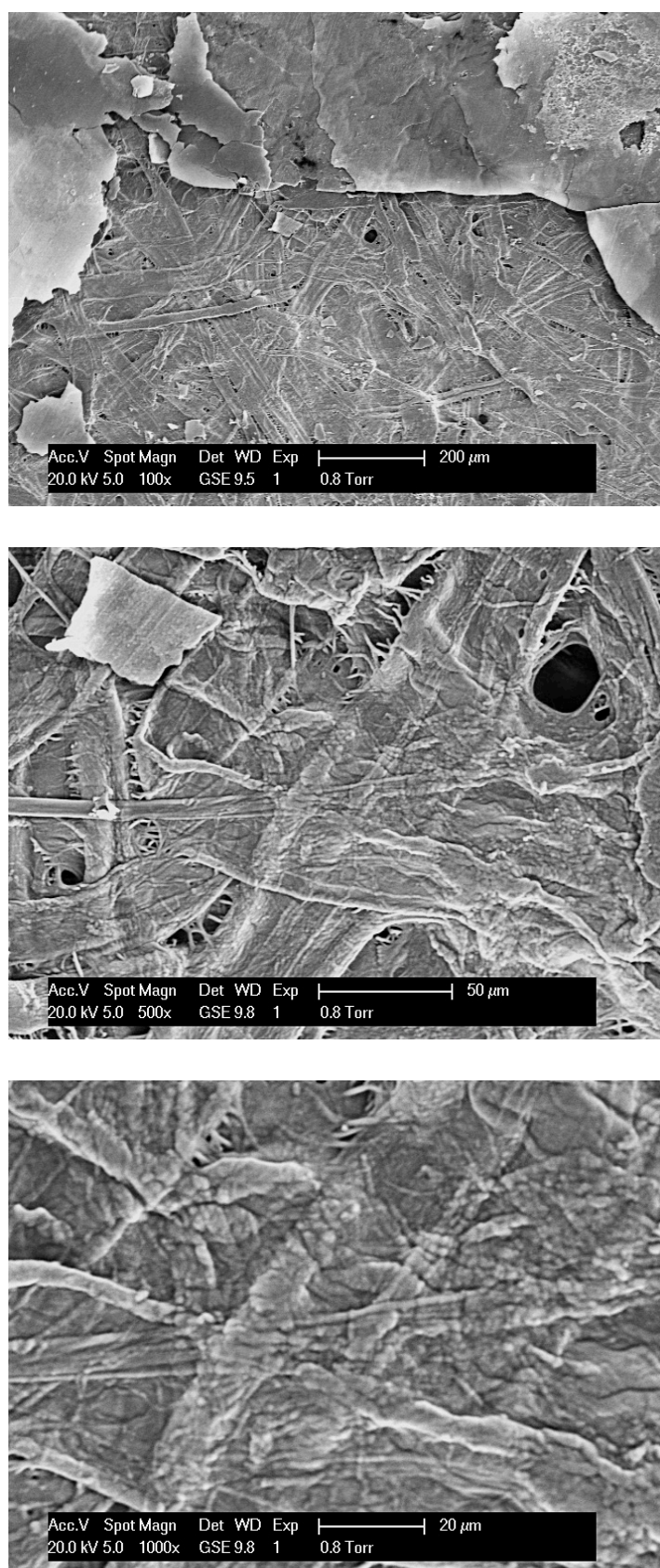


Figure A93 – Micrographs of paper sample at 100 x, 500 x and 1000 x magnification (7 days, 140 °C, 10000 mg kg⁻¹ DBDS, Air atmosphere).

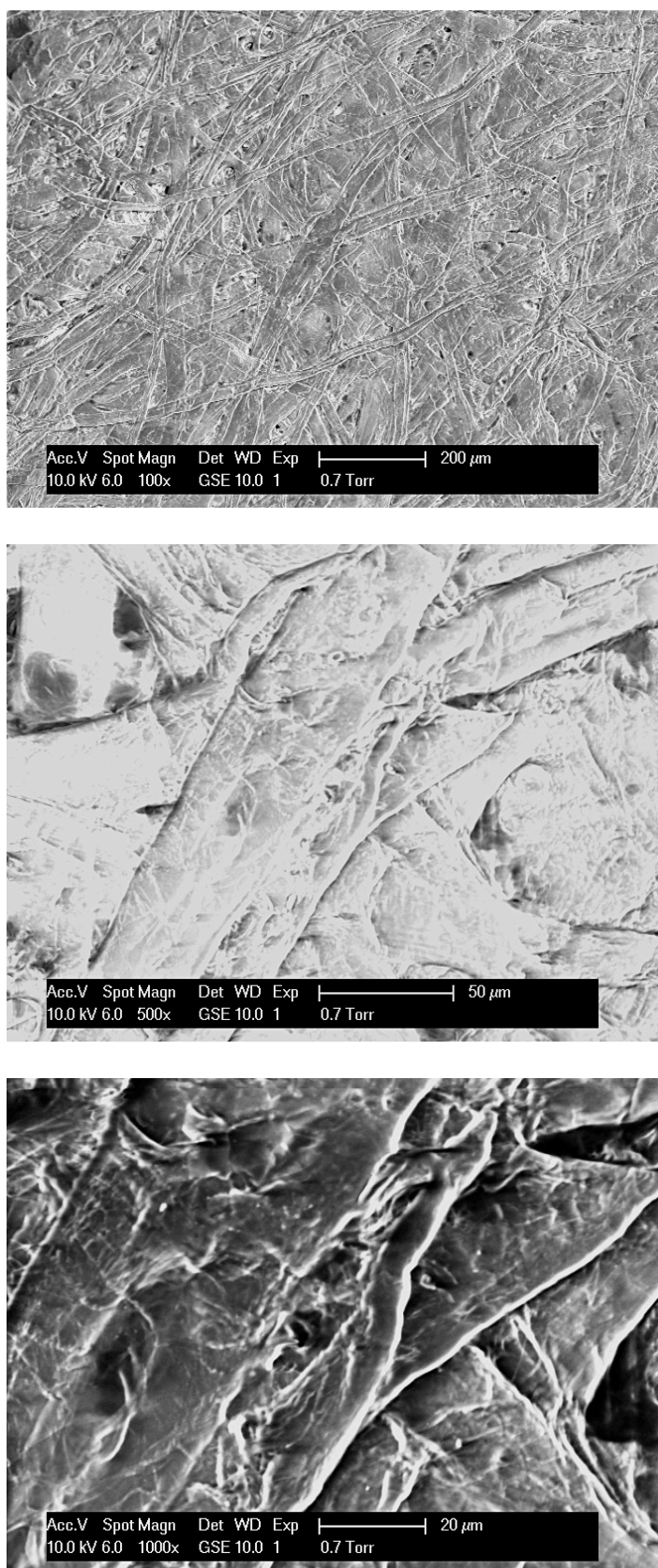


Figure A94 – Micrographs of paper sample at 100 x, 500 x and 1000 x magnification (7 days, 140 °C, 100 mg kg⁻¹ DBDS, N₂ atmosphere).

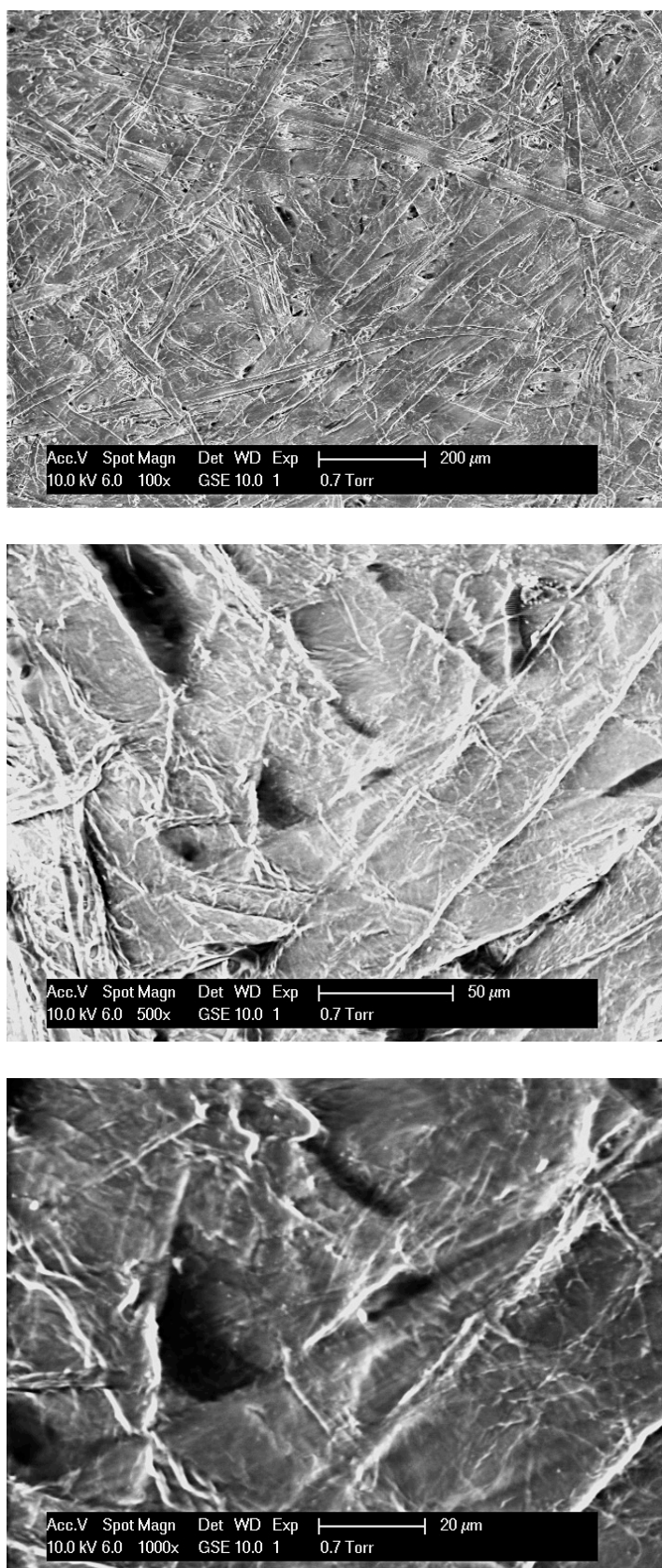


Figure A95 – Micrographs of paper sample at 100 x, 500 x and 1000 x magnification (7 days, 140 °C, 500 mg kg⁻¹ DBDS, N₂ atmosphere).

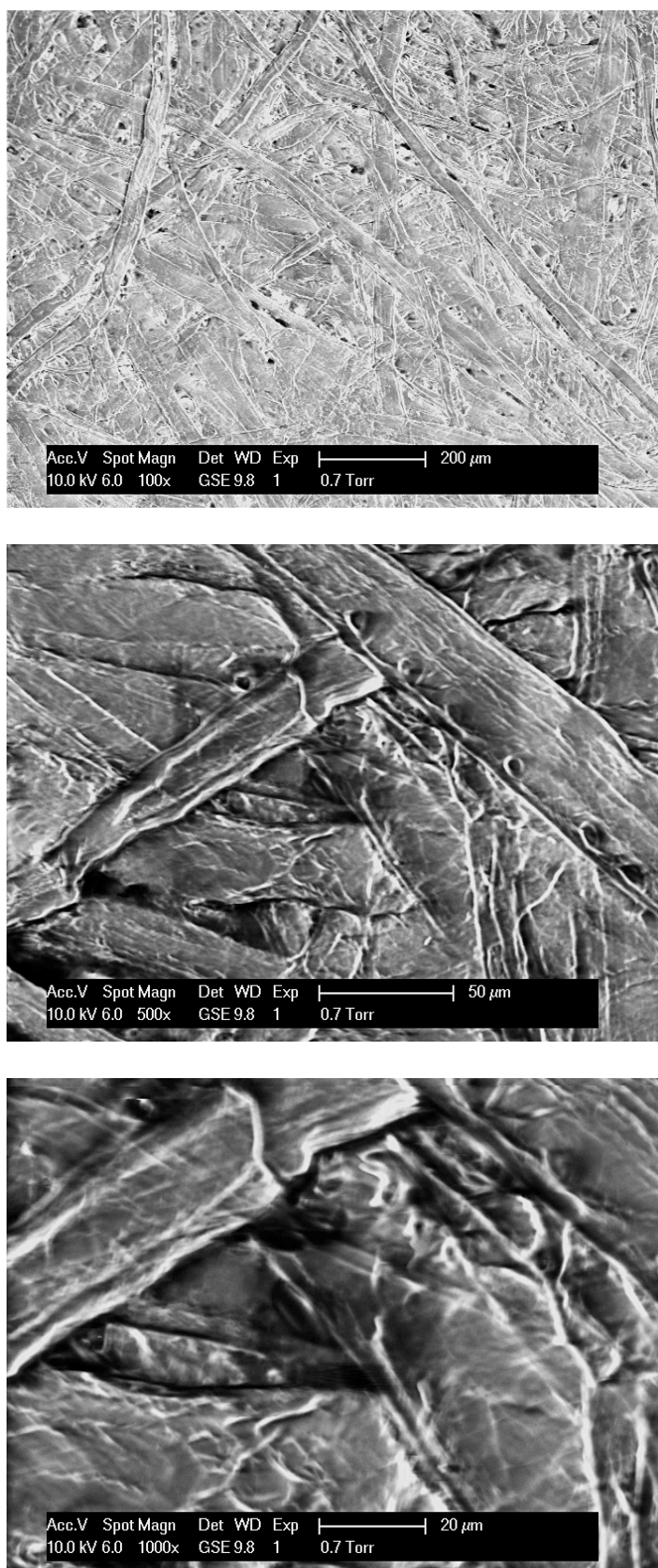


Figure A96 – Micrographs of paper sample at 100 x, 500 x and 1000 x magnification (7 days, 140 °C, 1000 mg kg⁻¹ DBDS, N₂ atmosphere).

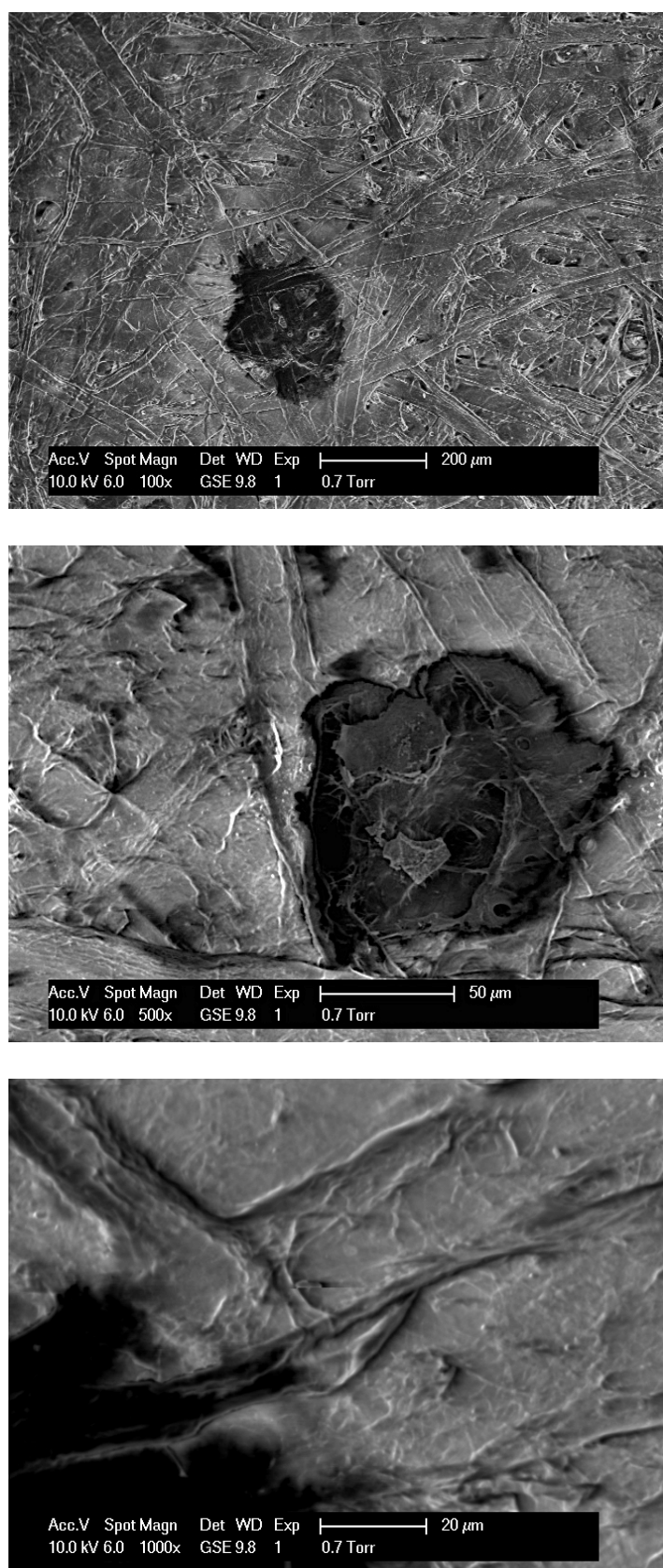


Figure A97 – Micrographs of paper sample at 100 x, 500 x and 1000 x magnification (7 days, 140 °C, 2000 mg kg⁻¹ DBDS, N₂ atmosphere).

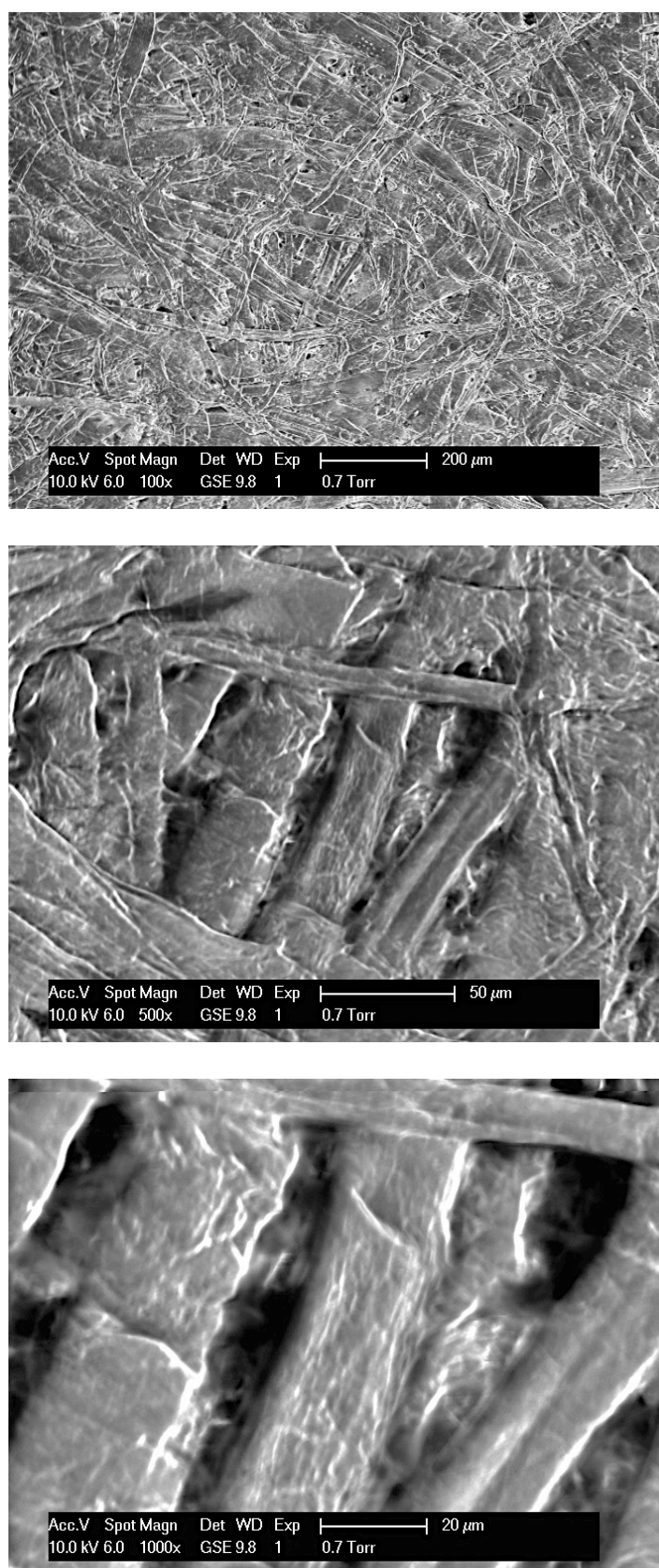


Figure A98 – Micrographs of paper sample at 100 x, 500 x and 1000 x magnification (7 days, 140 °C, 5000 mg kg⁻¹ DBDS, N₂ atmosphere).

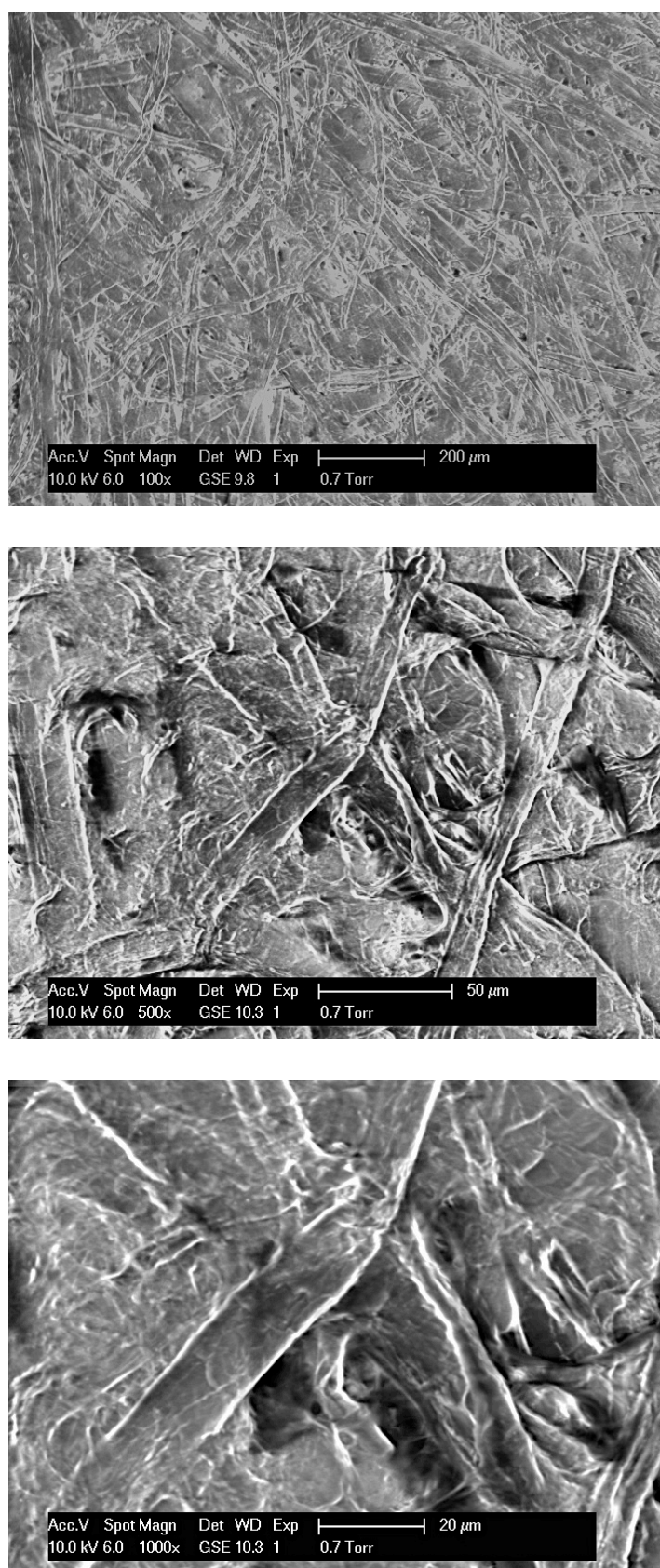


Figure A99 – Micrographs of paper sample at 100 x, 500 x and 1000 x magnification (7 days, 140 °C, 10000 mg kg⁻¹ DBDS, N₂ atmosphere).

A.3 Thermogravimetric Data

Dr Pedro S. Amaro performed TGA analyses on a Perkin Elmer Pyris 1. Multiple point temperature calibration was performed measuring Curie's point of Almel alloy (154.2 °C), Ni (355.3 °C), Perkalloy (596.0 °C) and Fe (780.0 °C) at a heating rate of 10 °C min⁻¹. Single point weight calibration was performed using a reference 100 mg mass. Air flow rate was set to 20 ml min⁻¹. The starting temperature was set to 50 °C and aged insulating Kraft paper samples (approx. 4 mg) were analysed in Pt pans at a heating rate of 10 °C min⁻¹. Extended data sets can be found as part of Dr Amaro Ph.D. thesis.⁵⁴

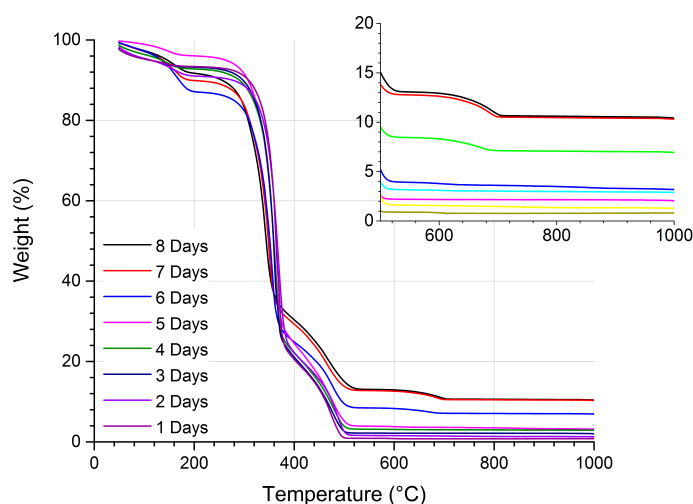


Figure A100 – Comparison between TGA traces of paper samples (1 to 8 days, 140 °C, 2000 mg kg⁻¹ DBDS, Air atmosphere).

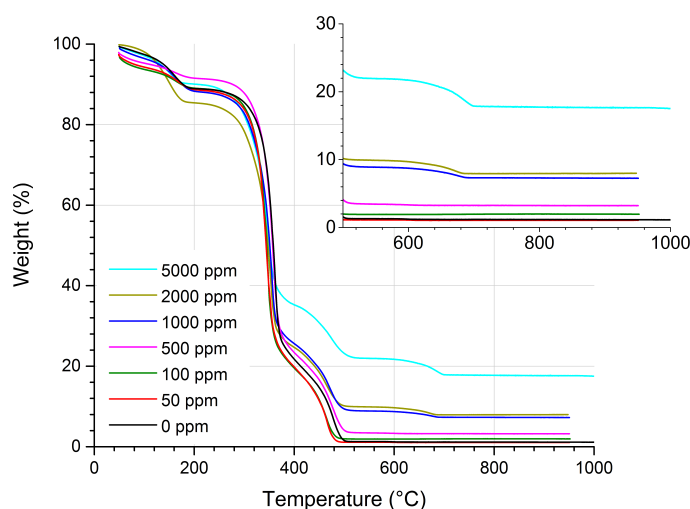


Figure A101 – Comparison between TGA traces of paper samples (7 days, 140 °C, 0 to 5000 mg kg⁻¹ DBDS, Air atmosphere).

Appendix B

B.1 Copyright permissions to reuse

The IEEE does not require individuals working on a thesis to obtain a formal reuse license, however, you may print out this statement to be used as a permission grant: Requirements to be followed when using any portion (*e.g.*, figure, graph, table, or textual material) of an IEEE copyrighted paper in a thesis:

- 1) In the case of textual material (*e.g.*, using short quotes or referring to the work within these papers) users must give full credit to the original source (author, paper, publication) followed by the IEEE copyright line © 2011 IEEE.
- 2) In the case of illustrations or tabular material, we require that the copyright line © [Year of original publication] IEEE appear prominently with each reprinted figure and/or table.
- 3) If a substantial portion of the original paper is to be used, and if you are not the senior author, also obtain the senior author's approval.

Requirements to be followed when using an entire IEEE copyrighted paper in a thesis:

- 1) The following IEEE copyright/ credit notice should be placed prominently in the references: © [year of original publication] IEEE. Reprinted, with permission, from [author names, paper title, IEEE publication title, and month/year of publication]
- 2) Only the accepted version of an IEEE copyrighted paper can be used when posting the paper or your thesis on-line.
- 3) In placing the thesis on the author's university website, please display the following message in a prominent place on the website: In reference to IEEE copyrighted material which is used with permission in this thesis, the IEEE does not endorse any of University of Southampton's products or services. Internal or personal use of this material is permitted. If interested in reprinting/republishing IEEE copyrighted material for advertising or promotional purposes or for creating new collective works for resale or redistribution, please go to:

http://www.ieee.org/publications_standards/publications/rights/rights_link.html to learn how to obtain a License from RightsLink. If applicable, University Microfilms and/or ProQuest Library, or the Archives of Canada may supply single copies of the dissertation.

B.2 XPS sample holder

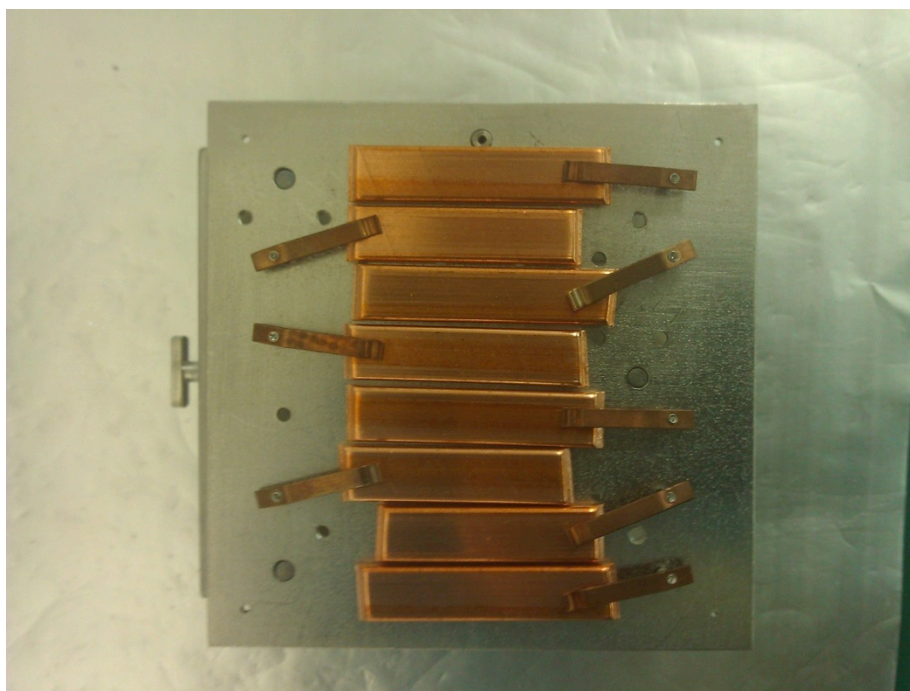


Figure A102 – Top view of the XPS sample holder with copper samples mounted and secured.

B.3 HD resolution CCD test results



Figure A103 – Copper samples inhibited with increasing amount (left to right) of Irgamet[®] 39 in Gemini X oil after the CCD test in the presence of 2000 mg kg⁻¹ of DBDS.





Figure A104 – Copper samples inhibited with increasing amount (left to right) of Irgamet[®] 39 in HyVolt III oil after the CCD test in the presence of 2000 mg kg⁻¹ of DBDS.





Figure A105 – Copper samples inhibited with increasing amount (left to right) of Irgamet[®] 39 in 10 GBN oil after the CCD test in the presence of 2000 mg kg⁻¹ of DBDS.

Appendix C

C.1 Copyright permission to reuse

[Home](#)
[Account Info](#)
[Help](#)




Title: Static secondary ion mass spectrometry investigation of corrosion inhibitor Irgamet®39 on copper surfaces treated in power transformer insulating oil

Author: Marco Facciotti, Pedro S. Amaro, Richard C.D. Brown, Paul L. Lewin, James A. Pilgrim, Gordon Wilson, Paul N. Jarman, Ian W. Fletcher

Publication: Corrosion Science

Publisher: Elsevier

Date: September 2015

Copyright © 2015 Elsevier Ltd. All rights reserved.

Logged in as:
Marco Facciotti
Account #: 3000897539

LOGOUT

Order Completed

Thank you very much for your order.

This is a License Agreement between Marco Facciotti ("You") and Elsevier ("Elsevier"). The license consists of your order details, the terms and conditions provided by Elsevier, and the [payment terms and conditions](#).

[Get the printable license.](#)

License Number	3677080770372
License date	Jul 27, 2015
Licensed content publisher	Elsevier
Licensed content publication	Corrosion Science
Licensed content title	Static secondary ion mass spectrometry investigation of corrosion inhibitor Irgamet®39 on copper surfaces treated in power transformer insulating oil
Licensed content author	Marco Facciotti, Pedro S. Amaro, Richard C.D. Brown, Paul L. Lewin, James A. Pilgrim, Gordon Wilson, Paul N. Jarman, Ian W. Fletcher
Licensed content date	September 2015
Licensed content volume number	98
Licensed content issue number	n/a
Number of pages	7
Type of Use	reuse in a thesis/dissertation
Portion	full article
Format	both print and electronic
Are you the author of this Elsevier article?	Yes
Will you be translating?	No
Title of your thesis/dissertation	A surface analytical chemistry approach to copper corrosion and its inhibition with benzotriazole derivatives in oil-filled power transformers
Expected completion date	Nov 2015
Estimated size (number of pages)	180
Elsevier VAT number	GB 494 6272 12
Permissions price	0.00 USD
VAT/Local Sales Tax	0.00 USD / 0.00 GBP
Total	0.00 USD

[ORDER MORE...](#)
[CLOSE WINDOW](#)

Copyright © 2015 [Copyright Clearance Center, Inc.](#) All Rights Reserved. [Privacy statement](#). [Terms and Conditions](#).
Comments? We would like to hear from you. E-mail us at customer@copyright.com

C.2 SSIMS data sets

Base Oil 20

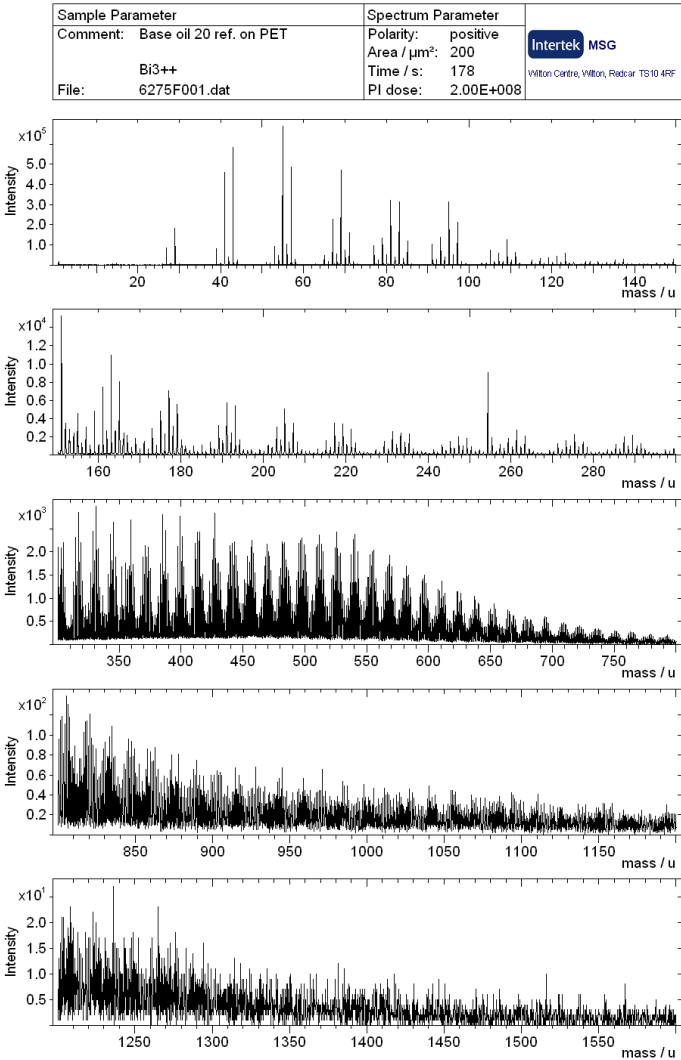


Figure A106 – Positive polarity secondary ion mass spectrum of Base Oil 20 on a PET film.

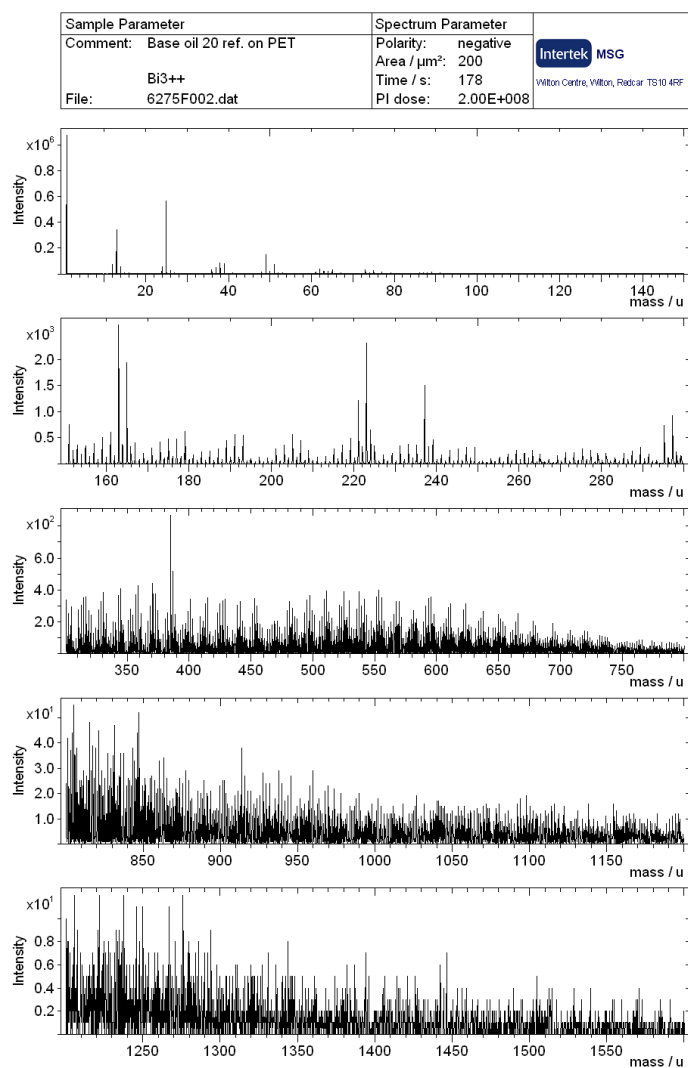


Figure A107 – Negative polarity secondary ion mass spectrum of Base Oil 20 on a PET film.

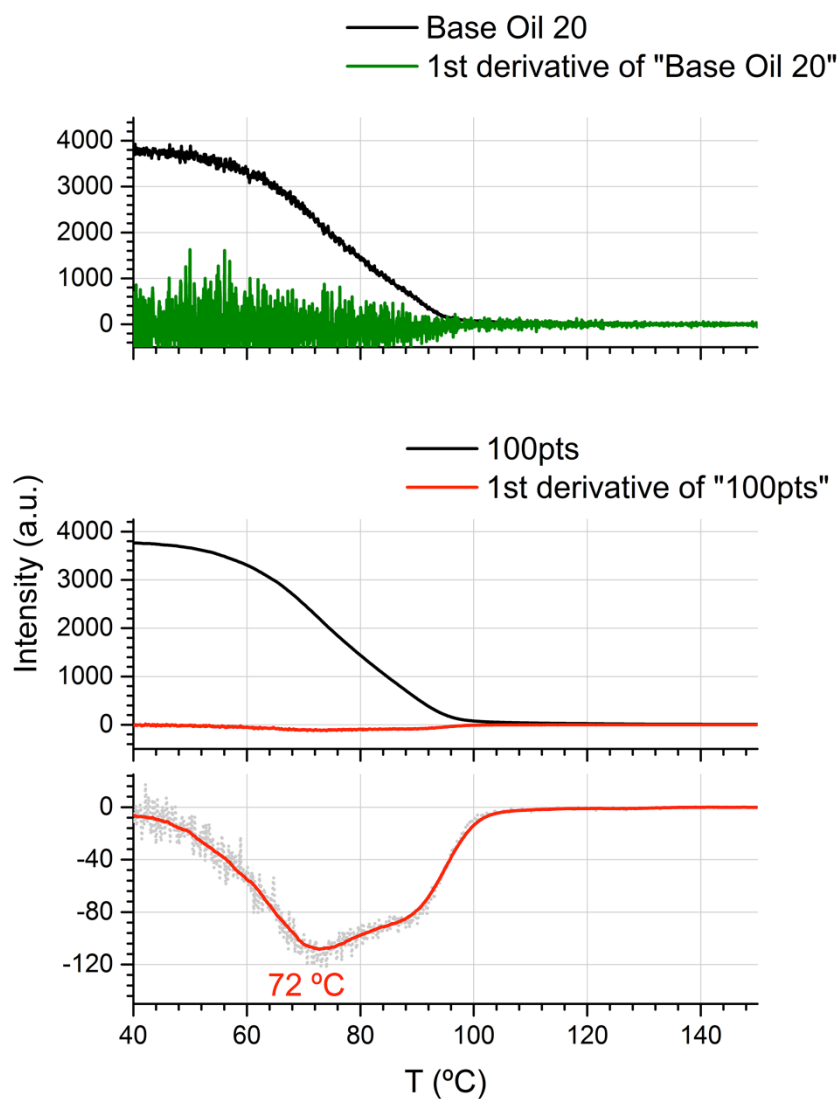


Figure A108 – Summary of the determination of T_p through TPD-SSIMS profiles processing: 1st differential (top) for m/z 132 on copper treated with 100 mg kg^{-1} of Irgamet[®]39 in Base Oil 20 at 70 $^{\circ}\text{C}$ for 24 hours; adjacent averaging smoothing at 100 points (middle); identification of the absolute minimum in the 1st differential plot (bottom).

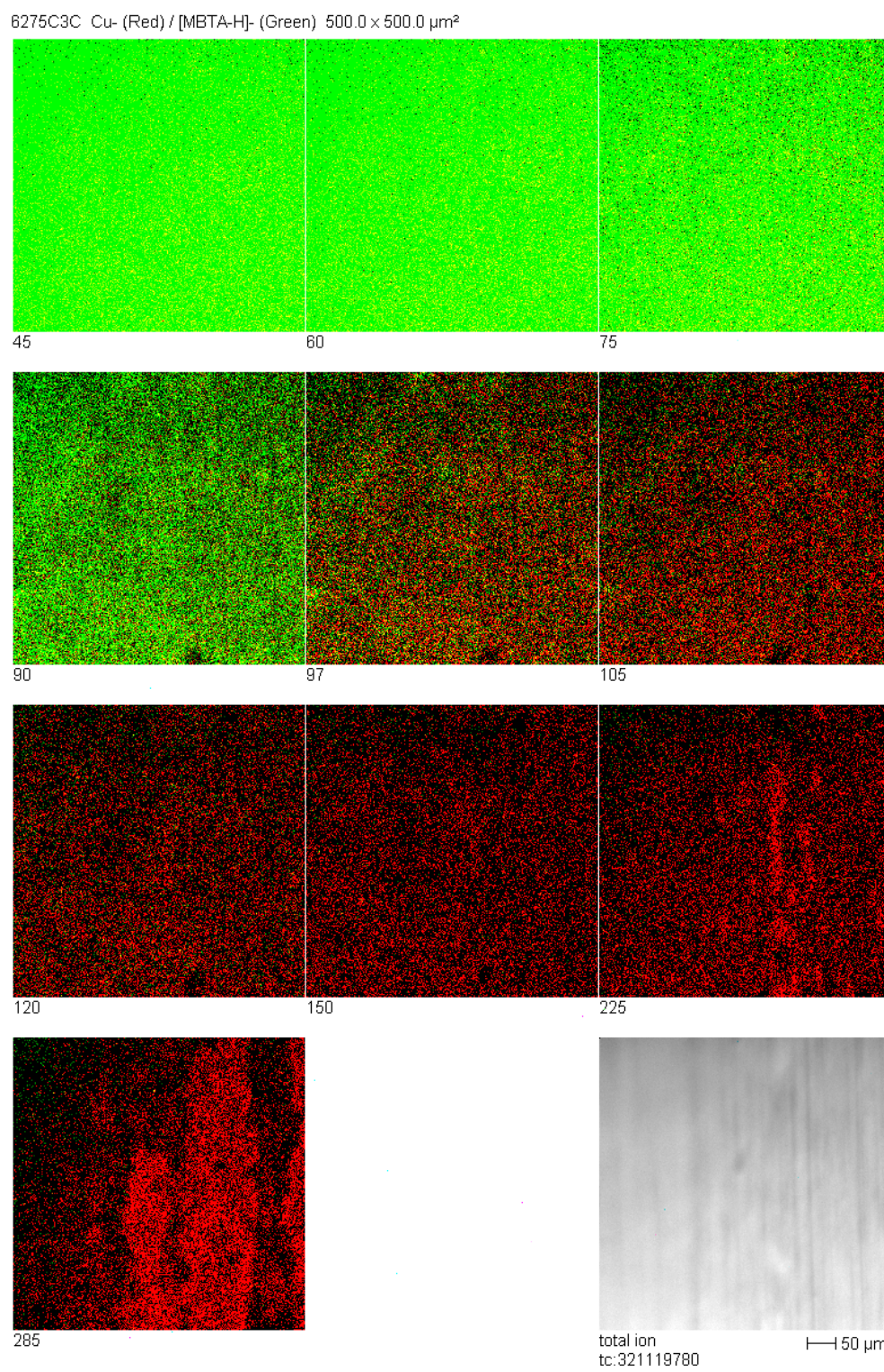


Figure A109 – Negative ion image from 45 °C to 285 °C of Cu (red) treated with 100 mg kg^{-1} of Irgamet[®] 39 (*i.e.* m/z 132, green) in Base Oil 20 at 70 °C for 24 hours.

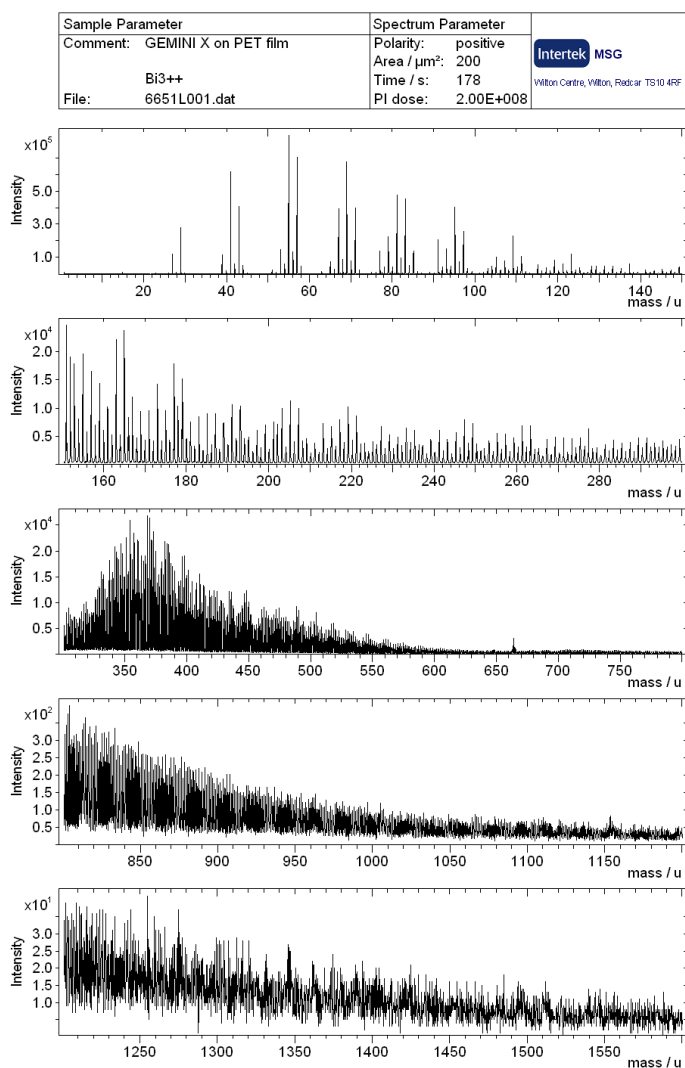
Gemini X oil

Figure A110 – Positive polarity secondary ion mass spectrum of Gemini X oil on a PET film.

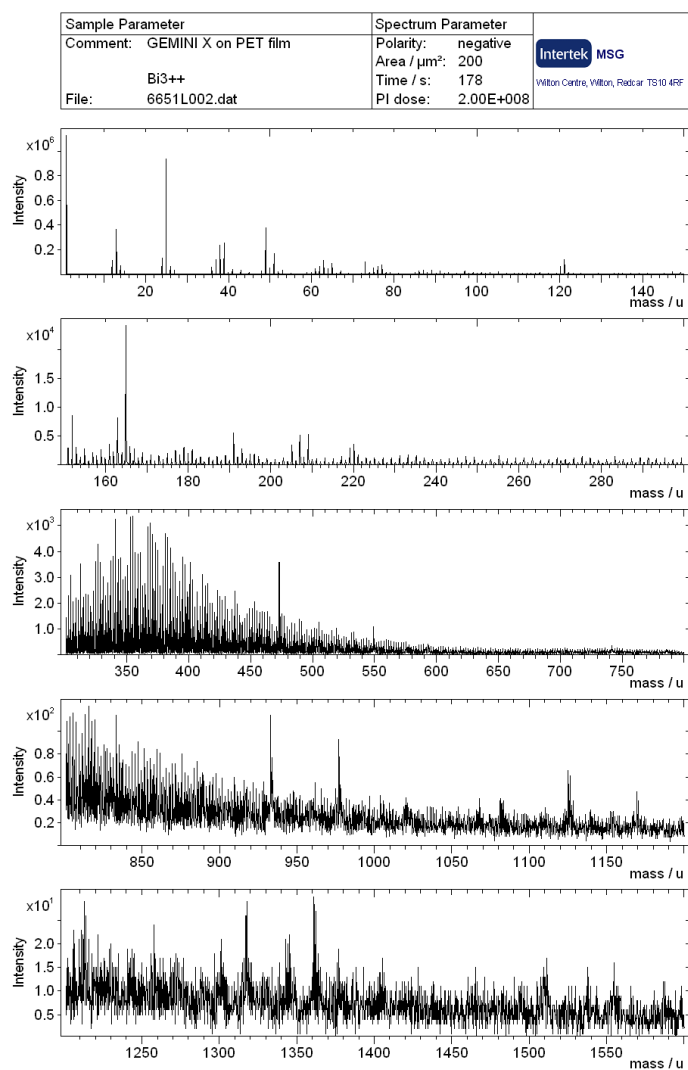


Figure A111 – Negative polarity secondary ion mass spectrum of Gemini X oil on a PET film.

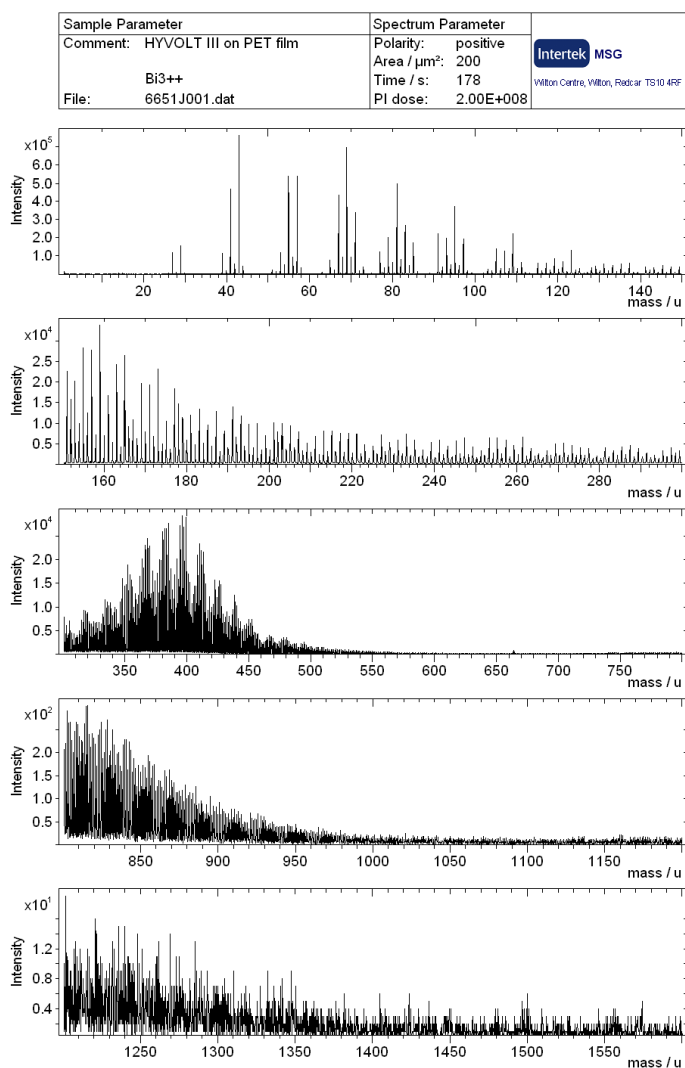
HyVolt III oil

Figure A112 – Positive polarity secondary ion mass spectrum of HyVolt III oil on a PET film.

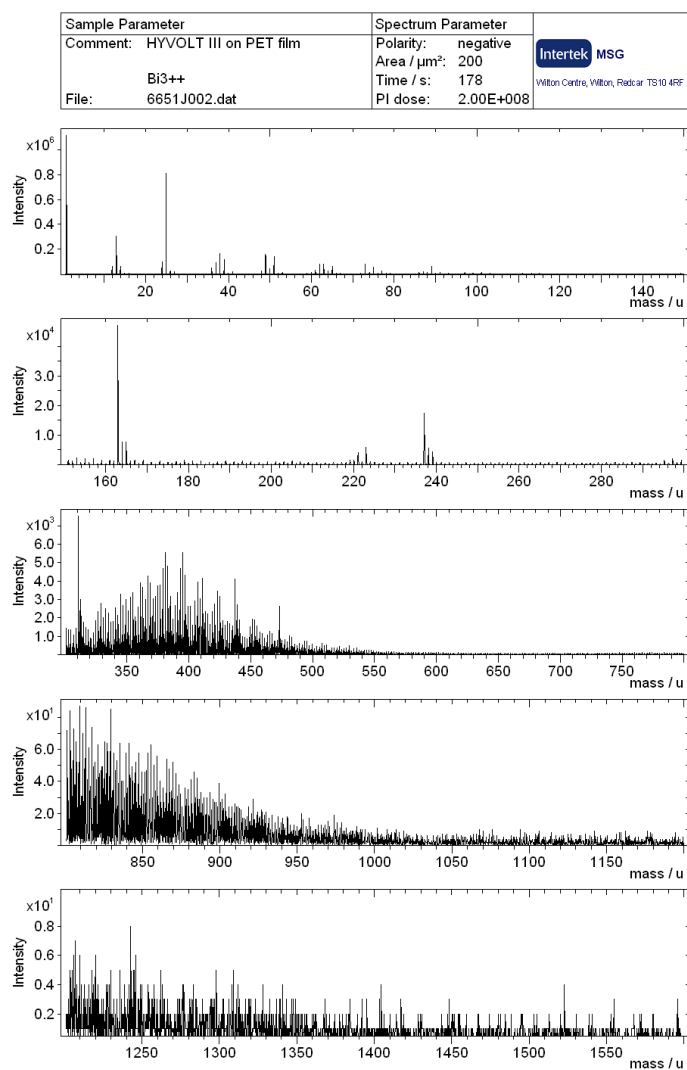


Figure A113 – Negative polarity secondary ion mass spectrum of HyVolt III oil on a PET film.

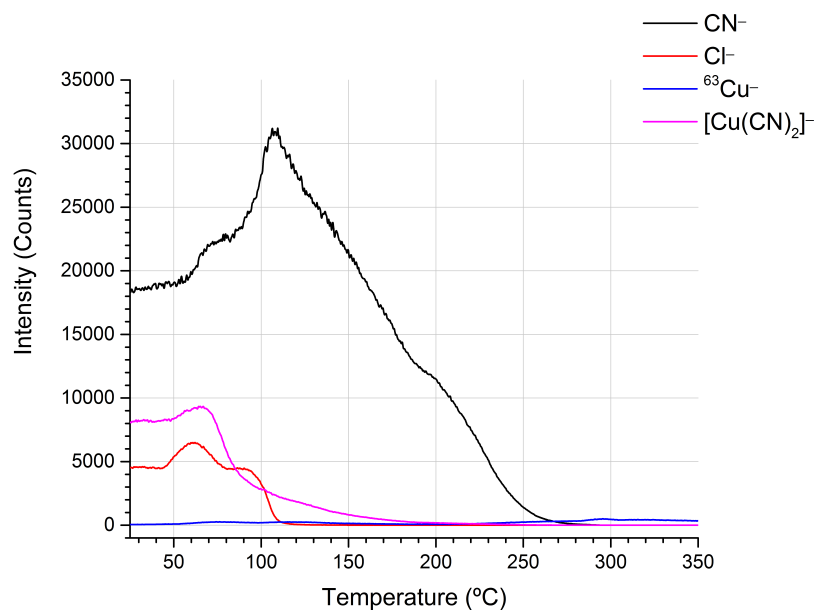


Figure A114 – TPD-SSIMS profiles for Cu^- , Cl^- and $\text{Cu}(\text{CN})_2^-$ on copper treated with 100 mg kg^{-1} of Irgamet[®] 39 in HyVolt III oil at 70 °C for 24 hours.

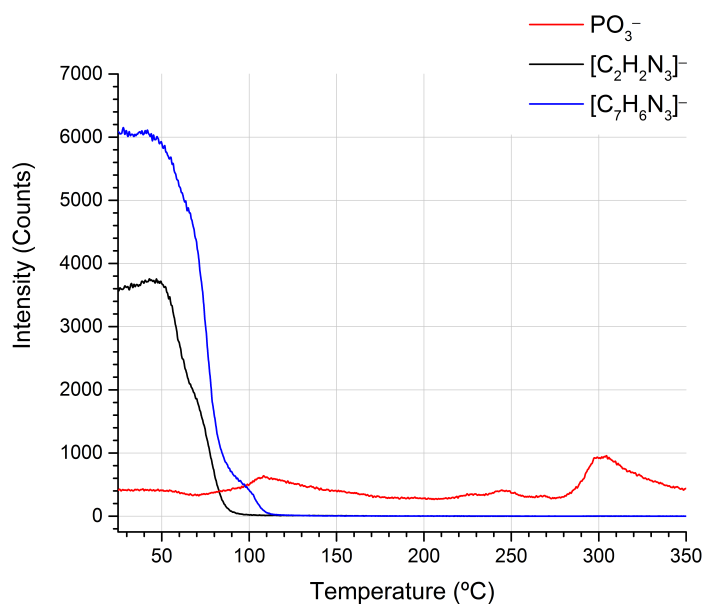


Figure A115 – TPD-SSIMS profiles for representative ions for the corrosion inhibitor and PO_3^- on copper treated with 100 mg kg^{-1} of Irgamet[®] 39 in HyVolt III oil at 70 °C for 24 hours.

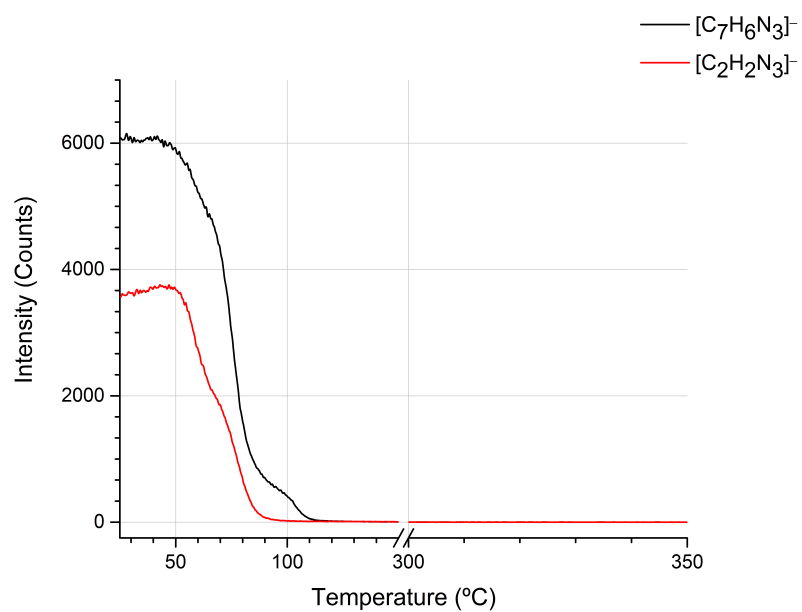


Figure A116 – TPD-SSIMS profiles for TTA deprotonated molecule (m/z 132) and TA ion (m/z 68) on copper treated with 100 mg kg⁻¹ of Irgamet[®] 39 in HyVolt III oil at 70 °C for 24 hours.

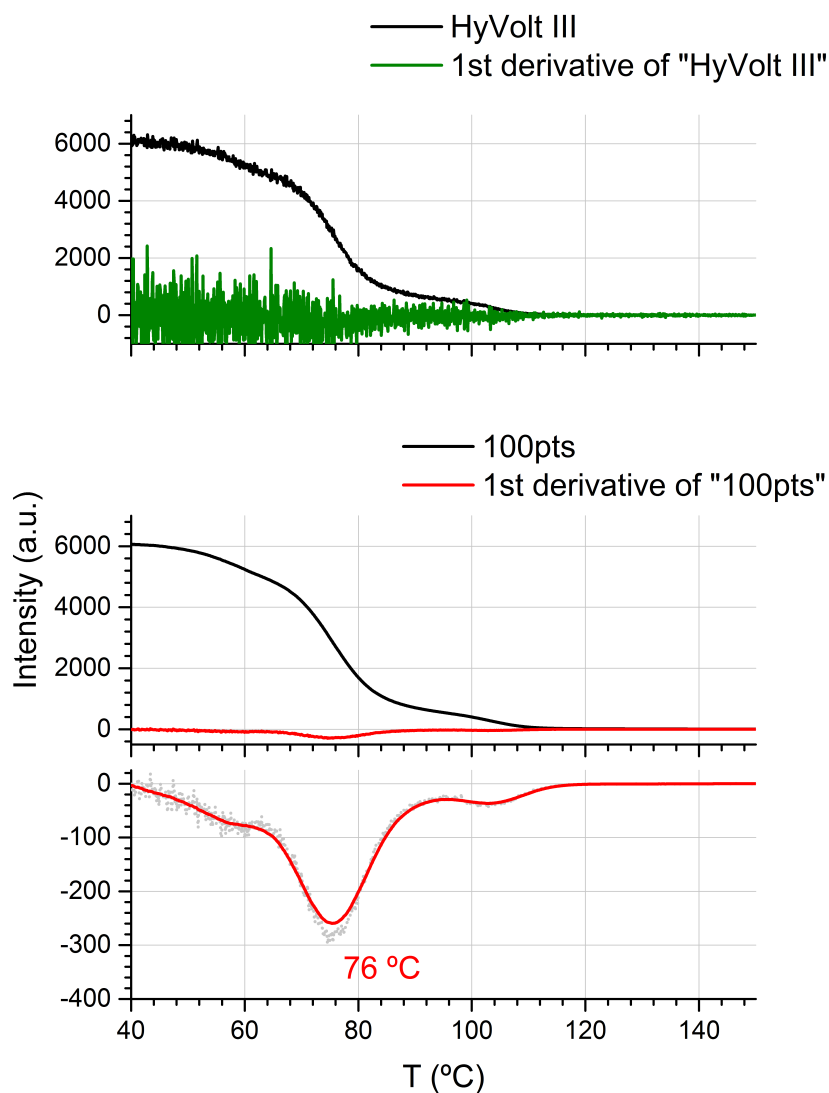


Figure A117 – Summary of the determination of T_p through TPD-SSIMS profiles processing: 1st differential (top) for m/z 132 on copper treated with 100 mg kg⁻¹ of Irgamet[®] 39 in HyVolt III oil at 70 °C for 24 hours; adjacent averaging smoothing at 100 points (middle); identification of the absolute minimum in the 1st differential plot (bottom).

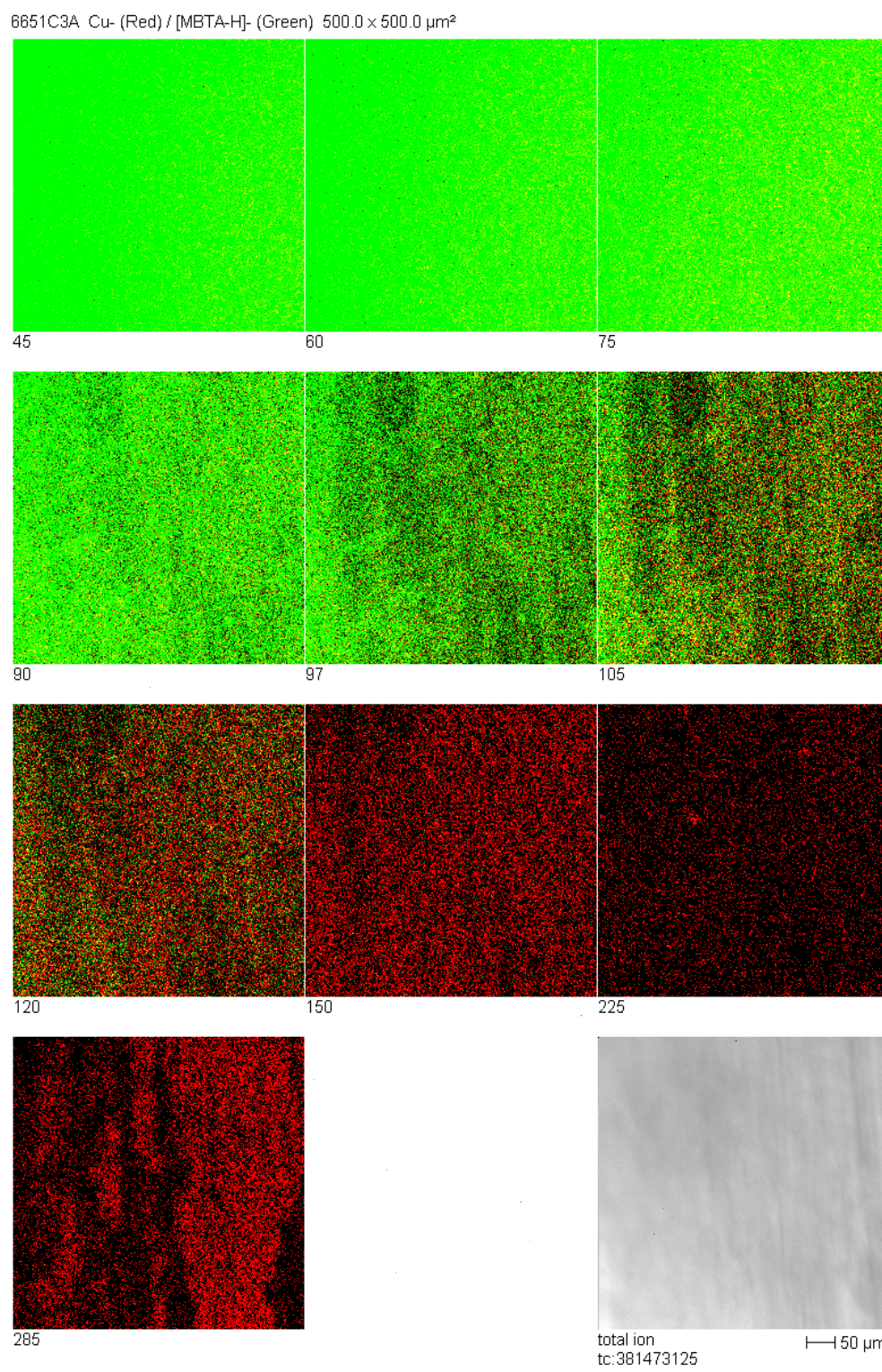


Figure A118 – Negative ion image from 45 °C to 285 °C of Cu (red) treated with 100 mg kg⁻¹ of Irgamet[®]39 (*i.e.* *m/z* 132, green) in HyVolt III oil at 70 °C for 24 hours.

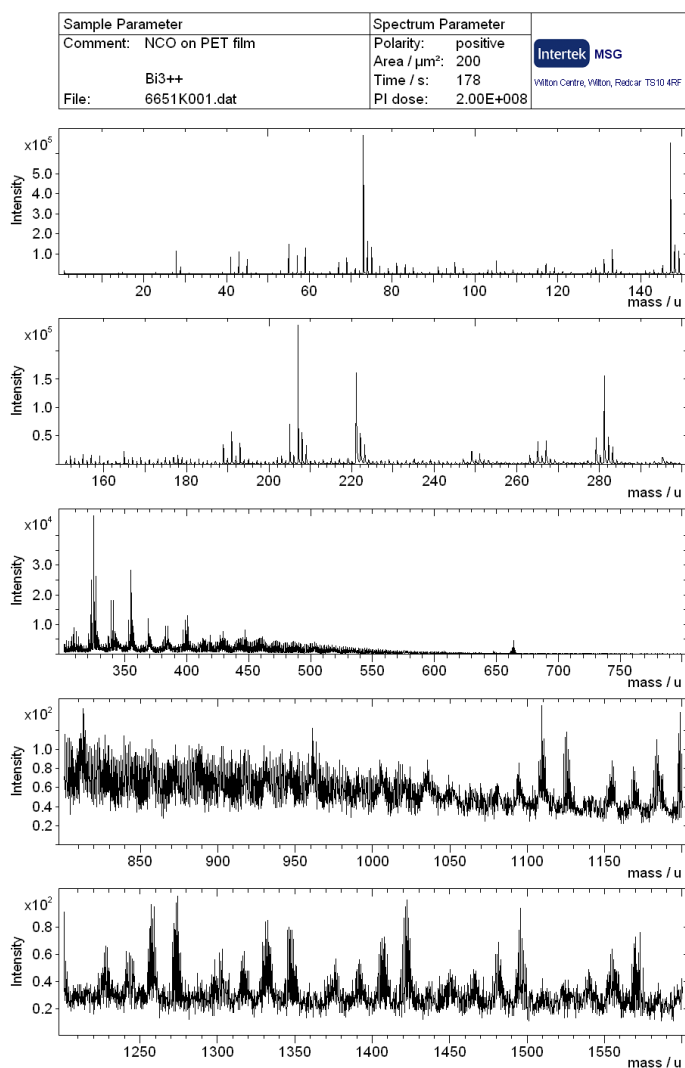
10 GBN oil

Figure A119 – Positive polarity secondary ion mass spectrum of 10 GBN oil on a PET film.

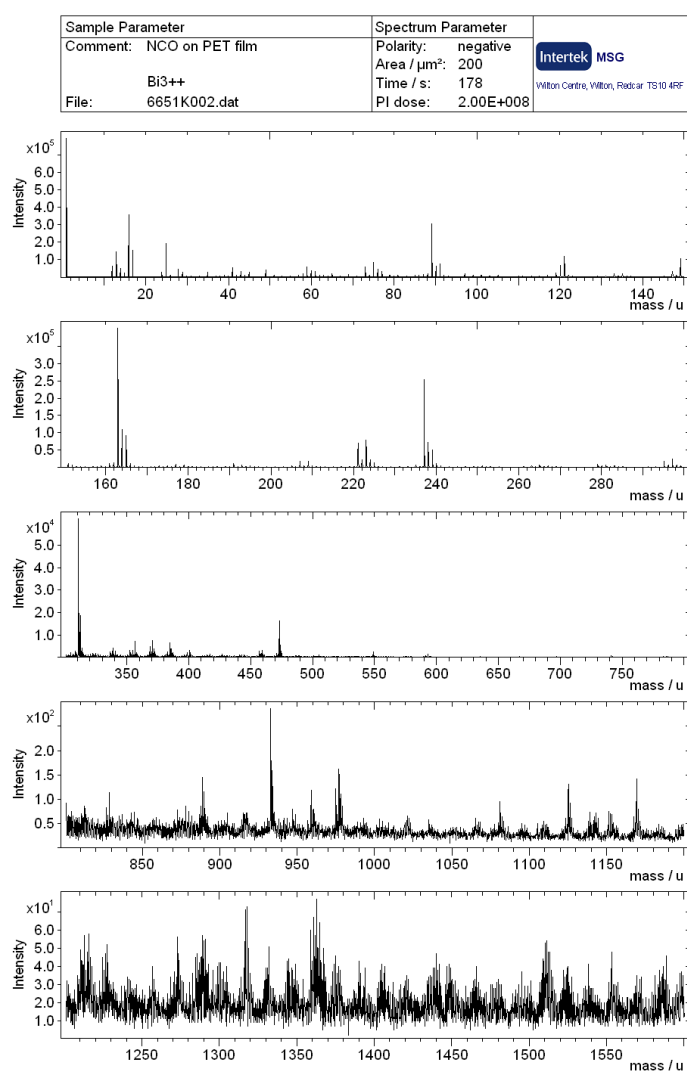


Figure A120 – Negative polarity secondary ion mass spectrum of 10 GBN oil on a PET film.

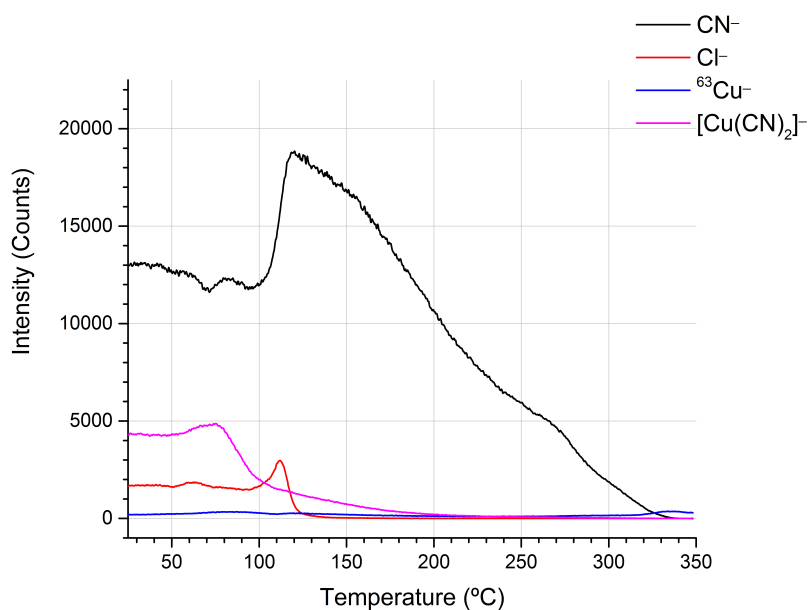


Figure A121 – TPD-SSIMS profiles for Cu^- , Cl^- and $\text{Cu}(\text{CN})_2^-$ on copper treated with 100 mg kg^{-1} of Irgamet[®] 39 in 10 GBN oil at 70 $^{\circ}\text{C}$ for 24 hours.

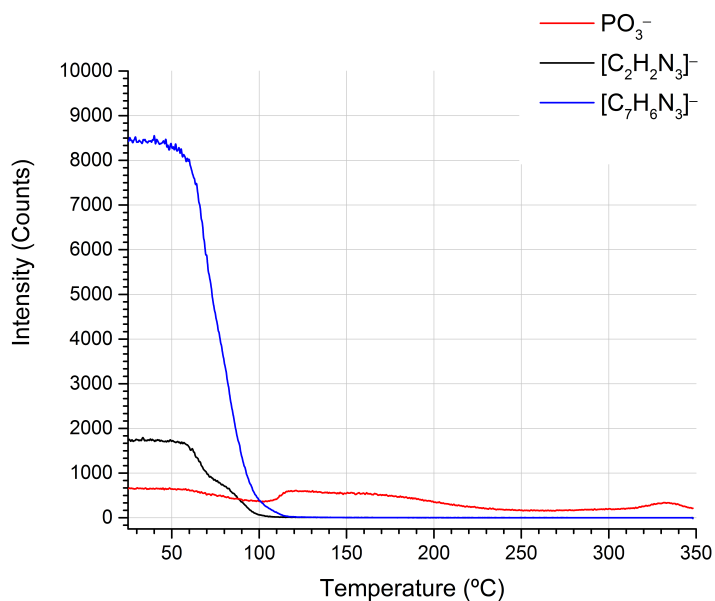


Figure A122 – TPD-SSIMS profiles for representative ions for the corrosion inhibitor and PO_3^- on copper treated with 100 mg kg^{-1} of Irgamet[®] 39 in 10 GBN oil at 70 $^{\circ}\text{C}$ for 24 hours.

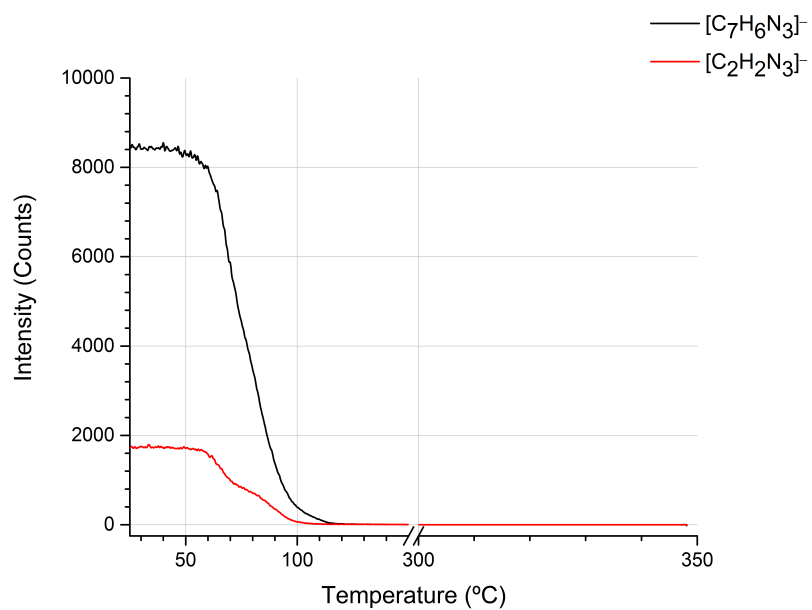


Figure A123 – TPD-SSIMS profiles for TTA deprotonated molecule (m/z 132) and TA ion (m/z 68) on copper treated with 100 mg kg⁻¹ of Irgamet[®] 39 in 10 GBN oil at 70 °C for 24 hours.

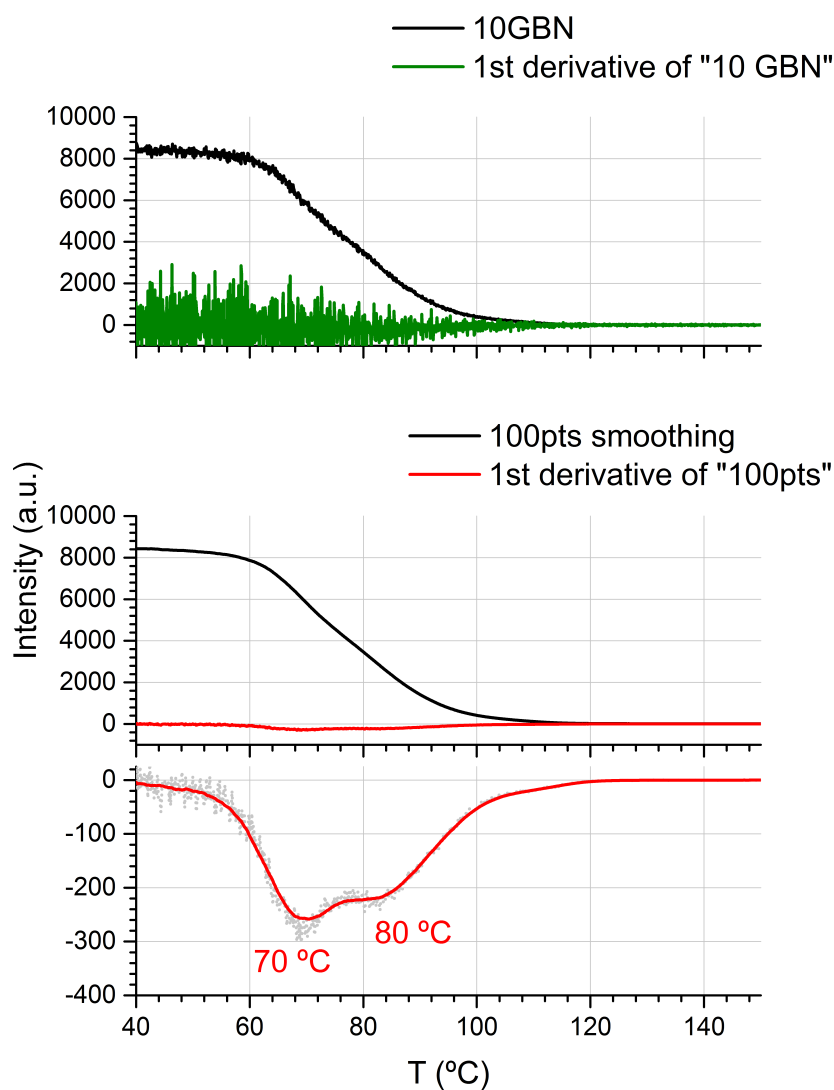


Figure A124 – Summary of the determination of T_p through TPD-SSIMS profiles processing: 1st differential (top) for m/z 132 on copper treated with 100 mg kg⁻¹ of Irgamet[®] 39 in 10 GBN oil at 70 °C for 24 hours; adjacent averaging smoothing at 100 points (middle); identification of the absolute minimum in the 1st differential plot (bottom).

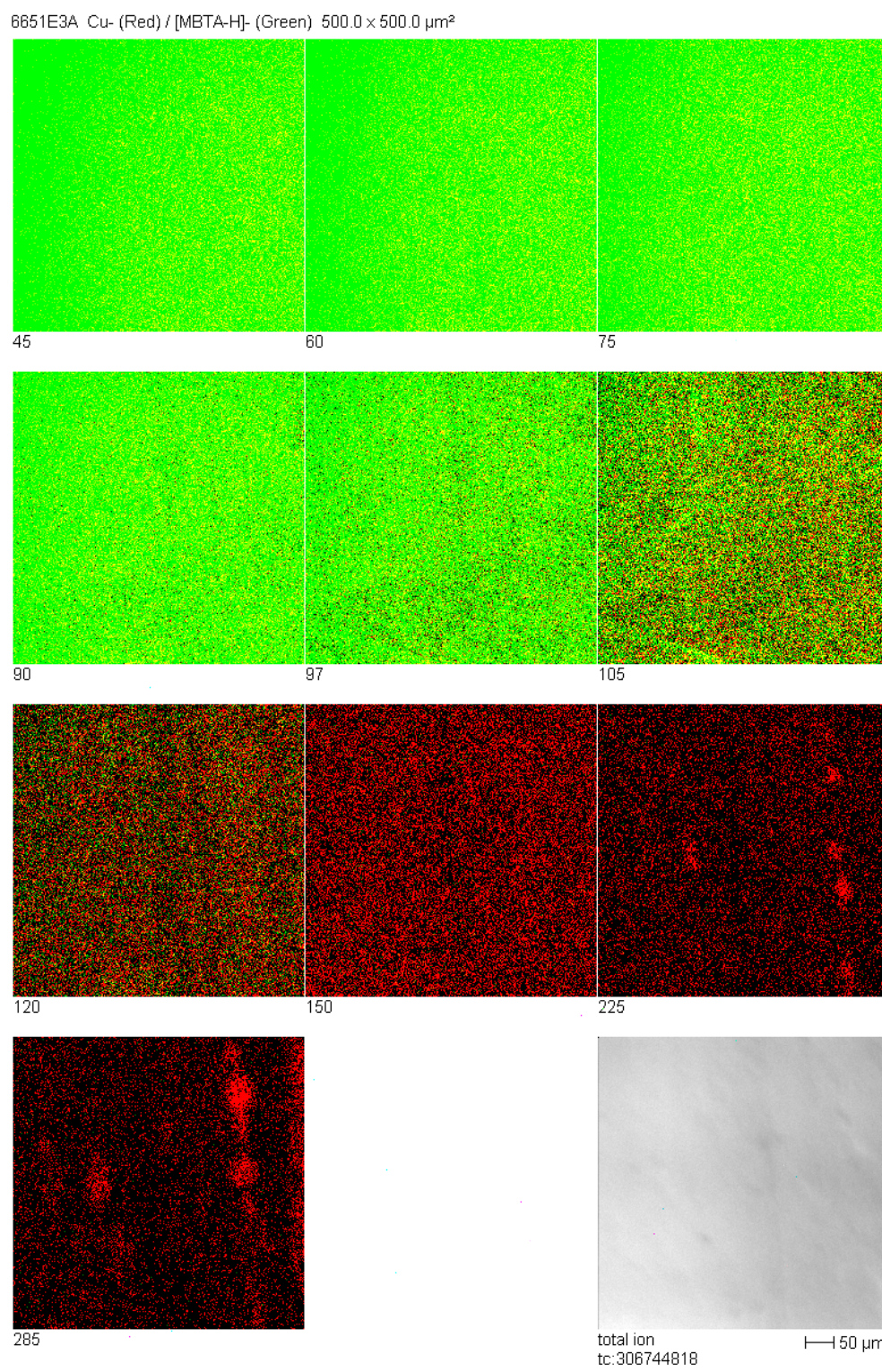


Figure A125 – Negative ion image from 45 °C to 285 °C of Cu (red) treated with 100 mg kg⁻¹ of Irgamet[®]39 (*i.e.* m/z 132, green) in 10 GBN oil at 70 °C for 24 hours.

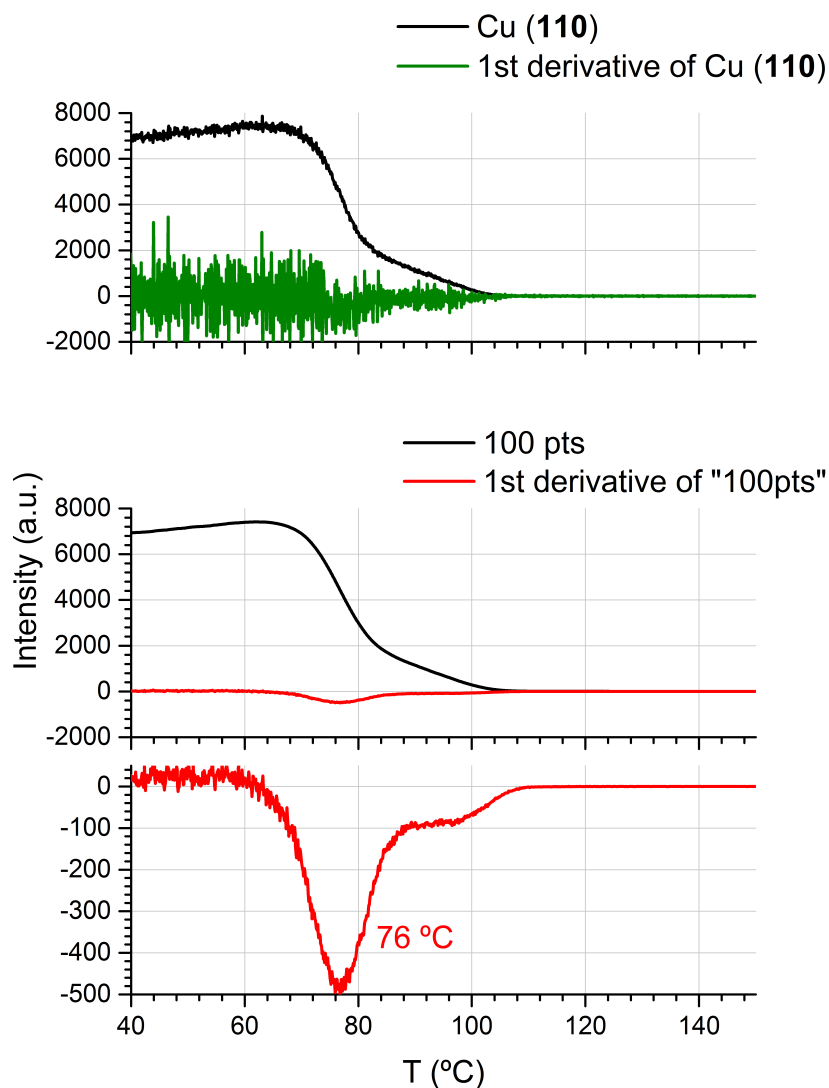
Cu(110) surface

Figure A126 – Summary of the determination of T_p through TPD-SSIMS profiles processing: 1st differential (top) for m/z 132 on Cu(110) treated with 100 mg kg⁻¹ of Irgamet[®]39 in Gemini X oil at 70 $^{\circ}\text{C}$ for 24 hours; adjacent averaging smoothing at 100 points (middle);

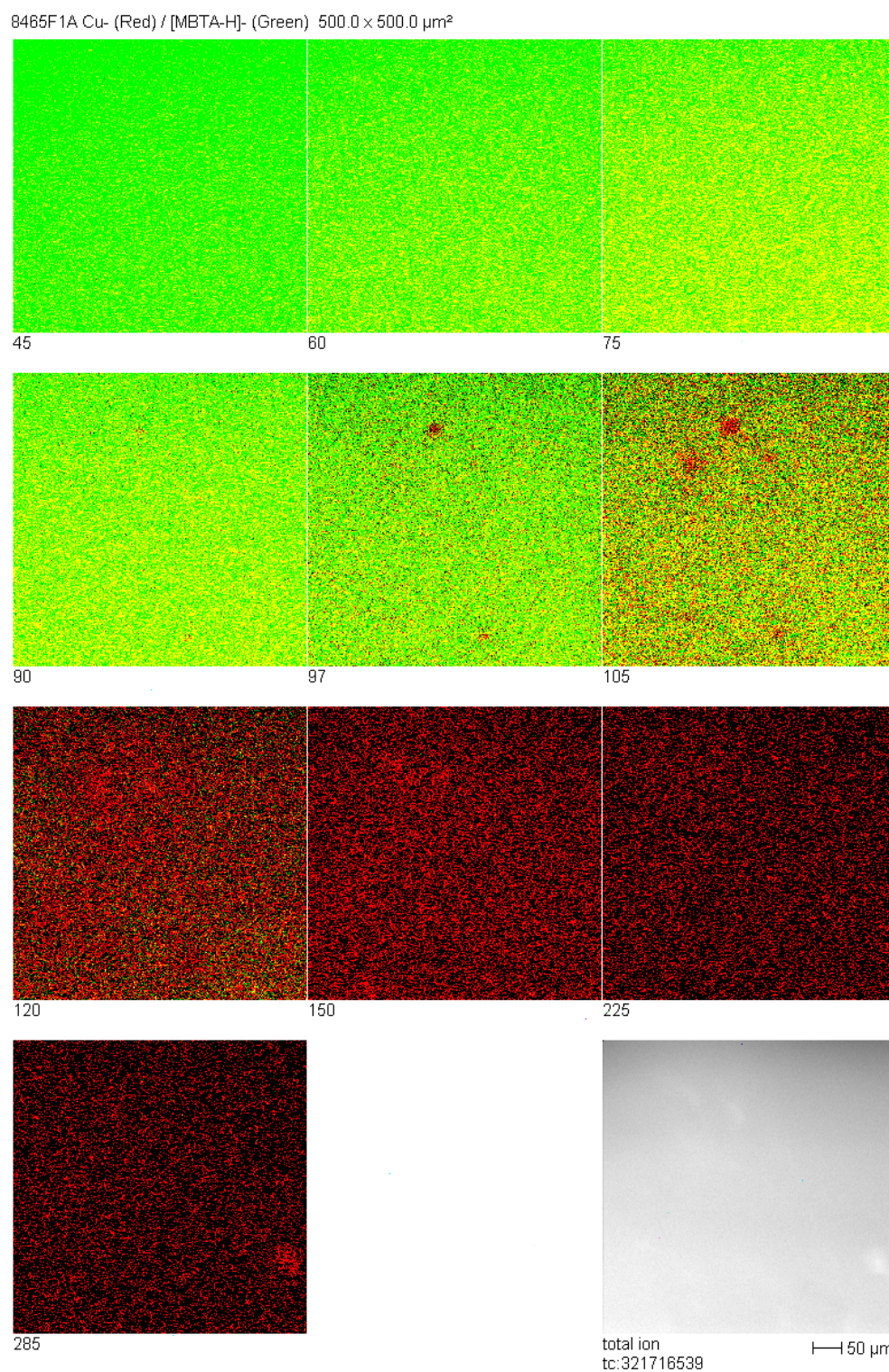


Figure A127 – Negative ion image from 45 °C to 285 °C of Cu(110) (red) treated with 100 mg kg^{-1} of Irgamet[®] 39 (*i.e.* m/z 132, green) in Gemini X oil at 70 °C for 24 hours.

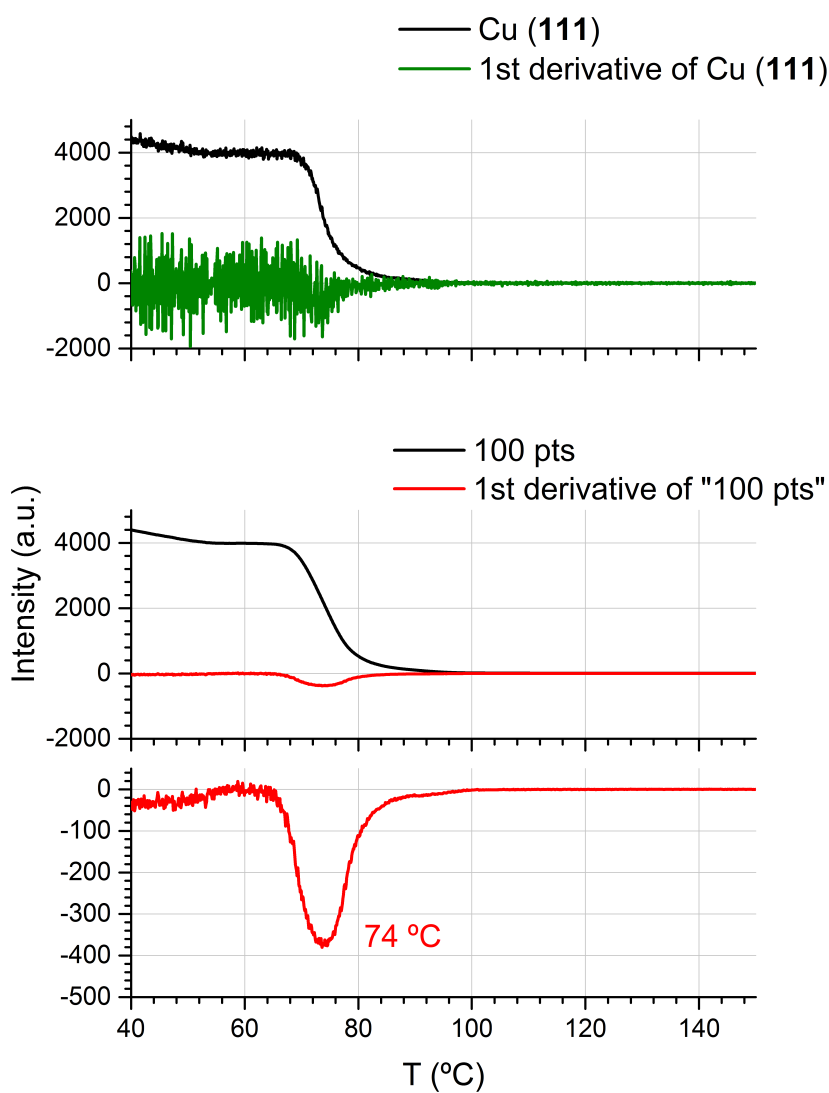
Cu(111) surface

Figure A128 – Summary of the determination of T_p through TPD-SSIMS profiles processing: 1st differential (top) for m/z 132 on Cu(111) treated with 100 mg kg⁻¹ of Irgamet[®]39 in Gemini X oil at 70 $^{\circ}\text{C}$ for 24 hours; adjacent averaging smoothing at 100 points (middle);

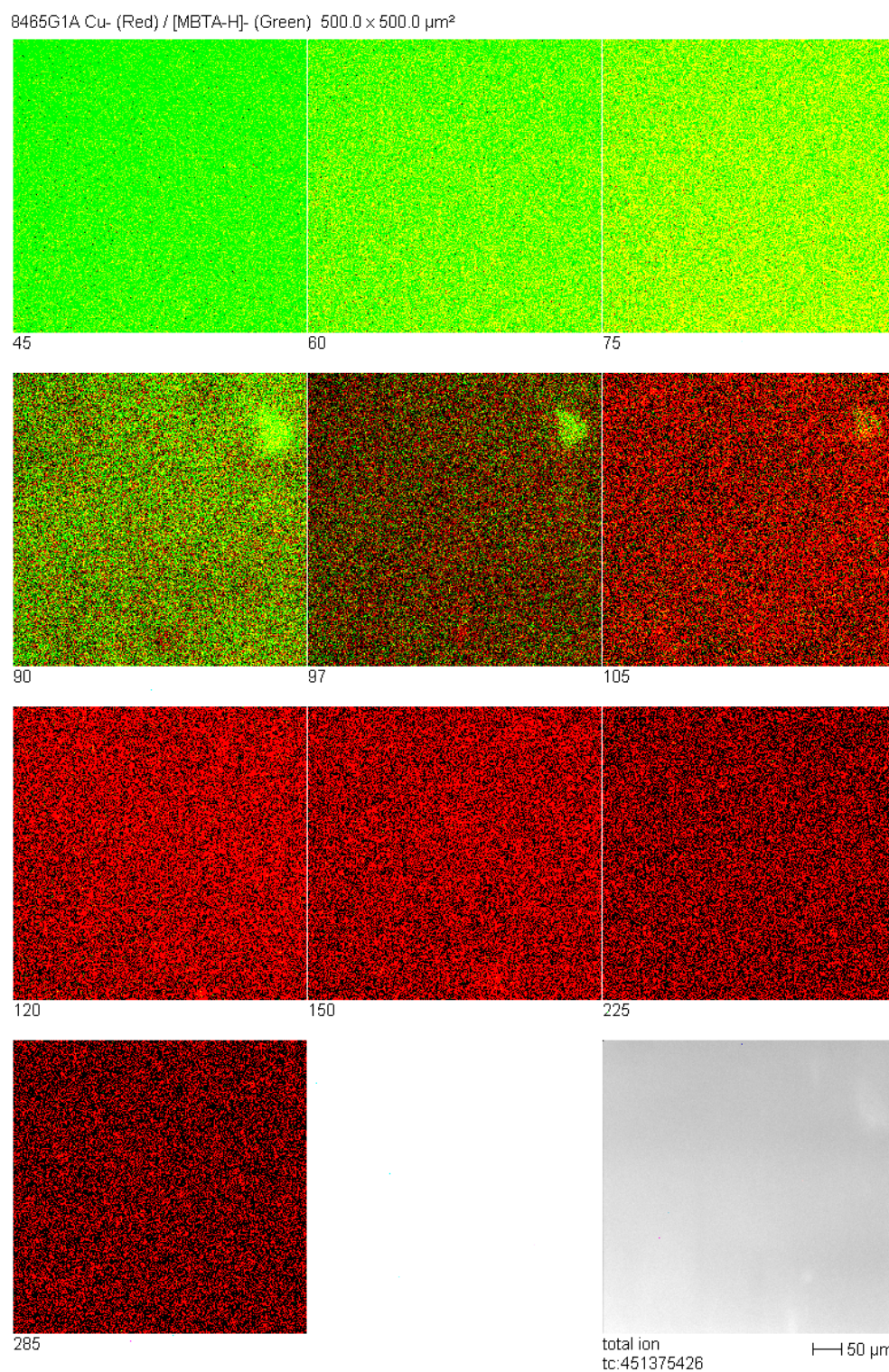


Figure A129 – Negative ion image from 45 °C to 285 °C of Cu (111) (red) treated with 100 mg kg⁻¹ of Irgamet[®] 39 (*i.e.* m/z 132, green) in Gemini X oil at 70 °C for 24 hours.

List of References

- (1) Faraday, M. Experimental Researches in Electricity. *Phil. Trans. R. Soc. Lond.* **1832**, 122, 472–478.
- (2) Maxwell, J. C. A Dynamical Theory of the Electromagnetic Field. *Phil. Trans. R. Soc. Lond.* **1865**, 155, 459–512.
- (3) Biscoe, J. History of public supply in the UK http://www.engineering-timelines.com/how/electricity/electricity_07.asp (accessed Jan 1, 2015).
- (4) *Digest of United Kingdom Energy Statistics (DUKES) 2014*; 2014.
- (5) Bartnikas, R. *Engineering Dielectrics: Volume III Electrical Insulating Liquids*; 1994.
- (6) Heathcote, M. J. *The J & P Transformer Book: A Practical Technology of the Power Transformer*; Newnes, 2007.
- (7) Winders, J. *Power Transformers: Principles and Applications*; Taylor & Francis, 2002.
- (8) Callan, N. LXXXVIII on a New Galvanic Battery. *Lond. Edinb. Dubl. Phil. Mag.* **1836**, 9, 472–478.
- (9) Zipenowski, K., Deri, M., Blathy, O. *Electric Distribution by Alternating Current*; 1888.
- (10) IEC TC 68. *Magnetic Materials (BS EN 60404)*; 2009.
- (11) Cotton, F.A., Wilkinson, G. *Advanced Inorganic Chemistry*; Fifth ed.; John Wiley & Sons, Inc., 1988.
- (12) IEC TC 10. *Copper and Copper Alloys (BS EN 13601)*; BSI, 2002; Vol. 3.
- (13) Solomon, S., Qin, D., Manning, M., Chen, Z., Marquis, M., Averyt, K.B., Tignor, M. and Miller, H. L. *Contribution of Working Group I to the Fourth Assessment Report of the Intergovernmental Panel on Climate Change*; Cambridge, UK and NY(USA), 2007.
- (14) Heywood, R. J. The Degradation Models of Cellulosic Transformer Insulation, Ph.D. thesis, University of Surrey, 1997.
- (15) IEC TC 10. *Fluids for Electrotechnical Applications. Unused Mineral Insulating Oils for Transformers and Switchgear (BS EN 60296)*; 2012.
- (16) Facciotti, M. Determination of Copper in Insulating Paper and Oils Used in Electrical Power Transformers and Its Effect on Dielectric Properties, M.Sc. thesis, University of Turin, 2010.

References

- (17) Rasco, J. M. Petroleum Refining Production of Naphthenic Transformer Oil Control of Corrosive Sulfur. In *74th Annual International Doble Client Conference*; Doble Engineering Company: Boston, MA, USA, 2007; Vol. 1275.
- (18) IEC TC 10. *Mineral Oil-Impregnated Electrical Equipment in Service. Guide to the Interpretation of Dissolved and Free Gases Analysis (BS EN 60599)*; 2007; Vol. 3.
- (19) ASTM D27. *Mineral Insulating Oils Used in Electrical Power Apparatus (ASTM D3487)*.
- (20) McNaught, A. D.; Wilkinson, A. *IUPAC Compendium of Chemical Terminology 2005*; 2nd ed.; Blackwell Scientific Publications, Oxford: Oxford, 2005.
- (21) Thethwayo, B. M.; Garbers-Craig, A. M. Laboratory Scale Investigation into the Corrosion of Copper in a Sulphur-Containing Environment. *Corros. Sci.* **2011**, *53*, 3068–3074.
- (22) Tran, T. T. M.; Fiaud, C.; Sutter, E. M. M. Oxide and Sulphide Layers on Copper Exposed to H₂S Containing Moist Air. *Corros. Sci.* **2005**, *47*, 1724–1737.
- (23) Tran, T. T. M.; Fiaud, C.; Sutter, E. M. M.; Villanova, A. The Atmospheric Corrosion of Copper by Hydrogen Sulphide in Underground Conditions. *Corros. Sci.* **2003**, *45*, 2787–2802.
- (24) Drach, A.; Tsukrov, I.; DeCew, J.; Aufrecht, J.; Grohbauer, A.; Hofmann, U. Field Studies of Corrosion Behaviour of Copper Alloys in Natural Seawater. *Corros. Sci.* **2013**, *76*, 453–464.
- (25) Armstrong, R. D.; Hall, C. A. The Corrosion of Metals in Contact with Ester Oils at Temperatures up to 200°C. *Corros. Sci.* **1994**, *36*, 463–477.
- (26) Fazal, M. A.; Haseeb, A. S. M. A.; Masjuki, H. H. Corrosion Mechanism of Copper in Palm Biodiesel. *Corros. Sci.* **2013**, *67*, 50–59.
- (27) Qian, Y.; Su, W. Research on Influencing Factors of Corrosive Sulfur Attacking Copper in Insulating Oil and Prevention. *IEEEJ Trans. Electr. Electron. Eng.* **2013**, *8*, 546–549.
- (28) Levin, M.; Wiklund, P.; Leygraf, C. Bioorganic Compounds as Copper Corrosion Inhibitors in Hydrocarbon Media. *Corros. Sci.* **2012**, *58*, 104–114.
- (29) Kalantar, A.; Levin, M. Factors Affecting the Dissolution of Copper in Transformer Oils. *Lubr. Sci.* **2008**, *20*, 223–240.
- (30) Ren, S.; Xu, Y.; Cao, X.; Zhong, L.; Yu, Q.; Jeanjean, R. A Research Summary of Corrosive Sulfur in Mineral Oils. In *Proceedings of the IEEE International Conference on Properties and Applications of Dielectric Materials*; 2009; pp. 353–356.
- (31) Scatiggio, F.; Tumiatti, V.; Maina, R.; Tumiatti, M.; Pompili, M.; Bartnikas, R. Corrosive Sulfur in Insulating Oils: Its Detection and Correlated Power Apparatus Failures. *IEEE Trans. Power Deliv.* **2008**, *23*, 508–509.

- (32) Bengtsson, C.; Dahlund, M.; Hajek, J. A. N.; Pettersson, L. F.; Gustafsson, K.; Leandersson, R.; Hjortsberg, A. *CIGRE A2-111 Oil Corrosion and Conduction Cu₂S Deposition in Power Transformer Windings*; 2006.
- (33) Lukic, J. M.; Milosavljevic, S. B.; Orlovic, A. M. Degradation of the Insulating System of Power Transformers by Copper Sulfide Deposition: Influence of Oil Oxidation and Presence of Metal Passivator. *Ind. Eng. Chem. Res.* **2010**, *49*, 9600–9608.
- (34) Han, Q.; Zhu, J.; Zhu, W.; Yang, X.; Lu, L.; Wang, X. Spontaneous Growth of Copper Sulfide Nanowires from Elemental Sulfur in Carbon-Coated Cu Grids. *Mater. Lett.* **2009**, *63*, 2358–2360.
- (35) Tumiatti, V.; Maina, R.; Scatiggio, F.; Pompili, M.; Bartnikas, R. Corrosive Sulphur in Mineral Oils: Its Detection and Correlated Transformer Failures. *Conf. Rec. IEEE Int. Symp. Electr. Insul.* **2006**, 400–402.
- (36) Lukic, J.; Wilson, G.; Scatiggio, F.; Rasco, J.; Dahlund, M.; Maina, R.; Peixoto, A.; Buchacz, T.; Smith, P.; Bertrand, Y.; et al. *CIGRE WG A2.40 Final Report - Copper Sulphide Long Term Mitigation and Risk Assessment (TB 625)*; 2015.
- (37) IEC TC 10. *Insulating Liquids. Test Method for Detection of Potentially Corrosive Sulphur in Used and Unused Insulating Oil (BS EN 62535)*; 2009.
- (38) Scatiggio, F.; Tumiatti, V.; Maina, R.; Tumiatti, M.; Pompili, M.; Bartnikas, R. Corrosive Sulfur Induced Failures in Oil-Filled Electrical Power Transformers and Shunt Reactors. *IEEE Trans. Power Deliv.* **2009**, *24*, 1240–1248.
- (39) Krawiec, S. Production of Corrosive Sulphur Free Transformer Fluids. In *Electrical Insulation Conference and Electrical Manufacturing Expo*; IEEE, 2007; pp. 76–79.
- (40) Arvidsson, L. Conditions for DBDS Induced Corrosive Sulfur Formation. In *Conference Record of the 2010 IEEE International Symposium on*; IEEE, 2010; pp. 1–4.
- (41) Hailing, J. Encyclopedia of Tribology. *Wear*, 1991, *150*, 382.
- (42) Amimoto, T.; Hosokawa, N.; Nagao, E.; Tanimura, J.; Toyama, S. Concentration Dependence of Corrosive Sulfur on Copper-Sulfide Deposition on Insulating Paper Used for Power Transformer Insulation. *IEEE Trans. Dielectr. Electr. Insul.* **2009**, *16*, 1489–1495.
- (43) Oweimreen, G. A.; Jaber, A. M. Y.; Abulkibash, A. M.; Mehanna, N. A. The Depletion of Dibenzyl Disulfide from a Mineral Transformer Insulating Oil. *IEEE Trans. Dielectr. Electr. Insul.* **2012**, *19*, 1962–1970.
- (44) Mizuno, K.; Toyama, S.; Kawai, H.; Tanimura, J.; Fujita, Y.; Kato, F.; Amimoto, T.; Hosokawa, N.; Nagao, E. Identification of Compounds Leading to Copper Sulfide Formation on Insulating Paper in Transformers and the Degradation of Suppressing Effect of 1, 2, 3-Benzotriazole and Irgamet® 39 in Insulating Oil. In *76th Annual International Doble Client Conference*; Doble Engineering Company: Boston, MA, USA, 2009; pp. IM – 7.

References

- (45) Facciotti, M.; Amaro, P. S.; Holt, A. F.; Brown, R. C. D.; Lewin, P. L.; Pilgrim, J. A.; Wilson, G.; Jarman, P. N. Contact-Based Corrosion Mechanism Leading to Copper Sulphide Deposition on Insulating Paper Used in Oil-Immersed Electrical Power Equipment. *Corros. Sci.* **2014**, *84*, 172–179.
- (46) Amimoto, T.; Nagao, E.; Tanimura, J.; Toyama, S.; Fujita, Y.; Kawarai, H.; Yamada, N. Identification of Affecting Factors of Copper Sulfide Deposition on Insulating Paper in Oil. *IEEE Trans. Dielectr. Electr. Insul.* **2009**, *16*, 265–272.
- (47) Whitfield, T. B.; Castle, J. E.; Saracco, C.; Ali, M. Transport of Copper over Paper in High-Voltage Electrical Insulation. *Surf. Interface Anal.* **2002**, *34*, 176–179.
- (48) Wiklund, P.; Levin, M.; Pahlavanpour, B. Copper Dissolution and Metal Passivators in Insulating Oil. *IEEE Electr. Insul. Mag.* **2007**, *23*, 6–14.
- (49) Kato, F.; Amimoto, T.; Nagao, E.; Hosokawa, N.; Toyama, S.; Tanimura, J. Effect of DBDS Concentration and Heating Duration on Copper Sulfide Formation in Oil-Immersed Transformer Insulation. *IEEE Trans. Dielectr. Electr. Insul.* **2011**, *18*, 1869–1876.
- (50) Kawarai, H.; Fujita, Y.; Tanimura, J.; Toyama, S.; Yamada, N.; Nagao, E.; Hosokawa, N.; Amimoto, T. Role of Dissolved Copper and Oxygen on Copper Sulfide Generation in Insulant Oil. *IEEE Trans. Dielectr. Electr. Insul.* **2009**, *16*.
- (51) Ren, S.; Zhong, L.; Yu, Q.; Cao, X.; Li, S. Influence of the Atmosphere on the Reaction of Dibenzyl Disulfide with Copper in Mineral Insulation Oil. *IEEE Trans. Dielectr. Electr. Insul.* **2012**, *19*, 849–854.
- (52) Kawarai, H.; Uehara, Y.; Mizuno, K.; Toyama, S.; Nagao, E.; Hosokawa, N.; Amimoto, T. Influences of Oxygen and 2,6-Di-Tert-Butyl-P-Cresol on Copper Sulfide Deposition on Insulating Paper in Oil-Immersed Transformer Insulation. *Dielectr. Electr. Insul. IEEE Trans.* **2012**, *19*, 1884–1890.
- (53) Toyama, S.; Mizuno, K.; Kato, F.; Nagao, E.; Amimoto, T.; Hosokawa, N. Influence of Inhibitor and Oil Components on Copper Sulfide Deposition on Kraft Paper in Oil-Immersed Insulation. *IEEE Trans. Dielectr. Electr. Insul.* **2011**, *18*, 1877–1885.
- (54) Amaro, P. S. Corrosive Sulphur in Large Transformers: Impact, Quantification and Detection, Ph.D. thesis, University of Southampton, 2015.
- (55) De Carlo, R. M.; Bruzzoniti, M. C.; Sarzanini, C.; Maina, R.; Tumiatti, V. Copper Contaminated Insulating Mineral Oils-Testing and Investigations. *IEEE Trans. Dielectr. Electr. Insul.* **2013**, *20*, 557–563.
- (56) De Carlo, R.; Sarzanini, C.; Bruzzoniti, M.; Maina, R.; Tumiatti, V. Copper-in-Oil Dissolution and Copper-on-Paper Deposition Behavior of Mineral Insulating Oils. *IEEE Trans. Dielectr. Electr. Insul.* **2014**, *21*, 666–673.
- (57) Bruzzoniti, M. C.; De Carlo, R. M.; Sarzanini, C.; Maina, R.; Tumiatti, V. Determination of Copper in Liquid and Solid Insulation for Large Electrical Equipment by ICP-OES. Application to Copper Contamination Assessment in Power Transformers. *Talanta* **2012**, *99*, 703–711.

- (58) Dahlund, M.; Atanasova-Höhlein, I.; Maina, R.; Dominelli, N.; Ohnstad, T.; Amimoto, T.; Claiborne, C.; Ese, M.-H.; Lukic, J.; Mezhvynskiy, V.; et al. *CIGRE WG A2-32 Final Report - Copper Sulphide in Transformer Insulation*; 2009.
- (59) Griffin, P. J.; Lewand, L. R. Understanding Corrosive Sulfur Problems in Electric Apparatus. In *74th Annual International Doble Client Conference*; Doble Engineering Company: Boston, MA, USA, 2007.
- (60) Mitchinson, P. M.; Lewin, P. L.; Jarman, P. A Mechanism for the Formation of Copper Sulphide in Oil Filled Electrical Equipment. In *Conference Record of the IEEE International Symposium on Electrical Insulation (ISEI)*; 2010; pp. 1–4.
- (61) Facciotti, M.; Amaro, P. S.; Brown, R. C. D.; Lewin, P. L.; Pilgrim, J. A.; Wilson, G.; Jarman, P. N. SSIMS Molecular Selective Imaging: A New Diagnostic Tool to Investigate Metal Passivators in Scrapped Transformers. In *2015 IEEE Electrical Insulation Conference (EIC)*; 2015; pp. 388–391.
- (62) Facciotti, M.; Amaro, P. S.; Brown, R. C. D.; Lewin, P. L.; Pilgrim, J. A.; Wilson, G.; Jarman, P. N. Passivators, Corrosive Sulphur and Surface Chemistry. Tools for the Investigation of Effective Protection. In *MyTransfo 2014: Oil and Transformer*; 2014; pp. 27–35.
- (63) Facciotti, M.; Amaro, P. S.; Brown, R. C. D.; Lewin, P. L.; Pilgrim, J. A.; Wilson, G.; Jarman, P. N.; Fletcher, I. W. Static Secondary Ion Mass Spectrometry Investigation of Corrosion Inhibitor Irgamet®39 on Copper Surfaces Treated in Power Transformer Insulating Oil. *Corros. Sci.* **2015**, *98*, 450–456.
- (64) Toyama, S.; Tanimura, J.; Yamada, N.; Nagao, E.; Amimoto, T. Highly Sensitive Detection Method of DBDS and the Elucidation of the Mechanism of Copper Sulfide Generation in Insulating Oils. *IEEE Trans. Dielectr. Electr. Insul.* **2009**, *16*, 509–515.
- (65) Jaber, A. M. Y.; Mehanna, N. A.; Abulkibash, A. M. Simultaneous Liquid-Liquid Extraction of Dibenzyl Disulfide, 2,6-Di-Tert-Butyl-P-Cresol, and 1,2,3-Benzotriazole from Power Transformer Oil prior to GC and HPLC Determination. *J. Sep. Sci.* **2012**, *35*, 750–757.
- (66) Bruzzoniti, M. C.; Maina, R.; Tumiatti, V.; Sarzanini, C.; De Carlo, R. M. Simultaneous Determination of Passivator and Antioxidant Additives in Insulating Mineral Oils by High-Performance Liquid Chromatography. *J. Liq. Chromatogr. Relat. Technol.* **2014**, *38*, 15–19.
- (67) Tumiatti, V.; Roggero, C.; Tumiatti, M.; Di Carlo, S.; Maina, R. State of the Art in Quantification of DBDS and Other Corrosive Sulfur Compounds in Unused and Used Insulating Oils. *IEEE Trans. Dielectr. Electr. Insul.* **2012**, *19*, 1633–1641.
- (68) Roggero, C.; Du, J.; Seemamahannop, R.; Kapila, S.; Tumiatti, V.; Tumiatti, M. Rapid and Specific Determination of Contaminants, by-Products, and Additives in Insulating Mineral Oils with Tandem Mass Spectrometry. *LC-GC Eur.* **2013**, *18*, 20–22, 24–25.

References

- (69) Bruzzoniti, M. C.; De Carlo, R. M.; Sarzanini, C.; Maina, R.; Tumiatti, V. Stability and Reactivity of Sulfur Compounds against Copper in Insulating Mineral Oil: Definition of a Corrosiveness Ranking. *Ind. Eng. Chem. Res.* **2014**, *53*, 8675–8684.
- (70) Holt, A. F.; Facciotti, M.; Amaro, P.; Brown, R. C. D.; Lewin, P. L.; Pilgrim, J. A.; Wilson, G.; Jarman, P. Silver Corrosion in Transformers. In *2013 Annual Report Conference on Electrical Insulation and Dielectric Phenomena*; IEEE, 2013; pp. 448–451.
- (71) Holt, A. F.; Facciotti, M.; Amaro, P.; Brown, R. C. D.; Lewin, P. L.; Pilgrim, J. A.; Wilson, G.; Jarman, P. An Initial Study into Silver Corrosion in Transformers Following Oil Reclamation. In *2013 IEEE Electrical Insulation Conference (EIC)*; IEEE, 2013; pp. 469–472.
- (72) Dahlund, M.; Johansson, H.; Lager, U.; Wilson, G. Understanding the Presence of Corrosive Sulfur in Previously Non-Corrosive Oils Following Regeneration. In *77th Annual International Doble Client Conference, Boston, MA, USA*; Doble Engineering Company: Boston, MA, USA, 2010; p. IM – 5.
- (73) Lewand, L. R. Passivators. *Neta World* **2006**, 1–3.
- (74) Waynick, J. A. The Development and Use of Metal Deactivators in the Petroleum Industry: A Review. *Energy & Fuels* **2001**, *15*, 1325–1340.
- (75) Kokalj, A.; Peljhan, S.; Finsgar, M.; Milosev, I. What Determines the Inhibition Effectiveness of ATA, BTAH, and BTAOH Corrosion Inhibitors on Copper? *J. Am. Chem. Soc.* **2010**, *132*, 16657–16668.
- (76) Mansikkamäki, K.; Ahonen, P.; Fabricius, G.; Murtomäki, L.; Kontturi, K. Inhibitive Effect of Benzotriazole on Copper Surfaces Studied by SECM. *J. Electrochem. Soc.* **2005**, *152*, B12.
- (77) Antonijevic, M. M.; Petrovic, M. B. Copper Corrosion Inhibitors. A Review. *Int. J. Electrochem. Sci.* **2008**, *3*, 1–28.
- (78) Al Kharafi, F. M.; Abdullah, A. M.; Ghayad, I. M.; Ateya, B. G. Effect of Sulfide Pollution on the Stability of the Protective Film of Benzotriazole on Copper. *Appl. Surf. Sci.* **2007**, *253*, 8986–8991.
- (79) Levin, M.; Wiklund, P.; Arwin, H. Adsorption and Film Growth of N-Methylamino Substituted Triazoles on Copper Surfaces in Hydrocarbon Media. *Appl. Surf. Sci.* **2007**, *254*, 1528–1533.
- (80) Wiklund, P. Chemical Stability of Benzotriazole Copper Surface Passivators in Insulating Oils. *Ind. Eng. Chem. Res.* **2007**, *46*, 3312–3316.
- (81) Kato, F.; Amimoto, T.; Nishiura, R.; Mizuno, K.; Toyama, S. Suppressive Effect and Its Duration of Triazole-Based Passivators on Copper Sulfide Deposition on Kraft Paper in Transformer. *IEEE Trans. Dielectr. Electr. Insul.* **2013**, *20*, 1915–1921.

- (82) Martins, M. A. G.; Gomes, A. R.; Pahlavanpour, B. Experimental Study of a Passivated Oil Corrosiveness, after Depletion of the Passivator. *IEEE Electr. Insul. Mag.* **2009**, *25*, 23–27.
- (83) Maina, R.; Tumiatti, V.; Pompili, M.; Bartnikas, R. Corrosive Sulfur Effects in Transformer Oils and Remedial Procedures. *IEEE Trans. Dielectr. Electr. Insul.* **2009**, *16*, 1655–1663.
- (84) Scatiggio, F.; Pompili, M.; Bartnikas, R. Oils with Presence of Corrosive Sulphur - Migration and Collateral Effects. *2009 IEEE Electrical Insulation Conference*, 2009.
- (85) Facciotti, M.; Holt, A. F.; Amaro, A. P. G. V; Brown, R. C. D.; Lewin, P. L.; Wilson, G.; Jarman, P. N. XPS Study on Direct Detection of Passivator Irgamet 39TM on Copper Surfaces Aged in Insulating Mineral Oil. In *2013 Annual Report Conference on Electrical Insulation and Dielectric Phenomena*; IEEE, 2013; pp. 1097–1100.
- (86) Allam, N. K.; Nazeer, A. A.; Ashour, E. A. A Review of the Effects of Benzotriazole on the Corrosion of Copper and Copper Alloys in Clean and Polluted Environments. *J. Appl. Electrochem.* **2009**, *39*, 961–969.
- (87) Finšgar, M.; Milošev, I. Inhibition of Copper Corrosion by 1,2,3-Benzotriazole: A Review. *Corros. Sci.* **2010**, *52*, 2737–2749.
- (88) Rudnick, L. R. Lubricant Additives: Chemistry and Applications; 2009; pp. 7–8, 28–29.
- (89) Levin, M. *Application of Copper Corrosion Inhibitors in Mineral Oil: Surface Analytical Studies and Corrosion Mitigation Evaluations*; Ph.D. thesis, KTH Royal Institute of Technology, 2012.
- (90) Chasan, D. E.; Ribeaud, M. Multiple Metal Corrosion Inhibitor, *Patent*, August 14, 2008.
- (91) Scatiggio, F.; Pompili, M.; Bartnikas, R. Effects of Metal Deactivator Concentration upon the Gassing Characteristics of Transformer Oils. *IEEE Trans. Dielectr. Electr. Insul.* **2011**, *18*, 701–706.
- (92) Finšgar, M.; Milosev, I. Corrosion Inhibitors for Copper and Stainless Steels in Chloride Solutions. In *Slov. Kem. Dnevi*; Univerza v Mariboru, Fakulteta za Kemijo in Kemijsko Tehnologijo, 2010; pp. finšgar1/1–finšgar1/11.
- (93) Schreifels, J. A.; Morris, R. E.; Turner, N. H.; Mowery, R. L.; Hues, S. M. Adsorption of a Metal Passivator onto Metal Surfaces. *Energy & Fuels* **1991**, *5*, 263–268.
- (94) Cao, P. G.; Yao, J. L.; Zheng, J. W.; Gu, R. A.; Tian, Z. Q. Comparative Study on Inhibition Effects of Benzotriazole for Metals in Neutral Solutions as Observed with Surface-Enhanced Raman Spectroscopy. *Langmuir* **2002**, *18*, 100–104.

References

- (95) Cao, P.; Gu, R.; Tian, Z. Electrochemical and Surface-Enhanced Raman Spectroscopy Studies on Inhibition of Iron Corrosion by Benzotriazole. *Langmuir* **2002**, *18*, 7609–7615.
- (96) Peljhan, S.; Kokalj, A. DFT Study of Gas-Phase Adsorption of Benzotriazole on Cu(111), Cu(100), Cu(110), and Low Coordinated Defects Thereon. *Phys. Chem. Chem. Phys.* **2011**, *13*, 20408–20417.
- (97) Kokalj, A.; Peljhan, S. Density Functional Theory Study of ATA, BTAH, and BTAOH as Copper Corrosion Inhibitors: Adsorption onto Cu(111) from Gas Phase. *Langmuir* **2010**, *26*, 14582–14593.
- (98) Jiang, Y.; Adams, J. B. First Principle Calculations of Benzotriazole Adsorption onto Clean Cu(111). *Surf. Sci.* **2003**, *529*, 428–442.
- (99) Chen, X.; Häkkinen, H. Divide and Protect: Passivating Cu(111) by Cu-(benzotriazole) 2. *J. Phys. Chem. C* **2012**, *116*, 22346–22349.
- (100) Kovačević, N.; Kokalj, A. DFT Study of Interaction of Azoles with Cu(111) and Al(111) Surfaces: Role of Azole Nitrogen Atoms and Dipole–Dipole Interactions. *J. Phys. Chem. C* **2011**, *115*, 24189–24197.
- (101) Kokalj, A.; Peljhan, S.; Koller, J. The Effect of Surface Geometry of Copper on Dehydrogenation of Benzotriazole. Part II. *J. Phys. Chem. C* **2014**, *118*, 944–954.
- (102) Kovačević, N.; Kokalj, A. The Relation between Adsorption Bonding and Corrosion Inhibition of Azole Molecules on Copper. *Corros. Sci.* **2013**, *73*, 7–17.
- (103) Kokalj, A.; Kovačević, N.; Peljhan, S.; Finšgar, M.; Lesar, A.; Milošev, I. Triazole, Benzotriazole, and Naphthotriazole as Copper Corrosion Inhibitors: I. Molecular Electronic and Adsorption Properties. *Chemphyschem* **2011**, *12*, 3547–3555.
- (104) Jiang, Y.; Adams, J. B.; Sun, D. Benzotriazole Adsorption on Cu₂O(111) Surfaces: A First-Principles Study. *J. Phys. Chem. B* **2004**, *108*, 12851–12857.
- (105) Kokalj, A.; Peljhan, S. Density Functional Theory Study of Adsorption of Benzotriazole on Cu₂O Surfaces. *J. Phys. Chem. C* **2015**, *119*, 150511123514009.
- (106) Kokalj, A. Ab Initio Modeling of the Bonding of Benzotriazole Corrosion Inhibitor to Reduced and Oxidized Copper Surfaces. *Faraday Discuss.* **2015**.
- (107) Finšgar, M. EQCM and XPS Analysis of 1,2,4-Triazole and 3-Amino-1,2,4-Triazole as Copper Corrosion Inhibitors in Chloride Solution. *Corros. Sci.* **2013**, *77*, 350–359.
- (108) Chadwick, D.; Hashemi, T. Adsorbed Corrosion Inhibitors Studied by Electron Spectroscopy: Benzotriazole on Copper and Copper Alloys. *Corros. Sci.* **1978**, *18*, 39–51.
- (109) Finšgar, M.; Kovač, J.; Milošev, I. Surface Analysis of 1-Hydroxybenzotriazole and Benzotriazole Adsorbed on Cu by X-Ray Photoelectron Spectroscopy. *J. Electrochem. Soc.* **2010**, *157*, C52.

- (110) Finšgar, M.; Peljhan, S.; Kokalj, A.; Kovač, J.; Milošev, I. Determination of the Cu₂O Thickness on BTAH-Inhibited Copper by Reconstruction of Auger Electron Spectra. *J. Electrochem. Soc.* **2010**, *157*, C295.
- (111) Roberts, R. F. X-Ray Photoelectron Spectroscopic Characterization of Copper Oxide Surfaces Treated with Benzotriazole. *J. Electron Spectros. Relat. Phenomena* **1974**, *4*, 273–291.
- (112) Oertel, M.; Klüsener, P.; Kempken, M.; Benninghoven, A.; Rother, H. J.; Holm, R. Combined SIMS/TPD Investigations of UHV-Prepared Tolyltriazole Overlayers on Cu, Ni and Au. *Appl. Surf. Sci.* **1989**, *37*, 135–146.
- (113) Dauchot, G.; Combarieu, R.; Repoux, M.; Delamare, F. TOF-SIMS Study of the Adsorption of Benzotriazole on Copper and Silver Surfaces: Kinetic Energies Distributions of Organic and Organometallic. In *Second. Ion Mass Spectrom., SIMS XII, Proc. Int. Conf., 12th*; Elsevier Science B.V., 2000; pp. 191–194.
- (114) Schreifels, J. A. The Interaction of a Metal Deactivator with Metal Surfaces. *Prepr. Pap. - Am. Chem. Soc. Div. Fuel Chem.* **1990**, *35*, 555–562.
- (115) Herlenius, N.; Rasco, J.; Casserly, E. New IEC 60296 (ed. 4) - From a Transformer Oil Manufacturer's Perspective. In *Transformer Life Management, TLM 2013*; Hannover/Dubai, 2013; pp. 1–5.
- (116) 10, T. *Detection and Determination of Specified Additives in Mineral Insulating Oils (IEC 60666)*; 2010.
- (117) ASTM D02.05. *Standard Test Method for Corrosiveness to Copper from Petroleum Products by Copper Strip Test (ASTM D130)*; 2012.
- (118) Russ, J. C. *Fundamentals of Energy Dispersive X-Ray Analysis*; Elsevier, 1984.
- (119) Lachance, G. R.; Claisse, F. *Quantitative X-Ray Fluorescence Analysis: Theory and Application*; Wiley, 1995.
- (120) Danilatos, G. D. Foundations of Environmental Scanning Electron Microscopy. *Adv. Electron. Electron Phys.* **1988**, *71*, 109–250.
- (121) Danilatos, G. D. Theory of the Gaseous Detector Device in the Environmental Scanning Electron Microscope. *Adv. Electron. Electron Phys.* **1990**, *78*, 1–102.
- (122) Danilatos, G. D. Environmental Scanning Electron Microscopy. In *In-situ microscopy in materials research*; Gai, P. L., Ed.; Kluwer Academic Publishers: Boston, MA, USA, 1997; p. 336.
- (123) Carlson, T. A. Photoelectron and Auger Spectroscopy. In; Plenum Press: New York, 1978.
- (124) Siegbahn Nordling C., Fahlman A., Nordberg R., Hamrin K., Hedman J., Johansson G., Bergmark T., Karlsson S.-E., Lindgren I., Lindberg B., K. *ESCA - Atomic, Molecular and Solid State Structure Studied by Means of Electron Spectroscopy*;

References

- Ser. IV, V.; Nova Acta Regiae Societatis Scientiarum Upsaliensis: Uppsala, Sweden, 1967.
- (125) Karslioglu, O.; Nemsak, S.; Zegkinoglou, I.; Shavorskiy, A.; Hartl, M.; Salmassi, F.; Gullikson, E. M.; Ng, M. L.; Rameshan, C.; Rude, B.; et al. Aqueous Solution/metal Interfaces Investigated in Operando by Photoelectron Spectroscopy. *Faraday Discuss.* **2015**.
- (126) Eistein, A. Does the Inertia of a Body Depend on Its Energy Content. *Ann. Phys. (N. Y).* **1905**, *17*, 821.
- (127) Fairley, N. *Introduction to XPS and AES*; Casa Software Ltd., 2009.
- (128) Edgell, M. J.; Paynter, R. W.; Castle, J. E. The Use of an Electron Flood Gun When Adopting Monochromatic AgL α Radiation for the XPS Analysis of Insulators. *Surf. Interface Anal.* **1986**, *8*, 113–119.
- (129) O'Connor, John, Sexton, Brett A., Smart, R. S. C. 23.4.3 Inelastic Mean Free Path in Polymers. In *Surface Analysis Methods in Materials Science*; Springer Science & Business Media, 2003; pp. 532–533.
- (130) Tanuma, S.; Powell, C. J.; Penn, D. R. Calculation of Electron Inelastic Mean Free Paths (IMFPs) VII. Reliability of the TPP-2M IMFP Predictive Equation. *Surf. Interface Anal.* **2003**, *35*, 268–275.
- (131) O'Connor, J.; Sexton, B. A.; Smart, R. S. C. 23.5 Secondary Ion Mass Spectrometry (SIMS). In *Surface Analysis Methods in Materials Science*; Springer Science & Business Media, 2009; pp. 537–540.
- (132) Mahoney, C. M.; Gillen, G. An Introduction to Cluster Secondary Ion Mass Spectrometry. In *Wiley Series on Mass Spectrometry - Cluster Secondary Ion Mass Spectrometry: Principles and Applications*; Mahoney, C. M., Ed.; John Wiley & Sons: Somerset, NJ, USA, 2013; p. 366.
- (133) Delcorte, A.; Restrepo, O. A.; Czerwinski, B. Cluster SIMS of Organic Materials: Theoretical Insights. In *Wiley Series on Mass Spectrometry - Cluster Secondary Ion Mass Spectrometry: Principles and Applications*; Mahoney, C. M., Ed.; Somerset, NJ, USA, 2013; p. 366.
- (134) Vickerman, J. C.; Briggs, D. Cluster and Polyatomic Primary Ion Beams. In *ToF-SIMS: Materials Analysis by Mass Spectrometry*; IM Publications, 2013; p. 732.
- (135) Mahoney, C. M. Surface Analysis of Organic Materials with Polyatomic Primary Ion Sources. In *Wiley Series on Mass Spectrometry - Cluster Secondary Ion Mass Spectrometry: Principles and Applications*; Mahoney, C. M., Ed.; Somerset, NJ, USA, 2013; p. 366.
- (136) Fahey, A. J. Ion Sources Used for Secondary Ion Mass Spectrometry. In *Wiley Series on Mass Spectrometry - Cluster Secondary Ion Mass Spectrometry: Principles and Applications*; Mahoney, C. M., Ed.; Somerset, NJ, USA, 2013; p. 366.

- (137) Tajmar, M.; Scharlemann, C. A. Development of Electric and Chemical Microthrusters. *International Journal of Aerospace Engineering*, 2011, 2011, 1–10.
- (138) Vickerman, J. C.; Briggs, D. Prologue: ToF-SIMS - An Evolving Mass Spectrometry of Materials. In *ToF-SIMS: Materials Analysis by Mass Spectrometry*; IM Publications, 2013; p. 732.
- (139) Redhead, P. A. Thermal Desorption of Gases. *Vacuum* **1962**, 12, 203–211.
- (140) Maina, R.; Tumiatti, V.; Bruzzoniti, M. C.; De Carlo, R. M.; Lukic, J.; Naumovic-Vukovic, D. Copper Dissolution and Deposition Tendency of Insulating Mineral Oils Related to Dielectric Properties of Liquid and Solid Insulation. In *IEEE International Conference on Dielectric Liquids (ICDL)*; 2011; pp. 1–6.
- (141) Plaza, S.; Mazurkiewicz, B.; Gruziński, R. Thermal Decomposition of Dibenzyl Disulphide and Its Load-Carrying Mechanism. *Wear* **1994**, 174, 209–216.
- (142) Slagle, K. H.; Reid, E. E. Action of Some Mercaptans in Hydrocarbon Solution on Copper and Copper Sulfide. *Ind. Eng. Chem.* **1932**, 24, 448–451.
- (143) Witt, D.; Klajn, R.; Barski, P.; Grzybowski, B. A. Applications, Properties and Synthesis of Ω -Functionalized N-Alkanethiols and Disulfides – the Building Blocks of Self-Assembled Monolayers. *Curr. Org. Chem.* **2004**, 8, 1763.
- (144) Colclough, T. Role of Additives and Transition Metals in Lubricating Oil Oxidation. *Ind. Eng. Chem. Res.* **1987**, 26, 1888–1895.
- (145) Amaro, P. S.; Facciotti, M.; Holt, A. F.; Pilgrim, J. A.; Lewin, P. L.; Brown, R. C. D.; Wilson, G.; Jarman, P. Tracking Copper Sulfide Formation in Corrosive Transformer Oil. In *2013 Annual Report Conference on Electrical Insulation and Dielectric Phenomena*; IEEE, 2013; pp. 144–147.
- (146) Krylova, V.; Andrulevičius, M. Optical, XPS and XRD Studies of Semiconducting Copper Sulfide Layers on a Polyamide Film. *Int. J. Photoenergy* **2009**, 2009, 1–8.
- (147) Darmstadt, H.; Garcia-Perez, M.; Adnot, A.; Chaala, A.; Kretschmer, D.; Roy, C. Corrosion of Metals by Bio-Oil Obtained by Vacuum Pyrolysis of Softwood Bark Residues. An X-Ray Photoelectron Spectroscopy and Auger Electron Spectroscopy Study. *Energy and Fuels* **2004**, 18, 1291–1301.
- (148) Subramanian, R.; Lakshminarayanan, V. Effect of Adsorption of Some Azoles on Copper Passivation in Alkaline Medium. *Corros. Sci.* **2002**, 44, 535–554.
- (149) Fang, B.-S.; Olson, C. G.; Lynch, D. W. A Photoemission Study of Benzotriazole on Clean Copper and Cuprous Oxide. *Surf. Sci.* **1986**, 176, 476–490.
- (150) Amimoto, T.; Nagao, E.; Tanimura, J.; Toyama, S.; Yamada, N. Duration and Mechanism for Suppressive Effect of Triazole-Based Passivators on Copper-Sulfide Deposition on Insulating Paper. *IEEE Trans. Dielectr. Electr. Insul.* **2009**, 16, 257–264.

References

- (151) Wan, T.; Qian, H.; Zhou, Z.; Gong, S. K.; Hu, X.; Feng, B. Suppressive Mechanism of the Passivator Irgamet 39 on the Corrosion of Copper Conductors in Transformers. *IEEE Trans. Dielectr. Electr. Insul.* **2012**, *19*, 454–459.
- (152) Pahlavanpour, B.; Sundkvist, K. *Mineral Insulating Oil Passivation Effectiveness of Passivation to Stop Copper Deposition*; Nynas Naphthenics Ltd.
- (153) Popova, I.; Yates Jr., J. T. Adsorption and Thermal Behavior of Benzotriazole Chemisorbed on Γ -Al₂O₃. *Langmuir* **1997**, *13*, 6169–6175.
- (154) Brusic, V. Copper Corrosion With and Without Inhibitors. *J. Electrochem. Soc.* **1991**, *138*, 2253.
- (155) Nynas AB. *Base Oil Handbook*; 2001.
- (156) Antonijevic, M. M.; Petrovic, M. B. Copper Corrosion Inhibitors. A Review. *Int. J. Electrochem. Sci.* **2008**, *3*, 1–28.
- (157) Peljhan, S.; Koller, J.; Kokalj, A. The Effect of Surface Geometry of Copper on Adsorption of Benzotriazole and Cl. Part I. *J. Phys. Chem. C* **2014**, *118*, 933–943.
- (158) Zumdhal, S. S.; Zumdhal, S. A. Covalent Bond Energies and Chemical Reactions. In *Chemistry*; Brooks/Cole Publishing Co., 1999; p. 1143.